DECIPHERING THE INDUCTION AND PATTERNING OF THE CONJUNCTIVAL PAPILLAE IN THE CHICKEN, GALLUS GALLUS

by

Karyn Allyson Jourdeuil

Submitted in partial fulfilment of the requirements
for the degree of Doctor of Philosophy

at

Dalhousie University
Halifax, Nova Scotia
November, 2015

DEDICATION

This thesis is dedicated to my family and friends, without whom I would not be here today.

It is, however, especially dedicated to:

My grandmother, Mary Neville. You are one of the strongest women I have ever known. Your dedication to your family is, and has always been, unwavering. Without you, none of us would have followed our dreams, myself included. I am eternally grateful for your continual love and support and could not have done this without you. I love you very much.

My mother, Denyse Neville. You have been so supportive of me over the years and have always encouraged me to follow my dreams. Who could ask for a better role-model?

My step-father, Vikram Venugopal. Your support and advice has permitted me to have this dream. Guess what? You're (hopefully, if I pass!) going to have your doctor! Yes, I know, still not the right kind of doctor!

Finally (but not least), this thesis is dedicated to Kevin Schleich, Shirley Neville, Phil Jourdeuil, Sue Jourdeuil, Chari Neville, and Jim Miller. I could not have done any of this without your encouragement and support.

I love you all very much.

TABLE OF CONTENTS

List of Tables x

List of Figures xi

Abstract xv

List of Abbreviations Used xvi

Acknowledgements xviii

Chapter 1: Introduction 1

1.1 – The Neural Crest 2

1.1.1 – Induction of the Neural Crest 6

1.1.1.1 – Induction of the Neural Plate Border 6

1.1.1.2 – The Neural Plate Border Specifier Genes 8

1.1.1.3 – The Neural Crest Specifier Genes 10

1.1.2 – The Specification of the Neuroectoderm, Non-Neural Ectoderm, and Pre-Placodal Region 12

1.2 – Early Eye Development and the Origin of the Periocular Mesenchyme 14

1.2.1 – Brief Overview of Early Eye Development 15

1.2.2 – Origin of the Periocular Mesenchyme 16

1.3 – The Sclerotic Ring 18

1.3.1 – The Conjunctival Papillae 21

1.3.1.1 – The Murray Stages of Papilla Morphogenesis (Murray, 1943) 22

1.3.1.2 – Induction and Patterning of the Conjunctival Papillae 25

1.3.1.2.1 – A Numbering Schema for the Conjunctival Papillae and the Modal Number per Eye 25

1.3.1.2.2 – The Relationship Between the Conjunctival Papillae and the Scleral Condensations 27

1.3.1.2.3 – Determining the Nature of Condensation Induction 29

1.3.2 – Conclusions 32

1.4 – Objectives 33

Chapter 2: Ablation of Neural Crest Signaling Centers Does Not Affect Papilla Patterning 36

2.1 – Introduction 36

2.1.1 – Background 36

2.1.2 – Epithelial-to-Mesenchymal Transition, Delamination, and Early Migration of the Neural Crest 37

2.1.3 – Migration of Neural Crest Cells into and Around the Eye 43

2.1.4 – Objectives 44

2.2 – Materials and Methods 45

2.2.1 – Egg Incubation 45

2.2.2 – Windowing Eggs 45

2.2.3 – Surgical Manipulations 46

2.2.4 – Embryo Fixation 48

2.2.5 – Imaging and Analysis 48

2.3 – Results 49

2.3.1 – Removal of the Otic Vesicle Epithelium 50

2.3.2 – Removal of the Epithelium Between the Otic Vesicle and the Eye 51

2.3.3 – Removal of Both the Otic Vesicle and Nasal Pit Epithelium 51

2.3.4 – Removal of the Epithelium Between the Nasal Pit and the Eye 52

2.3.5 – Removal of the Nasal Pit Epithelium 53

2.4 – Discussion 53

2.4.1 – Summary and Significance 57

Chapter 3: Conjunctival Papilla Regeneration Serves as a Mechanism of Epithelial Compensation 59

3.1 – Introduction 59

3.1.1 – Background 59

3.1.2 – Objectives 61

3.2 – Materials and Methods 62

3.2.1 – Egg Incubation and Windowing 62

3.2.2 – Surgical Manipulations 62

3.2.3 – Embryo Fixation 67
3.2.4 – Alkaline Phosphatase Staining 67
3.2.5 – *In Situ* Hybridization 68
3.2.6 – Cryosectioning 70
3.2.7 – Imaging and Analysis 71
3.3 – Results 72
3.3.1 – Epithelium Removal Prior to Conjunctival Papilla Induction does not affect the Patterning of the Other Conjunctival Papillae in the Ring 72
3.3.1.1 – Surgical Ablation at HH 29 73
3.3.1.2 – Surgical Ablation at HH 30 75
3.3.1.3 – Summary of Epithelium Removals 76
3.3.2 – Surgical Ablation of a Conjunctival Papilla Does not affect the Patterning of the other Conjunctival Papillae in the Ring 77
3.3.2.1 – Surgical Ablation at HH 30.5 78
3.3.2.2 – Surgical Ablation at HH 31 and HH 33 78
3.3.2.3 – Surgical Ablation at HH 34 79
3.3.2.4 – Summary of Papilla Ablations Between HH 30.5 and HH 34 80
3.3.3 – Testing the Limits of Conjunctival Papilla Regeneration during the Normal Period of Conjunctival Papilla Induction 80
3.3.3.1 – 1 Day Post-Surgery 82
3.3.3.2 – 1.5 Days Post-Surgery 82
3.3.3.3 – 2 Days Post-Surgery 83
3.3.3.4 – 2.5 Days Post-Surgery 84
3.3.3.5 – 3 and 3.5 Days Post-Surgery 84
3.3.3.6 – 5 Days Post-Surgery 85
3.3.3.7 – Summary of all Surgeries in this Section 87
3.3.4 – Testing the Limits of Conjunctival Papilla Regeneration Outside the Normal Period of Conjunctival Papilla Induction 87
3.3.4.1 – 1 Day Post-Surgery 88
3.3.4.2 – 2 Days Post-Surgery 89
3.3.4.3 – 4-5 Days Post-Surgery 89
3.3.4.4 – Summary of Surgical Ablation at HH 35 90

3.3.5 – How Does Papilla Regeneration Affect Condensation Induction and are the Known Molecular Pathways Used? 91

3.3.5.1 – 1 Day Post-Surgery 92

3.3.5.2 – 1.5 Days Post-Surgery 95

3.3.5.3 – 2 Days Post-Surgery 97

3.3.5.4 – 2.5 Days Post-Surgery 99

3.3.5.5 – 3 Days Post-Surgery 101

3.3.5.6 – Summary of In Situ Hybridization 102

3.4 – Discussion 104

3.4.1 – Towards Understanding the Patterning of the Conjunctival Papillae 104

3.4.2 – Towards Understanding the Regenerative Capacity of the Conjunctival Papillae 108

3.4.3 – A Conjunctival Papilla Removed at HH 35 Does not Regenerate yet a Condensation is Induced in the Underlying Mesenchyme 111

3.4.4 – The Regenerated Conjunctival Papilla Matures Faster in Order to Induce an Underlying Scleral Condensation during the Normal Inductive Period (HH 35-36) 112

3.4.5 – Summary and Significance 114

Chapter 4: Candidate Gene Expression During Conjunctival Papilla Development 116

4.1 – Introduction 116

4.1.1 – Background 116

4.1.2 – The Cranial Placodes 119

4.1.2.1 – Pre-Patterning of the Epithelium 120

4.1.2.2 – Induction of the Craniofacial Placodes 123

4.1.2.3 – Induction of Derivative Structures 128

4.1.2.3.1 – Neurogenic Cranial Placodes 128

4.1.2.3.2 – Non-Neurogenic Cranial Placodes 129

4.1.3 – The Cutaneous Placodes 130

4.1.3.1 – Hair Placodes 132

4.1.3.1.1 – Primary Wave of Hair Placode Development 133

4.1.3.1.2 – Secondary and Tertiary Waves of Hair Placode Development 135

4.1.3.2 – Feather Placodes 137
4.1.3.3 – Dental Placodes 139
4.1.4 – Objectives 141
4.2 – Materials and Methods 143
4.2.1 – Egg Incubation 143
4.2.2 – Candidate Gene Selection 143
4.2.3 – Primer Design 146
4.2.4 – Primer Rehydration 149
4.2.5 – RNA Extraction 149
4.2.6 – RNA Quantification 150
4.2.7 – cDNA Synthesis 150
4.2.8 – Polymerase Chain Reaction 150
4.2.9 – Gel Electrophoresis and Imaging 151
4.2.10 – Primer Validation 151
4.2.11 – Gene Sequencing 152
4.2.12 – RNA Extraction with Tissue Separation 153
4.2.13 – Presence versus Absence Analysis 153
4.2.14 – Primer Design with Conjugated T3 and T7 Binding Sites 153
4.2.15 – Validation of New Primers 155
4.2.16 – Ethanol Precipitation of DNA 156
4.2.17 – Purification of DNA from an Agarose Gel 156
4.2.18 – Plasmids 157
4.2.19 – Removing the Plasmids from Filter Paper 160
4.2.20 – Cloning 161
4.2.21 – Mini-Prep 161
4.2.22 – DNA Digest 161
4.2.23 – Gene Sequencing 161
4.2.24 – DIG-RNA Labeling (Probe Generation) 162
4.2.25 – DIG-High Prime DNA Labeling and Detection (Dot-Blot) 162
4.2.26 – *In Situ* Hybridization 162
4.2.27 – Cryosectioning 162

4.3 – Results 163

4.3.1 – Part A: Epithelial Competency Factors 163

4.3.2 – Part B: Candidate Gene Analysis 166

4.3.2.1 – Description of Selected Candidate Genes 166

4.3.2.2 – Candidate Gene Expression in the Epithelium and/or Mesenchyme: Presence versus Absence 170

4.3.2.3 – Results of In Situ Hybridization 171

4.3.2.4 – Summary of Candidate Gene Analysis 187

4.4 – Discussion 190

4.4.1 – Pre-Patterning of the Epithelium 191

4.4.2 – Investigating the Induction and Patterning of the Conjunctival Papillae and the Induction of the Underlying Scleral Condensations 195

4.4.2.1 – PROX1 195

4.4.2.2 – EDNRB 196

4.4.2.3 – INHBA 198

4.4.2.4 – DLX5 200

4.4.2.5 – GSC 203

4.4.2.6 – EYA1 204

4.4.2.7 – Summary of the Candidate Gene Analysis 205

4.4.3 – Conclusion 208

Chapter 5: Discussion and Conclusion 210

5.1 – Discussion 210

5.1.1 – Patterning of the Conjunctival Papillae 210

5.1.2 – Papillae Induction and Regeneration 214

5.1.3 – A New Stage of Conjunctival Papilla Development: The Conjunctival Placode 215

5.1.4 – A Third Category of Placodes – The Skeletogenic Placodes 220

5.1.4.1 – Limb Development: The Apical Ectodermal Ridge 221

5.1.4.2 – Evidence of Other Skeletogenic Placodes 224

5.2 – Conclusion 225

References 226

Appendix 1: Protocols 254

Appendix 2: *In Situ* Hybridization 273

Appendix 3: *Oc90* 280

LIST OF TABLES

Table 2.1: Summary of the results of epithelium removals between HH 14 and 18 49

Table 3.1: Table summarizing the results of epithelium removals directly above the ciliary artery between HH 29 and 30 73

Table 3.2: Table summarizing the results of papilla removals between HH 30 and 34 78

Table 3.3: Table summarizing the results of papilla removals between HH 30 and 34 after 1, 1.5, 2, 2.5, 3, 3.5, and 5 dps 81

Table 3.4: Table summarizing the results of papilla removals at HH 35 and then fixed after 1, 2, and 4 or 5 dps 88

LIST OF FIGURES

Figure 1.1: Schematics illustrating the NC populations and their derivatives....4

Figure 1.2: Fate map of the NC derivatives in the craniofacial skeleton of the chicken....5

Figure 1.3: A schematic summarizing the timing of NPB specification, NC specification, and NC migration in *Xenopus*, chick, zebrafish, and mouse....9

Figure 1.4: Schematic illustrating the location of the NC with respect to the non-neural ectoderm, the neural ectoderm, and the PPR including an overview of some of the genes that are involved at each step....14

Figure 1.5: A schematic illustrating the differences between the teleost scleral ossicles and the reptilian sclerotic ring....19

Figure 1.6: Schematic illustrating the M-stages of papilla development....24

Figure 1.7: Schematic illustrating the spatiotemporal pattern of conjunctival papilla induction....27

Figure 1.8: Schematic illustrating the different papilla regions....31

Figure 2.1: Schematic illustrating the ectopic ossicles (arrow) that were reported in a personal communication by Dr. J. Richman (University of British Columbia, Canada) after epithelium removal at the otic vesicle between HH 13 and 18....37

Figure 2.2: Schematic illustrating the migration of the cranial and cephalic NCCs....43

Figure 2.3: Schematic illustrating the area of epithelium removed in a HH 16 embryo....47

Figure 2.4: Results of epithelium removals performed between HH 14 and 18 and fixed between HH 33 and 38....50

Figure 3.1: A schematic illustrating the timeline of induction of the sclerotic ring....61

Figure 3.2: Diagram showing the surgery sites....64

Figure 3.3: Results of epithelium ablation at HH 29....75

Figure 3.4: Results of epithelium ablation at HH 30 76

Figure 3.5: Results of conjunctival papilla ablation at HH 34.....80

Figure 3.6: Results of conjunctival papilla ablation after 1 dps.....82

Figure 3.7: Results of conjunctival papilla ablation after 1.5 dps.....83

Figure 3.8: Results of conjunctival papilla ablation after 2 dps.....83

Figure 3.9: Results of conjunctival papilla ablation after 2.5 dps.....84

Figure 3.10: Results of conjunctival papilla ablation after 3 dps.....85

Figure 3.11: Results of conjunctival papilla ablation after 5 dps.....86

Figure 3.12: Results of conjunctival papilla ablation at HH 35 after 1 dps.....88

Figure 3.13: Results of conjunctival papilla ablation at HH 35 after 2 dps.....89

Figure 3.14: Results of conjunctival papilla ablation at HH 35 after 4-5 dps unstained (A) and stained with alkaline phosphatase (B).....90

Figure 3.15: Schematic summarizing the results of conjunctival papilla removals between HH 30-35 91

Figure 3.16: Schematic illustrating the two possible predicted scenarios of *Bmp2* expression in the regenerated conjunctival papillae as compared to the known expression of *Bmp2* 92

Figure 3.17: Results of *in situ* hybridization for *Bmp2* in the left (control) and right (surgery) eyes of the same embryo after surgical ablation of the conjunctival papilla directly above the ciliary artery at HH 34 after 1 dps (HH 35).....94

Figure 3.18: Results of *in situ* hybridization for *Bmp2* in the left (control) and right (surgery) eyes of the same embryo after surgical ablation of the conjunctival papilla directly above the ciliary artery at HH 34 after 1.5 dps (HH 35.5).....96

Figure 3.19: Results of *in situ* hybridization for *Bmp2* in the left (control) and right (surgery) eyes of the same embryo after surgical ablation of the conjunctival papilla directly above the ciliary artery at HH 34 after 2 dps (HH 36).....98

Figure 3.20: Results of *in situ* hybridization for *Bmp2* in the left (control) and right (surgery) eyes of the same embryo after surgical ablation of the conjunctival papilla directly above the ciliary artery at HH 34 after 2.5 dps (HH 36.5).....100

Figure 3.21: Results of *in situ* hybridization for *Bmp2* in the left (control) and right (surgery) eyes of the same embryo after surgical ablation of the conjunctival papilla directly above the ciliary artery at HH 34 after 3 dps (HH 37).....101

Figure 3.22: A summary of the expression of *Bmp2* in the surgery (right eye) of embryos from 1 dps through to 3 dps.....103

Figure 4.1: Schematic illustrating the establishment of the PPR and its subdivision into distinct placodes.....121

Figure 4.2: A schematic illustrating the induction and patterning of the hair, feather, and tooth placodes and their subsequent derivative structures.....135

Figure 4.3: A schematic illustrating the tissue dissected from the right and left eyes of samples for microarray analysis (dotted lines).....144

Figure 4.4: Summarizing the results of PCR for the candidate genes.....152

Figure 4.5: Results of *Prox1* PCR using the new primers to which T3 and T7 binding sites have been conjugated.....156

Figure 4.6: Summarizing the results of *in situ* hybridization of *β-catenin* at HH 30, HH 32, HH 34 and HH 35.....165

Figure 4.7: The results of gel electrophoresis for the six candidate genes.....170

Figure 4.8: Results of *in situ* hybridization for *Prox1*.....172

Figure 4.9: Results of *in situ* hybridization for *Ednrb*.....174

Figure 4.10: Results of *in situ* hybridization for *Inhba*.....176

Figure 4.11: Results of *in situ* hybridization for *Dlx5*.....180

Figure 4.12: Results of *in situ* hybridization for *Gsc*.....183

Figure 4.13: Results of *in situ* hybridization for *Eya1*.....186

Figure 4.14: Results of *in situ* hybridization for *Eya1*.....187

Figure 4.15: A schematic summarizing the expression of all my candidate genes during the induction and patterning of the conjunctival papillae and scleral ossicles between HH 30 and 35.5 189

Figure 4.16: A schematic summarizing the results of cryosectioning at the stage of strongest expression for each of the candidate genes 191

Figure 4.17: Schematic illustrating the possible gene interactions taking place during the induction of the conjunctival papillae and scleral condensations 207

ABSTRACT

The conjunctival papillae (CP), epithelial thickenings on the surface of the conjunctiva, are required for the induction of the underlying neural crest-derived, intramembranous scleral bones. Induction of the CP begins at Hamburger and Hamilton (HH) stage 30 (approximately 7 days post fertilization) and proceeds following a set temporospatial pattern. However, very little is known about the mechanisms or factors required for the induction and patterning of the CP. Therefore, I investigated a number of different aspects of CP development, namely: i) whether the inductive signal may be neural crest-derived, ii) how patterning is established within the ring of CP, and iii) whether known signaling factors for the development of other epithelial thickenings are required for CP development. To do this, a combination of surgical ablations and molecular techniques were used. Although I was unable to determine whether the neural crest-derived periocular mesenchyme is required for CP development, surgical ablation of either the epithelium or papilla directly above the ciliary artery (the first to form) between HH 29 and 34 demonstrated that the patterning of the CP is not dependent upon the first papilla to form. Furthermore, when a papilla was ablated between HH 30 and 34, this papilla was capable of regeneration. Further experimentation into this regenerative capacity highlighted that it serves as a mechanism of epithelial compensation to ensure that a complete ring of scleral condensations is induced in the underlying mesenchyme. Finally, using a candidate gene analysis, I was able to identify, for the first time, i) a gene that is likely required to establish epithelial competency prior to the induction of the CP, ii) genes that are expressed during the induction and patterning of the CP, and iii) novel genes likely involved in the induction of the condensations. This work has identified a new phase of papilla induction, the conjunctival placode, and suggests that a new category of placodes should be established, the skeletogenic placodes. This research will serve as a good basis for future research into both the CP and the induction and patterning of intramembranous bone.

LIST OF ABBREVIATIONS USED

AP – alkaline phosphatase

Bmp – bone morphogenetic protein

CDK – cyclin-dependent kinase

CNCC – cranial neural crest cells

CP – conjunctival papillae

DepC – diethyl pyrocarbonate

Dlx5 – distal-less homeobox 5

DNA – deoxyribonucleic acid

dpf – days post fertilization

dps – days post-surgery

Ednrb – endothelin receptor B

EMT – epithelial-to-mesenchymal transition

EtOH – ethanol

Eya1 – eyes absent homologue 1 (*Drosophila*)

Fgf – fibroblast growth factor

FoxD3 – forkhead box D3

GRN – gene regulatory network

Gsc – goosecoid homeobox

HH – Hamburger and Hamilton (1951) stages

Hh – hedgehog

Ihh – indian hedgehog

Inhba – inhibin beta A

kDa – kilo Dalton

LALI – local auto-activation and lateral inhibition

MeOH – methanol

MMP – matrix metalloproteases

mRNA – messenger RNA

M-stage – Murray stages of papilla development

NBF – neutral buffered formalin

NC – neural crest

NCC – neural crest cell

NC-GRN – neural crest gene regulatory network

NPB – neural plate border

Oc90 – otoconin 90

PBS – phosphate buffered saline

PBST – phosphate buffered saline with Tween20

PFA - paraformaldehyde

Ppa – partner of paired

PPR – pre-placodal region

Prox1 – prospero related homeobox 1

Ptc – patched

r - rhombomere

RNA – ribonucleic acid

RPE – retinal pigmented epithelium

Shh – sonic hedgehog

Six – sine oculis

Tgf-β – transforming growth factor beta

TIMP – tissue inhibitor of MMps

ACKNOWLEDGEMENTS

First and foremost, I would like to thank my supervisor, Dr. Tamara Franz-Odendaal. Seven years ago, Tamara gave a guest lecture in my developmental biology class on the neural crest. Prior to this lecture, I had had a keen interest in developmental biology stemming from the loss of my little sister at a young age from *spina bifida*, yet I don't think I had really thought it was possible for *me* to study in this field. A few months later, I walked into her office to see whether I would be able to work in her lab as an Honor's student. I don't quite remember how long it was that I had been in the lab for that Honor's degree before I began asking Tamara whether I could do my Master's with her; nor do I remember how long after beginning my Master's that I petitioned to upgrade to the Ph.D. program because I was unwilling to leave this fascinating field behind (as an aside, Tamara does a wonderfully hilarious impression of my wheedling to stay in her lab and do more work, which she recently shared with Christine and I). Seven years on and my curiosity in this field has only increased. Tamara has provided me with innumerable (and invaluable) opportunities – from learning new techniques to being able to travel internationally to attend conferences, which has allowed me to meet with the pre-eminent researchers in this field. Tamara has pushed me to develop into a confident, young researcher and it is due to her support and encouragement that I am the scientist I am today. Tamara, thank you, from the bottom of my heart for letting me into your lab that fateful day and believing in me. Without you, I would not be able to continue to follow my dreams.

I would also like to thank the members of my supervisory committee: Dr. Angelo Iulianella, Dr. Boris Kablar, Dr. William Baldridge, and Dr. Kazue Semba. The advice,

comments, and feedback with which you have provided me have been invaluable. I would also like to thank Dr. Iulianella and his student, Michelle Crawford, for teaching me primer design and teaching me how to trouble shoot *in situ* hybridization problems from newly designed probes. Additionally, I would like to thank Dr. Brian Hall who has provided helpful comments and criticisms throughout this degree and was kind enough to act as my external examiner for my Preliminary Examination.

Next, I would like to thank the members of the Franz-Odendaal Bone Development Lab. First of all, I would like to thank Megan Dufton and Kellie Cloney. You were my first lab mates and helped me to learn the ropes. Megan, you helped me learn how to be more confident in the lab. If it weren't for your lunch invitation, I may never have become comfortable enough to make such great lab friends. Kellie, you taught me a great deal about surgical manipulation in chick. You also taught me that for most problems, including dropped forceps, there is a solution if you know where to look for it. Next, I would like to thank James Jabalee. I don't know if I could have made it through the last two years of my degree if it weren't for you – your friendship, support, and help in the lab has been invaluable. *In situ* would not have been the same without you. Kaity and Christine, I would like to thank you for being the best lab-little sisters I could have ever imagined. I'm so glad both of you came into the lab and I don't think I could imagine my life without you two. I'd also like to thank Sew for everything. It has been so wonderful getting to know you and your family. Additionally, I would like to thank the rest of my many lab mates, past and present: Sally, Natalie, Matt, Jade, Justine, Sarah, Greg, Stephanie, Brittni, Zoe, Devin, Carolyn, Jochen, and Sara. You have all been fantastic lab mates and I couldn't think of a better bunch of people with whom to have spent the past seven years.

Last, but certainly not least, I would like to thank my family and boyfriend, Kevin. I can't even begin to describe the amount of support you have all given me over the past 6 years. All of you have sat through innumerable presentations, have proofed papers, and have studied with me (whether you wanted to or not) for exams. You have all been there for me through thick and thin. Very few families would drive 30 minutes to the lab late at night to drop off a supper and some company when experiments ran late or really, just put up with me in general. I certainly would not be where I am today if it weren't for all of you. You have all always told me that I could do whatever I set my mind to; advice that has driven me to push myself academically. I cannot adequately express how much you all mean to me – my thanks and love to all of you.

Chapter 1: Introduction

Patterning during development is one of the key mechanisms that drives species diversity. On a large scale, patterning specifies what kind of organism will be formed by an embryo. Patterning is also responsible for a number of smaller scale processes, such as whether a tooth will become an incisor or a molar, the type of hair (or feathers) an organism will develop and their distribution, as well as the type of bones that will form and their manner of ossification. While embryological patterning has been well characterized morphologically, our ability to understand how this is coordinated through inductive events and molecular cascades is fairly recent, beginning with the advent of gene and protein manipulations.

To date, most of the literature in this field has focused on the early development of the embryo and the development of structures that will affect human health (e.g. hair, tooth, and limb development); while other structures have received less attention, such as the sclerotic ring, the focus of this study. The sclerotic ring is composed of a number of overlapping neural crest-derived bony plates and is found within the eye of a number of teleosts and reptiles (Franz-Odendaal & Hall, 2006; Franz-Odendaal & Vickaryous, 2006; Franz-Odendaal *et al.*, 2007; Franz-Odendaal, 2008a). Unravelling the induction and patterning of the sclerotic ring has the potential to provide important insights into the development of other craniofacial bones (such as the neural crest-derived, flat calvarial bones) in vertebrates. As there are a number of developmental conditions that alter the patterning of craniofacial bones, such as craniosynostosis and cleft lip/palate (Shillito & Matson, 1968; Vanderas, 1987; Wilkie, 1997; Kabbani & Raghuveer, 2004; Arosarena,

2007), this research will also help to further our understanding of conditions that affect human health.

To this end, this thesis will examine an essential component of the sclerotic ring system, namely the conjunctival papillae. These conjunctival papillae are transient epithelial thickenings that form on the surface of the conjunctiva and are directly required for the induction and patterning of the underlying scleral bones (Coulombre & Coulombre, 1962). In the older literature and the Hamburger and Hamilton (HH) staging table, these epithelial thickenings are referred to as the scleral papillae (Hamburger & Hamilton, 1951; Fyfe & Hall, 1981; Hall, 1981a; Hall, 1981b; Fyfe & Hall, 1983; Fyfe *et al*., 1988); however, as they are not derived from the sclera, but rather from the conjunctiva, they are better referred to as the conjunctival papillae (Murray, 1943; Coulombre & Coulombre, 1962; Franz-Odendaal, 2008a; Duench & Franz-Odendaal, 2012) and will be referred to as such throughout this thesis.

This first chapter will provide an introduction to the neural crest, from which the sclerotic ring is derived; a brief introduction to the development of the eye and the origin of the periocular mesenchyme; as well as an in-depth discussion of the induction and patterning of the sclerotic ring.

1.1 – The Neural Crest

The neural crest (NC), from which the sclerotic ring is derived, is a unique cell population. First described as a strip of cells lying between the neural tube and the presumptive epidermis in 1868 by Wilhelm Heis, the NC was so named based on its position at the "crest" of the closing neural tube (reviewed in Betters *et al*., 2010; Bronner, 2012; Bronner & Le Douarin, 2012). The neural crest cells (NCC), which are unique to

vertebrates, are highly migratory and give rise to a large number of derivatives. These include both ectomesenchymal (i.e. cartilage, bone, odontoblasts, smooth muscle, mesenchymal cells, adipocytes, *etc*.) and non-ectomesenchymal (i.e. neurons, glia, melanocytes, chromaffin cells, *etc*.) derivatives (Figure 1.1A) which in turn make up the peripheral nervous system, the craniofacial skeleton, and the pigmentation of the skin to name but a few (Sauka-Spengler & Bronner-Fraser, 2008; Bronner & Le Douarin, 2012; Bronner, 2012; Ishii *et al*., 2012; Simões-Costa & Bronner, 2013; Ivashkin & Adameyko, 2013). Due to the ability of the NC to give rise to numerous structures, it is often referred to as a fourth germ layer (Hall, 2000; Prasad *et al*., 2012; Bronner & Le Douarin, 2012). Additionally, it is the evolution of the NC which is thought to have driven the evolution of the "New Head" (Gans & Northcutt, 1983). This evolution of a complex head and well innervated sensory structures enabled vertebrates to undergo radical changes in lifestyle and to inhabit new environments.

The NCCs are traditionally divided into five subpopulations based on axial level: cranial, cardiac, vagal, trunk, and sacral (Figure 1.1B). The cranial neural crest cells (CNCC) give rise to a large number of ectomesenchymal derivatives (described above) and as such also give rise to the majority of the craniofacial skeleton (including the sclerotic ring) (reviewed in Baker, 2005; Figure 1.2). The CNCCs can also give rise to melanocytes, Schwann cells, satellite glia of the cranial ganglia, parasympathetic neurons, sensory neurons (in some of the cranial sensory ganglia), and endocrine cells (Baker, 2005). The vagal NCCs extend from the first to the seventh somites in chick and contribute to the heart; including the musculo-connective elements of the major arteries and the aorticopulmonary septum of the heart (Baker, 2005). The cardiac NCCs, which arise from

the anterior region of the vagal NC (i.e. extend from the first to the third somites in the chicken embryo), contribute to the morphogenesis of the outflow region of the developing heart (Jiang *et al*., 2000). The vagal NCCs have also been shown to contribute to the anterior portion of the enteric nervous system and the parasympathetic nervous system; the rest of which are primarily derived from the sacral NCCs (Baker, 2005). Beyond the seventh somite lie the trunk NCCs, which contribute to the neurons and satellite glia of the sympathetic nervous system and the dorsal root ganglia as well as forming Schwann cells, melanocytes, and endocrine cells (Baker, 2005).

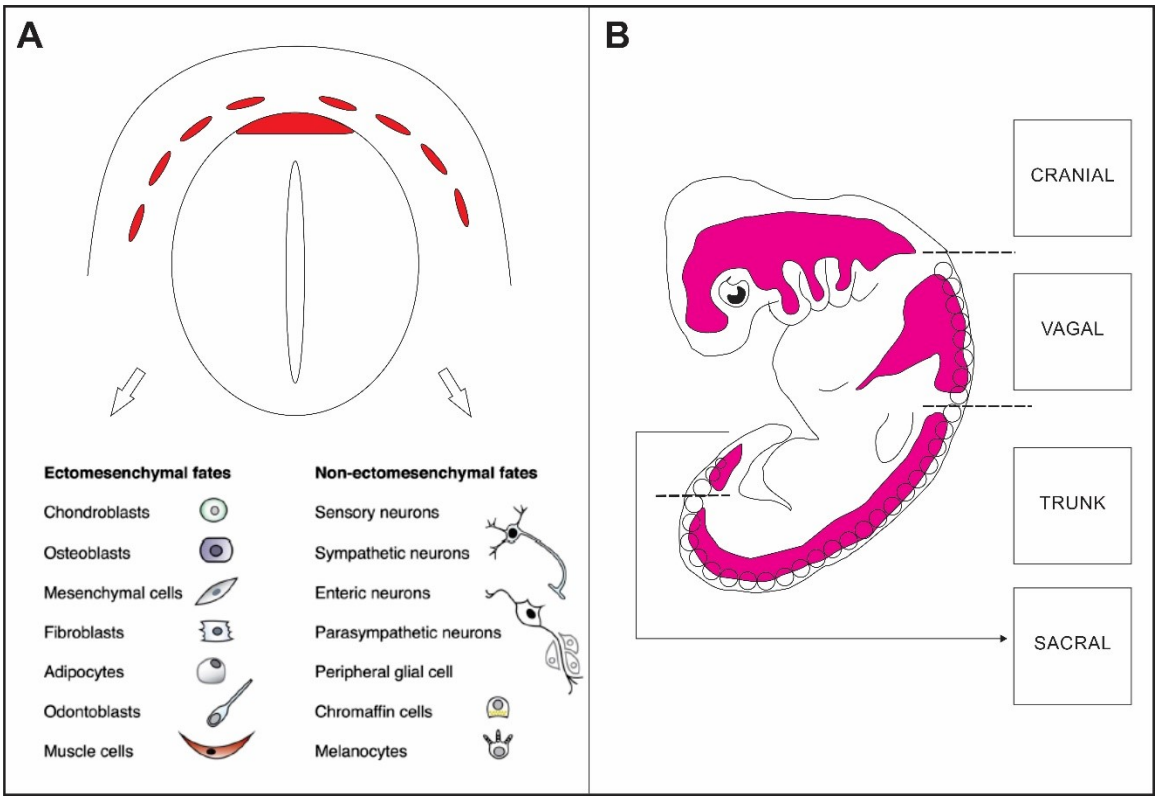

Figure 1.1: Schematics illustrating the NC populations and their derivatives. **A**) An illustration of the potential ectomesenchymal and non-ectomesenchymal fates of the NC. **B**) The division of the NC and a summary of their migratory pathways. The cardiac NC, which is not illustrated above, is derived from the anterior vagal NC. Adapted from Simões-Costa & Bronner (2013) and Ivashkin & Adameyko (2013).

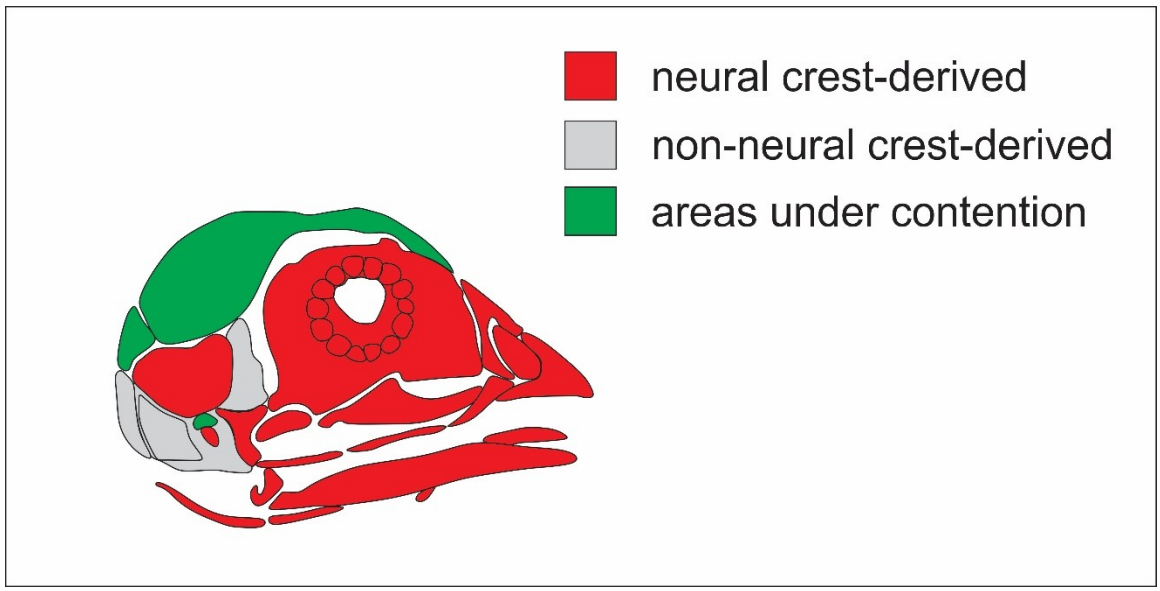

Figure 1.2: Fate map of the NC derivatives in the craniofacial skeleton of the chicken. This schematic highlights those regions which are known to be derived from the NC (red), those known to be derived from the mesoderm (grey), and those whose origin has not yet been determined (green). Adapted from Gross & Hanken (2008).

Of particular interest to this thesis are the NCCs capable of making bone, namely the CNCC. As only the CNCC are capable of forming bone, researchers have attempted to determine what differentiates the CNCC from the other subpopulations of the NC. Transplantation experiments between different axial levels have demonstrated that trunk NCCs, when transplanted into the cranial region, are capable of forming bone (Baker, 2005). This therefore suggests that fate restriction of NCC populations at the axial level is not a result of restricted potential but may rather be due to differential gene expression in each local environment (Baker, 2005). This hypothesis has received recent support as two enhancers, for the gene *forkhead box D3* (*FoxD3*) which is required for NC migration, have been identified with differential expression between the trunk and cranial NC subpopulations (Simões-Costa *et al*., 2012; Simões-Costa & Bronner, 2013).

However, prior to delving into a discussion of these CNCCs and their contribution to the sclerotic ring, I will provide an introduction to the way in which the NCCs are

induced at the neural plate border (NPB), as this inductive process is not only required for the NCCs but also for the induction and patterning of the cranial placodes and, subsequently, eye development (introduced below). Placodes will be discussed in more detail in Chapter 4 as they are particularly important to this thesis.

1.1.1 – Induction of the Neural Crest

The induction and specification of the NCCs is governed by a complex gene regulatory network (GRN) in which each step is temporally and spatially connected by transcription factors that cross-regulate each other and which may act redundantly (Sauka-Spengler & Bronner-Fraser, 2008) beginning during early gastrulation and continuing through neurulation (Sauka-Spengler & Bronner-Fraser, 2008; Stuhlmiller & García-Castro, 2012; Prasad *et al*., 2012; Simões-Costa & Bronner, 2013). Once the neural tube closes, the NCCs undergo an epithelial-to-mesenchymal transition (EMT), delaminate, and begin migrating; this latter process will be discussed in detail in Chapter 2. The rest of this section will focus on the induction of the NC prior to EMT.

1.1.1.1 – Induction of the Neural Plate Border

The first step in the establishment of the NC is its induction at the NPB between the neural and non-neural ectoderm beginning at early gastrulation in the chick (Sauka-Spengler & Bronner-Fraser, 2008; Stuhlmiller & García-Castro, 2012; Prasad *et al*., 2012; Simões-Costa & Bronner, 2013). It is characterized by tight control of signaling pathways, including: bone morphogenetic proteins (Bmp) and their inhibitors, fibroblast growth factors (Fgf) and WNT which are derived from both the ectoderm and mesoderm (reviewed in LaBonne and Bronner-Fraser, 1998; Prasad *et al*., 2012). The precise combinatorial code required for the induction of the NC is often species specific.

It was initially believed that NC induction could be explained by an ectodermal response to intermediate levels of Bmp, where high levels of Bmp secreted from the non-neural ectoderm is regulated by Bmp inhibitors (i.e. chordin, noggin, and follistatin) secreted from the neuroectoderm and the underlying paraxial mesoderm (Sauka-Spengler & Bronner-Fraser, 2008; Prasad *et al*., 2012; Bronner, 2012; Simões-Costa & Bronner, 2013). Additionally, a recent study in *Xenopus* has identified an essential regulator of Bmp activity, SNW1 (Wu *et al*., 2011). This regulator (SNW1) is dorsally expressed and required for NC induction independent from mesodermal formation; highlighting the requirement for Bmp in the induction of the NC (Wu *et al*., 2011). However, it soon became clear that other signaling pathways are required. Studies in *Xenopus* revealed that Fgf2, in combination with Bmp antagonists, can induce NC formation and that Fgf8 (from the paraxial mesoderm) is both required and sufficient to transiently induce the NC (reviewed in Sauka-Spengler & Bronner-Fraser, 2008 and Stuhlmiller & García-Castro, 2012). It is now believed that intermediate levels of Bmp are permissive, establishing a "competency zone" that allows other factors to induce the NC and also plays a role in the maintenance of the newly induced cell population (Sauka-Spengler & Bronner-Fraser, 2008; Stuhlmiller & García-Castro, 2012; Prasad *et al*., 2012).

Wnts have recently been proposed as an inductive signal for the NC (Stuhlmiller & García-Castro, 2012). Studies in *Xenopus* have demonstrated that overexpression of Wnt ligands can induce ectopic NPB and NC markers; while inhibition of Wnt signaling in the chick and *Xenopus* abrogates NC induction and later development (Sauka-Spengler & Bronner-Fraser, 2008; Stuhlmiller & García-Castro, 2012; Prasad *et al*., 2012). Additionally, Delta-Notch signaling has been implicated in the establishment of the NPB

in chick and *Xenopus*, where it is required upstream of Bmp expression to both promote NC formation and restrict it to the NPB (Sauka-Spengler & Bronner-Fraser, 2008; Stuhlmiller & García-Castro, 2012).

As is evident above, the complex relationship between the genes required to delineate the NPB has not been completely resolved; however, these signaling pathways act together to control the expression of downstream effector transcription factors that specify the NPB, known as the NPB specifier genes (Sauka-Spengler & Bronner-Fraser, 2008; Stuhlmiller & García-Castro, 2012; Prasad *et al*., 2012).

1.1.1.2 – The Neural Plate Border Specifier Genes

The NPB specifier genes, which include *Zic1*, *Msx1*, *Msx2*, *Dlx3*, *Dlx5*, *Pax3*, and *Pax7* are upregulated at the NPB shortly after NC induction in response to the complex interaction of the signaling pathways described above (Sauka-Spengler & Bronner-Fraser, 2008; Donoghue *et al*., 2008; Stuhlmiller & García-Castro, 2012; Prasad *et al*., 2012; Simões-Costa & Bronner, 2013). The expression of the NPB specifiers precedes the expression of the NC specifier genes and is thought to restrict the NPB from adopting neural plate or epidermal fates while maintaining the competence of the NPB to form cell types that are both ectomesenchymal and non-ectomesenchymal (Prasad *et al*., 2012; Simões-Costa & Bronner, 2013). The time at which these NPB specifier genes are upregulated and the specific combination of transcription factors involved is again species specific (Figure 1.3) (Stuhlmiller & García-Castro, 2012; Prasad *et al*., 2012; Simões-Costa & Bronner, 2013). Additionally, evidence from basal vertebrates has suggested that *Snail1* and *AP-2* may also function as NPB specifier genes shortly after the NPB specifiers described above and may also play a role in NC specification (Sauka-Spengler & Bronner-

Fraser, 2008). To date, little is known about the direct transcriptional targets of the NPB specifier genes and as such, further research will be required to improve our understanding of the complex relationships governing the current NC-GRN (Sauka-Spengler & Bronner-Fraser, 2008; Prasad *et al*., 2012).

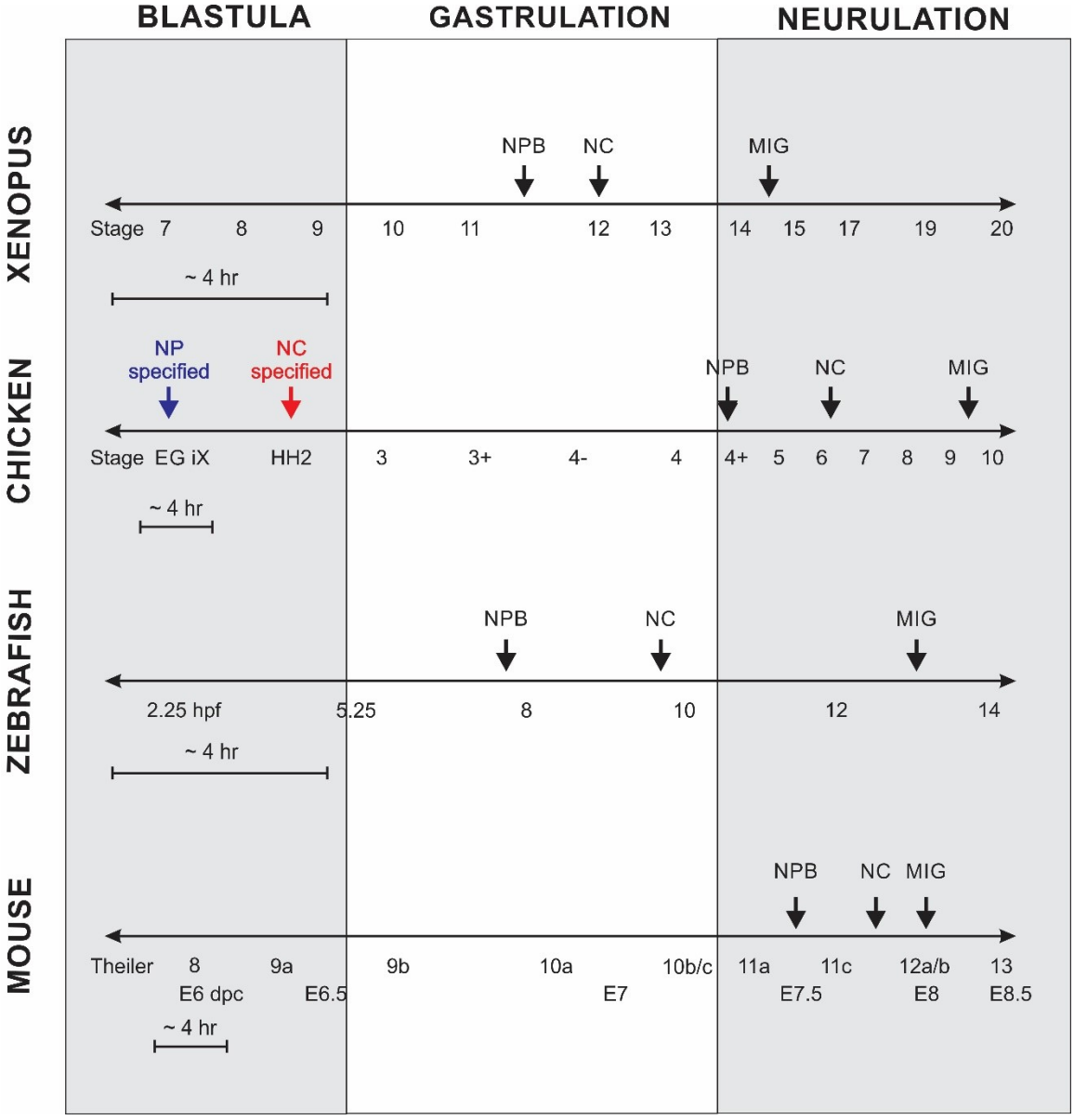

Figure 1.3: A schematic summarizing the timing of NPB specification, NC specification, and NC migration in *Xenopus*, chick, zebrafish, and mouse. Interestingly, in the chick, neural tissue is specified before the egg is laid (stage EG iX) and the NC is specified by HH 2 however, markers of the NPB and NC are not observed until after gastrulation. NPB:

neural plate border, NC: neural crest, MIG: NC migration. Adapted from Stuhlmiller & García-Castro (2012).

1.1.1.3 – The Neural Crest Specifier Genes

The upregulation of the NC specifier genes begins at the mid-gastrula stage in the chick (Basch *et al*., 2006; Prasad *et al*., 2012; Stuhlmiller & García-Castro, 2012). It is currently believed that there are two groups of NC specifier genes: early genes, such as *c-Myc* and *Id3* (as reviewed in Sauka-Spengler & Bronner-Fraser, 2008 and Prasad *et al*., 2012) and late genes, including *Snail1*, *Snail2*, *Sox8*, *Sox9*, *FoxD3*, *Twist*, *Ets1*, *AP2α*, *c-Myc*, and *Id* family members (Sauka-Spengler & Bronner-Fraser 2008; Prasad *et al*., 2012; Stuhlmiller & García-Castro, 2012; Simões-Costa & Bronner, 2013). The expression of these NC specifier genes is proposed to ultimately control NC behaviour, endowing the NCCs with the ability to undergo EMT, delamination, migration, and differentiation through the activation of the NC effector genes (Sauka-Spengler & Bronner-Fraser, 2008; Stuhlmiller & García-Castro, 2012; Simões-Costa & Bronner, 2013). The NC specifier genes also begin the process of specification of the NPB cells into the bona fide NC (Sauka-Spengler & Bronner-Fraser, 2008; Stuhlmiller & García-Castro, 2012). It should be noted, however, that these genes do not act alone; there is involvement of factors from all hierarchical levels of the NC-GRN in the establishment of the NC transcriptional state (Sauka-Spengler & Bronner-Fraser, 2008; Simões-Costa & Bronner, 2013). For instance, Fgf8 signaling, mediated by *Msx1*, induces the expression of *Snail2* and *FoxD3* in a Wnt-dependent manner (Sauka-Spengler & Bronner-Fraser, 2008). In *Xenopus*, Zic1 and Pax3/7 have been shown to induce expression of *Snail2* (reviewed in Prasad *et al*., 2012). A recent study by Wang *et al*., (2011) has also demonstrated the ability of the NC specifier

genes *tfap2a* and *FoxD3* to jointly maintain the balance of Bmp and Wnt signaling in the zebrafish to delineate the NC induction domain.

It is also important to consider the post-transcriptional (i.e. messenger ribonucleic acids (mRNA) and ribonucleic acid (RNA) binding proteins), post-translational (i.e. phosphorylation, SUMOylation, ubiquitination, and acetylation), and epigenetic regulation (i.e. histone modifiers, chromatin remodelling) of the NC specifier genes, as many of these regulatory genes are used reiteratively during NC development (Prasad *et al*., 2012). Studies have shown that post-translational ubiquitination of Snail proteins is an important mechanism of context-dependent control (Vernon & LaBonne, 2006; Prasad *et al*., 2012). Snail1/2 protein levels are regulated by an ubiquitin-proteasome system (UPS) and can be targeted for proteasomal degradation by partner of paired (Ppa) (Vernon & LaBonne, 2006; Prasad *et al*., 2012). SoxE factors, on the other hand, can be regulated post-translationally by both phosphorylation and SUMOylation (reviewed by Prasad *et al*., 2012). Additionally, a recent study by Roffers-Agarwal and colleagues (2012) has shown that the anti-phosphatase Paladin is able to modulate the activity of *Snail2* and *Sox10* genes in chick NC precursors. Another recent study by Jacques-Fricke and colleagues (2012) has investigated the role of *de novo* DNA methyltransferase *DNMT3b* in the developing NC of mice, as mice mutants for this methyltransferase display defects in the craniofacial skeleton and the cardiac ventricular septum. Although they determined that methyltransferase DNMT3b was not required in the CNCC, their study demonstrated that activity of this methyltransferase was required in the branchial arch mesendoderm and/or the cardiac mesoderm which later interact with the NCCs during the development of the craniofacial skeleton and the cardiac ventricular septum (Jacques-Fricke *et al*., 2012). While the above

summary offers only a brief description of the post-transcriptional, post-translational, and epigenetic modifications that may play a role in regulating the expression of the NC specifier genes, it will be necessary, in the future, to present a NC-GRN which incorporates this information in order to have a complete understanding of the induction and specification of the NC.

1.1.2 – The Specification of the Neuroectoderm, Non-Neural Ectoderm, and Pre-Placodal Region

It is also important to note here that the signaling factors required for the specification the NPB (i.e. Bmps, Fgfs, and Wnts) delineate not only the presumptive NC, but also play a role in the specification of the non-neural ectoderm, the neuroectoderm, and the pre-placodal region (PPR) (Harlow & Barlow, 2007; Schlosser *et al*., 2008; Whitlock, 2008; Bhat *et al*., 2013; Schlosser *et al*., 2014; Saint-Jeannet & Moody, 2014; Groves & LaBonne, 2014). The neural plate, which will give rise to the central nervous system, is initially characterized by the expression of high levels of Fgfs and the inhibition of both Wnts and Bmps (Sauka-Spengler & Bronner-Fraser, 2008; Stuhlmiller & García-Castro, 2012; Prasad *et al*., 2012; Simões-Costa & Bronner, 2013; Saint-Jeannet & Moody, 2014; Groves & LaBonne, 2014); while the non-neural ectoderm, on the other hand, which will give rise to the epidermis, is characterized by the expression of both Wnts and Bmps (Sauka-Spengler & Bronner-Fraser, 2008; Stuhlmiller & García-Castro, 2012; Prasad *et al*., 2012; Simões-Costa & Bronner, 2013; Saint-Jeannet & Moody, 2014; Groves & LaBonne, 2014). Additionally, shortly after the delineation of the NC, the PPR is established between the presumptive NC and the non-neural ectoderm (Harlow & Barlow, 2007; Schlosser *et al*., 2008; Whitlock, 2008; Bhat *et al*., 2013; Schlosser *et al*., 2014; Saint-Jeannet & Moody, 2014; Groves & LaBonne, 2014). This region, which will give

rise to the cranial placodes, is initially characterized by the expression of Fgfs and the inhibition of both Wnts and Bmps that are expressed in the non-neural ectoderm (Figure 1.4) (Saint-Jeannet & Moody, 2014; Groves & LaBonne, 2014). Therefore, due to their similar developmental induction, the cranial placodes share some superficial similarities with the NC (i.e. they are migratory and can generate multiple cell types, including sensory neurons and secretory cells) (Lassiter *et al*., 2014). While the induction and specification of the cranial placodes will be discussed in greater detail in Chapter 4, it is necessary to mention that one of these, the lens placode, is required for eye development, and is discussed below. Additionally, as I enter into a brief introduction of eye development, it will be important to consider the initial developmental landscape of the neuroectoderm, the NC, the cranial placodes (specifically the lens placode), and the epithelium as they are all critical for the induction and patterning of the vertebrate eye.

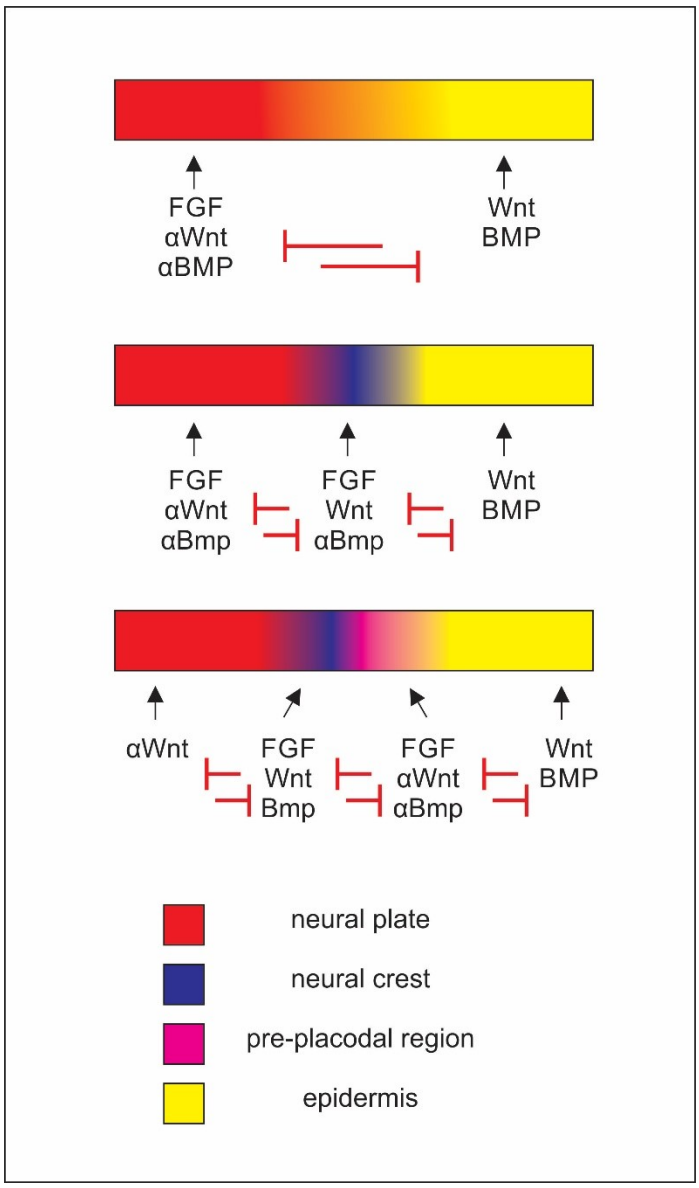

Figure 1.4: Schematic illustrating the location of the NC with respect to the non-neural ectoderm, the neural ectoderm, and the PPR including an overview of some of the signals that are involved at each step. Adapted from Groves & LaBonne (2012).

1.2 – Early Eye Development and the Origin of the Periocular Mesenchyme

The development of the vertebrate eye is complex and involves the coordination of a large number of tissues, including the neuroectoderm, the NC, the lens placode, and the surface ectoderm. As this topic is very broad and beyond the scope of this study, this

section will focus on the early development of the vertebrate eye up to the formation of the periocular mesenchyme, as this is the tissue from which the sclerotic ring is derived.

1.2.1 – Brief Overview of Early Eye Development

The development of the vertebrate eye begins during late gastrulation, shortly after the delineation of the presumptive NC at the NPB (Graw, 2010; Vergara & Canto-Soler, 2012; Sinn & Wittbrodt, 2013). It is first initiated with the establishment of a single eye field in the center of the anterior neuroectoderm by signaling from the underlying prechordal mesoderm (Graw, 2010; Vergara & Canto-Soler, 2012; Sinn & Wittbrodt, 2013). This single eye field is then split into two separate lateral domains during the establishment of the midline, which is mediated by expression of signaling factors from the midline prechordal region including Tgf-β, Fgf, and Hh family members (Graw, 2010; Vergara & Canto-Soler, 2012; Sinn & Wittbrodt, 2013). Once these eye fields have split, eye development is characterized by the evagination of the optic vesicles from the diencephalon (Graw, 2010; Vergara & Canto-Soler, 2012; Sinn & Wittbrodt, 2013). This evagination is the first morphological sign of eye development (Graw, 2010; Vergara & Canto-Soler, 2012; Sinn & Wittbrodt, 2013). The evagination of the optic vesicles continues until the optic vesicles have reached the surface epithelium (Martinez-Morales & Wittbrodt, 2009; Graw, 2010; Vergara & Canto-Soler, 2012; Sinn & Wittbrodt, 2013). This surface epithelium, just prior to contact with the evaginating optic vesicle, will begin to thicken, forming the lens placode (Grocott *et al*., 2011). Recent evidence has demonstrated that the alignment of the lens placodes and the optic vesicles is dependent upon signaling from the cephalic NC (i.e. a subsection of the CNCC which emigrates from the diencephalon and mesencephalon and migrates throughout the facial region) as the

NCCs repress lens formation everywhere except above the optic vesicles (Grocott *et al*., 2011). Once the optic vesicle has made contact with the lens placode, they invaginate simultaneously to form the lens and the optic cup (Martinez-Morales & Wittbrodt, 2009; Graw, 2010; Vergara & Canto-Soler, 2012; Sinn & Wittbrodt, 2013). The optic cup then becomes a bilayered structure of which the outer layer will become the retinal pigmented epithelium (RPE) and the inner layer will become the neural retina (Martinez-Morales & Wittbrodt, 2009; Graw, 2010; Vergara & Canto-Soler, 2012; Sinn & Wittbrodt, 2013). The hinge region, where the optic cup folds to generate the bilayered structure, gives rise to the iris and ciliary body (Graw, 2010; Vergara & Canto-Soler, 2012). The gene regulatory network responsible for the transformation of the optic vesicle into the optic cup and the subsequent specification of the RPE, neural retina, iris, and ciliary body are beyond the scope of this introduction and will not be discussed here. They are, however, well described in the following papers: Lamb *et al.,* 2007; Martinez-Morales & Wittbrodt, 2009; Graw, 2010; Vergara & Canto-Soler, 2012; Sinn & Wittbrodt, 2013. Additionally, as the subsequent development of the lens has been well reviewed elsewhere (Fuhrmann, 2010; Gunhaga, 2011) and it is not known to be involved in the development of the sclerotic ring, it will not be discussed further in this introduction.

1.2.2 – Origin of the Periocular Mesenchyme

It is important to further describe the formation of the NC-derived periocular mesenchyme as it will ultimately give rise to the scleral ossicles. During the invagination of the lens placode and the optic cup, the overlying epithelium repairs to replace the invaginating epithelium (Graw, 2010). This surface epithelium remains transiently attached to the lens via the lens stalk, but will ultimately become the corneal epithelium

(Graw, 2010). After the epithelium has repaired and the lens stalk has degenerated, the eye is invaded by the periocular NCCs from the surrounding mesenchyme (Creuzet *et al.*, 2005; Langenberg *et al*., 2008; Graw, 2010). The NC-derived cells that make up the periocular mesenchyme will give rise to the corneal stroma, the corneal endothelium, the ciliary muscle, the iris stroma, the sclera, the trabecular meshwork, the vasculature, the choroidal pericytes, and, in reptiles, the sclerotic ring (Creuzet *et al*., 2005; Franz-Odendaal, 2008a; Langenberg *et al*., 2008; Graw, 2010). The mechanisms, however, that govern the migration of these NCCs into the eye are not well understood (Creuzet *et al*., 2005; Langenberg *et al*., 2008). Fate mapping experiments in the chick have indicated that diencephalic NCCs invade the optic region from anterior and lateral directions, that mesencephalic NCCs invade the optic region from dorsal and medial directions, and that metencephalic NCCs invade the optic region from the latero-ventral direction (Creuzet *et al*., 2005). However, as these streams all converge and extensively overlap prior to invasion of the optic cup, it is currently unknown how or to what degree each of these NCC populations contribute to the periocular mesenchyme (Creuzet *et al*., 2005). Fate mapping experiments in other organisms, such as the zebrafish, have also demonstrated that the periocular mesenchyme is made up of cells from the diencephalon and mesencephalon but have had little success identifying which stream contribute to which component of the eye (Langenberg *et al*., 2008). Recent experiments in the Franz-Odendaal lab have begun to investigate the possible migratory pathways of the NCCs into the eye, however, these are in the preliminary stages and have suggested only that contributions are made from the temporal and nasal regions adjacent to the eye (K. Wilson, honours thesis, unpublished data).

1.3 – The Sclerotic Ring

The eye is a very complex organ with many components and serves a critical function in nearly all vertebrates, as it is responsible for vision. However, in order to maintain visual acuity and prevent the eye from distortion, there is an internal requirement for ocular support amongst vertebrates (Franz-Odendaal & Vickaryous, 2006). In some taxa (including: humans, placental and marsupial mammals, snakes, caecilians, lamprey, and hagfish), this intraocular support is solely provided by the dense connective tissue of the sclera (Franz-Odendaal & Vickaryous, 2006). In others, including most fish (chondrichthyans, teleosts, and non-tetropodan sarcopterygians), reptiles (birds, turtles, lizards, and crocodylians) as well as monotreme mammals; the dense connective tissue of the sclera is further reinforced by scleral cartilage (Franz-Odendaal & Vickaryous, 2006). Finally, among many reptiles (with the exception of snakes and crocodylians) and some teleost fish, the skeleton of the eye is additionally supported by a number of scleral bones, known as the scleral ossicles (Franz-Odendaal & Vickaryous, 2006; Franz-Odendaal & Hall, 2006). The morphology of this structural support differs greatly between teleosts and reptiles (Figure 1.5).

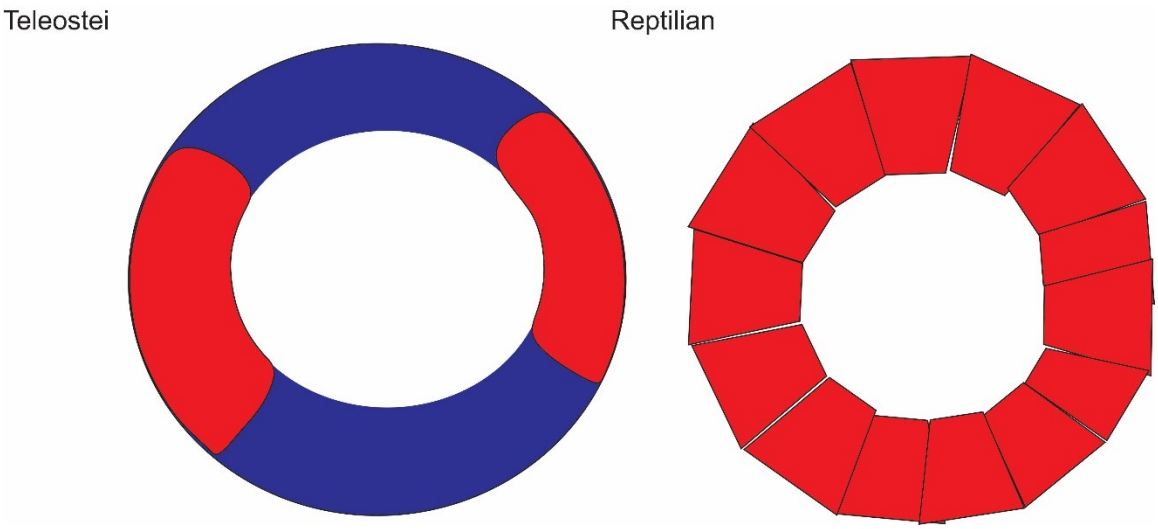

Figure 1.5: A schematic illustrating the differences between the typical teleost scleral ossicles and the reptilian sclerotic ring. Cartilage: blue; Bone: red.

In the teleost fish, the number and position of these scleral ossicles is highly constrained (Franz-Odendaal & Hall, 2006; Franz-Odendaal & Vickaryous, 2006; Franz-Odendaal *et al*., 2007; Franz-Odendaal, 2008b). Many teleost species develop two scleral ossicles within the ring of hyaline cartilage, anteriorly and posteriorly in the eye, while other teleosts will develop only one or none (Walls, 1942; Franz-Odendaal & Hall, 2006; Franz-Odendaal & Vickaryous, 2006; Franz-Odendaal *et al*., 2007; Franz-Odendaal, 2008b). The morphology of these scleral ossicles varies depending on the species; in some, the ossicles form as small elements in the anterior and posterior of the eye which are connected to one another by the ring of hyaline cartilage (Figure 1.5), while in others, the ossicles are large and can form a complete ring of bone (Franz-Odendaal, 2006; Franz-Odendaal & Hall, 2006; Franz-Odendaal & Vickaryous, 2006; Franz-Odendaal *et al*., 2007; Franz-Odendaal, 2008b). A comprehensive description of the morphology of the teleost sclerotic ring is presented in Franz-Odendaal (2008b), however it appears that these ossicles are not homologous to those of reptiles (Franz-Odendaal, 2011). The remainder

of this introduction will focus on the better understood reptilian scleral ossicles, with the chick as the model organism, as they are the focus of this Ph.D. research.

In most reptiles (including birds), the sclerotic ring is composed of a variable number of overlapping, NC-derived intramembranous (i.e. no cartilage precursor) bones, called scleral ossicles; which form at the corneal-scleral limbus of the eye (Slonaker, 1918; Slonaker, 1921; Curtis & Miller, 1938; Murray, 1943). In chicken, the sclerotic ring is usually made up of between 13 and 16 scleral ossicles, while the average number of ossicles per eye is 14 (Coulombre & Coulombre, 1962; Franz-Odendaal, 2008a). In addition, the number of ossicles has been shown to vary between the left and right eyes of the same embryo by one ossicle (Franz-Odendaal, 2008a). Unlike in teleost fish, this sclerotic ring forms independently from the hyaline cartilage, which surrounds the posterior portion of the eye (Coulombre & Coulombre, 1962). Due to its position in the eye, the sclerotic ring is believed to play an important role in ocular protection (Slonaker, 1918; Slonaker, 1921; Curtis & Miller, 1938).

The induction of the reptilian sclerotic ring is complex, with induction of a single bone in the ring taking place over a prolonged period of two days. As a quick overview, before more details are provided below, the induction and patterning of the sclerotic ring begins with the induction of the conjunctival papillae (Coulombre & Coulombre, 1962). The conjunctival papillae, which are epithelial thickenings of the conjunctiva, then undergo complex morphological development (Murray, 1943). During their development and maturation, these conjunctival papillae become inductively active, providing an inductive cue for the induction of the underlying scleral condensations in a 1:1 ratio (Coulombre & Coulombre, 1962). Once the conjunctival papillae have completed their inductive role and

the underlying condensations have begun to mineralize, the conjunctival papillae degenerate (Coulombre & Coulombre, 1962; Hall, 1981a). These mineralized scleral condensations, the scleral ossicles, continue to increase in size until they overlap, forming the sclerotic ring (Franz-Odendaal, 2008a). This sclerotic ring varies greatly in size and shape between species, from minute, delicate, and almost flat bones in the hummingbird to robust and tubular shaped bones in owls (Curtis & Miller, 1938). This variation in shape and size, in which the most robust sclerotic rings are found in high-flying and diving birds prevents corneal distortion during visual accommodation (which in birds and some reptiles involves anterior-posterior movement of the lens by the ciliary muscles, and/or changes in corneal curvature) (Slonaker, 1918; Slonaker, 1921; Curtis & Miller, 1938; Franz-Odendaal & Vickaryous, 2006).

Little is currently known about the mechanisms governing the induction and patterning of the conjunctival papillae. As this is the focus of my thesis, the following sections will provide a detailed introduction to what is currently known about these conjunctival papillae.

1.3.1 – The Conjunctival Papillae

The development of the sclerotic ring begins with the induction and patterning of a ring of transient, epithelial structures, known as the conjunctival papillae (Coulombre & Coulombre, 1962). The conjunctival papillae develop between the 7th and 8th days post fertilization (dpf), also known as HH 30-34 (Murray, 1943; Hamburger & Hamilton, 1951; Coulombre & Coulombre, 1962). After induction, the conjunctival papillae undergo a complex morphological development prior to becoming inductively active between 9 and 10 dpf (HH 35-36) (Coulombre & Coulombre, 1962; Hall, 1981a). After this inductive

role is completed, the conjunctival papillae begin to degenerate (11-12 dpf; HH 37-38) (Franz-Odendaal, 2008a).

The conjunctival papillae were first identified by Nussbaum in 1901 however their role in the induction of the underlying scleral condensations was not identified until 1962 (Coulombre & Coulombre, 1962). Early studies focused primarily on describing their complex morphological development (Nussbaum, 1901; Dabelov, 1927; and Murray, 1941 reviewed in Murray, 1943). This morphological development was broken down into six distinct stages (M-stages) by Murray in 1943.

1.3.1.1 – The Murray Stages of Papilla Morphogenesis (Murray, 1943)

The M-stages of papilla development are summarized in Figure 1.6. The six stages (M1-M6) occur between 7 and 10 dpf, HH 30 to 36. It is important to note, however, that this is the timing for the development of only the first of the 14 papillae to form and therefore the other papillae in the ring develop at slightly different stages. Below is the morphological description of the individual M-stages.

In the earliest stage, known as **M-stage 1**, the conjunctival papillae are characterized by a thickening of the basal epithelial layer while the periderm remains unchanged, resulting in a flat thickening of the epidermis; while the unspecialized epithelium between papillae is characterized as a flat, two-layered epithelium in which the basal (lower) layer is cubical in shape while the periderm (upper) layer tends to be flattened. By **M-stage 2**, the central portion of the papilla has increased in thickness, bulging slightly into the underlying mesenchyme and extending slightly above the surface of the epithelium. Murray (1943) attributed this increase in size to the migration of cells from the basal layer at the periphery of the papilla into the center of the papilla. More recent

studies, however, have attributed this increase in size to extensive cell proliferation within the papillae (Franz-Odendaal, 2008a). It is also during this second stage of papillary development that Murray first noted a thickening of the underlying mesenchyme directly beneath the central bulge of the papilla, the beginnings of the scleral ossicle condensation. The conjunctival papillae in **M-stage 3** have an increased downward bulge, called the "mesenchymal tongue". M-stage 3 is also marked by an increase in the projection of the papilla above the surface epithelium. At this stage, Murray noted, via histology, the presence of "fine collagen strands" arising from the basement membrane of the papillary tongue and descending into the underlying mesenchyme. Murray believed that these descending strands were a possible link between the conjunctival papillae and the underlying developing scleral bones. It should be noted, however, that although Murray assumed that these fibrils were collagen, they were later determined to be tenascin (Fyfe *et al*., 1988). By **M-stage 4**, the mesenchymal tongue of the papilla begins to regress due to the degeneration of the cells in this central mass. However, a more recent study by Franz-Odendaal (2008a) only identified limited cell death within in the papillae; therefore, the mechanism governing the degeneration of the mesenchymal tongue is currently unknown. This degeneration of the central mass, however, does not prevent the further extension of the papilla above the surface of the epithelium. At this stage, the underlying mesenchymal condensation is a thick aggregation of cells. The descending fibrous strands are more prominent at this stage, running both along the axial zone of the condensation and spreading outward into the more peripheral mesenchyme. Regression of the papilla's mesenchymal tongue continues into **M-stage 5**, which results in the slight involution of the basement membrane above that of the adjacent epithelium. This involuted area does not

pinch shut at this stage, but rather remains open to the underlying mesenchyme. The descending fibrous strands continue to descend from the basement membrane of the papilla into the enlarged, underlying, condensed mesenchyme. Finally, during **M-stage 6**, the papillae begin to degenerate. As the conjunctival papillae degenerate, the fibrous strands within the mesenchymal condensations begin to thicken and osteoblasts begin to differentiate within the skeletogenic condensation. In older samples, these fibrils have increased in number and osteoblasts are trapped in the matrix.

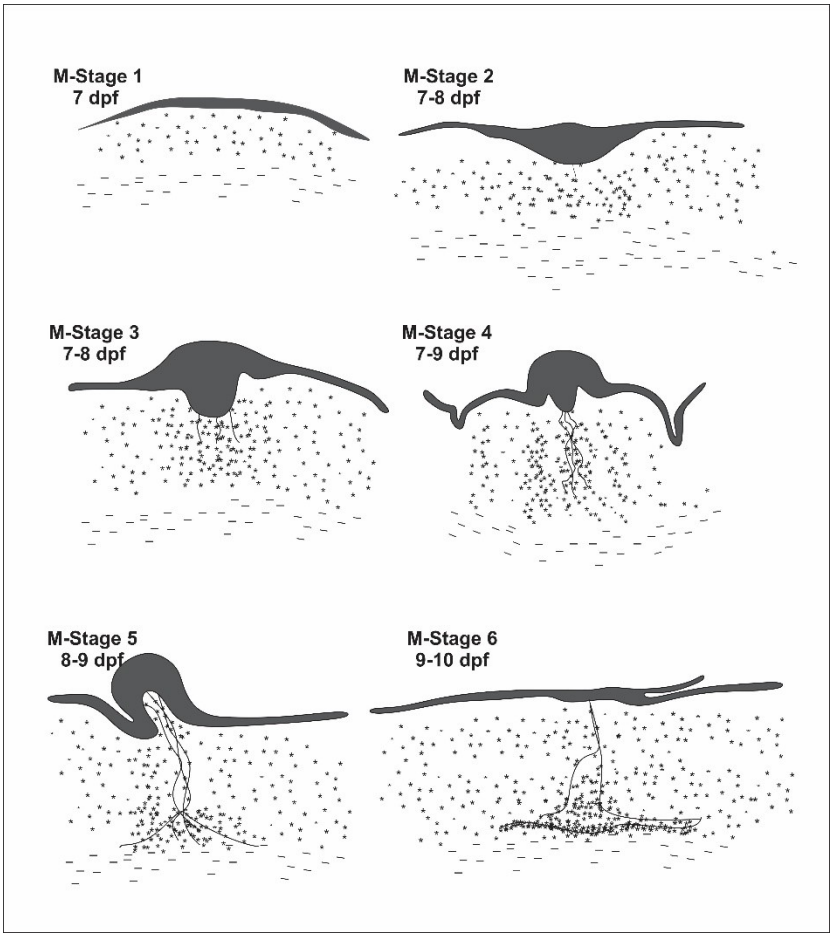

Figure 1.6: Schematic illustrating the M-stages of papilla development. Epithelium: dark grey; Mesenchyme: *; Descending fibrous strands are indicated. Adapted from Murray, 1943.

1.3.1.2 – Induction and Patterning of the Conjunctival Papillae

As mentioned above, the relationship between the conjunctival papillae and the underlying scleral condensations was not determined until 1962, when Coulombre and Coulombre undertook a detailed investigation of the conjunctival papillae and the induction of the scleral condensations. This study is one of the few, to this day (excluding this thesis and the work currently underway in the Franz-Odendaal lab) to focus on the manner in which the conjunctival papillae are induced and patterned. The following sections will discuss what little is currently known about the induction and patterning of the conjunctival papillae.

1.3.1.2.1 – A Numbering Schema for the Conjunctival Papillae and the Modal Number per Eye

One of the first steps that was taken towards unraveling the induction and patterning of the conjunctival papillae was to investigate the spatiotemporal sequence of papilla formation and the number of papillae that are induced. A first study into this patterning was conducted by Hamburger and Hamilton (1951) which was later expanded upon by Coulombre and Coulombre (1962), who established a numbering schema for the conjunctival papillae and scleral ossicles based on the position of the papilla/ossicle with respect to various anatomical landmarks in the eye. In this schema, the conjunctival papilla located directly above the choroid fissure was assigned the number 1; numbering then proceeded in a nasal direction, resulting in a counter-clockwise numbering schema in the right eye and a clockwise one in the left (Coulombre & Coulombre, 1962). In both the left and right eyes, this results in the placement of the 12^{th} conjunctival papilla directly above the ciliary artery (Coulombre & Coulombre, 1962). The authors concluded that papilla development proceeds as follows:

1. The first papilla to form, papilla number 12, is always located directly above the ciliary artery. Recent evidence suggests that there is no correlation between the timing of the induction of the conjunctival papillae and the developing vasculature in the eye (Jourdeuil & Franz-Odendaal, 2012).
2. After the first papilla has formed, the rest of the temporal group (papillae 10-13) are induced beginning at HH 31 (approximately 7-7.5 dpf). Concomitant with the development of the temporal group, the first papillae in the nasal group are induced.
3. At HH 32 (approximately 7.5 dpf), the rest of the nasal group is present on the surface of the eye (papillae 3-6) and the first papillae of the dorsal group are now visible.
4. The dorsal group of conjunctival papillae (papillae 7-9) then finish their induction at which time the first ventral papillae become visible. This occurs at HH 33 (approximately 7.5-8 dpf).
5. During HH 34 (approximately 8 dpf), the ventral conjunctival papillae finish their induction (papillae 14 and 2), at which time the last papilla to form (papilla number 1) is induced directly overlying the choroid fissure.

This timeline of papilla development, as described by Coulombre and Coulombre (1962) is summarized in Figure 1.7 below. This staggered spatiotemporal induction of the conjunctival papillae, in which each papilla forms at a slightly different time based on their position in the ring, has been described both in chicken and, more recently, in the turtle *Chelydra serpentina* (Coulombre & Coulombre, 1962; Franz-Odendaal, 2006). Additionally, Coulombre and Coulombre (1962) recorded the number of conjunctival papillae in each eye, noting that a normal ring is composed of 13-16 papillae, with a modal

number of 14, which is consistent with the strains of *Gallus gallus* used in this thesis. They did not, however, compare the number of papillae between the left and right eyes of the same individual, which was not investigated until 2008, when Franz-Odendaal (2008a) determined that there is a fluctuating asymmetry in 44% of individuals.

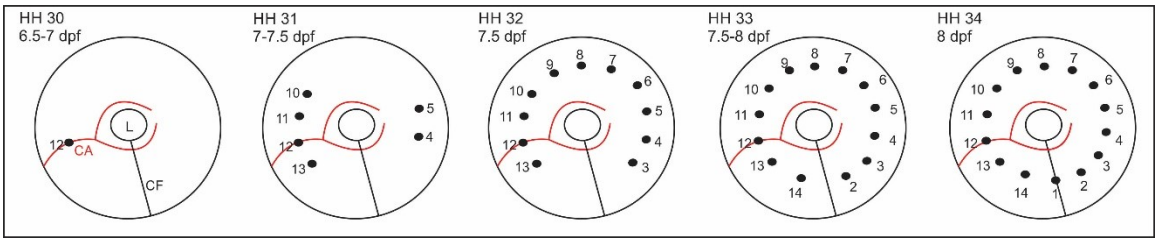

Figure 1.7: Schematic illustrating the spatiotemporal pattern of conjunctival papilla induction. CA: ciliary artery (red), CF: choroid fissure, L: lens.

1.3.1.2.2 – The Relationship Between the Conjunctival Papillae and the Scleral Condensations

Once the number and sequence of conjunctival papilla had been determined, it was possible to determine the relationship between the conjunctival papillae and the underlying scleral condensations (Coulombre & Coulombre, 1962). Observations by both Murray (1943) and Coulombre and Coulombre (1962) noted that the conjunctival papillae are located directly above the center of each underlying scleral condensation and that there is a 1:1 ratio of the number of conjunctival papillae to that of the condensations (Coulombre & Coulombre, 1962). Furthermore, the pattern in which the condensations were induced (temporal, nasal, dorsal, ventral) corresponded to that of the induction of the scleral condensations (Coulombre & Coulombre, 1962). Coulombre and Coulombre (1962) also noted that papilla degeneration occurred following this same spatiotemporal pattern only after ossification had begun in the underlying condensations.

The possible relationship between the conjunctival papillae and the underlying scleral condensations was first tested by Coulombre and Coulombre (1962), who surgically

ablated papilla number 12 (directly above the ciliary artery) at 7, 8, and 9 dpf (HH 30-35). The results of these experiments determined that the conjunctival papillae are required for the induction of the underlying scleral condensations until 9 dpf (HH 35), as no underlying condensation formed when papilla was removed either 7 dpf (HH 30) or 8 dpf (HH 34) (Coulombre & Coulombre, 1962). At 9 dpf (HH 35), however, a scleral condensation was often present at the site of surgery (Coulombre & Coulombre, 1962). During this experiment, they also fixed a number of samples in order to determine whether the conjunctival papillae were capable of regeneration (Coulombre & Coulombre, 1962). The results of these experiments suggested that the conjunctival papillae were not capable of regeneration (Coulombre & Coulombre, 1962). This will be discussed in more detail in Chapter 3.

In the next experiment, which investigated the relationship between the conjunctival papillae and the underlying condensations, chorioallantoic grafts were established of the temporal scleral mesenchyme (in the absence of the conjunctival epithelium and papillae) at 7, 8, 9, and 10 dpf (HH 30-36) (Coulombre & Coulombre, 1962). The results of this study provided further experimental evidence that the conjunctival papillae are required for the induction of the condensations as the scleral ossicles were generally only present in the grafts set up at 9 dpf (HH 35) or 10 dpf (HH 36) (Coulombre & Coulombre, 1962). This therefore suggested that the inductive event for the scleral condensations is completed by 10 dpf (HH 36). This was later re-investigated by Hall (1981a), who confirmed that the mesenchyme becomes specified to form a skeletogenic condensation only after HH 35.

Additional experiments by Hall (1981a and b), in which homotypic (i.e. epithelium and mesenchyme from the same origin) and heterotypic (i.e. epithelium and mesenchyme of different origins) grafts between the scleral and mandibular regions, were established on the chorioallantoic membrane at a variety of stages demonstrated that the inductive role played by the conjunctival papillae is permissive in nature (i.e. the mandibular epithelium can substitute for the scleral epithelium). Furthermore, these experiments indicated that the trapezoidal patterning of the scleral condensations must not be determined by the inductive cue but must rather be determined by the mesenchyme itself, as the scleral mesenchyme always generated normally patterned ossicle regardless of the source of the epithelium (Hall, 1981a and b). These recombination experiments also provided some interesting insights into papilla development, as the conjunctival papillae were not induced or maintained in grafted tissue (Hall, 1981a). This data suggested that papilla induction may require a specific mechanical component that is not present in chorioallantoic grafts (Hall, 1981a).

1.3.1.2.3 – Determining the Nature of Condensation Induction

After it had been determined that the conjunctival papillae are required for the induction and patterning of the underlying scleral condensations, attention turned to unravelling the mechanisms of this inductive event.

Early attention turned to the descending "collagen" strands described by Murray (1943). It was determined using a polyclonal antibody raised against tenascin and indirect immunofluorescence that these descending strands were most likely not collagen but rather tenascin, an extracellular matrix protein that has been shown to be involved in mesenchymal condensations (Fyfe *et al*., 1988). It was also hypothesized that these

descending strands may play a role in cell migration and/or division during the aggregation of the skeletal condensations (Van de Kamp & Hilfer, 1985; Fyfe *et al*., 1988).

Subsequent experiments attempted to determine the way in which this inductive event was mediated. An elegant series of experiments performed by Pinto and Hall (1991) determined that the inductive interaction between the conjunctival papillae and the underlying scleral condensations was mediated by a small diffusible factor with a molecular weight of approximately 3,500 to 6,000 daltons that was capable of diffusing up to 300 μm.

Possible candidates for this diffusible factor were not investigated until 2008, when Franz-Odendaal (2008a) performed an analysis of five candidate genes required for condensation induction. Of these candidates, *Sonic hedgehog* (*Shh*) was upregulated between HH 33 and 36. *In situ* hybridization determined that *Shh* was expressed in the conjunctival papillae between HH 35 and 36, the time at which the underlying scleral condensations are induced (Franz-Odendaal, 2008a). Furthermore, when *Hh* expression was ubiquitously inhibited by the implantation of a bead soaked in cyclopamine adjacent to a conjunctival papilla at HH 35 or 36, the underlying scleral condensation did not form (Franz-Odendaal, 2008a). This therefore suggested that Hh signaling may be required for condensation induction (Franz-Odendaal, 2008a). A subsequent study by Duench and Franz-Odendaal (2012) further investigated candidates for condensation induction. These candidate genes included *Patched* (*Ptc*), *Indian Hedgehog* (*Ihh*) and *Bmp*s-2, -4, and -7 (Duench & Franz-Odendaal, 2012). *In situ* hybridization demonstrated that *Ptc*, the Hh receptor, was first expressed in the conjunctival papillae at HH 35. By HH 36, *Ptc* was present in both the papillae and underlying mesenchyme, extending into the area

immediately adjacent to the papillae (which I have named the papilla-contiguous region [Figure 1.8]). Interestingly *Ihh* was co-expressed with *Ptc* at these stages (Duench & Franz-Odendaal, 2012). *Bmp2* was expressed in the papillae beginning at HH 34.5 and was downregulated at early HH 36 (Duench & Franz-Odendaal, 2012). *Bmp4* and *Bmp7* were not expressed in either the conjunctival papillae or underlying condensations. Additionally, when the expression of *Bmp* was ubiquitously inhibited by the implantation of a noggin soaked bead adjacent to a conjunctival papilla between HH 35 and 36, the underlying condensation did not form (Duench & Franz-Odendaal, 2012). Furthermore, there was a marked decreased in the expression of *Ihh* after noggin inhibition, demonstrating that the Bmp and Hh pathways are linked in the induction of the scleral condensations (Duench & Franz-Odendaal, 2012). Therefore, both Hh and Bmp families are involved in the induction and patterning of the underlying scleral condensations. In addition to the above, a small number of whole embryo screens and molecular studies have identified a few factors that are expressed in the conjunctival papillae. The role of these genes, which include *Claudin-1* (Simard *et al*., 2005) and *Cxcl4* (Ojeda *et al*., 2013), during the induction and patterning of the conjunctival papillae remain unknown.

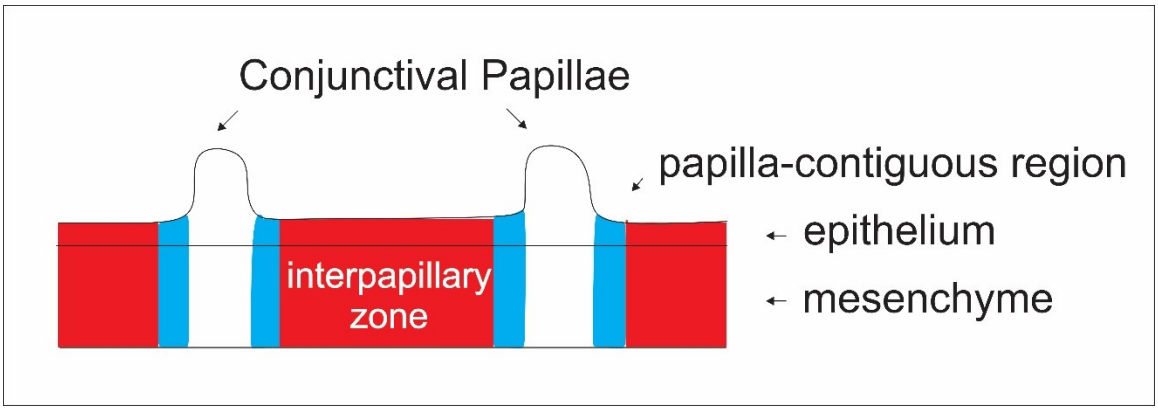

Figure 1.8: Schematic illustrating the different papilla regions. The papilla region (white), the papilla-contiguous region (light blue), and the interpapillary region (red). This schematic introduces the papilla-contiguous region and will be useful for future

characterization of gene expression in the papilla and underlying mesenchyme later in my thesis.

Although the scleral condensations are not the focus of my research, I must address one particular component of condensation development which was identified in the papilla ablations performed by Coulombre and Coulombre (1962), the molecular work by Franz-Odendaal (2008a) and Duench and Franz-Odendaal (2012) described above, and recent vascular perturbations by Jabalee and Franz-Odendaal (2015). In all of these experiments, when the induction of a scleral condensation was prevented (either by surgical ablation of the papilla or molecular inhibition), either the adjacent scleral condensation or the next one in the series to be induced increased in size in order to fill the space left unoccupied by the missing condensation. This suggests both that i) lateral inhibition between the condensations establishes the borders between condensations (and in the absence of this inhibitory factor, the adjacent condensations increase in size) and ii) that mesenchymal compensation occurs in this system (Coulombre & Coulombre, 1962; Franz-Odendaal, 2008a; Duench & Franz-Odendaal, 2012). This mesenchymal compensation suggests that there are redundancies in place to ensure the development of a complete sclerotic ring (Franz-Odendaal, 2008a; Duench & Franz-Odendaal, 2012).

1.3.2 – Conclusions

As described above, very little is known about the mechanisms that govern the induction and patterning of the conjunctival papillae. As similar epithelial-mesenchymal inductive interactions have now been shown to be required for the induction of craniofacial bones, unravelling the mechanisms and genes at play in this system, which is easily accessible and easy to manipulate, will provide important insights into craniofacial development and intramembranous ossification. As a number of development disorders

affect the development of craniofacial bones, insights into the mechanisms governing their induction will be of paramount importance for issues of human health and development.

1.4 - Objectives

The broad objective of this PhD research was to investigate induction and patterning of the conjunctival papillae. Each objective will be presented in a separate chapter (with the exception of Objectives 2 and 3 which are presented together); each chapter includes an Introduction, Methods, Results and Discussion section.

My specific objectives are as follows:

Objective 1: To determine whether surgical ablation of the epithelium at notable developmental landmarks (i.e. the otic vesicle and nasal pit), which have been shown to signal to the migrating NCCs, or the epithelium overlying NC migratory pathways early in development (i.e. prior to papillae formation) will disrupt the induction and patterning of the scleral condensations and/or conjunctival papillae. I hypothesized that signaling from the NCCs is required for conjunctival papillae induction and/or patterning. These data are presented in Chapter 2 and focuses on stages prior to papillae development.

Objective 2: To determine whether surgical ablation of the conjunctival epithelium (immediately prior to the formation of the papilla) or ablation of an individual papilla will affect the patterning of the other conjunctival papillae in the ring. While this topic was partly addressed by Coulombre and Coulombre (1962), they did not describe the effects (if any) on the adjacent conjunctival papillae. However, as Coulombre and Coulombre (1962) did not observe an alteration to the patterning of the underlying scleral condensations/ossicles, I hypothesized that the removal of

either the epithelium (at the site of future papilla formation) or a single papilla would not alter the patterning of the rest of the ring and therefore that other patterning mechanisms must establish papilla positioning at the corneal-scleral limbus. These data are presented in Chapter 3 and focus on the papillae stages of development.

Objective 3: During the analysis of the data in Objective 2, I determined that conjunctival papillae were capable of regeneration if the underlying basement membrane and scleral mesenchyme was not disturbed. My third objective was therefore to determine the limits of conjunctival papillae regeneration since Coulombre and Coulombre (1962) had shown papilla regeneration was not possible. This research examined whether a regenerated papilla was capable of inducing a scleral condensation and whether this represented a new aspect of compensation in the development of the sclerotic ring; in which, the conjunctival papillae matured faster to induce the condensation during the normal inductive period. I hypothesized that the regenerated conjunctival papillae are capable of condensation induction and that this represents an epithelial mechanisms of compensation to ensure the development of a complete sclerotic ring. These data are also presented in Chapter 3 and focus on the stages of papilla regeneration.

Objective 4: To identify potential candidate genes that are necessary for conjunctival papilla induction and patterning since none were known. My approach was to study a microarray dataset in order to identify potential candidates for the induction and patterning of the conjunctival papillae and to determine their spatiotemporal expression patterns throughout the induction and patterning of the

conjunctival papillae and subsequent induction of the scleral condensations (HH 28 through to HH 36). However, as the conjunctival papillae represent only a very small portion of the tissue sample analyzed during the microarray, the current literature for other systems which require epithelial thickenings (i.e. hair, feather, tooth, and the cranial placodes) was used in order to identify potential conjunctival papillae genes. These data are presented in Chapter 4.

This thesis will then conclude with Chapter 5, in which the findings of the thesis will be discussed in the context of the induction and patterning of the conjunctival papillae.

Chapter 2: Ablation of Neural Crest Signaling Centers Does Not Affect Papilla Patterning

2.1 – Introduction

2.1.1 – Background

As described in Chapter 1, the anterior periocular mesenchyme (in which the scleral ossicles form) is composed of NC-derived cells (Creuzet *et al.,* 2005; Kanakubo *et al*., 2006; Langenberg *et al*., 2008). Current experimental evidence in Dr. Franz-Odendaal's lab and the results of Hall's 1981(a) study led me to hypothesize that a signal from this NC-derived mesenchyme is responsible for the induction of the conjunctival papillae. This hypothesis received further support when Dr. Franz-Odendaal received a personal communication from Dr. J. Richman (University of British Columbia, Canada), which indicated that, when the epithelium was removed at the otic vesicle between HH 13 and 18, three ectopic ossicles formed outside the normal sclerotic ring between the temporal and dorsal groups of ossicles (Figure 2.1). As the epithelium is known to play a role in the migration and determination of the NC (Golding *et al.*, 2002; Golding *et al*., 2004; Teddy & Kulesa, 2004; Theveneau & Mayor, 2012) and NCCs have been shown to migrate along the epithelium in both the cranial and trunk regions (Bronner-Fraser, 1994; Creuzet *et al*., 2005; Graw, 2010; Theveneau & Mayor, 2012); I hypothesized that surgical ablation of the epithelium at the otic vesicle, as described by Dr. Richman, may alter the induction and patterning of derivative structures such as the scleral ossicles. Furthermore, this ablation may also affect the induction of the conjunctival papillae if they are indeed induced by signaling from the NC-derived periocular mesenchyme. Moreover, as the otic vesicle acts as a signaling center for the migration of the NC (i.e. produces factors, such as chemoattractants and chemorepulsants, that influence the migratory pathways of the NC;

Sechrist *et al*., 1993; Trainor *et al*., 2002; Theveneau & Mayor, 2012), I hypothesized that other signaling centers, such as the nasal pit, and the epithelium overlying the migratory pathways of the NC into the eye may also alter the induction and patterning of derivative structures such as the scleral ossicles and/or conjunctival papillae.

As the induction and patterning of the NC were introduced in Chapter 1, the introduction to this chapter will focus on NC EMT, delamination, and migration.

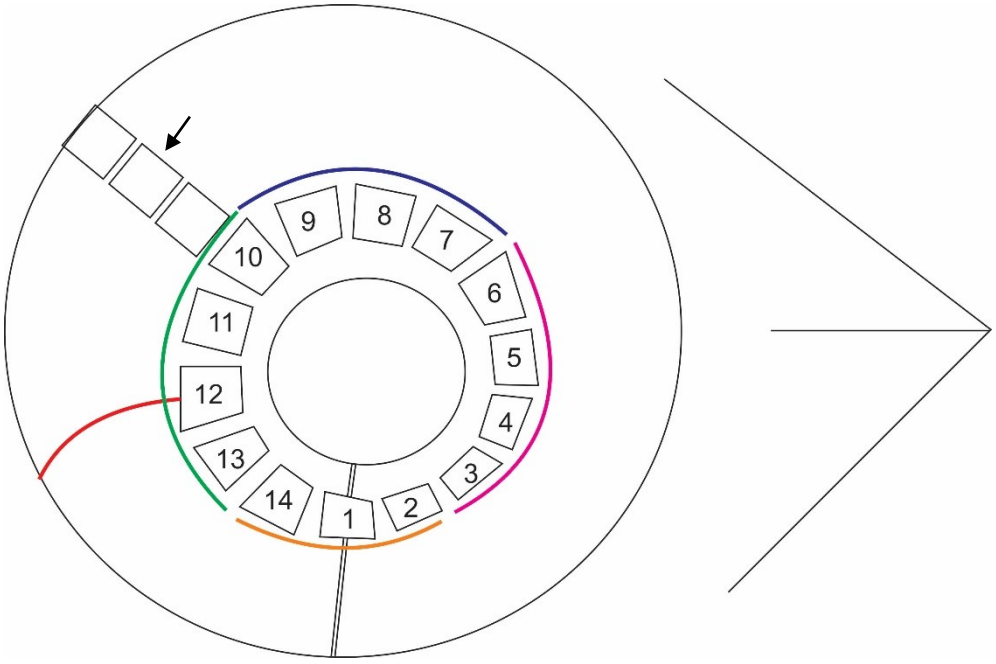

Figure 2.1: Schematic illustrating the ectopic ossicles (arrow) that were reported in a personal communication by Dr. J. Richman (University of British Columbia, Canada) after epithelium removal at the otic vesicle between HH 13 and 18. Numbers refer to ossicle position. Red line indicates the ciliary artery. Two parallel lines indicate the choroid fissure. Green line indicates the temporal group, pink line indicates the nasal group, blue line indicates the dorsal group, and orange line indicates the ventral group. Beak is indicated on the right of the schematic.

2.1.2 – Epithelial-to-Mesenchymal Transition, Delamination, and Early Migration of the Neural Crest

Prior to the onset of EMT, the NCCs are located at the apex of the closing neural tube in a fully polarized epithelium that is characterized by tight junctions and adherens junctions (Sauka-Spengler & Bronner-Fraser, 2008). As the neural tube closes (HH 8-9),

the NCCs undergo an epithelial-to-mesenchymal transition; a process by which epithelial cells are transformed from this tightly adherent, polarized epithelial layer into a population of dispersed mesenchymal cells (Sauka-Spengler & Bronner-Fraser, 2008; Bronner, 2012). This process is governed by changes in adhesive properties between cells, loss of apical-basal polarity, and cytoskeletal rearrangements that cause the NCCs to become highly motile and invasive (Sauka-Spengler & Bronner-Fraser, 2008; Bronner, 2012). Many of these same properties and genes are involved in tumour metastasis and therefore, this is an area of intense study (Kerosuo & Bronner-Fraser, 2012).

As described in Chapter 1, the NC specifier genes prime the NCC to undergo EMT and delaminate prior to migrating away from the neural tube (Sauka-Spengler & Bronner-Fraser, 2008; Stuhlmiller & García-Castro, 2012; Simões-Costa & Bronner, 2013). Many of the genes that control the downstream targets of EMT are also involved in the specification of the NC, such as *Sox10*, *Snail2*, and *Twist* (Sauka-Spengler & Bronner-Fraser, 2008; Stuhlmiller & García-Castro, 2012; Simões-Costa & Bronner, 2013). At least one of these genes, *Sox10*, has been shown to be epigenetically silenced by a repressive histone mark until the onset of EMT, at which point it is removed by JmjD2A (Bronner, 2012). These epigenetic modifications provide one explanation of how the NC becomes specified during gastrulation but only becomes migratory after neurulation (Basch, 2006; Bronner, 2012). During EMT, not only are the NCCs equipped with the molecular toolkit for migration but they must also maintain their multipotential nature; therefore, some of the genes expressed during EMT serve to restrict the NCCs from adopting ectomesenchymal fates while preserving neuronal and glial fates, an example of one such gene is *FoxD3* (reviewed in Prasad *et al*., 2012).

One of the NC specifier genes that is critically important to EMT is *Snail2* (Sauka-Spengler & Bronner-Fraser, 2008; Bronner, 2012; Prasad *et al*., 2012; Kerosuo & Bronner-Fraser, 2012). Snail2 plays a role in the down-regulation of Type I cadherins (i.e. E-cadherin, N-cadherin, and cadherin-6b) which characterize the adherens junctions of the epithelium (Sauka-Spengler & Bronner-Fraser, 2008; Prasad *et al*., 2012; Bronner, 2012; Kerosuo & Bronner-Fraser, 2012). This downregulation of Type I cadherins enables the upregulation of Type II cadherins (i.e. cadherin 5 and beyond) that characterize mesenchymal cells (Sauka-Spengler & Bronner-Fraser, 2008; Prasad *et al*., 2012; Bronner, 2012; Kerosuo & Bronner-Fraser, 2012). It is currently believed that this mediation of cadherins is both direct (as in the case of cadherin-6b) and via the activity of co-repressors, such as PHD12 and Sin3A in the chick in which PHD12 and Snail2 appear to interact with the Sin3A repressive complex (reviewed in Bronner, 2012). Additionally, this switch between Type I and Type II cadherins has been linked to acquisition of contact inhibition of locomotion (when cells move away from each other after cell-cell contact), a process that is required for both migration of the NCCs and cancer metastasis (Scarpa *et al.*, 2015). A recent study by Jhingory and colleagues (2010) has also identified the adherens junction molecule *neural alpha-catenin* (*aN-catenin*), which is a direct target of Snail2 and critical for chick NC migration. Snail2 has also been shown to play a role in the downregulation of claudins and occludins which mediate the dissolution of tight junctions and the transition to gap junctions (Sauka-Spengler & Bronner-Fraser, 2008).

In addition to the dissolution of adherens junctions and tight junctions, control of the cell cycle has been linked to EMT (Sauka-Spengler & Bronner-Fraser, 2008; Kerosuo & Bronner-Fraser, 2012; Prasad *et al.,* 2012). Again, Snail has been shown to induce cell

cycle arrest at the G1 phase by repressing cyclin D1 and cyclin D2 and maintaining high levels of p21, an inhibitor of cyclin-dependent kinase (CDK) activity (Sauka-Spengler & Bronner-Fraser, 2008; Kerosuo & Bronner-Fraser, 2012; Prasad *et al.*, 2012). Once cells begin delamination, expression of *Snail* decreases, enabling the cyclin levels to rise; thereby allowing the transition from the G1 phase to the S phase of the cell cycle (Sauka-Spengler & Bronner-Fraser, 2008; Kerosuo & Bronner-Fraser, 2012; Prasad *et al.*, 2012). Ets1 may also have a role in cell-cycle control as the presence of Ets1 in the CNCC and ectopic expression of Ets1 in the trunk NC has been shown to eliminate the need for cell-cycle arrest prior to delamination (reviewed in Prasad *et al.*, 2012).

After undergoing EMT, the newly motile NCCs must delaminate from the neural tube and begin active migration through their environment; requiring the NCCs to penetrate the basement membrane and invade extracellular matrices (Sauka-Spengler & Bronner-Fraser, 2008). In addition, the environments through which the NCCs will migrate are awash with intricate connective tissue barriers comprised of collagens, fibronectin, laminins, vitronectin, and proteoglycans (Sauka-Spengler & Bronner-Fraser, 2008). In order to be able to traverse these varied environments, NCCs require the proteolytic activity of membrane-bound and/or secreted matrix metalloproteases (MMPs) (Sauka-Spengler & Bronner-Fraser, 2008). The coordinated activities of these MMPs and their inhibitors (tissue inhibitors of MMPs; TIMPs) allow the NCCs to move through these tissues in response to precise signals and facilitates their migration away from the neural tube (Sauka-Spengler & Bronner-Fraser, 2008; Kerosuo & Bronner-Fraser, 2012).

This migration of NCCs occurs along set routes that differ based on axial level (Lanenberg *et al*., 2008; Gage *et al*., 2005; Kanakubo *et al*., 2006; Minoux & Rijli, 2010;

Ezin *et al*., 2011; Gammill & Roffers-Agarwal, 2010; Kulesa *et al*., 2004; Bronner, 2012). The migration and patterning of the NCCs involves numerous cell-cell and cell-environment interactions which have been best characterized in the CNCCs of the hindbrain and the trunk NCCs; however, as this thesis is primarily concerned with the CNCC, the migration patterns of the CNCCs will be the focus of this introduction.

It was previously believed that CNCC migration was pre-patterned in the neural tube such that the NCCs received a set molecular identity in the neural tube and would subsequently target and migrate to a region expressing the same molecular identity (Hunt *et al*., 1991 as described in Teddy & Kulesa, 2004). Additionally, the information carried by the pre-patterned NC would confer patterning information to the respective branchial arches (Noden, 1983 as in Teddy & Kulesa, 2004). It is now believed that the NCCs obtain patterning information during their migration through a combination of cell-cell and cell-environment interactions, including: chemotaxis, contact inhibition, contact guidance, and haptotaxis (Teddy & Kulesa, 2004; Kulesa *et al*., 2004; Kulesa *et al*., 2010; Theveneau & Mayor, 2012). Additionally, it has been demonstrated that the NCCs are not passively encountering their environment, but rather extend lamellipodia or short filopodia for local contact (< 20 μm) or extend filopodia over a long-distance (up to 100 μm) (Teddy & Kulesa, 2004; Kulesa *et al*., 2010; Theveneau & Mayor, 2012).

The CNCCs exit the rhombencephalon and migrate in distinct, segregated streams lateral to the even numbered rhombomeres (r) to the adjacent branchial arches (Figure 2.2) (Kulesa *et al*., 2004; Teddy & Kulesa, 2004; Bronner, 2012). This pattern of migration is well conserved between species and has been observed in chicken, zebrafish, mouse, and *Xenopus*; however, the mechanisms used to establish this segmental pattern of migration

often vary between species (Kulesa & Fraser, 2000; Kulesa *et al*., 2004; Teddy & Kulesa, 2004; Kulesa *et al*., 2010; Theveneau & Mayor, 2012). Recent evidence suggests that these NC-free zones lateral to r3 and r5 involve chemorepulsants that are secreted from the otic vesicle epithelium as, when this epithelium is ablated, NCCs will migrate into the areas lateral to r3 and r5 (Golding *et al.*, 2002; Golding *et al*., 2004; Teddy & Kulesa, 2004). Interestingly, however, grafts of ectopic otic vesicles attract rather than repel NCCs, illustrating that the complex mechanisms at play during the migration of the NCCs are not yet fully understood (reviewed in Theveneau & Mayor, 2012). It has been agreed however, that in addition to being a source of chemorepulsants, the otic vesicle also serves as a physical barrier NC migration from r3 and r5 (Sechrist *et al*., 1993; Trainor *et al*., 2002; Theveneau & Mayor, 2012). Furthermore, recent studies have focused on the cell-environment interactions that are required to target the individual streams to the correct branchial arch. It has been demonstrated that the Hh family plays a role in NC migration as loss of Hh results in increased apoptosis and decreased cell proliferation once the NCCs reach the branchial arches (Jeong *et al*., 2004). In addition, interactions between transmembrane neuropilins and their secreted ligands semaphorin*s* and VegF; receptors Cxcr4 and Cxcr7 and their ligand Sdf1; and Eph/Ephrins are intricately involved in chemotaxis to the correct branchial arches (Olesnicky Killian *et al*., 2009; McLennan *et al*., 2010, Banerjee *et al*., 2013).

In summary EMT, delamination and migration of the NC from the neural tube are complex processes that are not fully understood.

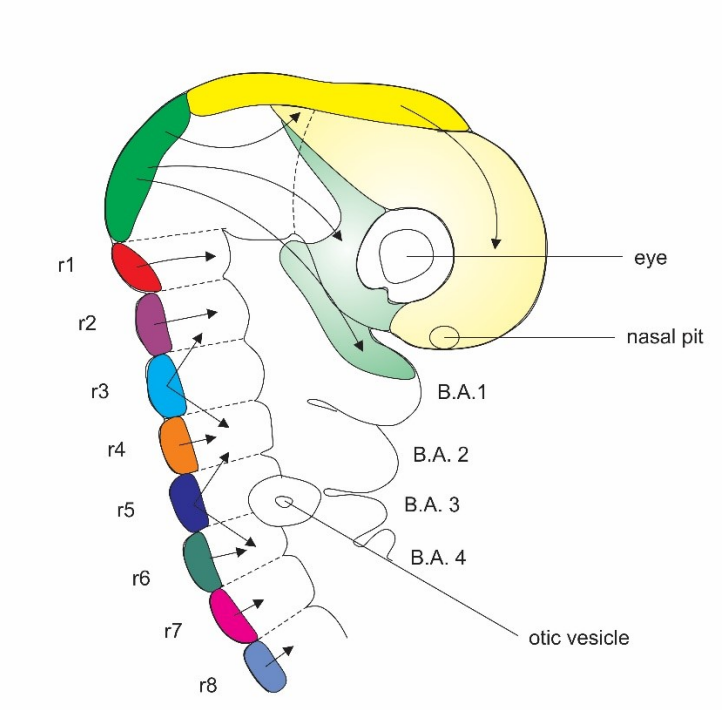

Figure 2.2: Schematic illustrating the migration of the cranial and cephalic NCCs. The cephalic NCCs migrate from the diencephalon (yellow), mesencephalon (green) and the Hox negative rhombomeres (r1 – red, r2 – purple, and the anterior of r3 – light blue). The migratory paths of the diencephalic and mesencephalic NC are shaded. The rest of the NCCs emigrate from the rhombomeres (r4 – orange, r5 – dark blue, r6 – dark green, r7 – pink, r8 – medium blue) into the branchial arches. Adapted from Le Douarin (2004).

2.1.3 – Migration of Neural Crest Cells into and Around the Eye

As this chapter is focused on the migration of the NCCs into and around the eye, the migration of the cephalic NC (i.e. a subdivision of the cranial NCC) will be described in some detail here. The cephalic NC originates from the diencephalon, the mesencephalon and the *Hox* negative region of the rhombencephalon (i.e. anterior to r3) (Figure 2.2) (Creuzet *et al*., 2005). The cephalic NCCs contribute to the neurocranium, the frontonasal process, the eye, and to a portion of the first branchial arch (LeDouarin, 2004; Creuzet *et al.,* 2005; Kanakubo *et al*., 2006). As described in Chapter 1, the diencephalic, mesencephalic, and metencephalic regions all contribute NCCs to the periocular mesenchyme; however, as there is extensive overlap of these streams prior to migration

into the eye, it is currently unknown to what degree each of the NC streams contribute to the periocular mesenchyme. Additionally, it is also unknown what mechanisms regulate the migration of the cephalic NCCs (Langenberg *et al*., 2008). One way in which directed migration may be achieved is through the release of signaling factors from the nasal pit, such as Fgf and Vegf (Hu & Marcucio, 2012). This expression of Fgf has been linked to the regulation of proliferation and differentiation in the migrating cephalic NC while expression of Vegf, a chemoattractant, may be directing the migration of the cephalic NC around the eye and into the frontonasal process (Hu & Marcucio, 2012). The role of these two genes has not yet been completely elucidated at the nasal pit (Hu & Marcucio, 2012). That the nasal pit may be acting as a signaling center to help regulate the migration of the NCCs is not surprising as the otic vesicle and the branchial arches, other landmarks along the migratory pathways of the NC, have also been shown to emit signaling factors that affect NC migration (Robinson *et al*., 1997; Xu *et al*., 2000; Golding *et al.*, 2002; Golding *et al*., 2004; Teddy & Kulesa, 2004; Olesnicky Killian *et al*., 2009; McLennan *et al*., 2010, Banerjee *et al*., 2013).

2.1.4 – Objectives

While it remains unclear which mechanisms govern the migration of the NCCs into the eye, signaling from the epithelium and surrounding mesenchyme during the migration of the NCC are known to play a significant role in the patterning of the NC as described above. Therefore, the objective of this chapter is to determine whether surgical ablation of known signaling centers for NCC migration (i.e. the otic vesicle and nasal pit) or the epithelium along NCC migratory routes prior to papillae formation will disrupt the induction and patterning of the scleral condensations and/or the conjunctival papillae.

2.2 – Materials and Methods

2.2.1 – Egg Incubation

Fertilized chicken eggs were obtained from Cox Bros. Farm (Truro, N.S., Canada) and stored at 4°C until incubated. Eggs were incubated horizontally in a forced-draft incubator at 37°C ± 1°C with a relative humidity of 40% ± 5%. Once in the incubator, eggs were turned twice daily until 2 days post fertilization (dpf) when they were windowed. Eggs were then returned to the incubator until the appropriate age for surgical manipulation. After surgical manipulation, windows were sealed and embryos were returned to the incubator until they reached the desired stage. All embryo staging was done according to HH staging guidelines (Hamburger & Hamilton, 1951). As development is a dynamic process during which many changes take place over a short period of time, half-stages were included in the analysis for greater accuracy. In cases where the results were the same for both whole- and half-stages, they will be discussed together.

2.2.2 – Windowing Eggs

Eggs were windowed following standard procedures (e.g. Silver, 1960). First, eggs were removed from the incubator and allowed to come to room temperature. Eggs were washed with 70% ethanol (EtOH; Central Stores, Dalhousie). An 18-gauge needle was used to remove 5-6 ml of albumin from the egg via a hole made in the pointed end. The hole in the end of the egg was then sealed using adhesive tape (Scotch Transparent Tape, 19 mm x 32.9 mm). A second hole was then made in the top of the egg which was only large enough to visualize the embryo. Embryos were treated with Penicillin-Streptomycin (40 µl of 5,000 units Penicillin and 5 mg Streptomycin; Sigma-Aldrich, P4458) and the hole was sealed with tape. Eggs were returned to the incubator until the desired stage for

surgical manipulation. It is important to note that the hole made in the surface of the shell during the initial windowing procedure is kept as small as possible. This permits the creation of a larger window prior to surgery and facilitates the removal of all of the tape residue from the initial window. Complete tape removal prior to surgery is critical in order to achieve a strong seal on the window post-surgery which increases embryo survival.

2.2.3 – Surgical Manipulations

A number of surgical manipulations were performed between HH 14 and 18 (50 to 69 hours post fertilization [hpf]).

To begin, eggs were removed from the incubator and the window was removed. The membranes above the embryo were stained with a drop of 0.3% neutral red (Sigma-Aldrich, N7005; Appendix 1) for visibility. These membranes were then opened using fine forceps (FST by Dumont #5 Mirror Finish, 1125-23). Embryos were staged according to all visible features, including somite number, angle of the head, and folding of the heart. The epithelium to be removed was then stained using nile blue phosphate (Sigma-Aldrich, N5632; Appendix 1). This allowed for the precise staining of only the epithelium, leaving the basal lamina and the underlying mesenchyme unstained. Once stained, the epithelium in one of the following five areas was gently removed using fine tungsten needles.

1. The otic vesicle epithelium (Figure 2.3A)
2. The nasal pit epithelium (Figure 2.3B)
3. Both the otic vesicle and nasal pit epithelia (Figure 2.3C)
4. The epithelium between the otic vesicle and the eye (Figure 2.3D)
5. The epithelium between the nasal pit and the eye (Figure 2.3E)

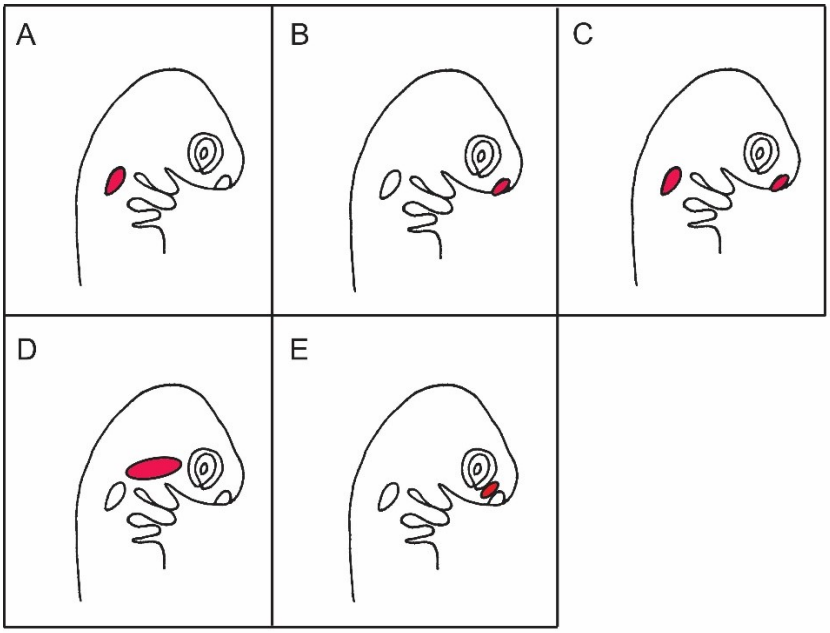

Figure 2.3: Schematic illustrating the area of epithelium removed in a HH 16 embryo. **A**) Otic vesicle epithelium. **B**) Nasal pit epithelium. **C**) Both otic vesicle and nasal pit. **D**) Epithelium between the otic vesicle and the eye. **E**) Epithelium between the nasal pit and the eye. Surgery sites are shown in red.

A number of controls were performed during these experiments. Windowing the eggs, staining the epithelium with both neutral red and nile blue phosphate, and then re-incubating the embryos had no noticeable developmental effect on the embryo (n=7). At most, there was a difference of one papilla between the left and right eyes, which is normal. As a control for the epithelium removals, the epithelium was "scratched". In these controls, the embryos developed normally and did not have a difference of more than one conjunctival papilla/scleral ossicle between the right and left eye (n=20).

Once the surgery/control experiment was completed, embryos were treated with another dose of Penicillin-Streptomycin and the window was re-sealed using tape. The eggs were then returned to the incubator in order to allow embryos to reach the desired stage for analysis.

2.2.4 – Embryo Fixation

Once embryos had reached the desired stage (between HH 34 and 38-39 [8 to 12-13 dpf]), eggs were removed from the incubator. These stages were chosen as they incorporate both the induction of the complete ring of conjunctival papillae (HH 30-34) and the induction of the underlying scleral condensations (HH 35-37) (Murray, 1943; Coulombre & Coulombre, 1962). As the underlying scleral condensations are unable to form without the inductive cue from an overlying conjunctival papilla (Coulombre & Coulombre, 1962), the number and pattern of condensations can serve as an approximate facsimile for the pattern of the conjunctival papillae in older embryos.

Embryos were removed from the egg and placed in a petri dish where they were quickly decapitated. Embryos were then washed in 0.85% chick saline (Appendix 1) and subsequently staged. After washing, embryos were fixed in 10% neutral buffered formalin (NBF; Fisher Scientific, 23-245-685) overnight at room temperature. After fixation, embryos were processed through a graded EtOH series (25%, 50%, 70%) and stored in 70% EtOH at room temperature.

2.2.5 – Imaging and Analysis

All images were taken using a Nikon DXM 1200C camera mounted on a Nikon SMZ 1000 dissecting microscope and analyzed using NIS-Elements software. Samples were examined for visible morphological changes around the eye, such as feather and eyelid morphology. Eyelids were then removed (in older samples) in order to see the conjunctival papillae and/or scleral condensations. Unstained papillae and condensations are easily visible without staining (Coulombre & Coulombre, 1962; Franz-Odendaal, 2008a; Jourdeuil & Franz-Odendaal, 2012). The number and position of the conjunctival

papillae and/or scleral condensations were recorded in both the left (control side) and right (surgery side) and any changes between these eyes were noted. All samples were then photographed.

2.3 – Results

In order to investigate the potential role of the NC in the induction and patterning of the scleral condensations and/or the conjunctival papillae, five surgical manipulations were performed in which the epithelium was ablated either at a known signaling center or along the migratory route of the NC. The results of each surgery are summarized in Table 2.1 and discussed individually below.

Table 2.1: Summary of the results of epithelium removals between HH 14 and 18. N represents the number of surgeries conducted on one eye per embryo.

Tissue Removed	Stage Removed	Stage Fixed	Result
Otic Vesicle	16-18	34-38	Eye Normal (n=6)
Nasal Pit	14-17	36.5-38	Eye Normal (n=6) Temporal Eyelid Missing (n=2) Additional Papilla (n=2)
Otic Vesicle and Nasal Pit	14-16	38-39	Eye Normal (n=6) Temporal Eyelid Missing (n=2) Eye 50% Reduced in Size (n=2)
Between Otic Vesicle and Eye	16-18	35-38	Eye Normal (n=10) Temporal Eyelid Missing (n=3)
Between Nasal Pit and Eye	16-18	35-39	Eye Normal (n=7) Temporal Eyelid Missing (n=1)
Control membranes	15-17	34-37	Eye Normal
Control epithelium	15-17	34-37	Eye Normal

2.3.1 – Removal of the Otic Vesicle Epithelium

The otic vesicle epithelium was removed from six embryos between HH 16 and 18 (51-69 hpf). These embryos were then allowed to develop until between HH 34 (i.e. once papillae induction is complete) and HH 38 (i.e. onset of condensation ossification). In all cases the patterning of the conjunctival papillae and underlying scleral condensations was completely normal (Figure 2.4A; Table 2.1). No ectopic ossicles or ectopic conjunctival papillae were observed either within the ring or outside of the ring of normal ossicles. Additionally, a difference of more than one conjunctival papilla/scleral ossicle between the right (surgery) and left (control) sides of the embryo was not observed, consistent with normal sclerotic ring development (Franz-Odendaal, 2008a).

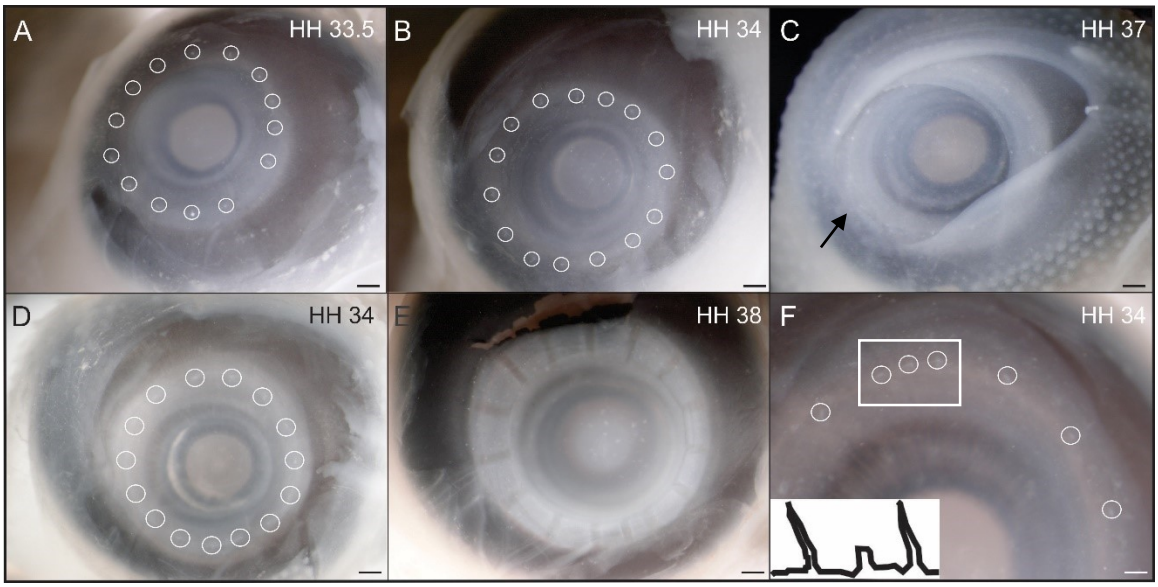

Figure 2.4: Results of epithelium removals performed between HH 14 and 18 and fixed between HH 33 and 38. **A**) Epithelium removal performed at the otic vesicle. Patterning of the conjunctival papillae is normal. **B**) Epithelium removal performed between the otic vesicle and the eye. Patterning of the conjunctival papillae is normal. **C**) An example of the temporal eyelid abnormality observed after epithelium removal between the otic vesicle and the optic cup, between the nasal pit and the optic cup, removal of both the otic vesicle and nasal pit, or of the nasal pit epithelium alone. The arrow indicates where the ridge of epithelium making up the temporal eyelid should be. **D**) Epithelium removal performed at both the otic vesicle and the nasal pit. Patterning of the conjunctival papillae is normal. **E**) Epithelium removal performed between the nasal pit and the eye. Patterning of the

scleral condensations is normal. **F**) Epithelium removal performed at the nasal pit. An additional papilla is present between the temporal and dorsal groups of conjunctival papillae (box). Inset figure shows the appearance of the conjunctival papillae in this region. Conjunctival papillae (white circles). Scale bars in A-E are 500 μm. Scale bar in F is 200 μm.

2.3.2 – Removal of the Epithelium Between the Otic Vesicle and the Eye

The epithelium between the otic vesicle and the eye was removed from ten embryos between HH 16 and 18 (51-69 hpf). These embryos were then allowed to develop until between HH 35 and 38. In all cases the patterning of the conjunctival papillae and the underlying scleral condensations was completely normal (Figure 2.4B; Table 2.1). No ectopic ossicles or ectopic conjunctival papillae were observed either within the ring or outside the ring of normal ossicles. Again, a difference of more than one conjunctival papilla/scleral ossicle between the right and left sides of the embryo was not observed, consistent with normal sclerotic ring development (Franz-Odendaal, 2008a). Interestingly, in three of these ten embryos (30%), the temporal portion of the eyelid did not form (Figure 2.4C) yet the nasal, dorsal, and ventral eyelid developed normally (i.e. becoming ellipsoidal in shape and reaching the ventral edge of the cornea). Additionally, in older samples (i.e. HH 38), feather germ formed on the temporal epithelium of the eyelid. This defect did not affect the nictitating membrane which is underneath the nasal eyelid epithelium.

2.3.3 – Removal of Both the Otic Vesicle and Nasal Pit Epithelium

The otic vesicle and nasal pit epithelium were removed together from eight embryos ranging in age between HH 14 and 16 (50-56 hpf). These embryos were then allowed to develop to between HH 38 and 39. In six of eight embryos (75%), the patterning of the scleral condensations was completely normal (Figure 2.4D; Table 2.1). No ectopic ossicles were observed either within the ring or outside of the ring of normal ossicles. A

difference of more than one scleral ossicle between the right and left sides of the embryo was not observed, consistent with normal sclerotic ring development (Franz-Odendaal, 2008a). Of these six embryos, two displayed the eyelid abnormality described in section 2.3.2 above (33%). In the other two embryos (25%), both eyes were severely reduced in size (by almost 50%) and displayed a concomitant reduction in the number of scleral ossicles. The eyes of both of these embryos were severely mottled and it was therefore difficult to determine the exact number of scleral ossicles present in the eye. It is possible that the surgical ablation of both the otic vesicle and nasal pit epithelium in these samples affected a critical stage of NC migration which resulted in the migration of fewer NCCs to the periocular mesenchyme, reducing the size of the eye. It is also possible that this phenotype is due to a genetic mutation, as in some control embryos (un-windowed eggs) for other projects, I have observed undersized eyes, embryos with only one eye, and Cyclops mutants (i.e. embryos with only a single, front-facing eye). Therefore, since i) no other surgeries resulted in this phenotype, ii) only a small number of samples displayed this reduction in eye size (25%), iii) because we cannot rule out genetic mutation, and iv) there was no obvious misplacement of the conjunctival papillae, these embryos will not be discussed further.

2.3.4 – Removal of the Epithelium Between the Nasal Pit and the Eye

The epithelium between the nasal pit and the eye was removed from seven embryos between HH 16 and 18 (51-69 hpf). These embryos were then allowed to develop to between HH 35 and 39. In all cases, the patterning of the conjunctival papillae and underlying scleral condensations was completely normal (Figure 2.4E; Table 2.1). No ectopic ossicles or ectopic conjunctival papillae were observed either within the ring or

outside of the ring of normal ossicles. Again, a difference of more than one conjunctival papilla/scleral ossicle between the right and left eyes of the embryo was not observed, consistent with normal sclerotic ring development (Franz-Odendaal, 2008a). Surprisingly, in one of seven embryos (14%), the temporal eyelid was again abnormal as described in section 2.3.3 above.

2.3.5 – Removal of the Nasal Pit Epithelium

The nasal pit epithelium was removed from eight embryos between HH 14 and 17 (50-64 hpf). These embryos were then allowed to develop to between HH 36 and 38. In six of eight embryos (75%), the patterning of the conjunctival papillae and underlying scleral condensations was completely normal. However, in two of eight embryos (25%), an extra papilla was observed between the temporal and dorsal groups of conjunctival papillae (Figure 2.4F; Table 2.1). This extra papilla was in close proximity to the other adjacent conjunctival papillae and these embryos had a difference of more than one conjunctival papilla between the right (surgery) and left (control) sides. I therefore conclude that this extra papilla is a true conjunctival papilla; however it appears to be at a younger developmental stage than the adjacent papillae (M3 versus M5), suggesting that it was induced later. Furthermore, I also noted the same eyelid abnormality as described above in 25% of the samples.

2.4 – Discussion

As described in the introduction to this chapter, the anterior periocular mesenchyme (from which the sclerotic ring is derived) is composed of NCCs. Recent, preliminary experiments in our lab show that NCCs migrate into the periocular mesenchyme from both the temporal and nasal regions between HH 16 and 20 (K. Wilson, unpublished data).

Additionally, it has been hypothesized that signals from the underlying ectomesenchyme may provide the inductive cue for the conjunctival papillae and may also direct their patterning (Hall, 1981a). Therefore, in order to investigate whether the NC may be involved in the induction and patterning of the conjunctival papillae and subsequent scleral ossicle development, I conducted a series of epithelium ablations at both known signaling centers and along the migratory routes of the cephalic NCCs.

In none of the surgical ablations performed in this study were ectopic ossicles obtained, either within or outside the normal ring of conjunctival papillae. Additionally, no alteration was observed in the patterning or induction of the conjunctival papillae when the epithelium was removed at the otic vesicle, between the otic vesicle and the eye, both the otic vesicle and the nasal pit, or between the nasal pit and the eye. In a small number of surgical ablations performed at the nasal pit between HH 14 and 17 (n=2 or 25%), an extra conjunctival papilla was present between the dorsal and temporal groups of papillae which was out of synchronization with the adjacent conjunctival papillae. These results suggest that signaling from the nasal pit epithelium to the migrating NCCs may play a role in the induction and patterning of the conjunctival papillae. However, this result was only obtained in the first two surgeries performed at the nasal pit and I was subsequently unable to replicate this result. It is possible that my inability to replicate this result is due to a fine-scale timing issue, whereby during these first two surgeries I was able to target the precise moment during which the NC were interacting with the nasal pit; a precise moment which eluded me in subsequent trials. Interestingly, this additional conjunctival papilla was always located in the inter-papillary zone between two adjacent papillae; a region which I hypothesize to express papilla inhibitors that act to establish the regular spacing of the

conjunctival papillae (Franz-Odendaal, pers. comm.). This may therefore suggest that the surgical manipulations performed at the nasal pit during this study not only altered the induction of the conjunctival papillae but also had an effect on their patterning. This will require further study.

It is possible that the above results, demonstrating that epithelium removals do not affect the patterning of the conjunctival papillae, may be due to a number of factors. First, the NCCs migrate over a prolonged period of time (beginning at approximately HH 8-9) (Stuhlmiller & García-Castro, 2012) and, as very little is known about the factors that govern the migration of the NCCs into the eye (see Section 2.1.3), it is difficult to ensure that the epithelium was removed at the precise stage at which the NCCs were being targeted by the signaling centers or migrating beneath the ablated epithelia. Furthermore, as ablations were performed during NCC migration (HH 14 and 18) but the conjunctival papillae are not induced until HH 30 (a full four days later), it is possible that the NCCs were able to compensate for the mispatterning caused by the surgical ablations. Additionally, embryonic epithelium regenerates rapidly (Nodder & Martin, 1997) therefore the window of time during which the epithelium was absent may have been too small to have an effect on NCC migration. Furthermore, the targeted site of epithelium ablation may not have been large enough to affect all of the underlying NCCs. Finally, it must also be considered that, while the induction of the conjunctival papillae may be due to an underlying NC-derived signal, the patterning of the conjunctival papillae may rather be due to specific patterns of epithelial competency. Therefore, the surgical ablation of the epithelium at both NC signaling centers and along the migratory routes of the NC may be unable to alter the patterning of the conjunctival papillae and/or scleral ossicles.

Thus, the epithelium removals performed during this study may have only targeted a small portion of the underlying NCCs. As it has been well documented that the migrating NCCs are in constant contact (and "talk amongst themselves"), as long as a portion of the stream received the instructive signal from the overlying epithelium, it would be possible to propagate that information to the rest of the NCCs in that stream. This interaction between NCCs is well documented, as when a portion of the trunk neural tube is surgically grafted into the cranial neural tube prior to delamination, the NCCs will migrate according to their new position, not the original position (Baker, 2005). Additionally, research in chimeras has also demonstrated the ability of the NC to self-regulate, such that; if a portion of the neural tube is grafted between two different avian species (e.g. a duck and a quail), both the host and donor sides will migrate according to their position but the final element generated by the donor NC will have a phenotype more similar to that of the donor than the host (Eames & Schneider, 2005; Jheon & Schneider, 2009). Overall, this suggests that the surgical ablation of signaling centers that I conducted may have had an insignificant effect on the migrating NCCs as the disruption in signaling to the underlying NCCs may not have been prolonged enough (likely only a half day) to alter the induction and patterning of the conjunctival papillae four days later considering the remarkable ability of NCCs to self-regulate.

An unexpected result of these experiments was the abnormal development of the temporal (posterior) region of the eyelid after epithelium removal at four sites: the nasal pit, both the otic vesicle and the nasal pit, between the otic vesicle and the eye, and between the nasal pit and the eye (N=8 of 39; 20%). This result was surprising as the temporal region of the eyelid is not near the site of epithelium removal in any of the surgical ablations

other than that between the otic vesicle and the eye. As the NC contributes to the development of the eyelids and the nictitating membrane (Creuzet *et al.,* 2005), it is possible that this was a result of the surgical ablations performed during this study.

Future studies into the role of the NC in the induction and patterning of the sclerotic ring should examine the effect of surgical ablation of the epithelium over a longer period of time (i.e. removing the epithelium at the target site once a day over multiple days) or other forms of disruption, such as the implantation of Nucleopore filters of various sizes beneath each of the signaling centers in order to restrict their contact with the underlying, migrating NCCs. Additionally, impermeable membranes could be implanted at various positions around the eye in order to restrict the immigration of the NCCs into the eye from various positions. It is possible that this will prove unsuccessful, as the NC has a marked ability to course-correct and may therefore simply migrate around the barrier. Furthermore, it may be possible to alter the course of the migrating NC through the implantation of a bead soaked with known chemoattractants in order to disrupt the migration of the NC into the eye. Performing these manipulations at a variety of stages will also help to elucidate the time at which the NCCs receive critical patterning information for the eye. Most importantly, however, it will be necessary to elucidate the pathways along which the NCCs migrate into the eye. This could be achieved by labeling different NC populations with different markers or using chick/quail chimeras.

2.4.1 – Summary and Significance

Although my results demonstrated that surgical ablation of the epithelium at known NCC signaling centers (i.e. nasal pit and otic vesicle) and along the migratory pathways of the NCCs do not have an effect on the induction and patterning of the conjunctival papillae,

this does not mean that the NCCs are not involved in the development of the conjunctival papillae. Additional studies are needed in order to fully elucidate the migratory pathways of NCCs into the developing eye and the factors governing this migration. The findings regarding epithelial competency and epithelial regeneration that were briefly alluded to above are interesting and are the focus of Chapter 3. As more is discovered about the factors governing the migration of the NCCs into the eye, researchers will be better equipped to unravel the mechanisms governing the induction and patterning of the tissues within the eye. This is of particular importance as the eyes occupy an important position within the head and a number of disorders affect the eye and associated tissues (e.g. Axenfeld-Rieger syndrome, anophthalmia, microphthalmia, *etc*.) (Lines *et al*., 2004; FitzPatrick & van Heyningen, 2005; Verma & FitzPatrick, 2007). Therefore, without a complete understanding of NCC migration and patterning later in development, we will not be able to fully understand these complex human craniofacial disorders.

Chapter 3: Conjunctival Papilla Regeneration Serves as a Mechanism of Epithelial Compensation

3.1 – Introduction

3.1.1 – Background

While the sclerotic ring has been of sporadic interest to researchers for the past 60 years, very little is known about the induction and patterning of the conjunctival papillae other than the timing of their development and their morphology as described in Chapter 1 and summarized in Figure 3.1. In order to gain insight into the development and function of these mysterious structures, Coulombre and Coulombre (1962) removed a single papilla (papilla 12, directly above the ciliary artery) from the eyes of embryos at 7 days (first papilla appears; HH 30), 8 days (induction of papillae completed; HH 34), and 9 days (beginning of condensation induction; HH 35) of age using Watchmaker's forceps. Ten specimens were fixed and serially sectioned immediately following conjunctival papilla removal while another ten specimens were fixed on each subsequent day of development (Coulombre & Coulombre, 1962). Histology of the immediately fixed samples showed that, in all cases, "the epithelium of the papilla was absent to, or just below, the level of the basement membrane" and that the "operation removed no more than the surface layer or two of mesenchymal cells" (Coulombre & Coulombre, 1962). However, in the other specimens, fixed on subsequent days and which were examined with reflective light, they noted that a conjunctival papilla, once removed, is unable to regenerate (Coulombre & Coulombre, 1962). In a subsequent experiment, these authors repeated these papilla removals and fixed embryos at 16 dpf (n=36). Based on their results, they concluded that, when a conjunctival papilla was removed prior to 9 dpf (HH 35-35.5), the underlying scleral ossicle either failed to appear or was greatly reduced in size (Coulombre &

Coulombre, 1962). In contrast, when a conjunctival papilla was removed at 9 dpf (HH 35), the underlying scleral ossicle subsequently develops and is of normal size (Coulombre & Coulombre, 1962). They additionally noted that, when this underlying scleral condensation failed to form, the adjacent condensations would increase in size until they met at the mid-point where they would overlap in order to close the gap (Coulombre & Coulombre, 1962). This skeletal compensation, they noted, did not change the original location of the condensation, but rather was accomplished by the in-growth of the bone into the "inter-ossicle space" (Coulombre & Coulombre, 1962). More recent experiments performed in Dr. Franz-Odendaal's lab (Franz-Odendaal, 2008a; Duench & Franz-Odendaal, 2012) have also demonstrated that the adjacent condensations are capable of compensation.

However, neither this study nor the more recent studies from our lab, have addressed whether the removal of this conjunctival papilla (#12) altered the patterning (i.e. spacing and positioning) of the other conjunctival papillae in the ring, as only ossicle patterning has been previously examined. As I hypothesize that a similar inhibitory factor may be required during the induction and patterning of the conjunctival papillae (i.e. lateral inhibition between papillae, an inhibitory factor in the inter-papillary zone, or some other unknown mechanism) in order to dictate conjunctival papilla development (Franz-Odendaal, pers. comm.); this is an important question to investigate.

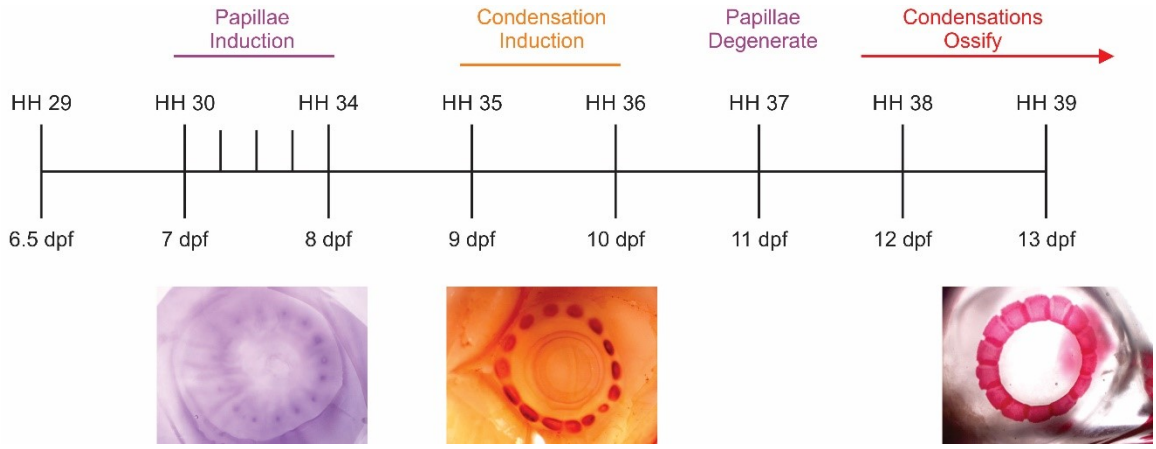

Figure 3.1: A schematic illustrating the timeline of induction of the sclerotic ring. The conjunctival papillae are induced between HH 30 and 34 which corresponds to 7 and 8 dpf. As HH 31, 32, and 33 occur between 7 and 8 dpf, they are represented by half-lines on the timeline. An *in situ* hybridization image of the conjunctival papillae stained for *Eya1* is show below HH 30 and 34. Once induced, the conjunctival papillae undergo a series of morphological changes in order to become capable of inducing the underlying scleral condensations between HH 35 and 36. The image below these stages shows the underlying scleral condensations, stained with alkaline phosphatase, an osteoblast marker. Once the conjunctival papillae have completed their inductive role, they begin to degenerate at HH 37. Subsequently, the condensations begin to ossify at HH 38. The ossification of the scleral ossicles continues into post-hatching chicks. The image below this stage shows the scleral ossicles stained with alizarin red S staining for mineralization.

3.1.2 – Objectives

My first objective for this aspect of my Ph.D. thesis research was to determine whether papillae patterning is coordinated around the ring. My approach to this question was two-pronged. First, I surgically removed the epithelium prior to the development of the first conjunctival papilla (i.e. the presumptive papilla region). Second, I replicated the experiment described by Coulombre and Coulombre (1962) to determine whether the first papilla to develop (papilla # 12, directly above the ciliary artery) affects or controls the patterning of the other conjunctival papillae in the ring. The specific methodology and results obtained are described in the following sections. While investigating these objectives, I discovered that an ablated conjunctival papilla can regenerate in some

instances. Based on this result, I then set out to determine the limits of this regenerative capability, by addressing the following questions:

i) Will a conjunctival papilla regenerate if it is removed during the normal period of papilla induction (between HH 31-33),

ii) Will a conjunctival papilla regenerate if it is removed at the end of papilla induction (HH 34),

iii) Will a conjunctival papilla regenerate if it is removed after the normal period of papilla induction (HH 35),

iv) How long does it take for a conjunctival papilla to regenerate; and

v) Is a regenerated conjunctival papilla able to induce an underlying scleral condensation and, if so, is this induction delayed or does it take place during the normal period of induction?

3.2 – Materials and Methods

3.2.1 – Egg Incubation and Windowing

Eggs were obtained from Cox Bros. Farm (Truro, N.S., Canada). Egg incubation and windowing were performed as described in Chapter 2.

3.2.2 – Surgical Manipulations

Two different types of surgeries were performed at different developmental stages using fine tungsten needles: i) removal of the epithelium directly above the ciliary artery prior to the induction of the first conjunctival papilla; this was conducted at HH 29 and 30 (N=27 Figure 3.2 A and B) and ii) removal of a conjunctival papilla; this was done at HH 30.5 (when the first conjunctival papilla has just formed, N=13), between HH 31-33 (during conjunctival papilla induction, N=31), at HH 34 (the end of conjunctival papilla

induction, N=63), and at HH 35 (after the normal period of conjunctival papilla induction, N=18) (Figure 3.2 C and D). The conjunctival papilla directly above the ciliary artery was targeted for surgical ablation because the position of induction of the first conjunctival papilla (i.e. directly above the ciliary artery) has been shown to be conserved between chicken and turtle (Franz-Odendaal, 2006) and also provides an accurate landmark for analysis. These surgeries were conducted through a window in the egg (as described in Chapter 2) and the embryos were treated with 40 µl Penicillin-Streptomycin after the procedure. The non-surgery eye served as a control in all experiments. In addition, surgery control experiments were also conducted. These are described below after the more detailed description of each surgery. As the chorioallantoic membrane extends across the embryos at these stages, an opening was created in the membrane to allow access to the underlying embryo. The strategy used to access the embryo varied based on the age of the embryo.

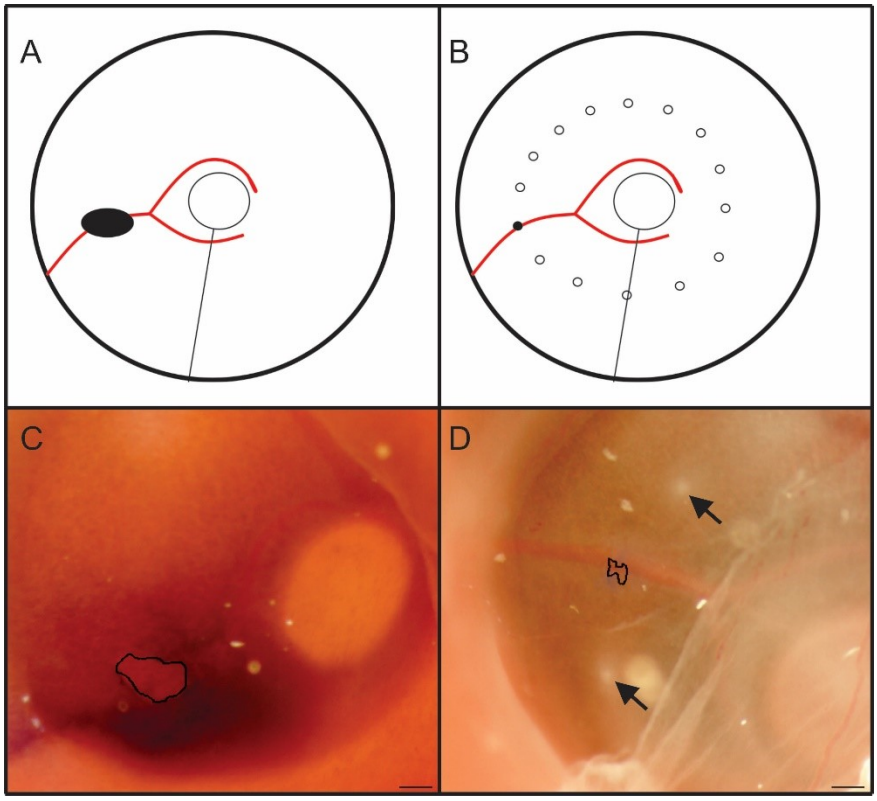

Figure 3.2: Diagram showing the surgery sites. **A**) Schematic illustrating the area of epithelium removed between HH 29 and 30, prior to papilla induction. **B**) Schematic illustrating the conjunctival papilla removed between HH 30 and 35. **C**) Photo taken during surgery showing the application of nile blue A (dark area surrounding ablated area) and the area of epithelium removed (black outline) directly above the ciliary artery. **D**) Photo taken during surgery showing the removal of the papilla directly above the ciliary artery (black outline) at HH 34. The two adjacent conjunctival papillae are indicated by arrows. All scale bars are 250 μm.

In younger samples (i.e. HH 29 and 30), a small hole was made in a chorioallantoic membrane-free region at the caudal end of the embryo. Once this hole had been made, it was then possible to carefully manoeuver the forceps along the edge of the chorioallantoic membrane, loosening and separating it from the underlying yolk sac. After the chorioallantoic membrane had been loosened and separated from the yolk sac, it was possible to fold it back, exposing the underlying embryo. In order to prevent the chorioallantoic membrane from obscuring the field of view during surgery, it was folded back onto the 70% EtOH cleaned eggshell. Once the embryo was exposed, a small hole

was made in the amniotic sac, allowing access to the embryo. The embryo was then staged according to all visible features, including the elbow and knee bends as well as the presence/absence of the egg tooth based on the HH staging table (1951). The epithelium directly above the ciliary artery was stained using nile blue A (as described in Chapter 2). The stained epithelium was then gently removed using fine tungsten needles. Following surgery, the chorioallantoic membrane was gently folded back across the embryo in a close approximation of its original position. The embryos were then treated with Penicillin-Streptomycin as described in Chapter 2. Following this, the window was sealed and the egg was returned to the incubator in order to allow the embryo to reach the desired stage.

In older samples (i.e. HH 31-35), the embryos were allowed to come to room temperature for approximately 30 minutes prior to surgery in order to slow the embryo's movements. Due to the age of the embryo, the chorioallantoic membrane completely surrounded the embryo and was well vascularized. An area of small vessels as close to the eye as possible was selected and these small vessels were pinched for a short time in order to form a clot that would divert the blood flow to the adjacent blood vessels. A small hole was then made in the center of this area. It should be noted that it was not always possible to create this hole directly above the eye as it depends on the position of the major vasculature of the chorioallantoic membrane and of the amniotic sac. Once the chorioallantoic membrane had been opened, an opening in the amniotic sac was made, the cut edges of which could be used to gently pull the embryo into position. Once in position, the embryo was re-staged based on all visible features (HH staging table, 1951). However, since very little of the embryo is visible due to the thick vasculature of the chorioallantoic membrane, the position of the eyelids and nictitating membrane, the number of

conjunctival papillae, and the days of incubation were most often used to determine a fairly accurate approximately of the age of the embryo. After the embryo was staged, the desired papilla (HH 31-35) was stained with nile blue A and gently removed using fine tungsten needles. As described above, the embryo was then treated with Penicillin-Streptomycin, the window sealed, and the egg returned to the incubator in order to allow the embryo to develop until the desired stage.

A number of controls were performed. The first surgical control involved gently tearing a hole in the chorioallantoic membrane and the amniotic sac of similar size to that created when performing the surgeries. This control was performed on both the younger and older samples (N=20). In the second control, the membranes were opened as described above and the conjunctival epithelium/papilla was treated with nile blue A as in the surgery experiments (N=7).

After surgical ablation, and once the embryos had reached the desired stage, a number of techniques were used to analyze the results. To evaluate the effect of surgical ablation on the other papillae in the ring the number and position of papillae in the ring were recorded (in both surgery and control eyes). In samples that were used to determine the regenerative capacity of the conjunctival papillae and the effect of regeneration on the underlying scleral condensations, alkaline phosphatase and *in situ* hybridization were also used to interpret the effects of papilla ablation.

On a side note, I also conducted 130 surgeries at these stages on a different strain of *Gallus gallus* when our normal local supplier culled their flock. Since the patterning of the conjunctival papillae was irregular in both the surgery and control embryos from this

strain, these samples are not discussed further. This observation, however, suggests that strain of chick should be taken into account when performing surgical ablations.

3.2.3 – Embryo Fixation

Once the embryos reached the desired stage of analysis (between HH 30 and 40), they were quickly decapitated and washed in 0.85% chick saline solution. Following this, samples were staged and fixed in either 10% neutral buffered formalin (NBF) overnight at room temperature or in 4% paraformaldehyde (PFA; Sigma-Aldrich, P6148, Appendix 1) in 1X PBS at 4°C overnight depending on the downstream experiment. NBF-fixed embryos were then dehydrated through a graded EtOH series (25%, 50%, 70%) and stored in 70% EtOH at room temperature. Embryos fixed in 4% PFA for alkaline phosphatase staining were washed in 1X PBS (Appendix 1) and then stored in 1X PBS at 4°C. Embryos fixed in 4% PFA destined for *in situ* hybridization, on the other hand, were washed in 1X PBST (Appendix 2) and then dehydrated through a graded methanol series (MeOH; EMD, MX0485-3) series (12.5%, 25%, 50%, 75%, 85%, 100%) and stored in 100% MeOH at -20°C until required.

3.2.4 – Alkaline Phosphatase Staining

The full protocol for alkaline phosphatase is given in Appendix 1. Briefly, embryos were prepared for enzymatic alkaline phosphatase staining by rehydration using a graded EtOH series (50%, 25%, dH_2O) and were then incubated in tris-maleate buffer (pH 8.3) for an hour at room temperature. The embryos were then incubated in alkaline phosphatase substrate solution at room temperature for an hour, following which, they were washed in a saturated sodium tetraborate solution. Following this, the samples were bleached

overnight in 3% hydrogen peroxide (Appendix 1) after which they were processed through a glycerol series (25%, 50%, 80%) for storage in 80% glycerol at 4°C in the dark.

3.2.5 – *In Situ* Hybridization

In situ hybridization was carried out on surgery samples at various time points post-surgery, namely 1 day post-surgery (dps), 1.5 dps, 2 dps, 2.5 dps, and 3 dps in order to determine the effect of regeneration on papilla maturation and condensation induction. A significant amount of time was spent trouble-shooting the *in situ* hybridization protocol during my degree. The final protocol is given in Appendix 2. All solutions were made using 0.1% diethyl pyrocarbonate (DepC; Sigma-Aldrich, D5758) treated water in order to prevent RNA degradation.

For all *in situ* hybridization reactions performed in this chapter (left and right eyes of 63 samples), a *Bmp2* plasmid obtained from Dr. Fallon's lab (Department of Anatomy, University of Wisconsin Medical School, USA) was used. *Bmp2* was selected because it has previously been shown to be expressed in the conjunctival papillae between HH 34.5 and HH 36 (Duench & Franz-Odendaal, 2012). As I used the mini-prep prepared for this 2012 publication, only the antisense probe was made. Additionally, as the protocol for *in situ* hybridization was modified during this study resulting in some inconsistent *in situ* hybridization results during the early phases of this objective, only samples performed after the final *in situ* hybridization protocol was established are included in this analysis. This excluded 48 *in situ* hybridization samples (1 dps, N=11; 1.5 dps, N=4; 2 dps, N=19; 2.5 dps, N=5; 3 dps, N=9; 4 dps, N=2) which will not be discussed, leaving a total sample number (across all stages) of 15.

Samples for *in situ* hybridization were dissected as follows: the head was bisected and the brain was removed. Subsequently, the posterior portion of the eye and the vitreous humor were removed. In older samples, the eyelids and nictitating membrane were also removed prior to *in situ* hybridization. After dissection, the samples were rehydrated through a graded MeOH series (85%, 75%, 50%, 25%, 12.5%). In order to ensure proper rehydration, embryos were left in each step of the methanol series until they sank. Samples were then washed in 1X PBST and left in a 10% hydrogen peroxide solution overnight. After bleaching, the samples were washed in 1X PBST and then permeabilized for 30 minutes with 20 µg/ml Proteinase K (Sigma-Aldrich, P8044). Following the permeabilization step, samples were fixed in 4% PFA with 0.25% glutaraldehyde (Sigma-Aldrich, G5822) for 20 minutes and then washed with 1X PBST. Samples were then transferred into a prehybridization solution and incubated at 60°C for 2 hours. During this 2 hour incubation, probe solutions were made using fresh prehybridization solution to which a variable amount of probe was added depending on the gene (initial probe concentrations were determined by dot-blot [Appendix 1] and then further titrated by *in situ* hybridization trial). Embryos were then incubated in probe solution overnight at 60°C. The following day, embryos were washed thrice for 20 minutes in Wash I and then thrice more in Wash II at 60°C. Following this, samples were rinsed in 1X TBST at room temperature before being placed in an antibody block for 2 hours at 4°C. During the antibody block, the antibody was pre-absorbed for 30 minutes at 4°C in 1 ml of 20% sterile filtered sheep serum (Sigma-Aldrich, S2263) containing a small amount of chick powder and the required amount of anti-digoxigenin-AP FAB fragments antibody (Roche, 11 093 274 910) based on the final volume of desired antibody solution. Prior to antibody

treatment, this 1 ml of pre-absorbed antibody was added to the final volume of 20% sheep serum and well mixed. Samples were then incubated overnight in antibody solution at 4°C. The following day, samples were rinsed in 1X TBST before being transferred to 1X TBST containing 2 mM (-)-tetramisole hydrochloride (levamisole; Sigma-Aldrich, L9756); in which they were left overnight at 4°C. For the following 3 days (4 nights), this 1X TBST solution containing 2 mM levamisole was changed daily in order to block endogenous expression of alkaline phosphatase. On the morning of the 4th day, a number of stock solutions were made, including 1X NTMT, 1X NTMT containing 2 mM levamisole, and the base solution for colour detection. Late that evening, 1X magnesium chloride (Fisher Scientific, BP214-500), 75 mg/ml nitrotetrazolium blue chloride stock (NBT; Sigma-Aldrich, N6876), and 50 mg/ml 5-bromo-4-chloro-3-indolyl phosphate p-toluidine salt stock (BCIP; Sigma-Aldrich, B6777) were added to the colour detection base solution to render it active. Samples were then incubated for approximately twelve hours in the dark at room temperature in this activated colour detection solution. The following morning, the color detection reaction was stopped by washing samples in 1X PBST containing 5 mM ethylenediaminetetraacetic acid disodium salt dihydrate (EDTA; Sigma-Aldrich, E5134). Samples were subsequently fixed in 4% PFA for 20 minutes and then re-washed twice in 1X PBST. Stained samples were stored in 1X PBS at 4°C until photographed after which they were transferred to a 50% glycerol solution (BDH, BDH1172-4LP) for long-term storage.

3.2.6 – Cryosectioning

In order to determine the spatial expression pattern of *Bmp2* in the epithelium and the mesenchyme, the developmental stage with the most representative expression was

selected for cryosectioning. To do this, the area with the strongest expression was dissected and orientated in a molten 1% agar solution (Appendix 1). The agar was placed at 4°C for 30 minutes to set. An agar block containing the embedded tissue sample was cut out and placed into a 30% sucrose solution (Appendix 1) and incubated overnight at 4°C. This incubation in 30% sucrose acts as a cryoprotectant for the tissue sample. The following day, the sample was mounted onto the cryosectioning chuck using Tissue Freezing Medium (Jung, 020108926) and then frozen for 10 minutes. The block was then sectioned until the sample was visible, at which point serial sections of the tissue sample were cut at 16 μm intervals at -25°C. All sections were placed on APTES coated slides (Appendix 1) and the coverslipped using an aqueous mounting medium (Fluoroshield; Sigma-Aldrich, F6182).

3.2.7 – Imaging and Analysis

All images were taken using either a Nikon DXM 1200C or a Nikon Digital Sight DS-5Mc camera mounted on either a Nikon SMZ 1000 dissecting microscope a Nikon Eclipse 50i compound microscope. All photographs were analyzed using NIS Elements BR 3.22.01 software. During surgical ablation of the epithelium directly above the ciliary artery, photographs were taken of each sample in order to record the area of epithelium removed. It was not possible to photograph the conjunctival papilla removals due to the thick membranes that overlay the embryo at this stage. Following surgery and fixation, the right and left eyes were photographed and analyzed for the number and position of the conjunctival papillae and/or scleral condensations. In older samples, the eyelids and nictitating eyelids were removed in order to see the conjunctival papillae or ossicles.

Surgical samples destined for *in situ* hybridization were photographed prior to *in situ* hybridization. They were then photographed post *in situ* hybridization prior to

dissection. The front half of the eye was then removed, followed by the anterior portion of the neural retina, the retinal pigmented epithelium, and the scleral cartilage (leaving just the epithelium and the mesenchyme). The eyes were then flat mounted on a slide, covered with a cover-slip, and photographed. This flat mounting of the sample allowed for consistent imaging and characterization of the expression in the entire ring of conjunctival papillae/scleral ossicles.

3.3 – Results

3.3.1 – Epithelium Removal Prior to Conjunctival Papilla Induction Does not affect the Patterning of the Other Conjunctival Papillae in the Ring

As described in Chapter 1, the first conjunctival papilla is always induced directly above the ciliary artery at HH 30. Following the induction of this first papilla, the induction of the rest of the papillae takes place over the next 24 hours of development (from HH 30 to 34). Little is known about the mechanisms governing the induction and patterning of the conjunctival papillae, therefore, in order to determine whether disrupting/preventing the induction of the first conjunctival papilla would have an effect on the induction and patterning of the other conjunctival papillae in the ring, I surgically ablated the epithelium directly above the ciliary artery prior to the induction of the first conjunctival papilla (between HH 29 and 30). After this surgical ablation, embryos were returned to the incubator and allowed to develop to the desired stage, as shown in Table 3.1. Each result will be described separately below.

Table 3.1: Table summarizing the results of epithelium removals directly above the ciliary artery between HH 29 and 30. Controls are described in the text. N, number of embryos. CA: ciliary artery.

Surgery Stage	Stage Fixed	N	Result
29	30.5	2	Presumptive papilla above CA
29.5	34-35	4	Papilla above CA
29	34-35	2	Epithelium not healed; small thickening at the border
29-29.5	38-40	6	Condensation ring normal
30	34	2	Papilla above CA
30	35-36	10	Papilla above CA
30	36	1	Epithelium not healed; small thickening at border
	Total N	27	

3.3.1.1 – Surgical Ablation at HH 29

The epithelium directly above the ciliary artery was surgically ablated from 14 embryos at HH 29-29.5 prior to the development of the first papilla after which the embryos were fixed at different stages of development (Table 3.1). HH 29 was chosen as it is the stage immediately before the first conjunctival papilla is visible in the epithelium (at HH 30). Of these 14 embryos, two were fixed after 1 day of incubation (HH 30.5), six were fixed after 2 to 3 days of incubation (HH 34-35), and six were fixed after 6 to 8 days of incubation (HH 38-40); the latter stage is when the scleral ossicles are clearly visible in the underlying mesenchyme and are undergoing mineralization. In all cases, the left eye was used as a control and was normal.

In samples that were fixed at HH 30.5, a very small thickening was visible in the epithelium located directly above the ciliary artery (N=2). This tiny thickening was very difficult to see and may represent a presumptive conjunctival papilla (Figure 3.3A). It may also, however, be scar tissue where the epithelium has repaired itself after surgery; however, as embryos have a marked ability for tissue repair without scarring (Nodder &

Martin, 1997), this is unlikely. It is also possible that this thickening is a mass of proliferated cells.

When the samples were fixed between HH 34 and 35 (when the complete ring of conjunctival papillae should be present), the results were variable (N=6, Figure 3.3B). In four samples (66%), the epithelium was completely repaired at the site of surgery and a thickening that was very similar in appearance to a conjunctival papilla was visible in the conjunctival epithelium directly above the ciliary artery. Although this thickening was often slightly displaced with respect to the ciliary artery (Figure 3.3B arrow). In the other two samples (33%), on the other hand, the epithelium at the site of surgery had not yet completely healed. In these samples, the area of epithelium ablated had been quite large and, while significantly reduced by the time of fixation, a small hole was still present at the site of surgery. Interestingly, in these two samples, a small thickening was present at the border of the surgery area (Figure 3.3C). This thickening may be a conjunctival papilla and could potentially explain the slight displacement of the conjunctival papillae noted in samples fixed at HH 34 and 35. In addition, no change was observed in the patterning of the other conjunctival papillae in the ring (N=6) (Figure 3.3B).

Similarly, when the conjunctival epithelium was removed directly above the epithelium at HH 29 and the samples were allowed to develop until between HH 38 and 40, the patterning and spacing of the scleral condensations was normal (N=6) (Figure 3.3D). This result was expected because a papilla was present directly above the ciliary artery in younger samples (HH 34 and 35) which would subsequently induce an underlying scleral condensation. These results further suggest that a delay in the induction of a single conjunctival papilla does not affect the patterning of the rest of the ring.

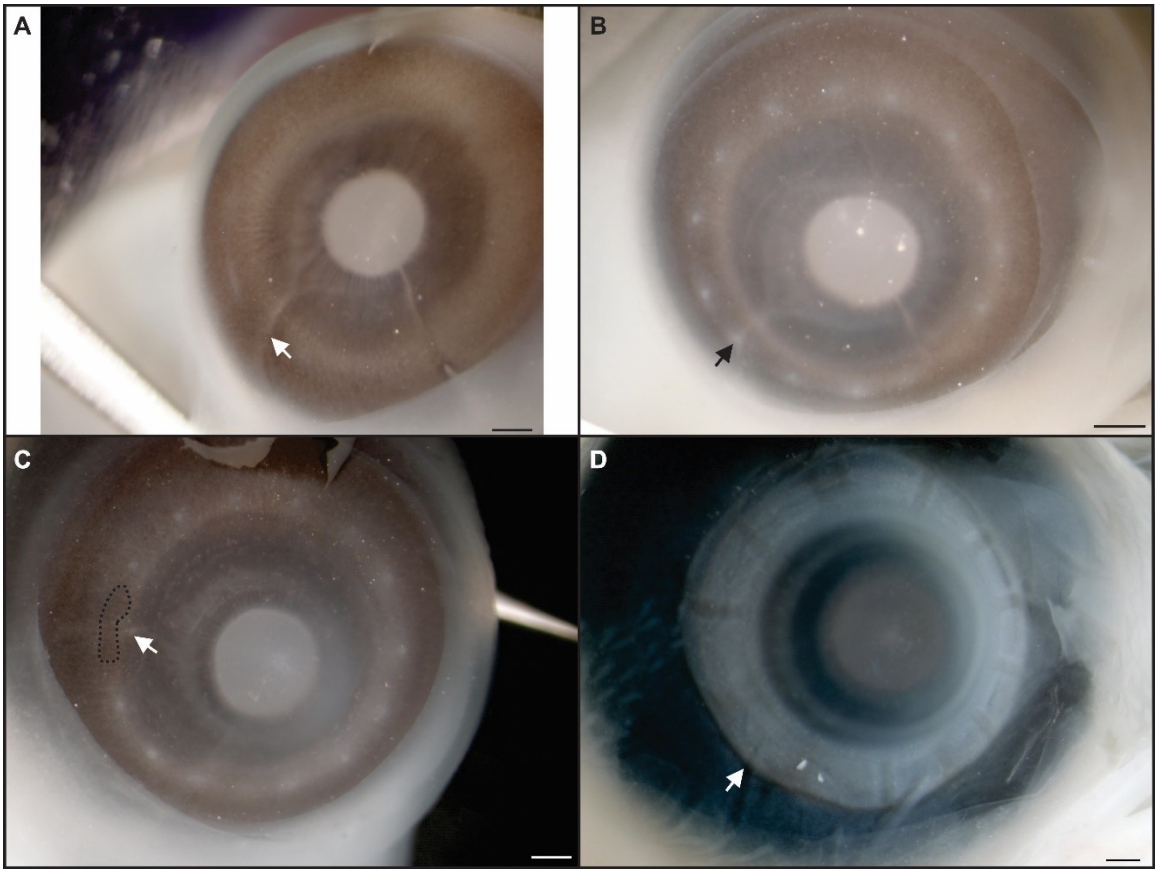

Figure 3.3: Results of epithelium ablation at HH 29. **A**) In samples fixed at HH 30.5, a very small, inconspicuous thickening was present directly above the ciliary artery (arrow). **B**) By HH 34, there is an obvious conjunctival papilla directly above the ciliary artery (arrow). **C**) In some samples the area of epithelium removed was quite large, the ablated area did not have time to completely repair before fixation at HH 34 (area outlined by dotted line). In these samples, a distinct thickening was visible in the epithelium above the ciliary artery, but was displaced with respect to the other papillae in the ring (arrow). **D**) By HH 40, a scleral condensation is present directly above the ciliary artery (arrow). All scale bars are 500 μm.

3.3.1.2 – Surgical Ablation at HH 30

As no alterations to the patterning of the conjunctival papillae was observed when the conjunctival epithelium directly above the ciliary artery was surgically ablated at HH 29, I performed the same surgical ablation at HH 30 immediately before the induction of the first conjunctival papilla in 14 embryos. In all cases, the left eye was used as a control and was normal.

When these embryos were fixed at HH 34, a small conjunctival papilla was present directly above the ciliary artery. In addition, all of the conjunctival papillae in the ring were present indicating there was no effect on their patterning (N=2, Figure 3.3A). Similarly, when an additional 10 samples were fixed slightly later (between HH 35 and 36), a small conjunctival papilla was present directly above the ciliary artery although this papilla was often slightly displaced (N=10) (Figure 3.3B). No effect on the patterning of the other conjunctival papillae in the ring was observed.

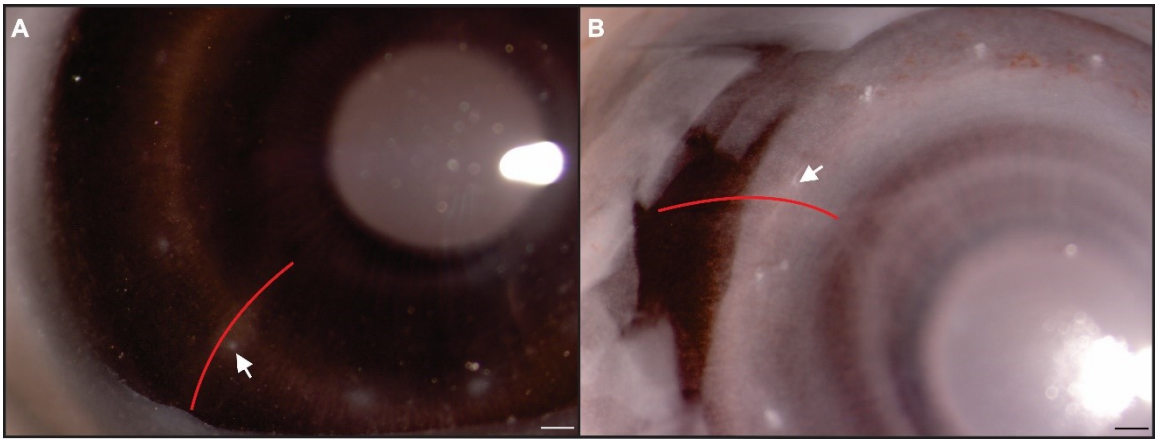

Figure 3.4: Results of epithelium ablation at HH 30. **A**) Sample fixed at HH 34 in which a papilla is visible at the site of surgery (arrow). All of the papillae in the ring are normally patterned. **B**) Sample fixed at HH 36 in which a papilla is visible at the site of surgery (arrow). All other papillae in the ring are normally patterned. All scale bars are 250 µm.

3.3.1.3 – Summary of Epithelium Removals

Collectively, the results of the above surgical manipulations indicate that the removal of the conjunctival epithelium directly above the ciliary artery does not alter the patterning or induction of the other conjunctival papillae in the ring. A conjunctival papilla was almost always present at the site of surgery; however, this papilla was sometimes slightly displaced with respect to the ciliary artery and appeared smaller than the adjacent papillae in the temporal region. This papilla was not measured. These results were

consistent across all 28 samples in which the conjunctival epithelium was removed prior to conjunctival papilla induction.

3.3.2 – Surgical Ablation of a Conjunctival Papilla Does not affect the Patterning of the other Conjunctival Papillae in the Ring

After determining that removing the conjunctival epithelium directly above the ciliary artery between HH 29 and 30 had no effect on the patterning of the rest of the conjunctival papillae in the ring (N=28), I wanted to investigate whether surgical ablation of the conjunctival papilla after it had formed (between HH 30.5 and 34) could affect the induction and patterning of the other conjunctival papillae in the ring. These results are summarized in Table 3.2. The left eye was again used as a control and, in all cases, was normal.

It should be noted that, while every effort was made to consistently remove the conjunctival papilla directly above the ciliary artery during this surgery, this papilla was not always accessible through the small hole in the chorioallantoic membrane and, in these cases, another conjunctival papilla (often in the nasal region) was removed (N=6 out of 27 surgeries). As the results of these surgical ablations was always the same as when the conjunctival papilla directly above the ciliary artery was removed, the results are presented together.

Table 3.2: Table summarizing the results of papilla removals between HH 30 and 34. Controls are described in the text. N represents the number of surgeries. CA: ciliary artery.

Surgery Stage	Stage Fixed	N	Result
30.5	33	2	Regenerated papilla present
30.5	38-39	2	
31-33	36.5	1	Regenerated papilla present
31-33	38-39	9	Condensation present at site of surgery
34	36-36.5	12	Regenerated papilla present
	Total N	26	

3.3.2.1 – Surgical Ablation at HH 30.5

At HH 30.5, there is only one conjunctival papilla in the ring. After surgical ablation, a small white thickening was observed directly above the ciliary artery but it was not obvious whether this was scar tissue or a new papilla developing (fixation at HH 33, N=2). The patterning of the other conjunctival papilla in the ring was normal. In embryos allowed to develop to between HH 38 and 40, I similarly observed no evidence that surgical ablation of the first conjunctival papilla had any effect on the patterning of the sclerotic ring, as a typical number of normally shaped and sized scleral condensations were present in the eye (N=2). These results suggest that the small thickening observed in the samples fixed at HH 33 may indeed be a small conjunctival papilla.

3.3.2.2 – Surgical Ablation between HH 31 and HH 33

When conducting the surgery between HH 31-33; which corresponds to the induction of the nasal, dorsal, and ventral groups of conjunctival papillae, a thickening was observed at the site of surgery which resembled a conjunctival papilla at HH 36.5 (N=9). There was again no effect on the induction and patterning of the other conjunctival papillae in the ring or the resulting underlying scleral condensations. By HH 38 and 39, a distinct

scleral condensation was present in the scleral mesenchyme beneath the surgery area, indicating that the regenerated papilla was capable of inducing an underlying ossicle.

3.3.2.3 – Surgical Ablation at HH 34

To complete this series of experiments, I also examined the result of surgical ablation of the conjunctival papilla directly above the ciliary artery at HH 34, when the complete ring of conjunctival papillae had been induced. Examination at HH 36, revealed the presence of a small conjunctival papilla at the site of surgery in all of the samples (N=11, Figure 3.5). This papilla appeared to be smaller than the other papillae in the temporal region; which was unusual, as it is usually the largest papilla in the ring. Additionally, this papilla was occasionally slightly displaced with respect to the ciliary artery. No changes in the patterning or spacing of the other conjunctival papillae in the ring were observed. The presence of a small conjunctival papilla at the site of ablation was particularly surprising as the induction of the conjunctival papillae ring is normally concluded by HH 34.

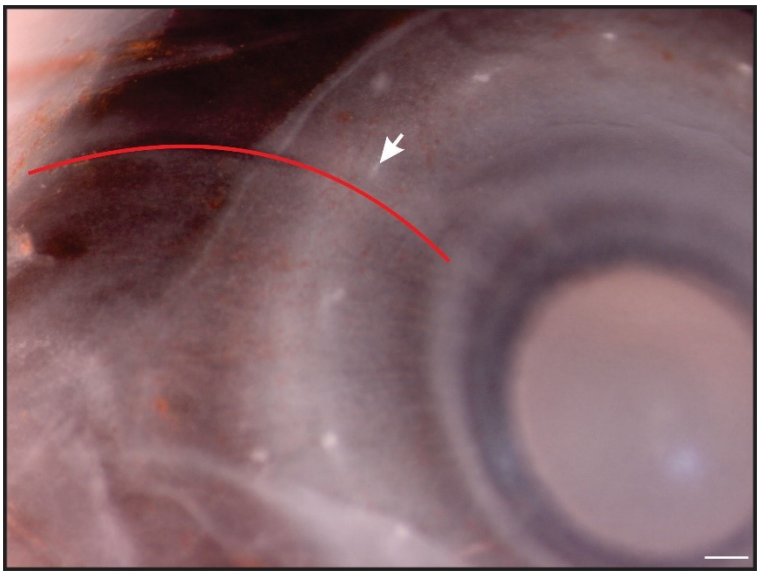

Figure 3.5: Results of conjunctival papilla ablation at HH 34. In samples fixed at HH 36, a small conjunctival papilla (arrow) is present above the ciliary artery (red line). It is sometimes slightly displaced with respect to the ciliary artery. Scale bar is 250 μm.

3.3.2.4 – Summary of Papilla Ablations between HH 30.5 and HH 34

Overall, these results indicate that the conjunctival papillae are capable of regeneration and, additionally, that the regenerated conjunctival papilla is able to induce a normally shaped and patterned scleral condensation. This is quite surprising as Coulombre and Coulombre (1962) found that, once removed, a conjunctival papilla was not capable of regeneration. This difference in results will be discussed below. These results additionally demonstrate that conjunctival papilla induction is possible over a longer temporal period than was previously believed, until at least HH 35.5, and that patterning of the rest of the ring is robust and unaffected.

3.3.3 – Testing the Limits of Conjunctival Papilla Regeneration during the Normal Period of Conjunctival Papilla Induction

Based on the above results, I wanted to further investigate the regenerative capacity of the conjunctival papillae. To do this, I repeated the previous experiments removing the conjunctival papilla directly above the ciliary artery at HH 30.5, between HH 31-33, and

at HH 34. Samples from each stage were then fixed after 1, 1.5, 2, 2.5, 3, 3.5, and 5 dps (N=81). In all cases, the left eye was used as a control and was normal. Results are summarized in Table 3.3.

Similarly to section 3.3.2 above, in a small number of samples (N=3; all three of which were fixed at 1 dps), I was not able to access the conjunctival papilla directly above the ciliary artery and one of the nasal papillae was removed instead. As the result of these surgeries were the same as the others (i.e. those that targeted the papilla directly above the ciliary artery), the results are presented together.

Table 3.3: Table summarizing the results of papilla removals between HH 30 and 34 after 1, 1.5, 2, 2.5, 3, 3.5, and 5 dps. N represents the number of surgeries. dps: days post-surgery, CA: ciliary artery. *Papillae were not measured.

dps	Surgery Stage	Stage Fixed	N	Result
1	31-32	34	3	No papilla present
	32-33	35	6	
	34	35	10	
1.5	31-32	34.5-35	2	Small presumptive papilla above CA
	34	35.5	3	
2	30.5	35	5	Small papilla above CA*
	31-33	35.5-36	3	
	34	36	17	
2.5	31-33	36-36.5	3	Papilla above CA
	34	36.5	6	Papilla above CA has begun to degenerate
3	30.5	36	4	Papilla above CA
	31-33	36.5	2	Papilla above CA has begun to degenerate
	34	37	8	
3.5	31-33	37	2	Papilla above CA is degenerating
5	34	39-40	5	Condensation under regenerated papilla
	34	39-40	2	Condensation under regenerated papilla appears smaller
		Total N	81	

3.3.3.1 – 1 Day Post-Surgery

In all cases, regardless of the stage at which the surgery was performed or the stage of fixation, there was no conjunctival papilla present at the site of surgery after 1 dps (N=19, Table 3.3; Figure 3.6). This indicates that it takes longer than one day for regeneration of the ablated conjunctival papilla to occur.

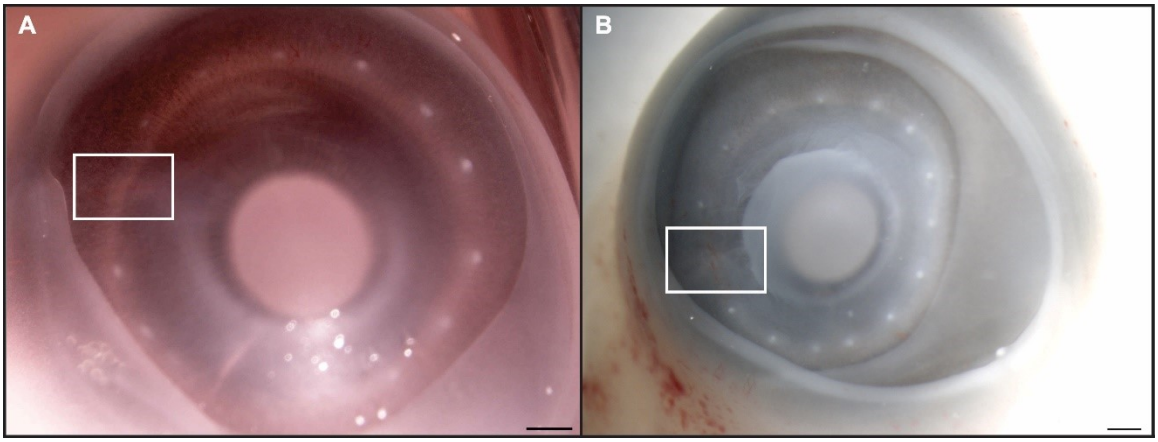

Figure 3.6: Results of conjunctival papilla ablation after 1 dps. When the surgery was performed at HH 31-32 and fixed at HH 34 (**A**) or performed at HH 34 and fixed at HH 35 (**B**), there was no papilla present directly above the ciliary artery (white box). All scale bars are 500 μm.

3.3.3.2 – 1.5 Day Post-Surgery

By 1.5 dps, a small presumptive conjunctival papilla was present directly above the ciliary artery (N=5) regardless of the stage at which the surgery was performed or the stage of fixation (Table 3.3; Figure 3.7). This result suggests that i) it takes approximately 1.5 days for a conjunctival papilla to start to regenerate and that ii) the epithelium is competent to respond to the (unknown) inductive cue until at least HH 35.5.

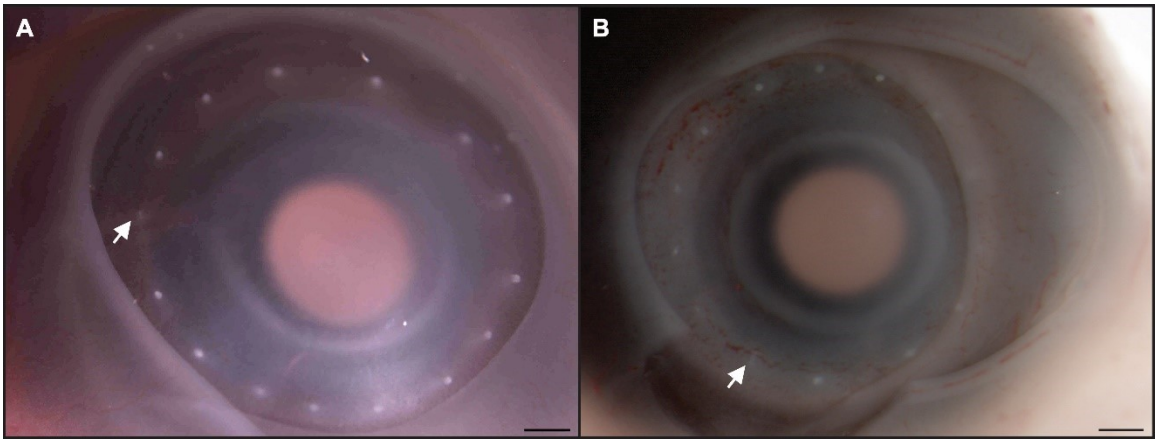

Figure 3.7: Results of conjunctival papilla ablation after 1.5 dps. **A**) Surgery performed at HH 31-32 and fixed at HH 34.5 and **B**) surgery performed at HH 34 and fixed at HH 35.5. In both cases, a small conjunctival papilla was visible in the epithelium directly above the ciliary artery (arrow). All scale bars are 500 µm.

3.3.3.3 – 2 Days Post-Surgery

By 2 dps, the regenerated conjunctival papilla was more obvious and appeared to have increased in size (N=25; Figure 3.8). Again, this result was the same regardless of the stage at which the surgery was performed (Table 3.3).

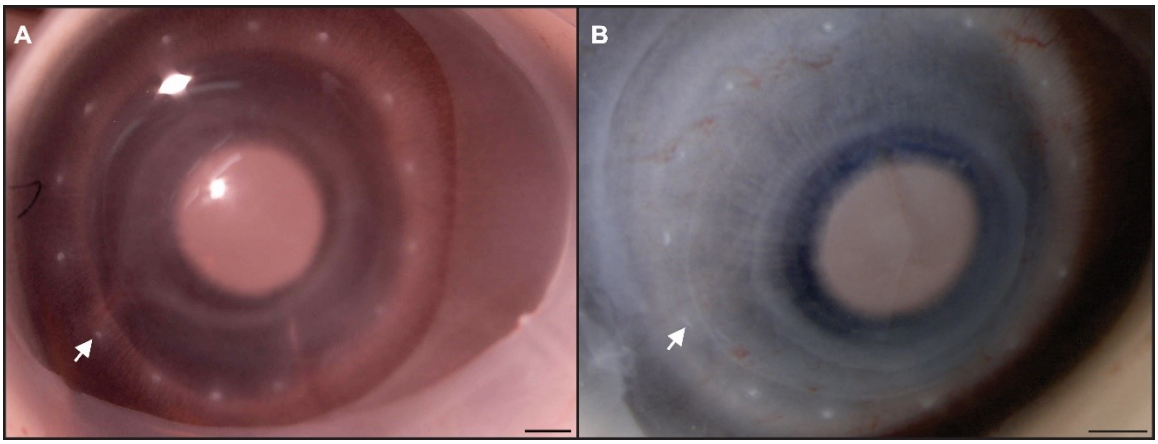

Figure 3.8: Results of conjunctival papilla ablation after 2 dps. **A**) Surgery performed at HH 31-32 and fixed at HH 35-35.5 and **B**) surgery performed at HH 34 and fixed at HH 36. In both cases a distinct papilla was visible directly above the ciliary artery (arrow). All scale bars are 500 µm.

3.3.3.4 – 2.5 Days Post-Surgery

Again, at 2.5 dps, a regenerated conjunctival papilla was always present directly above the ciliary artery regardless of the stage at which the ablation was performed or the stage at which the embryos were fixed (N=9; Table 3.3; Figure 3.9). In samples in which the papilla was ablated at HH 34, the smaller regenerated conjunctival papilla appeared to have already begun to degenerate (N=6; Figure 3.9B). As the conjunctival papillae normally degenerate after their inductive role is complete (Coulombre & Coulombre, 1962) this may indicate both i) that the inductive role of the regenerated conjunctival papillae is already complete by 2.5 dps (approximately HH 36.5) and/or ii) that it degenerates more quickly due to its smaller size.

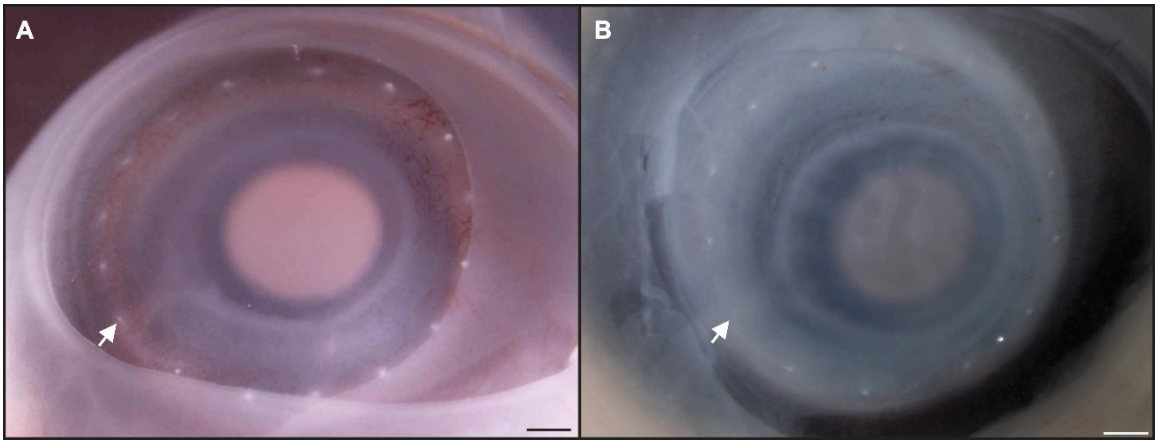

Figure 3.9: Results of conjunctival papilla ablation after 2.5 dps. **A**) Surgery performed at HH 31-32 and fixed between HH 35.5-36 and **B**) surgery performed at HH 34 and fixed at HH 36.5. In both cases, a distinct papilla was visible directly above the ciliary artery (arrow). In older samples, the regenerated papilla appears to have begun to degenerate, making it difficult to see. All scale bars are 500 µm.

3.3.3.5 – 3 and 3.5 Days Post-Surgery

Similarly, when the conjunctival papilla directly above the ciliary artery was surgically ablated and fixed at 3 dps, a regenerated conjunctival papilla was present at the site of surgery regardless of the stage at which the surgery was performed (N=14; Table

3.3). When the surgery was performed at HH 34 and fixed at HH 37 (N=8), the regenerated conjunctival papilla appears to have begun to degenerate, similar to the other conjunctival papillae in the temporal region (Figure 3.10). Interestingly, this papilla appears to be more degraded than the others in the temporal region. This may be because the regenerated conjunctival papilla has fewer cells than the others in the temporal region. A very similar result was observed at 3.5 dps (N=2). Degeneration of the papilla is a normal part of papillae development since these are transient structures; degeneration typically occurs by apoptosis at M-stage 6 (Murray, 1942). This result indicates that the regenerated conjunctival papilla is following the same transient developmental program as the other papillae in the ring.

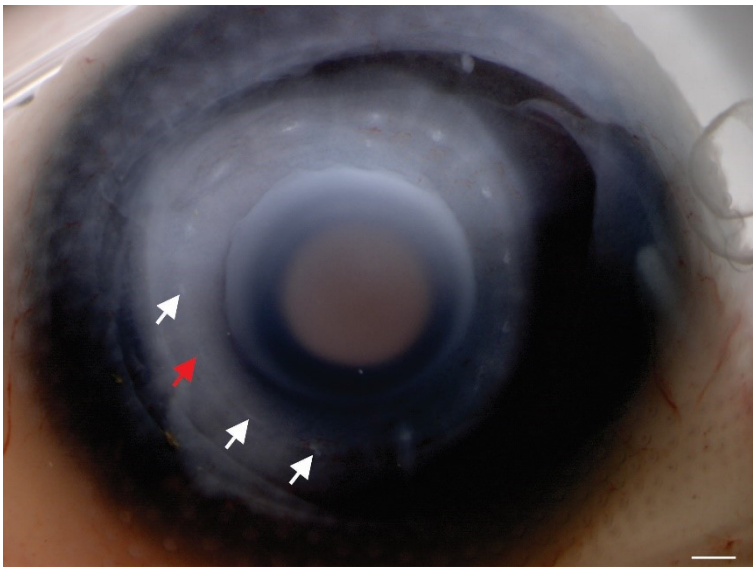

Figure 3.10: Results of conjunctival papilla ablation after 3 dps. The regenerated conjunctival papilla (red arrow) and those in the temporal region (white arrows) are degenerating compared to the other papillae in the ring. Scale bar is 500 μm.

3.3.3.6 – 5 Days Post-Surgery

In order to provide further evidence that the regenerated papilla was a true conjunctival papilla, I investigated whether it was capable of inducing an underlying scleral

condensation. To do this, I surgically ablated the conjunctival papilla directly above the ciliary artery at HH 34 and allowed the embryos to develop until HH 39-40 (N=7). In all seven embryos, a scleral condensation was present directly beneath the surgery site, above the ciliary artery. This results indicates that the regenerated papilla was a papilla with inductive capabilities (Figure 3.11). In five of these embryos (71%), the induced scleral condensations were of normal shape and size (Figure 3.11A). In the other two embryos, however, the resulting scleral condensation appears to be smaller than normal while the adjacent condensations seemed to have increased in size (Figure 3.11B). Measurements were not conducted because the aim was merely to show that a condensation was induced. It is possible that this alteration to the size of the underlying scleral condensation is due to the time at which the surgery was performed since a large number of surgeries were performed over the course of a single day, however, upon examining my lab notebook, I noted that these surgeries were performed earlier in the day than the others. It is thus unlikely that a disparity in the time at which the surgery was performed caused this effect.

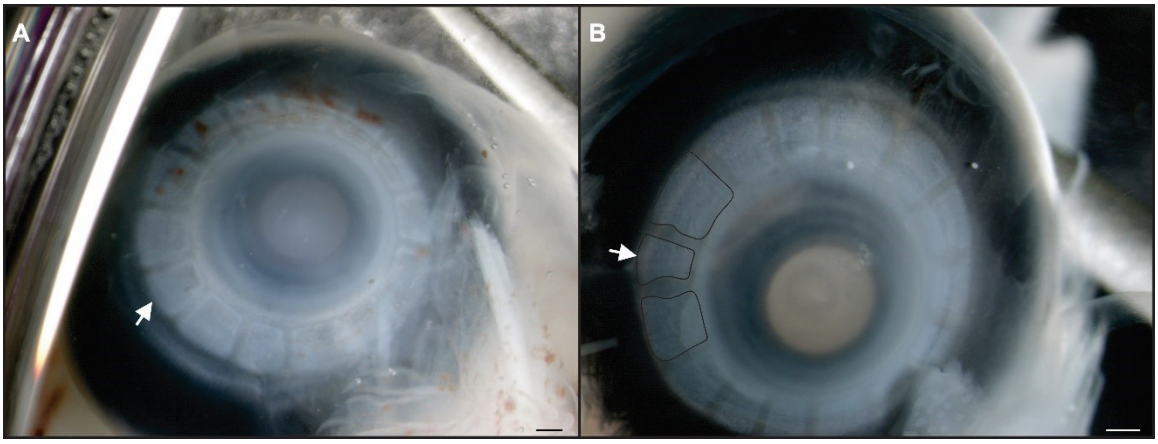

Figure 3.11: Results of conjunctival papilla ablation after 5 dps. **A**) When the conjunctival papilla directly above the ciliary artery was ablated at HH 34 and the embryos were fixed at HH 40, there was a normally shaped and patterned scleral condensation directly above the ciliary artery (arrow). **B**) In a small number of samples (N=2), the scleral condensation that was induced (arrow) appeared smaller than the adjacent condensations. Condensations have been traced in black for clarity. All scale bars are 500 μm.

3.3.3.7 – Summary of all Surgeries in this Section

Overall, these surgery results suggest that:

1. The inductive cue that induces a papilla is perhaps present longer than was previously reported,
2. That the epithelium remains competent to respond to the inductive cue for the conjunctival papillae until at least HH 35.5, and
3. That it takes approximately 1.5 dps for an ablated conjunctival papilla to regenerate. Once regenerated, these conjunctival papillae develop similarly to the other conjunctival papillae in the ring; namely, progressing through the M-stages of development, inducing an underlying scleral condensation, and finally degenerating.

3.3.4 – Testing the Limits of Conjunctival Papilla Regeneration Outside the Normal Period of Conjunctival Papilla Induction

My next objective was to determine the ability of the conjunctival papillae to regenerate (and subsequently induce an ossicle), when the papilla is removed outside of the normal period of conjunctival papilla induction (i.e. at HH 35, when induction of the mesenchyme has commenced and the papillae are mature). Thus, to investigate this, I removed the conjunctival papilla directly above the ciliary artery at HH 35 and subsequently fixed the embryos at 1, 2, and 4-5 dps (Table 3.4). As in all previously described surgeries, the left eye was used as a control and was completely normal.

Unfortunately, due to the age of the embryos and the thickness of the chorioallantoic membrane vasculature at this stage, I had more difficulty accessing the conjunctival papilla directly above the ciliary artery during surgical ablation. In such

samples, one of the nasal papillae were removed instead (10 out of 18 embryos). The results were similar for both groups and are therefore presented together.

Table 3.4: Table summarizing the results of papilla removals at HH 35 and then fixed after 1, 2, and 4 or 5 dps. N represents the number of surgeries.

dps	Surgery Stage	Stage Fixed	N	Result
1	35	36-36.5	5	No papilla present
2	35	37-37.5	5	No papilla present; condensation in mesenchyme
4-5	35	39-40	8	Ossicle present at site of surgery
		Total N	18	

3.3.4.1 – 1 Day Post-Surgery

At 1 dps, no conjunctival papilla was observed at the site of surgery (N=5; Figure 3.12). Normally, at this stage (approximately HH 36), distinct papillae are present.

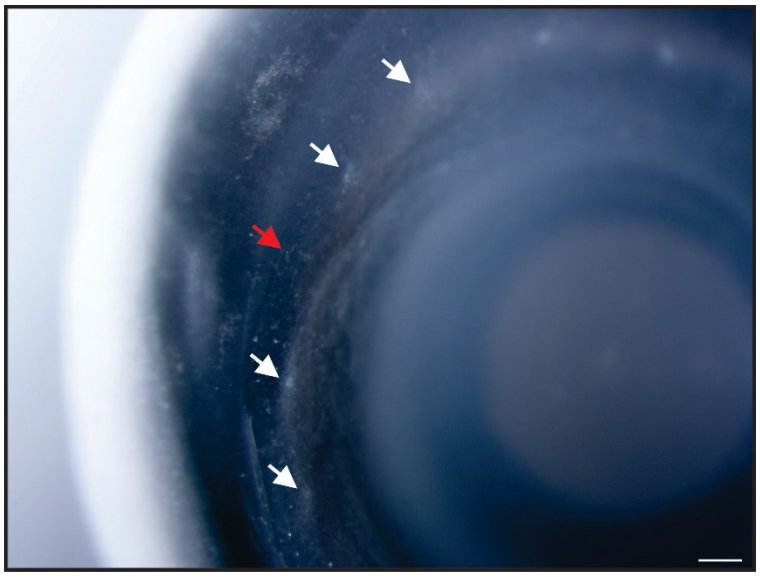

Figure 3.12: Results of conjunctival papilla ablation at HH 35 after 1 dps. There is no obvious conjunctival papilla at the site of surgery (red arrow). Adjacent conjunctival papillae are indicated by the white arrowheads. Scale bar is 500 µm.

3.3.4.2 – 2 Days Post-Surgery

By 2 dps, there was still no evidence of a conjunctival papilla at the site of surgery (N=5); whereas, at this stage (approximately HH 37) papillae are usually in advanced stages of degeneration and ossicle condensations are present (Figure 3.13). Curiously, despite this lack of a conjunctival papilla, a scleral condensation was visible at the site of surgery in the underlying scleral mesenchyme (Figure 3.13). The only explanation for this result is that there is enough inductive signal in the mesenchyme prior to HH 35 to induce an ossicle and that the papilla-generated inductive signal does not need to be maintained beyond this stage.

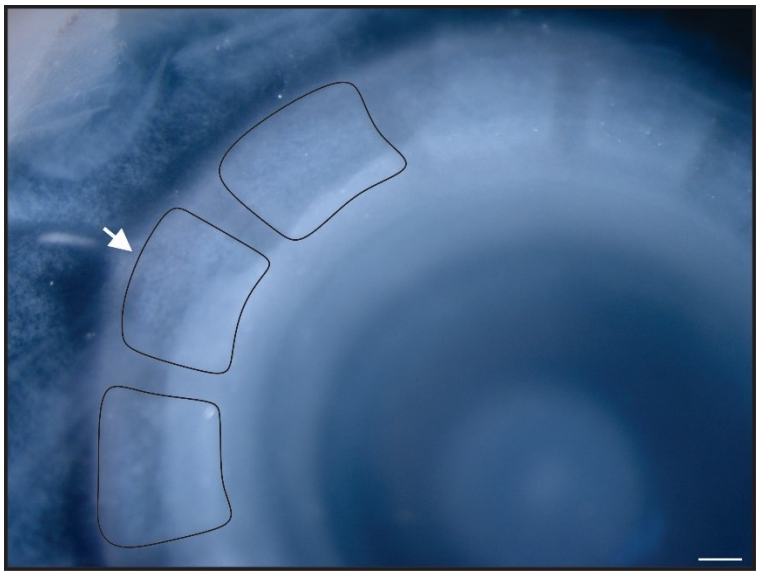

Figure 3.13: Results of conjunctival papilla ablation at HH 35 after 2 dps. No conjunctival papilla was observed at the site of surgery however, a normally shaped and patterned scleral condensation was present (arrow). The condensations have been traced for clarity. Scale bar is 500 μm.

3.3.4.3 – 4-5 Days Post-Surgery

After 4 or 5 dps (HH 39-40), a complete ring of scleral condensations was present and clearly visible in the eye (N=8, Figure 3.14A). This result also indicates that the induction and patterning of the underlying scleral condensation continued despite the

absence of the overlying conjunctival papilla. In order to confirm that the scleral condensation observed at the site of surgery in the 4-5 dps embryos was a normal scleral condensation, the eye of one sample was stained for enzymatic activity of alkaline phosphatase. In both the control and surgery eye, all scleral ossicles in the ring expressed alkaline phosphatase normally, indicating that they were skeletogenic in nature. Additionally, these condensations were all of a similar size, having begun to overlap one another (Figure 3.14B). This suggests that a normal scleral condensation was induced when the conjunctival papilla was surgically ablated at HH 35, despite the absence of the overlying conjunctival papilla post-surgery.

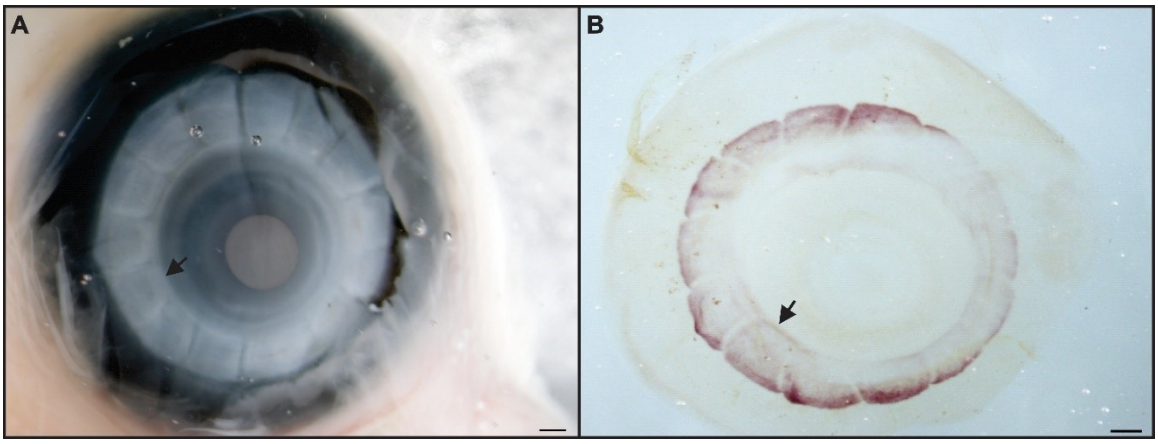

Figure 3.14: Results of conjunctival papilla ablation at HH 35 after 4-5 dps unstained (**A**) and stained with alkaline phosphatase (**B**) Black arrow indicates the condensation at the site of surgery. All scale bars are 500 μm.

3.3.4.4 – Summary of Surgical Ablation at HH 35

Overall, these results indicate that a conjunctival papilla is not capable of regeneration when ablated at HH 35. This is most likely because enough of the inductive signaling molecules have already reached the underlying mesenchyme. These results also suggest that the inductive cascade initiated by the conjunctival papillae does not need to be

maintained beyond HH 35. The results of the conjunctival papillae ablations presented in Sections 3.3.3 and 3.3.4 are summarized in Figure 3.15 below.

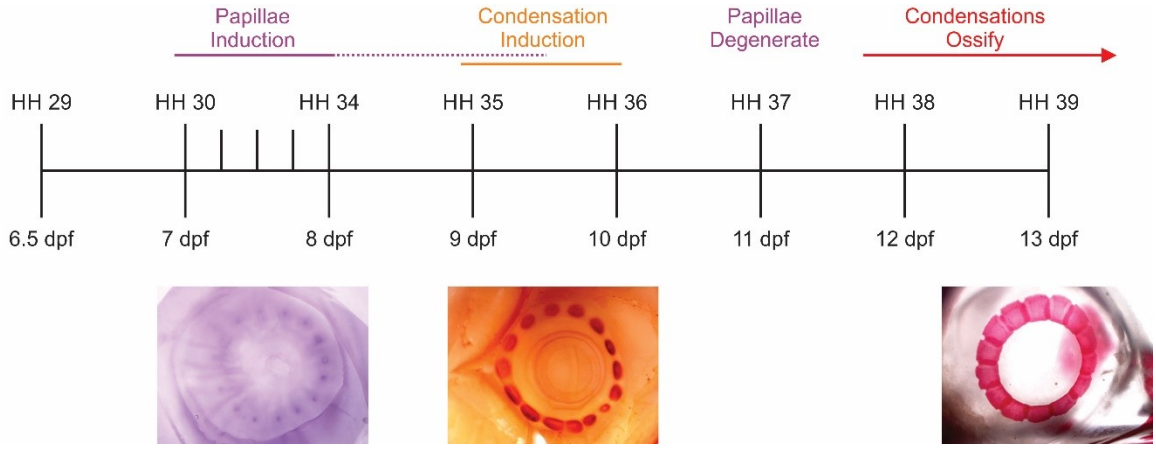

Figure 3.15: Schematic summarizing the results of conjunctival papilla removals between HH 30-35. This study has demonstrated that the conjunctival papillae are capable of regeneration until HH 35.5, a full day and a half longer than was previously believed. These data also suggest that the epithelium remains competent to respond to an inductive cue (which is also present) until HH 35.5 (dotted purple line). This regenerated conjunctival papilla is then able to induce an underlying scleral condensation.

3.3.5 – How Does Papilla Regeneration Affect Condensation Induction and Are the Known Molecular Pathways Used?

Once I determined that the conjunctival papillae are capable of regeneration and that a regenerated papilla is able to induce an underlying scleral condensation, I wanted to better understand how a small regenerated conjunctival papilla is capable of inducing the underlying scleral condensation. My approach was to repeat the above experiment (i.e. removing the conjunctival papilla at HH 34 and fixing these samples at 1, 1.5, 2, 2.5, and 3 dps) and then analyzing the samples using *in-situ* hybridization for *Bmp2*, a gene which has been previously shown to be expressed in the conjunctival papillae between HH 34.5 and early HH 36 and which plays a role in the induction of the underlying scleral condensations (Duench & Franz-Odendaal, 2012).

Specifically, I wanted to determine whether a conjunctival papilla, once it has begun to regenerate, will i) mature faster in order to induce the underlying scleral condensation during the normal inductive period (i.e. HH 35-36; 1-2 dps) or ii) mature over a period of 1-2 days (the normal time period) subsequently inducing the underlying scleral condensation with a delay (i.e. at HH 37; 3 dps). These two scenarios are summarized in Figure 3.16.

Since timing was critical in this analysis, only those samples in which the conjunctival papilla directly above the ciliary artery was ablated were used.

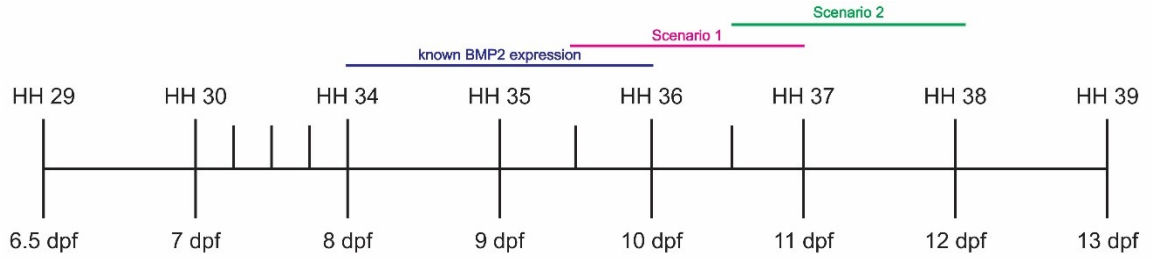

Figure 3.16: Schematic illustrating the two possible predicted scenarios of *Bmp2* expression in the regenerated conjunctival papillae as compared to the known expression of *Bmp2*.

3.3.5.1 – 1 Day Post-Surgery

In the control (left) eye of embryos after 1 dps (approximately HH 35), there is strong expression of *Bmp2* in the conjunctival papillae of the nasal, dorsal, and ventral regions (N=2; Figure 3.17A and B). In the temporal region, the conjunctival papillae have begun to downregulate their expression of *Bmp2* after having induced *Bmp2* expression in the underlying scleral mesenchyme (Figure 3.17B, arrow). This mesenchymal expression is confined to the small, ovoid scleral condensation.

Similarly, in the surgery (right) eye of embryos after 1 dps, strong expression in the conjunctival papillae of the nasal, dorsal, and ventral regions was observed (N=2). The

temporal conjunctival papillae adjacent to the ciliary artery have begun to downregulate their expression of *Bmp2* after having induced *Bmp2* expression in the underlying scleral condensations (Figure 3.17C and D). At the site of surgery, on the other hand, a small conjunctival papilla strongly expressed *Bmp2* (Figure 3.17E). This conjunctival papilla is not yet visible using brightfield microscopy (Figure 3.17C). Interestingly, the expression of *Bmp2* in this papilla was out of synchronization with the adjacent conjunctival papillae, which have downregulated *Bmp2* (Figure 3.17E). The regenerated conjunctival papilla has also begun to induce the expression of *Bmp2* in the underlying scleral condensation, however, the induction of this condensations has been delayed as compared to the adjacent temporal condensations as it appears more similar to the condensations of the nasal group (i.e. later induced) than the adjacent temporal condensations. This suggests that the regenerated conjunctival papilla matures quickly in order to induce an underlying scleral condensation during the normal timeline of condensation induction (i.e. between HH 35-36) with only a slight delay compared to the adjacent temporal conjunctival papillae. This most accurately describes scenario 1 presented above.

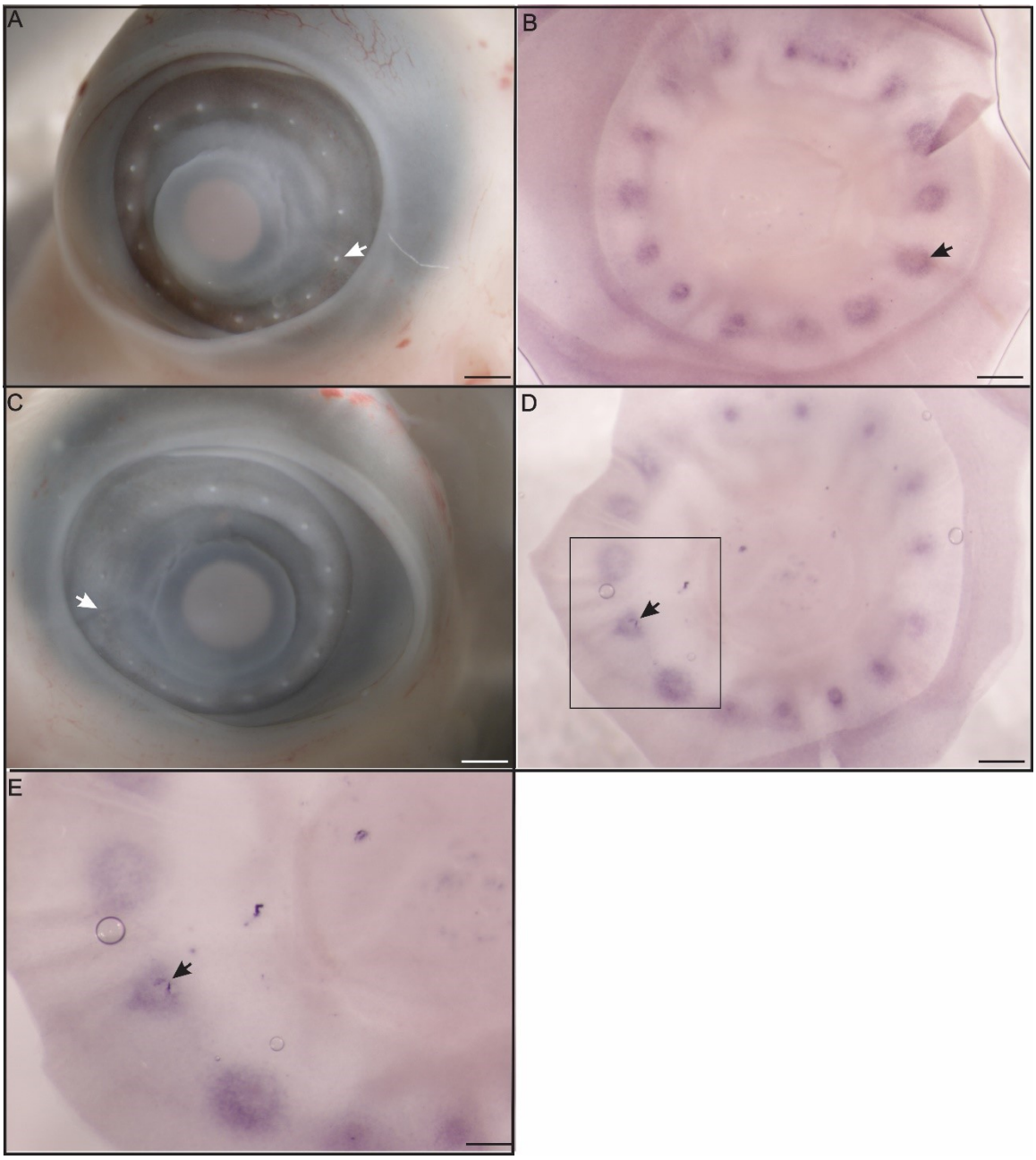

Figure 3.17: Results of *in situ* hybridization for *Bmp2* in the left (control) and right (surgery) eyes of the same embryo after surgical ablation of the conjunctival papilla directly above the ciliary artery at HH 34 after 1 dps (HH 35). In all images, an arrow indicates the papilla at the ciliary artery. **A**) Brightfield image of control eye. **B**) The same control eye after *in situ* hybridization. The temporal conjunctival papillae have downregulated *Bmp2* while the condensations have begun to express *Bmp2* in this region. **C**) Brightfield image of surgery eye. The new conjunctival papilla is not yet visible in brightfield image but was detected by its expression of *Bmp2* in D. **D**) The same surgery eye after *in situ* hybridization. The regenerated papilla is expressing *Bmp2* while it has been downregulated in the other temporal conjunctival papillae. This regenerated papilla has also induced expression in the underlying scleral condensation. The boxed area is shown

at a higher magnification in E. **E**) High magnification image of the temporal region of the surgery eye. The adjacent scleral papillae have downregulated *Bmp2*. Scale bars in A and C are 500 μm, scale bars in B and D are 200 μm, scale bar in E is 100 μm.

3.3.5.2 – 1.5 Days Post-Surgery

In the control (left) eye of embryos after 1.5 dps (approximately HH 35.5), both the temporal and nasal conjunctival papillae have downregulated their expression of *Bmp2* (N=2, Figure 3.18B). Dorsal and ventral conjunctival papillae, on the other hand, still express *Bmp2*; this expression, however, is not as strong as it was at 1 dps. A *Bmp2* expressing scleral condensation is visible underneath the conjunctival papillae of the temporal, dorsal, and ventral regions. These scleral condensations are largest on the temporal side of the eye (Figure 3.18A and B).

Similarly, in the surgery (right) eye of embryos at 1.5 dps, the dorsal and ventral papillae still express *Bmp2*, although this expression is not as strong as it was at 1 dps (N=2; Figure 3.18D and E). Directly above the ciliary artery, the regenerated conjunctival papilla, which is now visible using brightfield microscopy (Figure 3.18C), no longer expresses *Bmp2* (Figure 3.18E). Scleral condensations are clearly visible beneath the conjunctival papillae in the temporal, dorsal, and ventral regions. The condensations are largest in the temporal region. The condensation beneath the regenerated conjunctival papillae has increased in size, similarly to all other condensations (Figure 3.18 D).

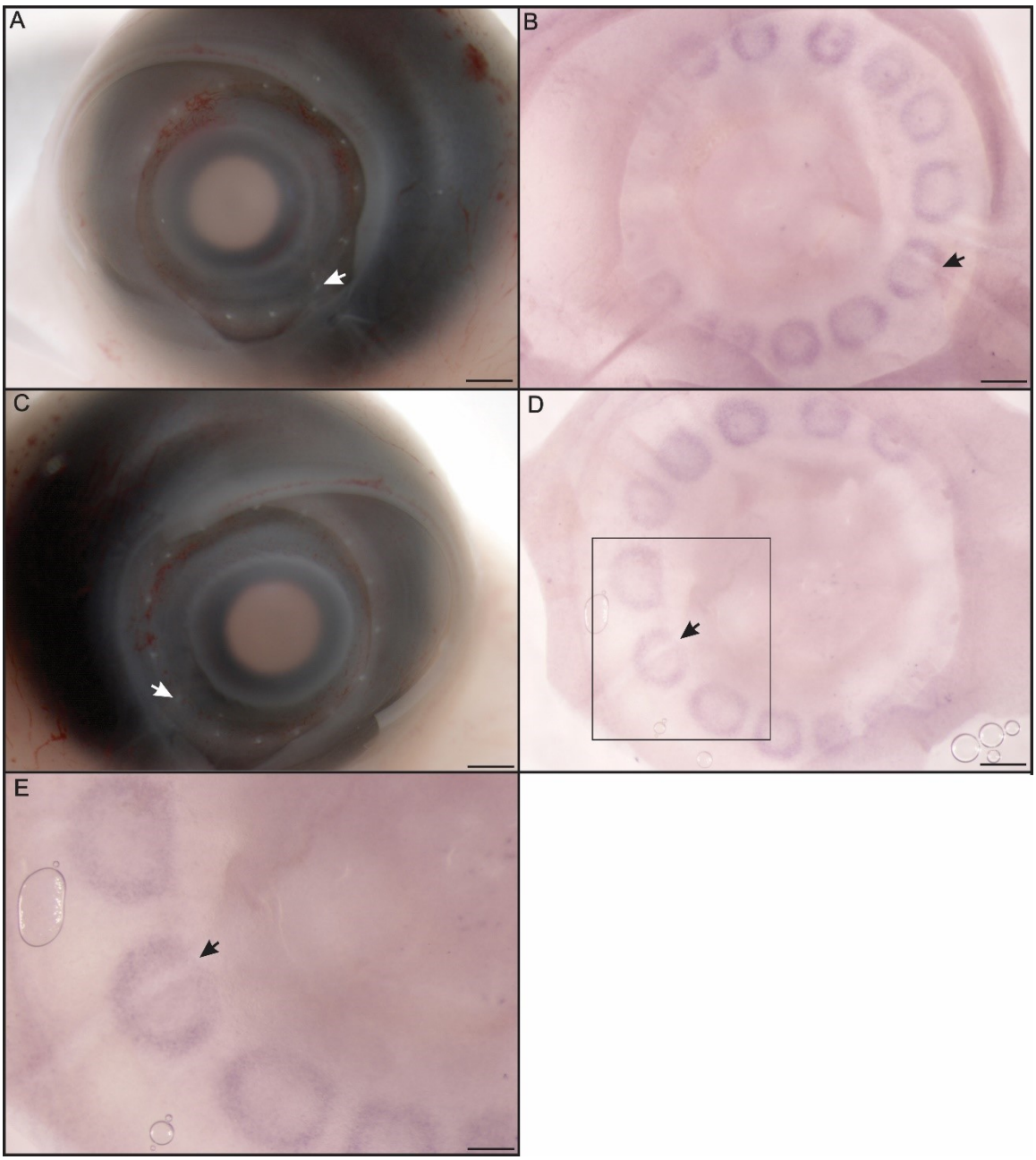

Figure 3.18: Results of *in situ* hybridization for *Bmp2* in the left (control) and right (surgery) eyes of the same embryo after surgical ablation of the conjunctival papilla directly above the ciliary artery at HH 34 after 1.5 dps (HH 35.5). In all images, an arrow indicates the ciliary artery. **A**) Brightfield image of control eye. **B**) The same control eye after *in situ* hybridization. The temporal and conjunctival papillae have downregulated *Bmp2* and the condensations, which still express *Bmp2*, have increased in size. **C**) Brightfield image of surgery eye. A small papilla is now visible at the site of surgery. **D**) The same surgery eye after *in situ* hybridization. The regenerated papilla has downregulated expression of *Bmp2* and the underlying condensation appears to have increased in size as have all of the other condensations in the ring. The box indicates the area that is shown at a higher magnification in E. **E**) High magnification image of the

temporal region of the surgery eye. The regenerated conjunctival papilla has downregulated *Bmp2* expression and the underlying condensation expresseses *Bmp2*. Scale bars in A and C are 500 μm, scale bars in B and D are 200 μm, and scale bar in E is 100 μm.

3.3.5.3 – 2 Days Post-Surgery

In the control (left) eyes of embryos at 2 dps (approximately HH 36), all of the conjunctival papillae in the ring have downregulated their expression of *Bmp2* (N=4; Figure 3.19A and B). The scleral condensations have continued to increase in size and have a strong border of *Bmp2* expression.

Similarly, in the surgery (right) eyes of embryos at 2 dps, all of the conjunctival papillae have downregulated their expression of *Bmp2* (N=4, Figure 3.19D). Under brightfield microscopy, the regenerated conjunctival papilla seems to have increased in size (Figure 3.19C). *In situ* hybridization revealed that the scleral condensations in the temporal region have also increased in size as in the control eye (Figure 3.19D). Furthermore, cryosectioning of a surgery eye at 2 dps confirms that *Bmp2* expression at this stage is limited only to the underlying scleral condensations and has been downregulated in all temporal conjunctival papillae, including the regenerated papilla (Figure 3.19E). Additionally, cryosectioning revealed that the regenerated papilla is filiform in shape indicating that it has matured through the M-stages of papilla development and is now similar to the other papillae in the eye (Figure 3.19E and F).

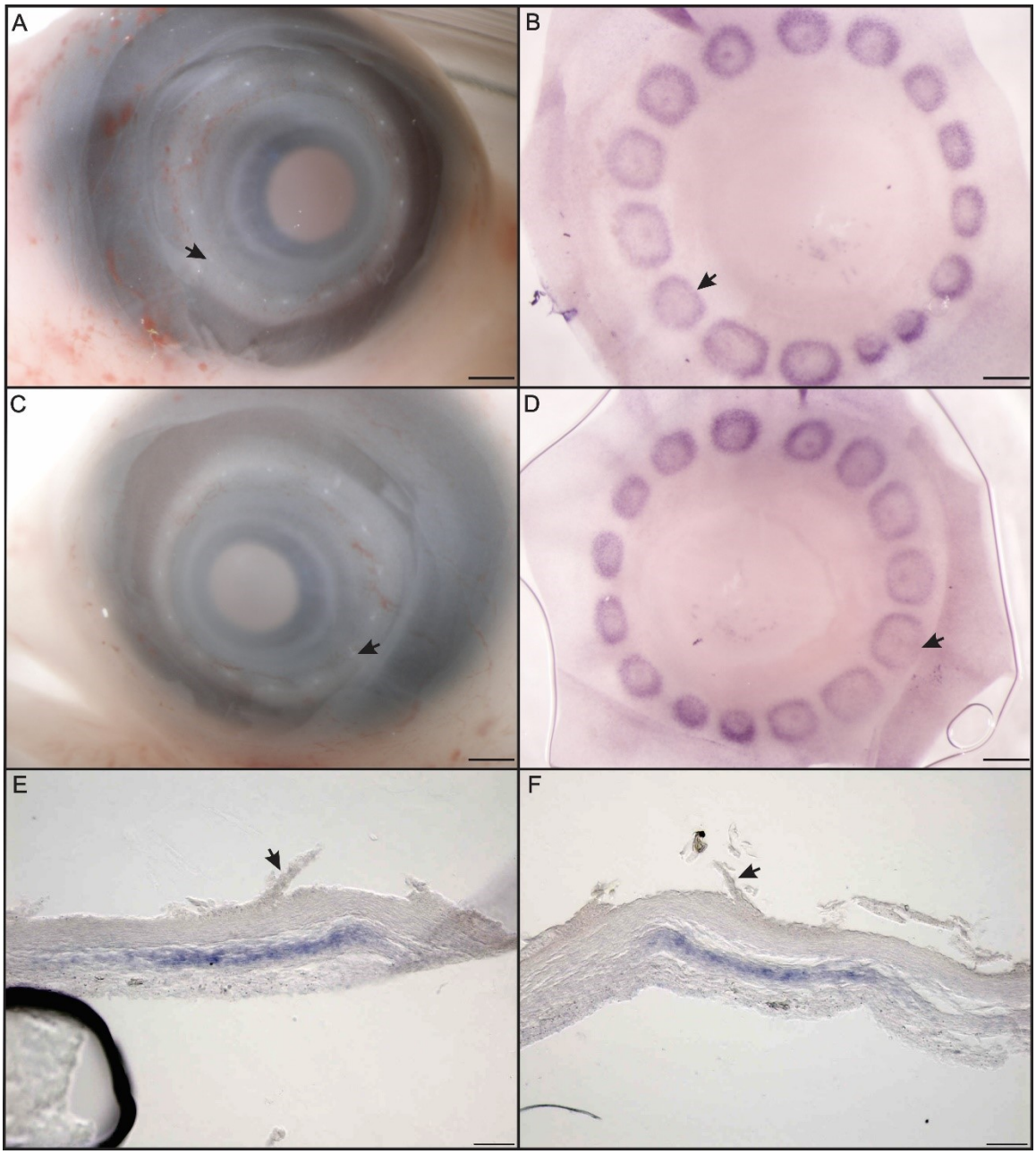

Figure 3.19: Results of *in situ* hybridization for *Bmp2* in the left (control) and right (surgery) eyes of the same embryo after surgical ablation of the conjunctival papilla directly above the ciliary artery at HH 34 after 2 dps (HH 36). In all images, the ciliary artery is indicated by an arrow. **A**) Brightfield image of control eye. **B**) The same control eye after *in situ* hybridization. All of the scleral condensations have increased in size and strongly express *Bmp2*. **C**) Brightfield image of surgery eye. A small papilla is visible at the site of surgery (arrow). **D**) The same surgery eye after *in situ* hybridization. All of the scleral condensations in the ring have increased in size and strongly express *Bmp2*. **E**) Cryosection through the conjunctival papilla and scleral condensation directly above the ciliary artery in the control eye. There is a distinct papilla which is filiform in shape (arrow). *Bmp2* expression has been downregulated in the conjunctival papilla and is now

strongly expressed in the underlying scleral condensation. **F**) Cryosection through the regenerated conjunctival papilla and underlying condensation. The papilla is filiform in shape and is now at the same M-stage as the ciliary artery papilla shown in E . There is no expression of *Bmp2* in the regenerated papilla but the underlying condensation expresses *Bmp2* similarly to the other condensations in the temporal region. Scale bars in A and C are 500 μm, scale bars in B and C are 200 μm, scale bars in E and F are 20 μm.

3.3.5.4 – 2.5 Days Post-Surgery

By 2.5 dps (approximately HH 36.5) in the control (left) eye, the temporal conjunctival papillae have become hard to see and appear to have begun degenerating (3.20A). The scleral condensations have increased in size and are trapezoidal in shape, more closely resembling the mature shape of the scleral condensation (N=4; Figure 3.20B). The boundaries of these scleral condensations is clearly demarcated by a region devoid of *Bmp2* expression (Figure 3.20B), however they have begun to downregulate their expression of *Bmp2*, compared to earlier stages (compare Figure 3.20B to Figure 3.19B).

The surgery (right) eye of the 2.5 dps embryos are very similar to the control eyes (N=4, Figure 3.20D). Under brightfield microscopy, the conjunctival papillae in the temporal region have become hard to see as they have begun degenerating (Figure 3.20C). The scleral condensations are trapezoidal in shape and have begun to downregulate the expression of *Bmp2* (Figure 3.20D). In one sample, the scleral condensations in the temporal region have begun to overlap and no *Bmp2*-free gap is present between the scleral condensations (not shown). This indicates that the scleral condensation, induced with a slight delay by the regenerated conjunctival papilla, has compensated for the delay in its induction by 2.5 dps (HH 36.5), as it downregulates expression of *Bmp2* similarly to the other temporal scleral condensations.

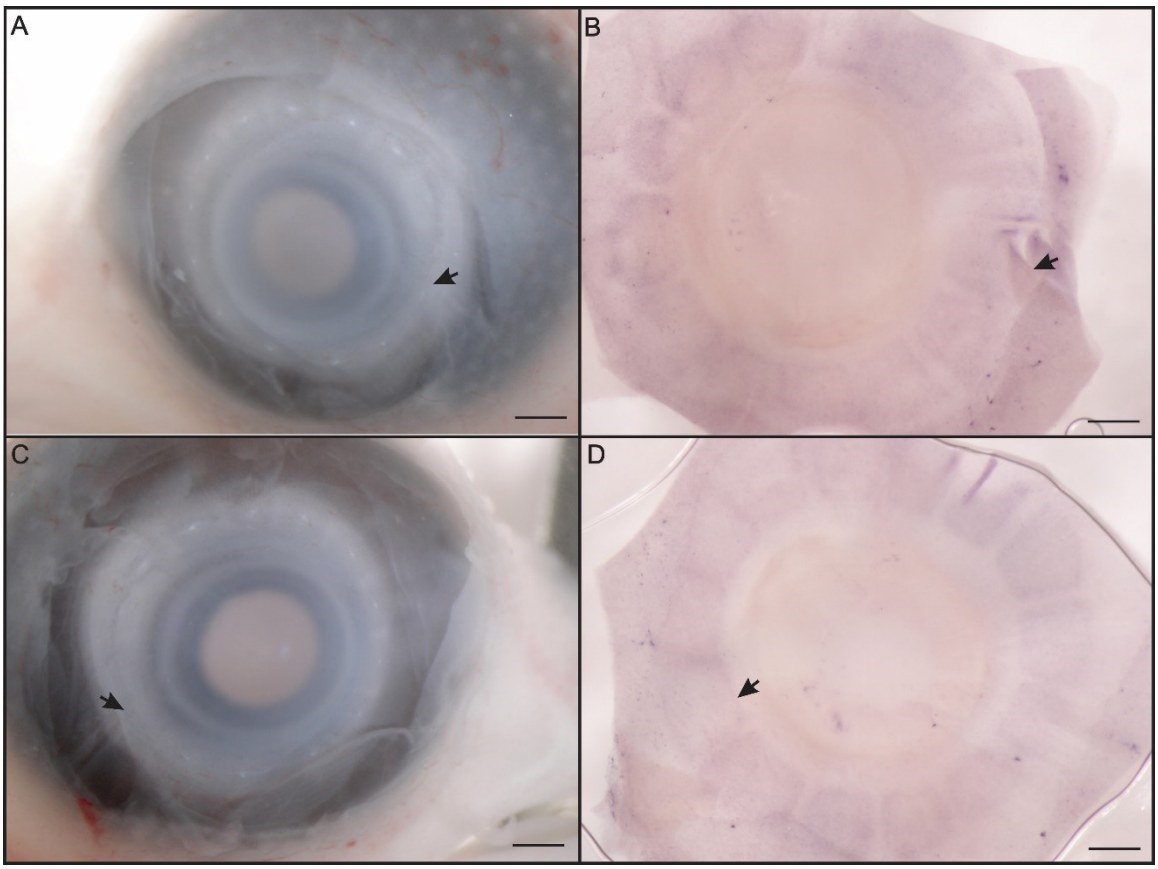

Figure 3.20: Results of *in situ* hybridization for *Bmp2* in the left (control) and right (surgery) eyes of the same embryo after surgical ablation of the conjunctival papilla directly above the ciliary artery at HH 34 after 2.5 dps (HH 36.5). The ciliary artery is indicated by an arrow in all images. **A**) Brightfield image of control eye. The papilla above the ciliary artery is degenerating. **B**) The same control eye after *in situ* hybridization. All of the scleral condensations have increased in size and have begun to downregulate *Bmp2* expression. **C**) Brightfield image of surgery eye. A small papilla is visible at the site of surgery and is degenerating. **D**) The same surgery eye after *in situ* hybridization. All of the scleral condensations in the ring have increased in size and have begun to downregulate *Bmp2* expression. The condensation at the site of surgery is also downregulating *Bmp2* expression. Scale bars in A and C are 500 μm, scale bars in B and D are 200 μm.

3.3.5.5 – 3 Days Post-Surgery

In the control eyes of embryos at 3 dps (approximately HH 37), the conjunctival papillae are degenerating (Figure 3.21A) while the underlying condensations have continued to increase in size (N=2). The scleral condensations have continued to downregulate their expression of *Bmp2* and borders between the scleral condensations have become difficult to see (Figure 3.21B).

There is very little difference between the control and surgery eyes at this stage (N=2). The conjunctival papillae are degenerating and are quite hard to see (Figure 3.21C). The scleral condensations have increased in size, further downregulating their expression of *Bmp2*, and the borders between condensations are difficult to see (Figure 3.21D).

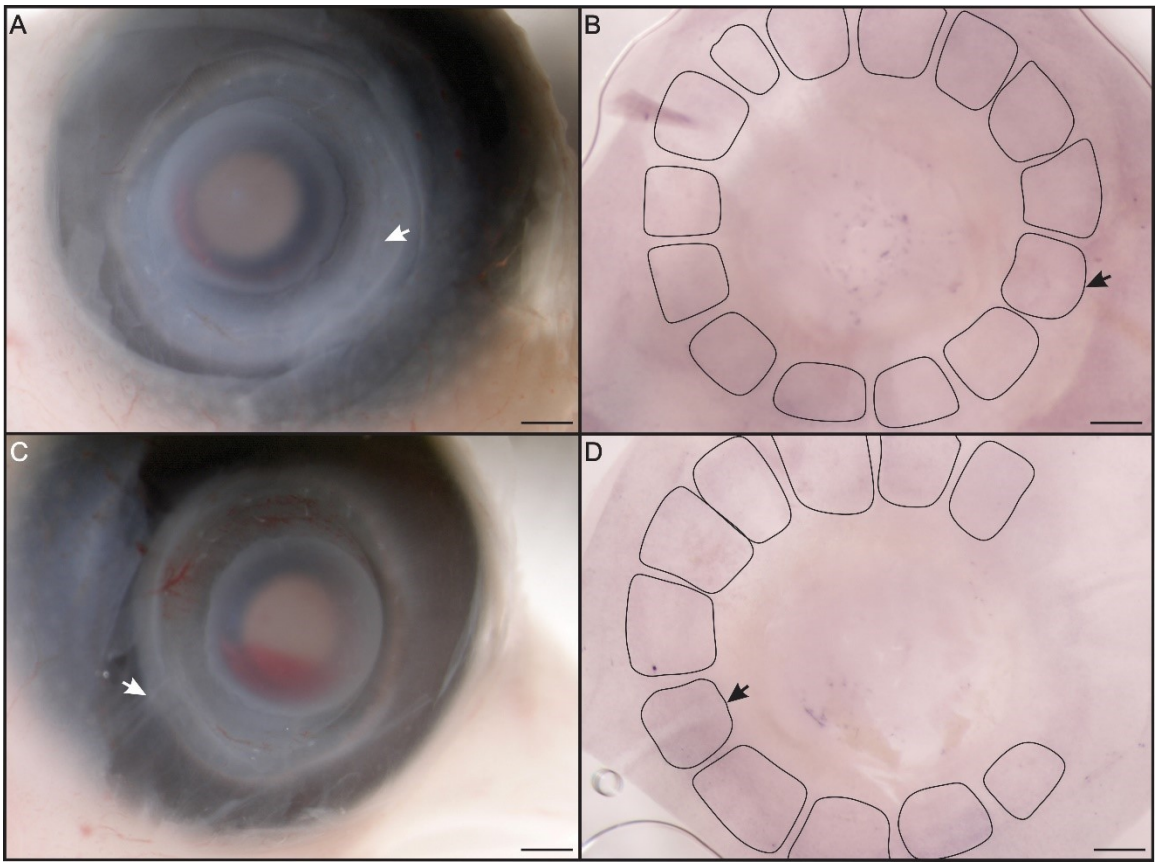

Figure 3.21: Results of *in situ* hybridization for *Bmp2* in the left (control) and right (surgery) eyes of the same embryo after surgical ablation of the conjunctival papilla

directly above the ciliary artery at HH 34 after 3 dps (HH 37). The ciliary artery is indicated by an arrow in all images. **A**) Brightfield image of control eye. The papilla above the ciliary artery is degenerating. **B**) The same control eye after *in situ* hybridization. All of the scleral condensations have increased in size and now only very faintly express *Bmp2*. **C**) Brightfield image of surgery eye. The regenerated papilla is no longer visible and is almost fully degenerated. **D**) The same surgery eye after *in situ* hybridization. All condensations have increased in size and now only faintly express *Bmp2*. Condensations have been traced for clarity except for those which were not fully visible. Scale bars in A and C are 500 μm, scale bars in B and D are 200 μm.

3.3.5.6 – Summary of In Situ Hybridization

The temporal and spatial pattern of *Bmp2* expression observed in the regenerated conjunctival papilla suggests that the first scenario I proposed is correct. That is, that the papilla matures quickly in order to induce an underlying condensation with a slight delay during the normal inductive period (i.e. between HH 35 and 36). Once ablated, the epithelium regenerates (which takes approximately one day). As soon as this epithelium is repaired the epithelium begins to thicken, re-forming the conjunctival papilla. Immediately, the regenerated papilla begins to express *Bmp2*, skipping the normal one-to-two day maturation period (Figure 3.22A). Thus, the regenerated conjunctival papilla does not need to reach the filiform stage prior to becoming inductively active, enabling it to induce the underlying scleral condensation during the normal period of condensation induction (i.e. between HH 35 and 36); however, with a slight delay as compared to the rest of the temporal group. This is likely an important epithelial compensatory mechanism in place to ensure that all condensations are induced and of similar size. By 1.5 dps, the regenerated conjunctival papilla has downregulated its expression of *Bmp2* (Figure 3.22B) and the underlying scleral condensation has increased in size similarly to all other condensations in the ring. By 2 dps, the scleral condensation induced by the regenerated conjunctival papilla is indistinguishable from the other condensations in the temporal

region (Figure 3.22C). As all of the scleral condensations in the ring have downregulated their expression of *Bmp2* by 2.5 dps, this suggests that the condensation induced by the regenerated papilla has now fully compensated for the delay in its induction (Figure 3.22D). As such, by 3 dps, all of the condensations in the ring have continued to downregulate their expression of *Bmp2* and the condensation induced by the regenerated papilla, which has begun to overlap the adjacent condensations, is indistinguishable from the other condensations in the temporal region (Figure 3.22E).

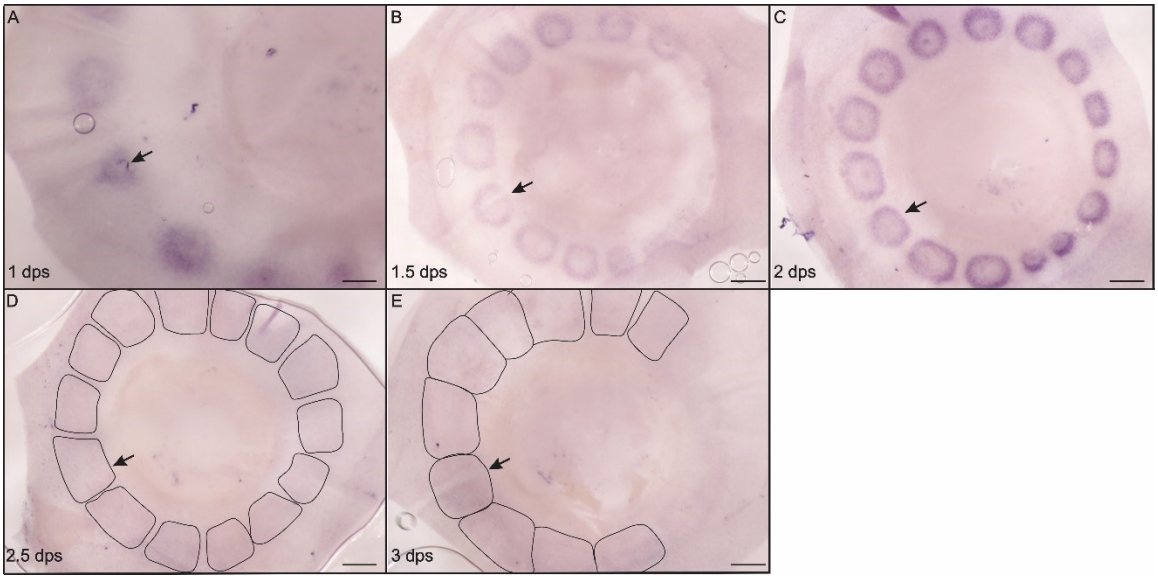

Figure 3.22: A summary of the expression of *Bmp2* in the surgery (right) eye of embryos from 1 dps through to 3 dps. The ciliary artery is indicated by an arrow in all images. **A**) At 1 dps (HH 35), the regenerated conjunctival papilla expresses *Bmp2* with a slight delay as compared to the other temporal conjunctival papilla and has begun to induce an underlying scleral condensation. **B**) At 1.5 dps (HH 35.5), the regenerated conjunctival papilla has downregulated its expression of *Bmp2*. The underlying scleral condensations have all increased in size. **C**) By 2 dps (HH 36), all of the condensations have increased in size and the condensation beneath the regenerated papilla is indistinguishable from the others in the temporal region. **D**) By 2.5 dps (HH 36.5), all of the scleral condensations have downregulated expression of *Bmp2*, including the condensation induced by the regenerated conjunctival papilla. **E**) By 3 dps (HH 37), all of the scleral condensations have continued to downregulate *Bmp2* expression. Condensations have been traced for clarity in D and E. Scale bars are 200 μm

3.4 – Discussion

As there have only been two studies to date that have specifically examined the induction and patterning of the conjunctival papillae (Coulombre & Coulombre, 1962; Hall, 1981a and b), this discussion will be somewhat limited. The results of this study, however, have yielded a number of new insights into papilla development and will provide a good baseline for future studies.

3.4.1 – Towards Understanding the Patterning of the Conjunctival Papillae

As described in Chapter 1 and earlier in this chapter, the first papilla to form is always located directly above the ciliary artery and this patterning has been conserved in at least two of the species examined to date, namely the chicken and the turtle (Coulombre & Coulombre, 1962; Franz-Odendaal, 2006; Duench & Franz-Odendaal, 2012). Subsequently, the rest of the papillae are induced in four distinct groups: i) temporal, ii) nasal, iii) dorsal, and iv) ventral. The papillae within each of these groups are evenly spaced from one another and this spacing is maintained across groups. Furthermore, I have hypothesized that the spacing between the conjunctival papillae is mediated by local inhibition between papillae (Franz-Odendaal, pers. comm.). Therefore, in order to begin unravelling the mechanisms governing the induction and patterning of the conjunctival papillae, I surgically ablated the conjunctival epithelium directly above the ciliary artery between HH 29 and 30 (prior to the induction of the first conjunctival papilla) in order to assess the effect of this ablation on the induction and patterning of the other conjunctival papillae in the ring. I then surgically ablated a conjunctival papilla from the ring at a number of later stages (HH 30.5 to 34) during the induction and patterning of the

conjunctival papillae in order to assess the effect of this ablation on the patterning of the conjunctival papillae.

In all surgeries, removal of the conjunctival epithelium directly above the ciliary artery prior to the induction of the first papilla had no effect on the patterning of the other conjunctival papillae in the ring. Furthermore, the epithelium at the site of surgery was quickly repaired and a conjunctival papilla was induced above the ciliary artery, although this papilla was sometimes slightly displaced with regards to the ciliary artery. These results were very interesting as they demonstrated that the first conjunctival papillae to form does not provide patterning information for the other conjunctival papillae in the ring. Furthermore, this highlights that there may be two levels of patterning occurring during the induction of the conjunctival papillae: i) a temporal pattern (i.e. the induction of four distinct groups: temporal, nasal, dorsal, and ventral around the corneal-scleral limbus) and ii) a spatial pattern (i.e. the spacing between the conjunctival papillae).

Many other placodes are also patterned at both the temporal and spatial levels, including feather placodes, hair placodes, and tooth placodes (Wolpert, 1998; Eames & Schneider, 2005; Drew *et al*., 2007; Duverger & Morasso, 2009; Koussoulakou *et al*., 2009; Bei, 2009; Catón & Tucker, 2009; Cobourne & Sharpe, 2010; Lin *et al*., 2011; Jiang *et al*., 2011; Porntaveetus *et al*., 2011; Matalova *et al*., 2012; Sennett & Rendl, 2012; Painter *et al*., 2012; Yue *et al*., 2012; Chuong *et al*., 2013). For example, in the feather, the induction and patterning of the placodes is divided into tracts (Mou *et al*., 2011; Chuong *et al*., 2013). In chick, the first row of placodes to form is known as the primary tract and it is a single row of placodes down the center of the back in which all of the placodes are evenly spaced (Mou *et al*., 2011; Chuong *et al*., 2013). Once this tract has formed, the subsequent tracts

form in a hexagonal grid established by the position of the placodes in this initial tract (Mou *et al*., 2011; Chuong *et al*., 2013). This hexagonal arrangement of the feather placodes is thought to be mediated by a number of factors: i) the local expression of placodal genes accompanied by the expression of placode inhibitors in the inter-placodal region, restricting placode formation to areas of low inhibition and ii) the arrangement of the underlying mesenchyme into a diamond-shaped array of dense extracellular matrix, restricting placode formation to the center of this diamond where the extracellular matrix is less dense (Stuart *et al*., 1972; Sengel, 1990; Miura, 2007; Mou *et al*., 2011; Jiang *et al*., 2011; Li *et al*., 2012; Painter *et al*., 2012; Wells *et al*., 2012; Chuong *et al*., 2013). It should be noted, however, that the spatiotemporal patterning of the cutaneous placodes (such as the example of feather placodes given above) are linear. The first tract forms and all subsequent placodes are patterned outward from this tract.

In the conjunctival papillae system, on the other hand, the temporal and spatial patterning is not linear. The first group (temporal) is induced on one side of the eye while the second group (nasal) forms opposite it a few hours later. The third (dorsal) and fourth (nasal) groups both form opposite one another, but are located between the temporal and nasal groups. It is currently unknown how this patterning is established, how the conjunctival papillae are patterned within each group, and furthermore, how spacing is achieved between the individual papillae of adjacent groups. The results of my surgical ablations, however, have led me to hypothesize that the patterning of the conjunctival papillae is first established based on timing (i.e. the establishment of each group) and then at the spatial level (i.e. the spacing of each papilla). As such, some signal or other mechanism (such as the migration of the NCCs into the eye) establishes each of the regions

that will give rise to the conjunctival papillae (i.e. the temporal, nasal, dorsal, and ventral groups). After the first papilla is induced, a second patterning mechanism kicks in within each of these groups which is then responsible for the patterning and spacing of each of the individual papillae. Furthermore, I hypothesize that a reaction-diffusion model, such as the local auto-activation and lateral inhibition (LALI) model proposed by Meinhardt and Grier (Meinhardt, 2012) may most accurately govern the spacing of the individual papillae. In such a model, an autocatalytic (i.e. drives its own production) activator and an inhibitor interact to establish a stationary pattern (Roth, 2011; Meinhardt, 2012; Ball, 2015). Importantly, however, these two chemicals (or signaling cascades) must have different rates of diffusion, in which the inhibitor diffuses farther and faster than the activator (Roth, 2011; Meinhardt, 2012; Ball, 2015). As such, the activity of the activator becomes sequestered to a small area surrounded by inhibitor and other zones of activator activity can only be established at areas of low activator concentration (Roth, 2011; Meinhardt, 2012; Ball, 2015). This provides a particularly attractive model for the patterning of the conjunctival papillae for a number of reasons: i) when a conjunctival papilla is ablated it always regenerates at the site of ablation and ii) it provides an elegant solution for how consistent spacing is established between papillae despite their induction in opposite groups. If a LALI model is responsible for the spacing of the conjunctival papillae, then the papillae of the first two groups to form (temporal and nasal) would be able to provide the patterning cues for the spacing of the papillae in later forming dorsal and ventral groups through the activity of the long range inhibitor. This will require further study.

However, many other questions still remain to be answered with regards to the patterning of the conjunctival papillae. Some of these include: why the first papilla to form

is always located directly above the ciliary artery, the mechanism by which the conjunctival papillae are restricted to the corneal-scleral limbus, and how additional papillae are integrated into the ring without disturbing the patterning of the other papillae. While some of these have received a small amount of attention, much more research must be done before it will be possible to fully understand the complexities of the patterning of the conjunctival papillae.

3.4.2 – Towards Understanding the Regenerative Capacity of the Conjunctival Papillae

That the conjunctival papillae are capable of regeneration when removed prior to HH 34 was very surprising as a previous study by Coulombre and Coulombre (1962) stated that when a conjunctival papilla was removed it was unable to regenerate. Additionally, if the papilla was ablated prior to HH 35, the underlying scleral ossicle would fail to appear or be greatly reduced in size (Coulombre & Coulombre, 1962). I hypothesize that the inability of the conjunctival papilla to regenerate in Coulombre and Coulombre's (1962) study may have been due to the way in which the surgeries were performed. In their study, the conjunctival papilla was removed by being pulled off the surface of the epithelium using Watchmaker's forceps, which they acknowledge damaged the underlying basal lamina and removed the first few layers of the underlying mesenchyme. Furthermore, Hall (1981a and b) demonstrated that the inductive cue for the conjunctival papillae may be mesenchymal in origin because papillae are neither induced nor maintained when the epithelium was separated from the underlying mesenchyme during their inductive period (between HH 30 and 34). In my experiments, a more sensitive removal method was used which did not damage the underlying basal lamina or scleral mesenchyme, leading me to

hypothesize that Coulombre and Coulombre (1962) damaged an important area necessary for papilla induction.

When a conjunctival papilla was ablated at HH 34 and fixed after 1, 1.5, 2, 2.5, 3, 3.5, and 5 dps, the regenerated conjunctival papilla was first visible at the site of surgery at 1.5 dps (HH 35.5). This is a full one and a half days after the last conjunctival papilla is normally induced in the eye, extending the previously established timeline for the induction and patterning of the conjunctival papillae. Additionally, these results suggest that i) the inductive cue for the conjunctival papillae is present in the eye until at least HH 35.5 and ii) that the conjunctival epithelium remains competent to respond to this inductive cue until at least HH 35.5.

It is also possible that this inductive cue may no longer be actively produced but has been "trapped" by the basement membrane or the extracellular matrix, which has been shown in the literature to act as a sink for secreted factors in other systems (Pinto & Hall, 1991; Hynes, 2009). Gradual release of this factor from either the ECM or the basement membrane would thus enable the induction of the conjunctival papillae for a limited period of time after the inductive factor is no longer being actively produced. Additionally, it should be noted that it is currently unknown whether the factors responsible for the induction and patterning of the conjunctival papillae are secreted or require cell-cell contact. Thus, identifying the nature of the inductive interaction, the factors involved, and the way in which the conjunctival papillae are regenerated will require further study.

Regardless of whether the inductive cue is being actively expressed or is has been trapped by the basal lamina, in order to respond to the inductive cue, the epithelium must remain competent. My research shows that the conjunctival epithelium must maintain its

competency until at least HH 35.5. This may thus suggest that the factors which have been shown to be required for epithelial competency in other systems, such as β-catenin, Wnts, and the ectodysplasin (Eda/Edar) family may play a role in maintaining epithelial competency in the conjunctival epithelium as well (Wolpert, 1998; Eames & Schneider, 2005; Widelitz, 2008; Zhang *et al*., 2009; Cui et al., 2010; Duverger & Morasso, 2009; Dhouailly, 2009; Sayama *et al*., 2010; Enshell-Seijffers *et al*., 2010; Jiang *et al*., 2011; Painter *et al*., 2012; Sennett & Rendl, 2012; Huang *et al*., 2012; Woo *et al*., 2012; Suksaweang *et al*., 2012; Wells *et al*., 2012 Chuong *et al*., 2013; Myung *et al*., 2013; O'Connor *et al*., 2013). It also serves to highlight the similarities between the other placodes and the conjunctival papillae, which will be addressed in Chapter 4. Furthermore, by determining which factors are involved in establishing and maintaining epithelial competency in this system, it may be possible to determine which non-neurogenic placodal systems the conjunctival papillae resemble most closely molecularly.

Moreover, the regeneration of an ablated conjunctival papilla suggests that a mechanism of epithelial compensation is in place to guarantee the induction of a complete ring of scleral condensations in the underlying mesenchyme. As mechanisms of mesenchymal compensation have been previously demonstrated by Coulombre and Coulombre (1962), Franz-Odendaal (2008a), and Duench and Franz-Odendaal (2012); whereby, when the induction of a scleral condensation is abrogated by either surgical (Coulombre & Coulombre, 1962) or molecular means (Franz-Odendaal, 2008a; Duench & Franz-Odendaal, 2012) either the adjacent condensations or one in the opposite side of the ring will increase in size until the gap left open by the missing condensations has been filled, resulting in the development of a complete sclerotic ring. My results are therefore

not altogether surprising. These compensatory mechanisms would serve to provide redundancy in the system, ensuring that a complete sclerotic ring is induced and normally patterned prior to adulthood. Redundancy is common in developmental systems (Pinyopich *et al*., 2003; Fukushige *et al*., 2006; Suzuki *et al*., 2007; Peterkin *et al*., 2007) and so the scleral ossicle system is not unusual in this regard. It is likely that this redundancy has developed in the sclerotic ring system given its importance in visual accommodation as the sclerotic ring has been hypothesized to prevent the distortion of the eye (Curtis & Miller, 1938).

3.4.3 – A Conjunctival Papilla Removed at HH 35 Does not Regenerate yet a Condensation is Induced in the Underlying Mesenchyme

I next wanted to determine whether a conjunctival papilla (when removed at HH 35, outside of the normal period of conjunctival papilla induction and coinciding with the beginning of scleral condensation induction) was capable of regeneration and if so, whether it could induce an underlying scleral condensation. In all cases (N=18), when the conjunctival papilla was ablated at HH 35, there was no evidence of a regenerated conjunctival papilla at the site of surgery at any of the stages examined (1, 2, and 4-5 dps). This suggests that the factors responsible for the induction and patterning of the conjunctival papillae (i.e. inductive signal and/or epithelial competency) are no longer present by HH 36 or 37. It is therefore possible to conclude, based on the results of these surgical ablations that the window of conjunctival papilla induction and patterning extends from HH 30 through to HH 35.5. Furthermore, in all cases (N=13), by HH 37 (2 dps) a scleral condensation was visible in the underlying mesenchyme. These results therefore confirm the results of previous studies (Coulombre & Coulombre, 1962; Hall, 1981a),

indicating that the inductive event is well underway at HH 35 and that the conjunctival papilla is no longer required after HH 35 for the induction of the underlying condensation.

3.4.4 – The Regenerated Conjunctival Papilla Matures Faster in Order to Induce an Underlying Scleral Condensation during the Normal Inductive Period (HH 35-36)

Once the limits of conjunctival papilla regeneration were determined, I then wanted to investigate how a regenerated conjunctival papilla was able to induce an underlying scleral condensation. As discussed in the results above, I presented two different scenarios: 1) the regenerated conjunctival papilla will mature faster in order to induce the underlying scleral condensation during the same inductive period as the other conjunctival papillae in the ring, although with a slight delay and 2) after regeneration, the conjunctival papilla will mature over a period of one-to-two days (depending on position in the ring) as does a normally induced conjunctival papilla and will then induce the underlying scleral condensation outside of the normal inductive period. The results of this study most closely resembled the first scenario presented.

It is important to note that this is the first study to demonstrate expression of *Bmp2* in the underlying scleral condensations beginning at HH 35. This discrepancy from the previous study in which *Bmp2* was examined is due to the newly designed *in situ* hybridization protocol, which is more sensitive than the one previously used in the Franz-Odendaal lab (Duench & Franz-Odendaal, 2012). *Bmp2* expression in the underlying scleral condensations is important for a number of reasons.

Bmp2 is expressed in the underlying scleral condensations of the temporal region at HH 35 (1 dps in this study). This is significant because *Bmp2* is a gene required for differentiation of mesenchymal cells into the skeletogenic lineage (Lu, 2007, Chen *et al*., 2012), indicating that the condensation is already present in the underlying mesenchyme

by HH 35 and is becoming specified to a skeletogenic fate. Recent studies in the Franz-Odendaal lab have also identified the expression of alkaline phosphatase in the scleral condensations beginning at HH 35 (K. Wilson, unpublished data), demonstrating that these differentiated osteoblasts are active.

Furthermore, the expression of *Bmp2* in the scleral condensation in the absence of the conjunctival papilla indicates that the skeletogenic event has already occurred. This may therefore suggest that the induction of the scleral condensation takes place slightly earlier than was previous believed, between HH 34 and 35, at least in the temporal region. These results also demonstrate that the inductive cue from the conjunctival papillae is not required in order for the condensation to achieve the required size for mineralization.

These results also provide insights into two of the requirements for condensation mineralization. As demonstrated by Atchley and Hall (1991) there are cellular parameters that are fundamental to the development of a condensation. These include: i) a critical number of cells, ii) time of condensation initiation, iii) the mitotically active fraction, iv) the rate of cell division, and v) the rate of cell death (Atchley & Hall, 1991; Hall & Miyake, 1995). While previous research has investigated the time of condensation induction, the rate of cell division, and cell death in these condensations (Coulombre & Coulombre, 1962; Hall, 1981a; Franz-Odendaal, 2008a), the minimum number of cells required in the condensation before the preosteogenic cells are able to differentiate remains unknown. This study, however, provides an interesting method with which to investigate this critical cell density. As *Bmp2* is expressed in the scleral condensation prior to the onset of alkaline phosphatase, it may be possible, using a coordinated timeline of *Bmp2* and alkaline phosphatase activity to determine the required condensation size and cellular density

required for differentiation of osteoblasts at the center of the condensation. Additionally, as described above, the timing of *Bmp2* expression in the underlying condensation may indicate that the induction of the underlying scleral condensations may actually begin earlier than previously reported (Coulombre & Coulombre, 1962; Hall, 1981a), between HH 34 and 35, rather than at HH 35 and 36.

3.4.5 – Summary and Significance

This work has contributed substantially to our understanding of the induction and patterning of the conjunctival papillae, an area that has not been studied since the 1980s. My results show that:

i) Surgical ablation of the conjunctival epithelium prior to the induction of the first papilla does not alter the induction and patterning of the conjunctival papillae suggesting that the patterning of the conjunctival papillae is not dependent on the first papilla to form. This also suggests that there may be two levels of patterning in the conjunctival papillae system: temporal (i.e. group level) and spatial (i.e. patterning between papillae).

ii) These studies have indicated, for the first time, that the conjunctival papillae are capable of regeneration as long as the underlying mesenchyme and basal lamina are not damaged during the surgical ablation. This, therefore, provides further support for the hypothesis that the inductive cue for the conjunctival papillae originates in the mesenchyme.

iii) These studies have demonstrated that conjunctival papilla induction is possible until HH 35.5, a full one and a half days longer than was previously believed. This must also mean that the conjunctival epithelium remains competent to

respond to an inductive cue until at least HH 35.5 and that this inductive cue must still be available (i.e. either actively produced or stored in the basal lamina).

iv) This study has also examined the limits of regeneration, demonstrating that regeneration is possible when a conjunctival papilla is ablated at up to and including HH 34, that is takes 1.5 days for a papilla to regenerate, and that a regenerated papilla is able to induce a normal scleral condensation.

v) Furthermore, by using *in situ* hybridization for *Bmp2*, I was able to demonstrate that a regenerated conjunctival papilla matures faster in order to induce a condensation during the normal period of condensation induction. My results also suggested that induction may take place slightly earlier than was previously believed (between HH 34 and 35), as small condensations are visible via *Bmp2*-staining in the mesenchyme of the temporal region at HH 35. The identification of an early condensation marker may enable future researchers to determine the critical condensation size required for ossification of intramembranous bones.

vi) Finally, this study has identified a mechanism of epithelial compensation which ensures the induction of a complete ring of scleral condensations. This epithelial compensation provides an additional level of redundancy in the scleral ossicle system to the previously identified mesenchymal compensation. This discovery may provide clues into the evolutionary history of the sclerotic ring.

Chapter 4: Candidate Gene Expression During Conjunctival Papilla Development

4.1 – Introduction

4.1.1 – Background

Based on the results of the experiments in the previous Chapters, there is mounting evidence to suggest that the conjunctival papillae share many similarities with the other placodes. Both the cranial placodes and the cutaneous placodes are epithelial thickenings that give rise to a diverse array of derivative structures including sensory organs and cutaneous appendages such as hair, feathers, scales and teeth; many of which have enabled the radiation of vertebrates into diverse habitats. In all cases, these placodes are transient in nature, are similarly induced (i.e. similar inductive cascades are involved), and are responsible for the temporospatial patterning of their respective derivative structures. Yet, these epithelial placodes are often not considered together because they do not share the same developmental origin (i.e. the cranial placodes are studied in isolation from the cutaneous placodes) (Schlosser, 2006). However, when the induction and patterning of these placodes are considered in detail, they are all governed by similar processes, which can be summarized as follows:

1. An initial inductive phase or pre-patterning of the epithelium in which the epithelium becomes competent to respond to an inductive signal (Baker & Bronner-Fraser, 2001; Zou *et al*., 2004; Baker, 2005; Schlosser, 2005; Schlosser, 2006; Meulemans & Bronner-Fraser, 2007; Kourakis & Smith, 2007; Schlosser *et al*, 2008; Widelitz, 2008; Whitlock, 2008; Duverger & Morasso, 2009; Chen *et al*., 2009; Catón & Tucker, 2009; Bei, 2009; Cobourne & Sharpe, 2010; Sayama *et al*., 2010; Enshell-Seijffers *et al*., 2010; Lin *et al*., 2011;

Sennett & Rendl, 2012; Huang *et al*., 2012; Woo *et al*., 2012; Myung *et al*., 2013; Suksaweang *et al*., 2012; Wells *et al*., 2012; ; Grocott *et al*., 2012; Chuong *et al*., 2013; Bhat *et al.*, 2013; Groves & LaBonne, 2014; Schlosser *et al*., 2014; Saint-Jeannet & Moody, 2014).

2. The induction of an epithelial thickening (i.e. the placode) in response to an inductive signal (usually from the underlying mesenchyme) (Ferguson *et al*., 1998; Wolpert, 1998; Baker & Bronner-Fraser, 2001; Baker, 2005; Schlosser, 2005; Eames & Schneider, 2005; Schlosser, 2006; Zhang *et al*., 2009; Dhouailly, 2009; Cui et al., 2010; Duverger & Morasso, 2009; Catón & Tucker, 2009; Chen *et al*., 2009; Koussoulakou *et al*., 2009; Bei, 2009; Takahashi *et al*., 2010; Sayama *et al*., 2010; Jiang *et al*., 2011; Painter *et al*., 2012; Sennett & Rendl, 2012; Chuong *et al*., 2013; O'Connor *et al*., 2013; Groves & LaBonne, 2014; Saint-Jeannet & Moody, 2014; Schlosser *et al*., 2014).
3. The induction of a subsequent structure by the placode (i.e. the placode derivative), which can involve a number of different processes (e.g. complex morphogenetic movements, cellular migration, diffusion gradients, *etc*.) (Wolpert, 1998; Zou *et al*., 2004; Eames & Schneider, 2005; Drew *et al*., 2007; Meulemans & Bronner-Fraser, 2007; Whitlock, 2008; McCabe & Bronner-Fraser, 2009; Duverger & Morasso, 2009; Liu *et al*., 2008; Bei, 2009; Catón & Tucker, 2009; Koussoulakou *et al*., 2009; Chen *et al*., 2009; Enchell-Seijffers *et al*., 2010; Sayama *et al*., 2010; Jackman *et al*., 2010; Garcia *et al*., 2011; Jiang *et al*., 2011; Landin *et al*., 2012; Painter *et al*., 2012; Yue *et al*., 2012; Clavel *et*

al., 2012; Sennett & Rendl, 2012; Chuong *et al*., 2013; Bhat *et al*., 2013; Lassiter *et al.*, 2014; Saint-Jeannet & Moody, 2014; Maier *et al*., 2014).

This mounting evidence thus raises the question of whether the conjunctival papillae in the scleral ossicle system may also have a placode stage. In the literature, feather, hair, and tooth development begin with the formation of an epithelial placode which subsequently undergoes a significant morphological development and will either project above or below the epithelium at which point they are referred to as either a papilla or a germ (the nomenclature in the tooth field is different) (Ferguson *et al*., 1998; Dhouailly, 2009; Chen *et al*., 2009; Koussoulakou *et al*., 2009; Lin *et al*., 2011; Jiang *et al*., 2011; Sennett & Rendl, 2012; Woo *et al*., 2012; Clavel *et al*., 2012; Chen & Chuong, 2012; Myung *et al*., 2013; Chuong *et al*., 2013). Additionally, in all of these systems, the epithelial placode also induces an underlying mesenchymal thickening, which is known as a papilla (i.e. feather papilla, hair papilla, dental papilla) (Ferguson *et al*., 1998; Dhouailly, 2009; Chen *et al*., 2009; Koussoulakou *et al*., 2009; Lin *et al*., 2011; Jiang *et al*., 2011; Sennett & Rendl, 2012; Woo *et al*., 2012; Clavel *et al*., 2012; Chen & Chuong, 2012; Myung *et al*., 2013; Chuong *et al*., 2013). These mesenchymal papillae frequently give rise to all of or part of the derivative structure (e.g. the dental papilla gives rise to the dentin and pulp of the tooth [Koussoulakou *et al*., 2009; Porntaveetus *et al*., 2011]) and often, together with other mesenchymal structures, make up the stem cell niche responsible for the replacement of cutaneous structures (e.g. dermal papillae and dermal sheath have the ability to induce and form hair bulbs [Matsuzaki & Yoshizato, 1998]) (Rendl *et al.,* 2005; Widelitz, 2008; Duverger & Morasso, 2009; Jiang *et al*., 2011; Yue *et al*., 2012; Huang *et al.,* 2012; Woo *et al*., 2012; Sennett & Rendl, 2012). As the conjunctival papillae begin

with an initial thickening, undergo a subsequent morphological maturation (generating the papilla itself), are required for the induction and patterning of derivative structures (the scleral ossicles), and are transient in nature (degenerate after condensation induction at HH 37); it seems plausible that this initial, uncharacterized stage is that of a conjunctival placode. It is also possible that this initial stage was not noted during the initial characterization of the conjunctival papillae because their role in the induction of the scleral condensations was not discovered until the 1960s (Coulombre & Coulombre, 1962).

I therefore set out to determine whether the conjunctival papillae system also includes a placodal stage. The introduction to this chapter will therefore focus on the two groups of placodes, the cranial placodes and the cutaneous placodes.

4.1.2 – The Cranial Placodes

As early as 1983, Northcutt and Gans suggested that many of the evolutionary novelties of the vertebrate head can be traced back to two embryonic tissues: the NC, which I described in Chapters 1 and 2, and the cranial placodes (Northcutt & Gans, 1983; Kourakis & Smith, 2007; Schlosser, 2014). The cranial placodes are a secondary population of progenitor cells that are able to give rise to sensory structures and accessory sensory structures of the vertebrate head such as the olfactory epithelium; the inner ear; the lens of the eye; neurons in some of the cranial sensory ganglia; and, in some vertebrates, the lateral line (Whitlock, 2008; Padanad & Riley, 2011; Saint-Jeannet & Moody, 2014; Steventon *et al*., 2014). As was described in Chapter 1, the NCCs and the cranial placodes are both induced in the NPB region in the anterior region of the embryo during early development (Harlow & Barlow, 2007; Schlosser *et al*., 2008; Whitlock, 2008; Bhat *et al*., 2013; Schlosser *et al*., 2014; Saint-Jeannet & Moody, 2014; Groves & LaBonne, 2014) and

the cranial placodes share some similarities with the NCCs, namely: their ability to give rise to sensory neurons and their transient migratory nature (Lassiter *et al*., 2014). The placodes formed in this region are therefore able to give rise to both neurogenic (i.e. olfactory, profundal, trigeminal, epibranchial, hypobranchial, otic, and lateral line) and non-neurogenic (i.e. adenohypophyseal and lens) placodes (Zou *et al*., 2004; Meulemans & Bronner-Fraser, 2007; Harlow & Barlow, 2007; Kourakis & Smith, 2007; Schlosser *et al*., 2008; Canning *et al*., 2008; Knabe *et al*., 2009; O'Neill *et al*., 2012; Saint-Jeannet & Moody, 2014; Steventon *et al*., 2014).

Regardless of the type of cranial placode (i.e. neurogenic or non-neurogenic), their induction and patterning involves the three main steps described above, namely: the pre-patterning of the epithelium, the induction of the placodes themselves, and finally the subsequent induction of their derivative structures; which will be described in the following sections.

4.1.2.1 – Pre-Patterning of the Epithelium

The first step in the development of the cranial placodes is the pre-patterning of a molecularly distinct, horse-shoe shaped band of epithelium that extends approximately from the first pair of somites and surrounds the anterior of the embryo (Figure 4.1A) (Baker & Bronner-Fraser, 2001; Baker, 2005; Schlosser, 2005; Schlosser, 2006; Whitlock, 2008; Bhat & Riley, 2011; Schlosser *et al*., 2014). This horse-shoe shaped band of epithelium, known as the PPR lies between the non-neural epithelium and the presumptive NC (Schlosser, 2005; Schlosser, 2006; Meulemans & Bronner-Fraser, 2007; Harlow & Barlow, 2007; Schlosser, 2014; Groves & LaBonne, 2014; Saint-Jeannet & Moody, 2014). However, prior to the formation of this PPR, the embryo must first establish both the

presumptive neural and non-neural tissue and subsequently the presumptive NC region (Harlow & Barlow, 2007; Schlosser *et al*., 2008; Whitlock, 2008; Bhat *et al*., 2013; Schlosser *et al*., 2014; Saint-Jeannet & Moody, 2014; Groves & LaBonne, 2014). As the induction and delineation of this region was described in detail in Chapter 1, it will not be revisited here.

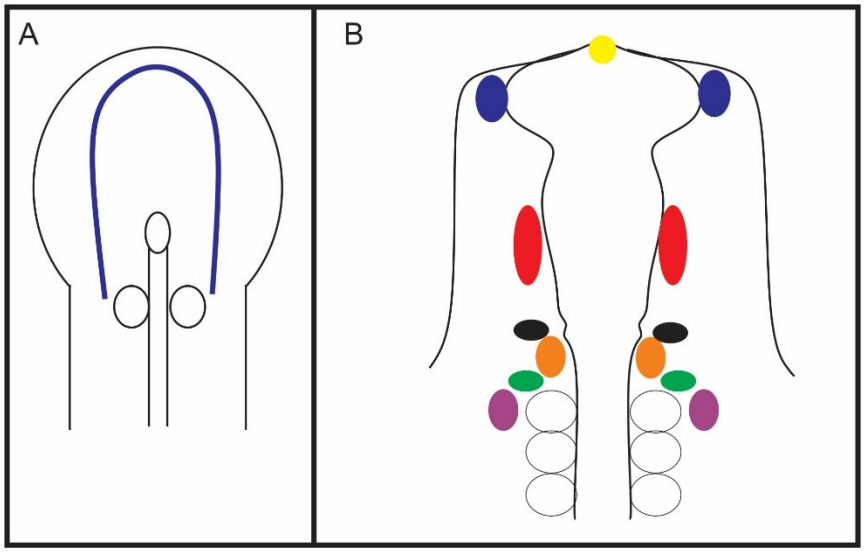

Figure 4.1: Schematic illustrating the establishment of the PPR and its subdivision into distinct placodes. **A**) The PPR: a horse-shoe shaped band of epithelium that extends approximately from the first pair of somites and surrounds the anterior of the embryo (blue). **B**) An illustration of the cranial placodes. Yellow: the unpaired adenohypophysis; Blue: the lens placodes; Red: the trigeminal placodes; Purple: the epibranchial placodes; Orange: the otic placodes; Uncolored circles: somites. Adapted from Jidigam and Gunhaga, 2013.

Shortly after the delineation of the presumptive NC region, the PPR becomes distinguishable from all other tissues in the region by the expression of Fgf and the suppression of both Wnts and Bmps (Groves & LaBonne, 2014). After this initial delineation, the PPR becomes defined by expression of members of the Six (homologous to the *Drosophila sine oculis* gene) family and by its activating co-factor Eya (*eyes absent*) and its repressive co-factors Groucho and Dach (*Dachshund*) (Baker & Bronner-Fraser, 2001; Zou *et al*., 2004; Baker, 2005; Schlosser, 2005; Schlosser, 2006; Meulemans &

Bronner-Fraser, 2007; Schlosser *et al*, 2008; Whitlock, 2008; Kourakis & Smith, 2007; Grocott *et al*., 2012; Bhat *et al.*, 2013; Groves & LaBonne, 2014; Schlosser *et al*., 2014; Saint-Jeannet & Moody, 2014). However, it should be noted that it is currently unclear whether the effects of Fgfs, Wnts, and Bmps on the induction of *Six* and *Eya* genes is direct or indirect because very little is known about the regulatory enhancers controlling the expression of pre-placodal genes (Groves & LaBonne, 2014). The exception to this statement is that of *Six*1, for which a single enhancer has so far been identified; however, this regulatory element did not contain binding sites for the direct transcriptional effectors of the Fgf, Bmp, or Wnt pathways (Sato *et al*., 2010; Sato *et al*., 2012; Groves & LaBonne, 2014). Contained within this enhancer was, however, a binding site for Msx1, a protein that has been shown in other systems (e.g. tooth) to be regulated by the expression of Bmps (Groves & LaBonne, 2014). There is, however, evidence that the expression of *Six* and *Eya* genes are regulated by other transcription factors that are expressed earlier in the NPB (Groves & LaBonne, 2014). One such of these regulatory interactions is that of *Distal-less* gene family members *Dlx*3 and *Dlx*5 which have been shown in zebrafish, *Xenopus*, and chick to upregulate expression of both *Six* and *Eya* genes (Groves & LaBonne, 2014; Saint-Jeannet & Moody, 2014). Additionally, knock-down of these *Dlx* genes can attenuate expression of pre-placodal genes (Groves & LaBonne, 2014). Other transcription factors, such as Iroquois (*Irx*), which are expressed in the PPR just prior to the expression of *Six* and *Eya* genes have been shown to positively regulate their expression (Schlosser, 2008; Groves & LaBonne, 2014; Saint-Jeannet & Moody, 2014; Schlosser *et al*., 2014). Furthermore, it has been shown that *Irx* genes, in some circumstances, can be regulated by both Fgfs and Bmps (Groves & LaBonne, 2014).

Thus, the induction of the PPR, similar to the induction of the presumptive NC, involves a very complex combinatorial code of gene expression. These signaling pathways act together to control the expression of downstream effectors that specify the PPR. These transcription factors also work to sharpen the boundaries between the non-neural epithelium, the PPR, the presumptive NC, and the neural ectoderm through positive autoregulation and mutual inhibition (Groves & LaBonne, 2014; Saint-Jeannet & Moody, 2014). For example, in the PPR, *Dlx*5 and *Gata*3 are initially required for the induction of *Six* and *Eya* genes; subsequently, once expression of *Six* and *Eya* genes has been initiated, their expression is maintained through positive autoregulation while the *Dlx*5 and *Gata*3 genes are repressed by a *Six*1; *Eya*1/2 complex (Baker, 2005; Schlosser, 2005; Schlosser, 2006; Bhat *et al*., 2013; Groves & LaBonne, 2014; Schlosser *et al*., 2014; Saint-Jeannet & Moody, 2014). However, until more is known about the regulatory elements of down-stream factors (i.e. *Six* and *Eya* genes for the placodes and NC specifier genes for the NC) that delineate these territories in the NPB region, our understanding of placodal pre-patterning at the NPB will remain incomplete.

4.1.2.2 – Induction of the Craniofacial Placodes

During the early development of the craniofacial placodes (i.e. once *Six* and *Eya* expression has been upregulated and the PPR has become distinct from the presumptive NC), the placodal field is multi-potential. This was initially demonstrated by Jacobson (1963) who showed, through transplantation experiments in amphibians, that within the ectoderm adjacent to the anterior neural plate, cells were competent to give rise to any placode (Saint-Jeannet & Moody, 2014). Further experiments demonstrated that when the PPR was rotated along its anterior-posterior axis at the early neurula stage, placodes formed

largely based on their new position (Jacobson, 1963 reviewed in Saint-Jeannet & Moody, 2014). However, if the same experiment was performed only hours later, the placodes largely developed based on their original position in the PPR (Jacobson, 1963 reviewed in Saint-Jeannet & Moody, 2014). These experiments therefore suggested that, while the cells in the PPR are originally competent to develop into any placode, there is a progressive restriction to their ability over time (Jacobson, 1963 reviewed in Saint-Jeannet & Moody, 2014). It was later determined that this initial ground state, in which *Six*1 and *Eya*1 are expressed throughout the entire PPR, was characteristic of the lens placode (Bailey *et al*., 2006). This lens fate was subsequently reprogrammed through the establishment of molecularly distinct sub-regions (along the anterior-posterior axis) which, through combinatorial gene expression, give rise to specific placodes (Schlosser, 2005; Schlosser, 2006; Schlosser *et al*., 2014). It has been determined that expression of *Six* and *Eya* genes, while characteristic of the PPR as a whole, may also be responsible for this segregation of the PPR into the anterior and posterior zones through the induction of a number of down-stream target genes (Schlosser *et al*., 2014).

The *Six* and *Eya* proteins are able to induce a large number of downstream targets due to the way in which co-factor binding alters Six's ability to bind to DNA. As mentioned above, the vertebrate Six gene family (*Six1-6*) is able to form both activating and repressive complexes with its co-factors Eya, Groucho, and Dach (Schlosser, 2005; Schlosser, 2006; Neilson *et al*., 2010; Groves & LaBonne, 2014; Saint-Jeannet & Moody, 2014). The *Six* genes are characterized by a homeodomain-type DNA-binding region and an N-terminal Six domain (SD) that binds to its co-factors (Kawakami *et al*., 2000; Groves & LaBonne, 2014; Saint-Jeannet & Moody, 2014). Eya proteins themselves are unable to

bind directly to DNA and can only access the nuclear compartment by binding to other transcription factors via the C-terminally located Eya domain (ED) (Kawakami *et al.*, 2000; Zou *et al*., 2004; Meulemans & Bronner-Fraser, 2007; Fortunato *et al*., 2014; Saint-Jeannet & Moody, 2014). Thus, Eya proteins can interact with many of the Six proteins, and also with many other transcription factors, therefore enabling them to be critical modifiers of Six protein function. This Six-Eya signaling cascade is not restricted solely to the delineation of the PPR, but rather is part of a highly conserved regulatory network termed the "Retinal Determination Gene Network" or the "Pax-Six-Eya-Dach" network (Kawakami *et al.*, 2000; Fortunato *et al*., 2014). This regulatory network has been identified in both insects and vertebrates and is involved in a variety of developmental processes (Kawakami *et al.*, 2000; Fortunato *et al*., 2014). *Pax* expression has also been recorded in the PPR, however it seems that, in the PPR, *Pax* expression is downstream of *Six,* unlike what has been described in *Drosophila* (Kawakami *et al.*, 2000; Fortunato *et al*., 2014). Thus, differential interactions of the three Six (*Six1, Six2,* and *Six4*) family genes with the four Eya (*Eya1, Eya2, Eya3,* and *Eya4*) family members and co-repressors Groucho and Dach can give rise to a wide variety of downstream gene expression patterns, serving to help segregate the PPR into distinct sub-regions (Kawakami *et al.*, 2000; Fortunato *et al*., 2014; Groves & LaBonne, 2014; Saint-Jeannet & Moody, 2014). The mechanisms governing how differential gene expression is established in these sub-regions, however, it not completely understood.

This differential gene expression pattern between the anterior and posterior regions is first observed at the early neurula stage in most model organisms (Schlosser, 2005; Schlosser, 2006; Schlosser *et al*., 2014). The sub-division of this region utilizes both the

down-stream targets of the Six-Eya regulatory network and many of the transcription factors that were required for the initial establishment of the PPR. This thus suggests that the adjacent tissues (both mesenchymal and epithelial) influence the induction and patterning of the placodes themselves. During the early neurula stage of embryogenesis, the anterior sub-region is characterized by the expression of such genes as *Bmp*s, *Fgf*s, *Otx2, Pax6, Six3*, and *Six6* to name but a few (Baker & Bronner-Fraser, 2001; Baker, 2005; Schlosser, 2005; Schlosser, 2006; Groves & LaBonne, 2014; Saint-Jeannet & Moody, 2014; Schlosser *et al*., 2014). The anterior sub-region will give rise to both neural and non-neural placodes, including the adenohypophyseal, olfactory, and lens placodes (Meulemans & Bronner-Fraser, 2007; Bhat & Riley, 2011; Bhat *et al*., 2013; Schlosser *et al*., 2014; Saint-Jeannet & Moody, 2014; Groves & LaBonne, 2014). The posterior sub-region, on the other hand, is characterized by the expression of such genes as *Wnt*s, *Gbx2, Irx1, Irx2A, Irx3, Pax2*, and *Pax8* (Meulemans & Bronner-Fraser, 2007; Bhat & Riley, 2011; Bhat *et al*., 2013; Schlosser *et al*., 2014; Saint-Jeannet & Moody, 2014; Groves & LaBonne, 2014). The posterior placodal sub-region will give rise only to neural placodes, including the otic, epibranchial, laterial line (in some species), and hypobranchial placodes (Meulemans & Bronner-Fraser, 2007; Bhat & Riley, 2011; Bhat *et al*., 2013; Schlosser *et al*., 2014; Saint-Jeannet & Moody, 2014; Groves & LaBonne, 2014). Interestingly, the trigeminal placodes form between these two placodal sub-regions in an area that is primarily characterized by the expression of *Wnt*s, *Pdgf*, and the *Irx* family genes (Saint-Jeannet & Moody, 2014). As both the anterior and posterior sub-regions are still able to give rise to more than one type of placode, they have also been referred to as "equivalence domains" or "equivalence groups" (Schlosser, 2006; Saint-Jeannet & Moody, 2014).

Though each sub-region can be characterized by the expression of specific genes, it must be noted that the boundaries of gene expression within these domains are not always the same. For instance, Bmp signaling, while restricted to the anterior sub-region is never expressed at the level of the adenohypophyseal placode (Saint-Jeannet & Moody, 2014). Additionally, while Bmp is expressed at the levels of the presumptive olfactory and lens placodes, expression in the olfactory region is transient, as prolonged expression of Bmp transforms the olfactory placode to a lens fate (Saint-Jeannet & Moody, 2014).

After these distinct sub-regions have been established, these factors and their downstream targets become restricted to progressively smaller areas within each domain, thus establishing the molecular identity of the individual placodes (Figure 4.1B) (Saint-Jeannet & Moody, 2014). This combinatorial code of gene expression therefore provides a molecular signature for each sensory placode which will, in turn, drive their development into mature sensory organs (Meulemans & Bronner-Fraser, 2007; Bhat & Riley, 2011; Bhat *et al*., 2013; Schlosser *et al*., 2014; Saint-Jeannet & Moody, 2014; Groves & LaBonne, 2014). It is currently not understood whether large-scale cellular migration is required for the development of the cranial placodes, as previous studies have yielded contradictory results (reviewed in Steventon *et al*., 2014). In *Xenopus* and zebrafish, experiments have shown that the migration of the NC is required for placode formation as the migration of the NCCs "push" the placodal cells into position whereas in other species, these large-scale cellular re-arrangements have not been observed (Theveneau *et al*., 2013; Steventon *et al*., 2014). Thus, while we have begun to unravel the induction and patterning of the cranial placodes, much remains to be uncovered before the processes and genes governing their development are fully understood.

4.1.2.3 - Induction of Derivative Structures

As there are so many different cranial placodes, each giving rise to different derivatives, I will be discussing their further development only briefly. This discussion will be presented by type, beginning with the neurogenic placodes.

4.1.2.3.1 - Neurogenic Cranial Placodes

The neurogenic placodes, which contribute sensory neurons to the peripheral nervous system, include the olfactory, profundal, trigeminal, epibranchial, hypobranchial, otic, and lateral line placodes (Meulemans & Bronner-Fraser, 2007; Whitlock, 2008; McCabe & Bronner-Fraser, 2009; Bhat *et al*., 2013; Lassiter *et al.*, 2014). The molecular factors responsible for neurogenic placode development include Pax2, Pax3, Pax8, Dmrt4, Islet1, Tbx2, and others which have been summarized in a number of excellent reviews, and as such, will not be further discussed here (Krimm, 2007; Canning *et al*., 2008; Padanad & Riley, 2011; Bhat & Riley, 2011; Bhat *et al*., 2013; Schlosser *et al*., 2014; Saint-Jeannet & Moody, 2014). The development of the neurogenic derivatives (i.e. placodal sensory neurons) are defined by two key cellular processes: i) neuronal determination, where primed progenitor epithelial cells are selected for a neuronal fate and undergo neurogenesis and neuronal differentiation, and ii) delamination from the epithelium, whereby cells detach from their epithelial neighbours and escape through a break in the basement membrane in the mesenchyme as migratory sensory neuroblasts, a process different from the EMT observed in the NC (Graham *et al*., 2007; Lassiter *et al*., 2014). The specification, neuronal determination, and delamination of these neurogenic placodes is governed by a number of factors, including Notch, Fgfs, Wnts, and Bmps. For a comprehensive review of the genetic cascades responsible for the induction and patterning

of the trigeminal, epibranchial, otic, and olfactory placodes see Lassiter *et al.* (2014); of the lateral line, see Piotrowski & Baker (2014); of the otic and olfactory placodes, see Maier *et al*. (2014); whereas for an overall review, see Schlosser & Northcutt (2000) and Schlosser (2006). As the neurogenic cranial placodes bear little resemblance to non-neurogenic derivatives, they are irrelevant to the discussions here about the conjunctival papillae and will therefore not be further discussed.

4.1.2.3.2 - Non-Neurogenic Cranial Placodes

The non-neurogenic placodes, on the other hand, which include the lens and adenohypophyseal placodes, do not contribute sensory neurons to the peripheral nervous system; rather, they contribute specialized epithelial structures to regions that are independently innervated (Zou *et al*., 2004; Meulemans & Bronner-Fraser, 2007; Whitlock, 2008; McCabe & Bronner-Fraser, 2009; Garcia *et al*., 2011; Saint-Jeannet & Moody, 2014; Maier *et al*., 2014).

The adenohypophyseal placode is the most anterior placode to develop and, unlike all other cranial placodes, is not paired (Zou *et al*., 2004; Meulemans & Bronner-Fraser, 2007; Whitlock, 2008; McCabe & Bronner-Fraser, 2009; Garcia *et al*., 2011; Saint-Jeannet & Moody, 2014; Maier *et al*., 2014). After specification (via Pitx3, Lhx3, Six6, and Msx1), the adenohypophyseal placode undergoes a dorsal out-pocketing to form Rathke's Pouch in the midline oral ectoderm of the roof of the oral cavity (McCabe & Bronner-Fraser, 2009; Saint-Jeannet & Moody, 2014). Expression of Bmp is also required for the induction of the placode and the initial evagination of the oral ectoderm to form the pouch rudiment (Takuma *et al*., 1998; Baker & Bronner-Fraser, 2001; McCabe & Bronner-Fraser, 2009; Saint-Jeannet & Moody, 2014). This out-pocketing will form the "epithelial" part of the

pituitary gland (Baker & Bronner-Fraser, 2001; McCabe & Bronner-Fraser, 2009; Saint-Jeannet & Moody, 2014). Where the adenohypophysis contacts the diencephalon, the neurohypophysis is formed, providing the "neural" part of the pituitary gland (Saint-Jeannet & Moody, 2014). After the adenohypophysis has formed the "epithelial" portion of the pituitary gland, different endocrine cells are generated within it in a precise temporal and spatial order (Baker & Bronner-Fraser, 2001; Schlosser, 2006; Whitlock, 2008; McCabe & Bronner-Fraser, 2009). For an excellent review of this process, see Baker & Bronner-Fraser (2001).

The lens placodes, on the other hand, are a set of bilateral placodes that form at the lower border of the anterior region of the PPR, mediated by the expression of Mafb, Foxe3, Sox1, and Pax6 (Baker & Bronner-Fraser, 2001; Schlosser, 2006; Bhat & Riley, 2011; Garcia *et al*., 2011; Bhat *et al*., 2013; Schlosser *et al*., 2014). In response to contact from the evaginated diencephalon, these placodes thicken and then invaginate (along with the diencephalon) to form the lenses of the paired eyes (Martinez-Morales & Wittbrodt, 2009; Graw, 2010; Vergara & Canto-Soler, 2012; Sinn & Wittbrodt, 2013). While the eye is innervated after the formation of the neural retina (derived from the diencephalon), the lens placode contributes the specialized epithelial structure (lens) which is required for vision (Fuhrmann, 2010; Gunhaga, 2011). For an excellent review of this process, see Baker & Bronner-Fraser (2001).

4.1.3– The Cutaneous Placodes

Although the cutaneous placodes have often been referred to interchangeably as "cutaneous papillae" or "cutaneous germ" in the literature, they are epithelial thickenings that are responsible for the induction and patterning of all ectodermal (cutaneous)

appendages, including: teeth; feathers; hair; mammary, sweat, and salivary glands; and scales (Ferguson *et al*., 1998; Wolpert, 1998; Eames & Schneider, 2005; Zhang *et al*., 2009; Dhouailly, 2009; Cui et al., 2010; Duverger & Morasso, 2009; Catón & Tucker, 2009; Chen *et al*., 2009; Koussoulakou *et al*., 2009; Bei, 2009; Takahashi *et al*., 2010; Sayama *et al*., 2010; Jiang *et al*., 2011; Painter *et al*., 2012; Sennett & Rendl, 2012; Chuong *et al*., 2013; O'Connor *et al*., 2013). Similarly to the cranial placodes, the structures derived from these cutaneous placodes are vertebrate specific and were instrumental in allowing the radiation of vertebrates into various climates (e.g. through insulation due to the evolution of hair, feathers, and scales), into various habitats (e.g. via evolution of feathers in flying vertebrates), and enabled the consumption of varied food types (e.g. via evolution of different types of teeth) to name but a few. Cutaneous placodes are also ultimately responsible for the temporal and spatial organization of these cutaneous appendages (Ferguson *et al*., 1998; Wolpert, 1998; Eames & Schneider, 2005; Zhang *et al*., 2009; Dhouailly, 2009; Cui et al., 2010; Duverger & Morasso, 2009; Catón & Tucker, 2009; Chen *et al*., 2009; Koussoulakou *et al*., 2009; Bei, 2009; Takahashi *et al*., 2010; Sayama *et al*., 2010; Jiang *et al*., 2011; Painter *et al*., 2012; Sennett & Rendl, 2012; Chuong *et al*., 2013; O'Connor *et al*., 2013). Additionally, as with the cranial placodes, these cutaneous placodes are highly evolutionarily conserved, with similar signaling cascades required for their development across species and types of skin appendage (Ferguson *et al*., 1998; Wolpert, 1998; Eames & Schneider, 2005; Zhang *et al*., 2009; Dhouailly, 2009; Cui et al., 2010; Duverger & Morasso, 2009; Catón & Tucker, 2009; Chen *et al*., 2009; Koussoulakou *et al*., 2009; Bei, 2009; Takahashi *et al*., 2010; Sayama *et al*., 2010; Jiang *et al*., 2011; Painter *et al*., 2012; Sennett & Rendl, 2012; Chuong *et al*., 2013; O'Connor *et al*., 2013).

This high degree of conservation, however, does not imply that these structures are homologous or that they have evolved together. The similarity in the genetic cascades involved in their induction and patterning may rather imply that these cascades have been similarly co-opted or, simply, that similar gene regulatory networks are required for the induction of an epithelial thickening (Ferguson *et al*., 1998; Wolpert, 1998; Eames & Schneider, 2005; Zhang *et al*., 2009; Dhouailly, 2009; Cui et al., 2010; Duverger & Morasso, 2009; Catón & Tucker, 2009; Chen *et al*., 2009; Koussoulakou *et al*., 2009; Bei, 2009; Takahashi *et al*., 2010; Sayama *et al*., 2010; Jiang *et al*., 2011; Painter *et al*., 2012; Sennett & Rendl, 2012; Chuong *et al*., 2013; O'Connor *et al*., 2013). To date, this has not been well investigated and therefore, requires further study.

As described earlier, the induction and patterning of the cutaneous placodes also involves three main steps: i) pre-patterning of the epithelium, ii) induction of the placodes via mesenchymal-epithelial signaling, and iii) induction and patterning of the derivative structures. As the cutaneous placodes give rise to a wide variety of derivative structures, there is a large variation in the molecular signals that drive this subsequent differentiation. As hair, feather, and dental placode development are among the best understood, they will serve as the focus of the subsequent sections.

4.1.3.1 – Hair Placodes

Hair placode development, as with all other placodes, proceeds through an ordered series of epithelial-mesenchymal interactions (Figure 4.2) (Rendl *et al*., 2005; Törnqvist *et al*., 2010; Woo *et al*., 2012; Sennett & Rendl, 2012). However, there is also a temporal component to the regulation of hair development, especially in mammals (Duverger & Morasso, 2009; Sennett & Rendl, 2012). It is this combination of molecular and temporal

regulation that coordinates to produce the many different types of hair, including: eyelashes, vibrissae (whiskers), tail hairs, guard hairs, awl/auchene hairs, and zigzag hairs (Duverger & Morasso, 2009; Enchell-Seijffers *et al*., 2010; Sayama *et al*., 2010; Clavel *et al*., 2012; Sennett & Rendl, 2012). As hair development has been best studied in the mouse, I will restrict the following discussion to the mouse model.

4.1.3.1.1 - Primary Wave of Hair Placode Development

In the mouse, there are three waves of hair development, referred to as the primary, secondary, and tertiary waves (Duverger & Morasso, 2009; Sennett & Rendl, 2012; Clavel *et al*., 2012). The primary wave of hair development begins around embryonic day (E) 13.5 and gives rise to the guard hairs of the pelage (Cui et al., 2010; Duverger & Morasso, 2009; Enshell-Seijffers *et al*., 2010; Sayama *et al*., 2010; Sennett & Rendl, 2012; Clavel *et al*., 2012). These are long, straight hairs with sensory functions that protrude above the coat and represent only about 1-3% of the total number of hairs in the coat (Cui et al., 2010; Duverger & Morasso, 2009; Enshell-Seijffers *et al*., 2010; Sayama *et al*., 2010; Sennett & Rendl, 2012; Clavel *et al*., 2012). The induction of the primary wave of hair development begins when a signal from the underlying mesenchyme induces a thickening in the overlying epithelium (Duverger & Morasso, 2009; Törnqvist *et al*., 2010; Woo *et al*., 2012; Sennett & Rendl, 2012). Prior to this inductive signal, there is widespread expression of Wnt ligands and β-catenin in the epithelium (Duverger & Morasso, 2009; Sayama *et al*., 2010; Enshell-Seijffers *et al*., 2010; Sennett & Rendl, 2012; Huang *et al*., 2012; Woo *et al*., 2012; Myung *et al*., 2013). These factors help establish the competency of the epithelium so that it can respond to the inductive signal from the mesenchyme (Cui et al., 2010; Sennett & Rendl, 2012; Woo *et al*., 2012). This pre-patterning leads to the induction

of other placodal factors, including Edar (ectodysplasin A receptor) and Dkk4 (dickkopf) which, if inhibited, will abrogate placode formation (Cui et al., 2010; Sayama *et al*., 2010; Duverger & Morasso, 2009; Sennett & Rendl, 2012). There is also, at this time, the localized expression in the mesenchyme of Sox2 and Sdc1 beneath each "pre-placode" (Sennett & Rendl, 2012). Beyond this point of hair development, it has proven difficult to isolate which genes are responsible for each individual step, as they appear almost simultaneously (Sennett & Rendl, 2012). It is known, however, that Fgfs and Bmps are required for both the induction and patterning of the hair placodes, although the exact family members required have not yet been determined (Duverger & Morasso, 2009; Cui et al., 2010; Sennett & Rendl, 2012). At E13.5, Edar expression becomes restricted to the placode while Eda expression is restricted to the inter-placodal regions (Zhang *et al*., 2009; Cui et al., 2010; Sayama *et al*., 2010; Duverger & Morasso, 2009; Sennett & Rendl, 2012). It is thought that this restricted Eda expression serves two functions: i) to promote placodal fate by suppressing Bmp2 and upregulating the Bmp inhibitors Ccn2 and follistatin and ii) the upregulation of Shh in the placode by Eda, which, along with Pdgfa regulates cell proliferation and drives invagination into the underlying mesenchyme, producing the hair shaft (Sennett & Rendl, 2012). The restriction of Bmp expression by Eda and Fgf is critical for hair placode formation, as mice deficient in noggin lack all but the primary hair follicles (this process has been excellently reviewed by Sennet & Rendl (2012) and will not be discussed further here). The regular spacing of the placodes is thought to be regulated by a LALI model and has, to date, come the closest to meeting all of the requirements of a Turing model (Sick *et al*., 2006; Economou & Green, 2014). Cell adhesion and planar cell

polarity are also hypothesized to play a role in establishing the pattern of hair placode development (Duverger & Morasso, 2009; Chen & Chuong, 2012).

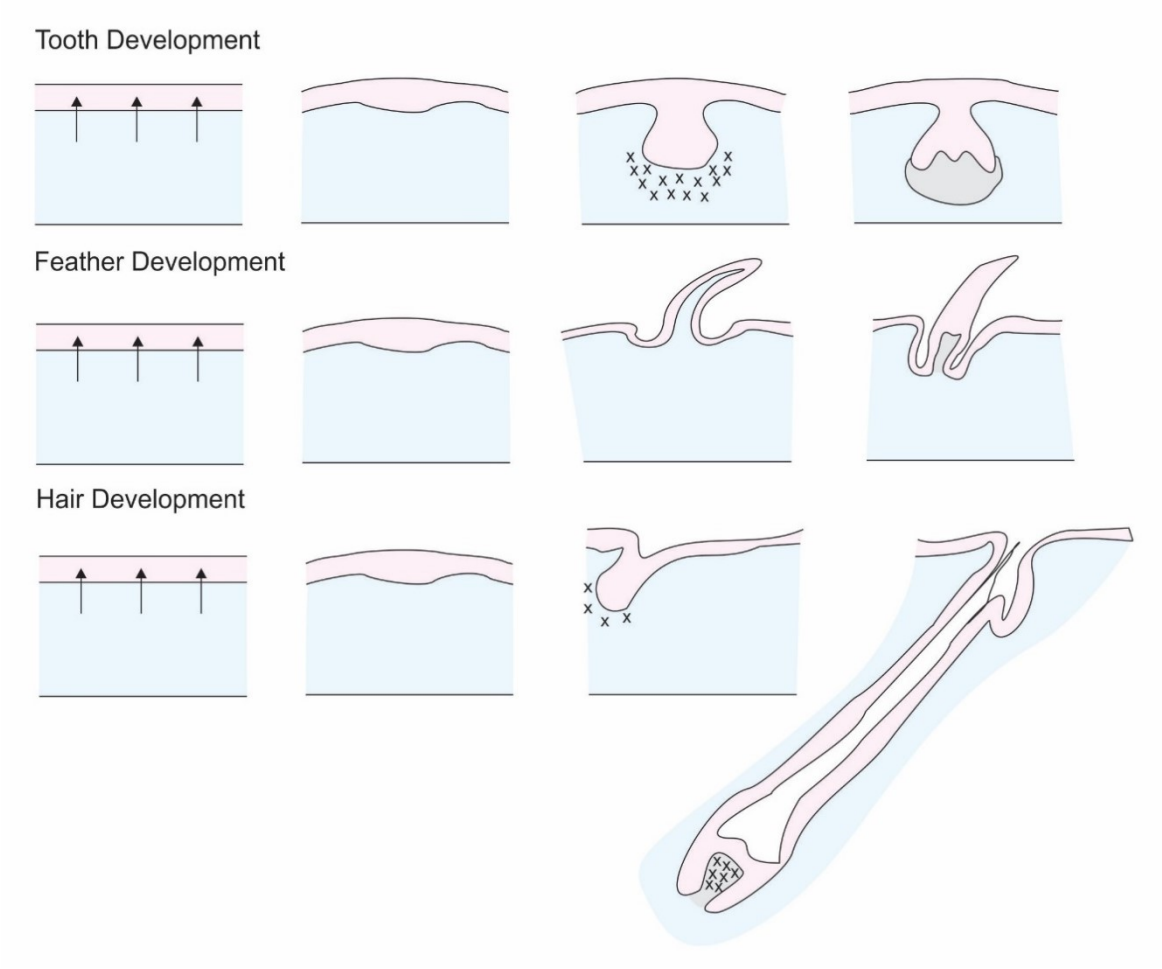

Figure 4.2: A schematic illustrating the induction and patterning of the hair, feather, and tooth placodes and their subsequent derivative structures. This process begins with the acquisition of epithelial competency and is followed by the initiation of a mesenchymal-epithelial signal cascade. This inductive cascade results in the induction of a placode. This placode then undergoes complex morphogenetic movements, invagination into the underlying mesenchyme and the induction of the derivative structures. Epithelium: pink; mesenchyme: blue; mesenchymal condensation: crosses; dermal papilla: light grey. Tooth adapted from Tucker and Sharpe, 2004; Feather adapted from Prum, 1999; and Hair adapted from Fuchs, 2007.

4.1.3.1.2 - Secondary and Tertiary Waves of Hair Placode Development

The secondary wave of hair placode induction begins around E16 and will give rise to the awl and auchene hairs; while the tertiary wave of hair placode induction begins

around E18 and will produce zigzag hairs (Cui et al., 2010; Duverger & Morasso, 2009; Sayama *et al*., 2010; Sennett & Rendl, 2012). Awl hairs are straight, though shorter than the guard hairs and will contribute approximately 30% of the coat (Duverger & Morasso, 2009; Enshell-Seijffers *et al*., 2010; Clavel *et al*., 2012). Zigzag hairs, on the other hand, are the most abundant hair type of the coat and are responsible for insulation (Duverger & Morasso, 2009). These are characterized by 3-4 alternating bends, causing them to resemble a zigzag (Duverger & Morasso, 2009; Enshell-Seijffers *et al*., 2010; Sayama *et al*., 2010; Clavel *et al*., 2012; Sennett & Rendl, 2012). The auchene hairs are the least well understood type of hair and only contributes nominally to the coat (Duverger & Morasso, 2009). These secondary and tertiary waves develop very similarly to the primary hairs, though the key factors change in the subsequent waves (Cui et al., 2010; Sennett & Rendl, 2012). For example, while expression of noggin is present in the dermal papilla during primary hair follicle development, it is not a critical factor for the induction and patterning of primary hair follicles as mutants lacking noggin expression develop normal guard hairs (Cui et al., 2010; Sennett & Rendl, 2012). In noggin mutants, however, no secondary or tertiary hair types will develop (Sennett & Rendl, 2012). This provides a fantastic example of how temporal regulation, paired with the same genetic cascades, can provide varied phenotypes. This may also be due, in part, to pioneer factors, which are transcription factors that bind directly to condensed chromatin in an ATP-independent process, enabling the transcription of different downstream products at different times (Groves & LaBonne, 2014). No pioneer factors have yet been identified or described in this system.

4.1.3.2 – Feather Placodes

Feather development, similar to hair development, is regulated through both molecular and temporal mechanisms (Wolpert, 1998; Eames & Schneider, 2005; Drew *et al*., 2007; Jiang *et al*., 2011; Painter *et al*., 2012; Yue *et al*., 2012; Chuong *et al*., 2013). During feather development, the placodes are organized into distinct tracts (macro-organization) such as spinal and femoral tracts and are also organized within each tract, where the primary row develops first and subsequent placodes form in a hexagonal grid (micro-organization) (Mou *et al*., 2011; Chuong *et al*., 2013). Again, similar molecular factors are involved in the development of all feather placodes (described below), however the primary row in each tract is regulated differently from the subsequent rows (Wolpert, 1998). It is currently unknown what molecular factors regulate the complex micro-organization of the feather field; however, it likely involves an epithelial-mesenchymal induction and acquisition of competence (Wolpert, 1998; Drew *et al*., 2007; Dhouailly, 2009).

Feather placode development begins, in the chick, around E8 with widespread expression of Wnt7a, β-catenin, gremlin, and Wnt11 in the epithelium (Widelitz, 2008; Suksaweang *et al*., 2012; Wells *et al*., 2012 Chuong *et al*., 2013). There is then an inductive cue from the underlying mesenchyme, the identity of which is currently unknown (Wolpert, 1998; Eames & Schneider, 2005; Dhouailly, 2009). After this inductive signal from the underlying mesenchyme has been initiated, the expression of Wnt7a and β-catenin become restricted to the feather placodes while gremlin and Wnt11 become restricted to the inter-placodal regions (which will give rise to the inter-follicular tendon, muscle, and dermis) (Mou *et al*., 2011; Jiang *et al*., 2011; Li *et al*., 2012; Painter *et al*., 2012; Wells *et*

al., 2012; Chuong *et al*., 2013). Eda and Edar/Edaradd are both involved in feather development, where *Eda* is expressed in the inter-placodal region and Edar is restricted to the feather placode; however, it is currently unknown whether the role of Eda/Edar is similar to that in hair (regulating Bmp expression and upregulating Shh in the placode) or not (Drew *et al.,* 2007; Painter *et al*., 2012; Chuong *et al*., 2013). While the exact pattern of molecular expression is not known, a group of placodal activators and inhibitors have been determined (Wolpert, 1998; Drew *et al*., 2007). Activators include: Fgf2 and -4, noggin, follistatin, Bmp7, Tgf-β2, β-catenin, Wnt3a, Shh, and many others while the inhibitors include: Bmp2 and -4, delta-1, soluble FGFRs, Wnt11, and Egf (Wolpert, 1998; Eames & Schneider, 2005; Dhouailly, 2009; Jiang *et al*., 2011; Painter *et al*., 2012; Chuong *et al*., 2013; O'Connor *et al*., 2013). This complex regulation of activators and inhibitors establishes the spatial patterning of the hexagonally arranged feather placodes through lateral inhibition (which is believed to adhere to Turing's model, although this has not yet been conclusively demonstrated) and cell adhesion properties (Eames & Schneider, 2005; Mou *et al*., 2011; Li *et al*., 2012). The extracellular matrix has also been implicated in the patterning of the feather placode (Stuart *et al*., 1972; Sengel, 1990; Miura, 2007). Interestingly, the hexagonal patterning of each tract is individual to each chick, indicating that patterning is individually established in each chick by epigenetic factors (Chuong *et al*., 2013). Following placode development and patterning, the molecular cascade diverges from that of other placodes, with rapid proliferation and the extension of the placode above the epithelium (Figure 4.2) (Eames & Schneider, 2005; Drew *et al*., 2007; Widelitz, 2008; Dhouailly, 2009; Jiang *et al*., 2011; Mou *et al*., 2011; Li *et al*., 2012; Ng *et al*., 2012; Painter *et al*., 2012; Yue *et al*., 2012; Suksaweang *et al*., 2012; Wells *et al*., 2012). This

has been well reviewed by elsewhere and will not be discussed further here (Eames & Schneider, 2005; Drew *et al*., 2007; Widelitz, 2008; Dhouailly, 2009; Jiang *et al*., 2011; Mou *et al*., 2011; Li *et al*., 2012; Ng *et al*., 2012; Painter *et al*., 2012; Yue *et al*., 2012; Suksaweang *et al*., 2012; Wells *et al*., 2012).

4.1.3.3 – Dental Placodes

Tooth development, in the mouse, begins at E10 with widespread expression of Wnts and Shh (Mammoto *et al*., 2011; Lin *et al*., 2011). This expression acts to define the oral (non-odontogenic) and dental (odontogenic) epitheliums, restricting Shh expression to the dental epithelium (Koussoulakou *et al*., 2009; Lin *et al.*, 2011; Tucker & Fraser, 2014). This dental epithelium, at E11, will thicken to form the dental lamina (Liu *et al.*, 2008; Bei, 2009; Koussoulakou *et al*., 2009; Cobourne & Sharpe, 2010; Zhou *et al*., 2011; Matalova *et al*., 2012; Tucker & Fraser, 2014). At this phase of tooth development, the instructive ability resides within the epithelium and overexpression of Wnts at this stage will result in the formation of supernumerary teeth (Chen *et al*., 2009; Catón & Tucker, 2009; Bei, 2009; Cobourne & Sharpe, 2010; Lin *et al*., 2011). Shortly after E11, the mesenchyme acquires inductive ability and by E11.5, the dental placodes form, a process requiring expression of Fgfs and Wnts, and the inhibition of Bmps (Liu *et al*., 2008; Bei, 2009; Koussoulakou *et al*., 2009; Mammoto *et al*., 2011; Zhou *et al*., 2011; Landin *et al*., 2012). The exact inductive cascade for these placodes, as with other placodes, is currently not well understood, although it is known that epithelial expression of Fgf8 and Bmp4 is required for *Pitx2* expression, a marker of the dental lamina, and the induction of underlying mesenchymal transcription factors, such as *Msx1*/*2*, *Pax9* (Ferguson *et al*., 1998; Catón & Tucker, 2009; Chen *et al*., 2009; Koussoulakou *et al*., 2009; Bei, 2009; Takahashi *et al*.,

2010). Furthermore, if the expression of either *Pax9* or *Pitx2* is abrogated, teeth will not form (Liu *et al*., 2008; Catón & Tucker, 2009; Chen *et al*., 2009; Koussoulakou *et al*., 2009; Bei, 2009; Zhou *et al*., 2011). After the establishment of the dental lamina, distinct placodes will form, and it is thought that each placode will give rise to an individual type of tooth (Liu *et al*., 2008; Bei, 2009; Koussoulakou *et al*., 2009; Mammoto *et al*., 2011). The mouse, however, has evolved a partial dentition, in which only one pair of incisors form separated by a diastema (or tooth-less region) from three pairs of molars (Koussoulakou *et al*., 2009; Bei, 2009; Catón & Tucker, 2009; Cobourne & Sharpe, 2010; Lin *et al*., 2011; Porntaveetus *et al*., 2011; Matalova *et al.*, 2012). As the second and third pairs of molars form by a different mechanism (reviewed by Catón & Tucker, 2009; Cobourne & Sharpe, 2010; Juuri *et al*., 2013; Tucker & Fraser, 2014), they will not be discussed further here. Therefore, the mouse only forms dental placodes for a pair of incisors and molars. The formation of the diastema has been attributed to weak expression of *Pax9* and the downregulation of *Shh* expression in the placodes, causing the pre-placodes to degenerate (Koussoulakou *et al*., 2009; Bei, 2009; Catón & Tucker, 2009; Cobourne & Sharpe, 2010).

As mentioned above, epithelial expression of Bmp4 and Fgf8 are also required for the induction of mesenchymal expression of *Msx1* and *Barx1*, respectively (Koussoulakou *et al*., 2009; Catón & Tucker, 2009). These genes, once activated, induce the expression of Bmp4 and Fgf8 in the underlying mesenchyme and create discrete expression fields, where mutual antagonism restricts expression of Bmp4 and Msx1 to the anterior dental field (which will form the incisors) and Fgf8 and Barx1 to the posterior dental field (which will form the molars) (Koussoulakou *et al*., 2009; Catón & Tucker, 2009). Additionally,

this mesenchymal expression of Msx1 represses Osr2, restricting Osr2 to the lingual oral mesenchyme (Zhou *et al*., 2011). Osr2 in turn restricts Msx1 expression to the dental mesenchyme (Zhou *et al*., 2011). In the absence of Osr2, supernumerary teeth will develop in the lingual aspect of the oral epithelium, outside of the normal dental field (Zhou *et al*., 2011). It should also be noted that it is difficult to identify the genetic cascades involved in the induction of the dental placode, as there seems to be redundancy in the genes involved (Liu *et al*., 1998; Chen *et al*., 2009; Koussoulakou *et al*., 2009; Porntaveetus *et al*., 2011). In species lacking dentition, such as the chick, the signaling pathways required for the early odontogenic development have been conserved, likely because this signaling cascade has been co-opted from the combinatorial code required for maxilla and mandible development (Chen *et al*., 2000; Tucker & Fraser, 2014).

Once the placodes have formed, Shh expression in the placodes is required for localized cell proliferation, which drives the invagination into the underlying mesenchyme (Liu *et al*., 2008; Bei, 2009; Catón & Tucker, 2009; Koussoulakou *et al*., 2009; Chen *et al*., 2009; Jackman *et al*., 2010; Landin *et al*., 2012) this is referred to as the bud stage. The subsequent stages of tooth development, including the cap and bell stages have been excellently reviewed by Koussoulakou and colleagues (2009), Bei (2009); Caton and Tucker (2009), and Cobourne and Sharpe (2009) and will not be discussed here (Figure 4.2).

4.1.4 – Objectives

The primary objective of this chapter was to investigate the similarities between the induction and patterning of the conjunctival papillae and that of other placodes in order to

provide evidence to rename the initial stage of conjunctival papillae development the conjunctival placode. This question was addressed in two ways:

i) By investigating a possible competency factor that may be required prior to the induction and patterning of the conjunctival papillae.

I chose to address this question after it was determined in Chapter 3 that the conjunctival papillae were able to regenerate; suggesting that the epithelium was competent to respond to an inductive cue until HH 35.5. The chosen competency factor (*β-catenin*) was based on the literature of the cutaneous placodes. *β-catenin* expression was examined at HH 28 and 29 (prior to the induction of the first conjunctival papilla), at HH 30 (when the first conjunctival papilla forms), between HH 31-34 (during the induction and patterning of the ring of conjunctival papillae), and at HH 35 (beginning of the induction of the scleral condensations).

ii) By investigating six candidate genes that may be involved in the induction and patterning of the conjunctival papillae.

Candidate genes were selected using data from a microarray analysis performed in the Franz-Odendaal lab (unpublished). However, as the conjunctival papillae represent only a very small portion of the tissue sample analyzed during the microarray, the current literature for other systems which require epithelial placodes (i.e. cranial and cutaneous placodes) was used in order to identify potential conjunctival papillae genes. Six genes were identified as likely candidates involved in the development of the conjunctival papillae. They were then analyzed at HH

30, 31, 33, 34, and 35.5 in order to investigate their spatiotemporal expression patterns during the induction and patterning of the conjunctival papillae and the subsequent induction of the underlying scleral condensations.

This study is the first to investigate an epithelial competency factor prior to the induction and patterning of the conjunctival papillae and the first to investigate the molecular mechanisms governing the induction and patterning of the conjunctival papillae.

4.2 – Materials and Methods

4.2.1 – Egg Incubation

Eggs were obtained from Cox Bros. Farm (Truro, N.S., Canada) and A.C.A. Co-Operative Limited (Kentville, N.S., Canada) and stored at 4°C until incubated. Eggs were incubated horizontally in a forced-draft incubator as described in Chapter 2, although these eggs were left un-opened. Embryos were fixed in 4% PFA as described in Chapter 3 and then processed for *in situ* hybridization.

4.2.2 – Candidate Gene Selection

The microarray data from which the initial list of candidate genes were selected was obtained in 2009 (Franz-Odendaal, unpublished data). For this analysis, approximately half of the eye was dissected from the left and right eye of each sample, after which the neural retina, RPE, vitreous humour, lens, sclera, and scleral cartilage were removed; leaving only the conjunctival epithelium and scleral mesenchyme. The dissected tissue centered on the ciliary artery and included both the two papillae dorsal and ventral to the ciliary artery (Figure 4.3). Samples were collected at HH 30 (prior to the induction of the first papilla), HH 34 (when the ring of conjunctival papillae is complete), HH 35

(which marks the beginning of the induction of the underlying scleral condensations), HH 36 (end of the induction period for the scleral condensations), and HH 37 (scleral condensations faintly visible in the underlying mesenchyme). As the area of interest represents only a small amount of tissue, samples were collected from a total of six embryos per stage analyzed. This pooling of samples also served to compensate for slight variations in the stage of each embryo. Two experimental replicates were included for each stage. Biological replicates were not included as the tissues from multiple embryos were pooled. The microarray analysis was performed at the London Regional Genomics Center in London, Ontario (Canada).

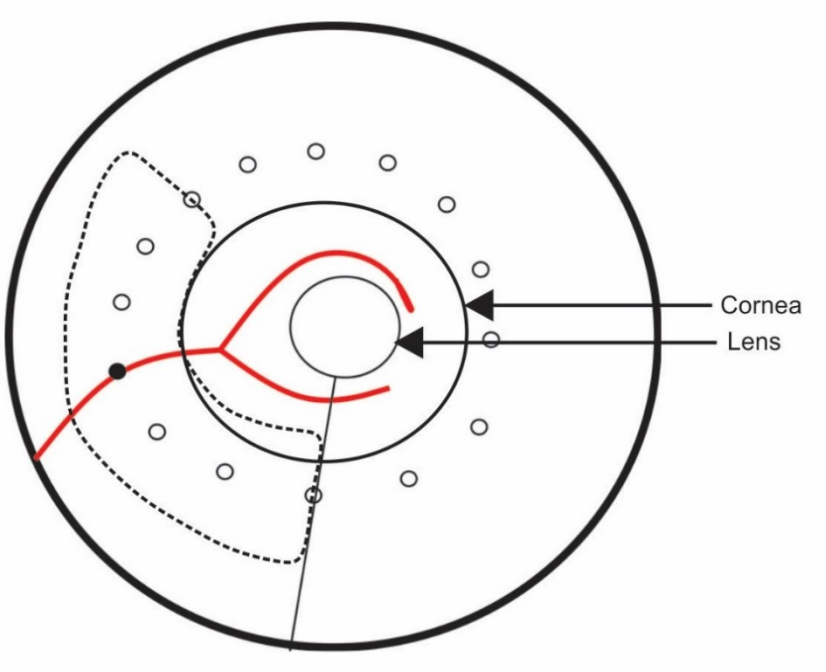

Figure 4.3: A schematic illustrating the tissue dissected from the right and left eyes of samples for microarray analysis (dotted lines). Ciliary artery (red); ciliary artery papilla (black).

The London Regional Genomics Center also performed an ANOVA for each stage comparison. As I was only interested the induction and patterning of the conjunctival papillae, my analysis focused on the differential gene expression between HH 30 and 34, the stages at which the conjunctival papillae are induced. Thus, this analysis included genes that were turned on or off during conjunctival development. However, it also included genes involved in other processes (such as cell migration and cell proliferation) as well as genes involved in the development of other systems (e.g. the vasculature in the scleral mesenchyme).

To begin my analysis, I created a list of those genes that had a greater than or equal to 1.5 fold increase or decrease between HH 34 and 30. This fold change value was chosen as a fold-change of 1.5 or 2 is standard in the literature. This yielded a list of 267 genes that decreased between HH 34 and 30 and 375 genes that increased over this time period.

The function of each of these genes was then analyzed using Gene Ontology (www.geneontology.org). Genes that had been shown to play a role in signal transduction, epithelial-mesenchymal signaling, inner ear development, eye development, inductive events, known signaling pathways (i.e. Shh, Wnt, Bmp, Fgf), placode development, feather development, or tooth development, were identified as potential targets to be compared to the literature. On the other hand, genes that had been shown to play a role in ion binding, cardiac function, musculature, catalytic pathways, endothelial development, protein phosphorylation, DNA repair, RNA binding, and extracellular matrices were discarded. In so doing, the list was reduced to a total of 36 genes. This reduced list was then compared to the literature for the induction and patterning of other placodes, papillae, and placode derivatives (i.e. lens development, inner ear development, hair development, *etc.*). This

resulted in a list of seven candidate genes: *Prox1, Oc90, Ednrb, Inhba, Dlx5, Gsc,* and *Eya1*. The specific role played by each of these ten genes in the literature will be discussed in the results below.

4.2.3 – Primer Design

As very few of these candidate genes had been investigated in the chick at the beginning of this study, primers were designed for each candidate. The protocol used to design the primers is detailed in Appendix 1. The primers and target gene sequence for each candidate gene is presented below. It should be noted that the RefSeq used to design the primers for *Oc90* has since been removed from the NCBI website as it was found to be erroneous. For that reason, *Oc90* will not be included in the subsequent analysis, but will be presented in Appendix 3.

PROX1

AAGCAGGCAAACCAAGAGAAGAAGAGTTGACATTGGAGTGAAAAGG
>>>>>>>>>>>>>>>>>>>>>>>>>
ACGGTAGGGACAGCATCTGCATTTTTTGCAAAGGCAAGAGCGACGTTT

TTTAGTGCCATGAATCCCCAAGGTTCAGAGCAGGATGTTGAGTATTCA

GTGGTGCAGCATGCAGATGGGGAAAAGCCAAATGTACTCCGCAAGCT

GCTGAAGAGGGCGAACTCGTATGAAGATGCCATGATGCCTTT
<<<<<<<<<<<<<<<<<<<<<<<<<

Product size: 231 bp

Start	Len	TM	GC%	Seq
97	20	59.99	45.00	AAGCAGGCAAACCAAGAGAA
327	20	60.04	45.00	AAAGGCATCATGGCATCTTC

EDNRB

TGACTTGCTGCACATCATCATCGACATCCCCATCAGCGTCTACAAGCT
>>>>>>>>>>>>>>>>>>>>>>>>>>>>
ACTTGCAGAGGACTGGCCCTTTGGTGTCGAAATGTGTAAATTAGTGCC

CTTCATTCAAAAGGCATCAGTGGGCATCACAGTGTTGAGTTTGTGTGC

CCTCAGTATAGACAGGTACCGAGCAGTTGCT
<<<<<<<<<<<<<<<<<<<<<<<<<<<<

Product size: 175 bp

Start	Len	TM	GC%	Seq
185	20	59.99	45.00	TGACTTGCTGCACATCATCA
359	20	59.94	55.00	AGCAACTGCTCGGTACCTGT

INHBA

GCCACCAAGAAACTCCATGTGGGAAAGGTGGGAGATGATGGCTATGT
>>>>>>>>>>>>>>>>>>>>>>>>>>>>
GGAAATAGAGGATGATGTTGGAAGAAGAGCAGAATGAATGAAGTTGT

GGAGCAACCTCAGAAATCATCACTTTTGCAGAATCAGGAACACCCAA
<<<<<<<<<<<<

GAAAACGTTGC
<<<<<<<<<<<<<

Product size: 154 bp

Start	Len	TM	GC%	Seq
494	20	59.97	50.00	GCCACCAAGAAACTCCATGT
647	20	60.02	45.00	GCAACGTTTTCTTGGGTGTT

DLX5

ACAAACAAACGACGACGACAACGACAAACAAACAAACAAAAAAAAG
>>>>>>>>>>>>>>>>>>>>>>>>>>>>
GTTAAAATGTGTAAAGCTTGTGCATGTAACTTATTGCATTTCAAAGGA

ACCCTTTTTTATACCGTGCGGACGTTTTTCGGCTCAGCTGTGGACACTG
<<<<<<<<<<<<<<<<

TCAATGG
<<<<<<<<

Product size: 151 bp

Start	Len	TM	GC%	Seq
1023	20	60.20	45.00	ACAAACAAACGACGACGACA
1173	20	60.16	55.00	CCATTGACAGTGTCCACAGC

GSC

CCACGTCTGGGTATTTCGTTTCCTGGAAGAGGTTTTCCAGCGCTTCGAG
>>>>>>>>>>>>>>>>>>>>>>>>
CTGCTCGTCAGTGAAGATAGTCCGGTGCCGTCTTTTCCGCCTGCAGTGC

AGCTGGTTGAGTAACTGCAGCTCCGTCCGGGACAAAGTGCCTACGTTC

ATGTAGGGCAACATCTGATGGGGAACAGGGGACATCAGCACCGACCC

AGCGCCCTCGTAACCTACGAACAGACAGACGAGACGA
<<<<<<<<<<<<<<<<<<<<<<<<<<<<

Product size: 230 bp

Start	Len	TM	GC%	Seq
496	20	59.85	50.00	CCACGTCTGGGTATTTCGTT
725	20	60.18	55.00	TCGTCTCGTCTGTCTGTTCG

EYA1

AAATTGGCATTCCGCTACAGACGAGTAAAAGAAATATATAATACCTAC
>>>>>>>>>>>>>>>>>>>>>>>>
AAAAACAATGTTGGAGGTCTTCTTGGTCCAGCAAAAAGAGGCTTGGCT

ACAACTAAGAGCAGAAATTGAAGCTTTGACGGATTCCTGGTTAACACT

TGCACTGAAAGCACTCACCCTTATTCATTCAAGGACAAATTGTGTGAA

CATCCTTGTAACAACTACTCAACTAATTCCGGCTCTGG
<<<<<<<<<<<<<<<<<<<<<<<<

Product size: 232 bp

Start	Len	TM	GC%	Seq
4	20	60.10	45.00	AAATTGGCATTCCGCTACAG
235	20	60.21	50.00	CCAGAGCCGGAATTAGTTGA

4.2.4 – Primer Rehydration

In order to rehydrate the primers, a volume of TE Buffer (Appendix 1) was added to each primer equal to the nanomolar weight of each oligonucleotide sequence multiplied by ten; generating a 100 μM concentration of primer. TE Buffer was used for the rehydration process as it binds to magnesium, rendering it inactive, protecting the oligonucleotides from degradation. Following the rehydration process, primers were divided into 20 μl aliquots and frozen at -20°C.

4.2.5 – RNA Extraction

The RNeasy Mini Kit (Qiagen, 73304) was used for all RNA extractions and the protocol is given in Appendix 1. Tissue disruption was performed using a BioMasher (VWR, 82031-456). In order to ensure consistency between the extracted RNA for microarray validation and the microarray itself, the same area of tissue was dissected from both the left and right eye of six embryos at each of HH 30 and 34 as was described in section 4.2.2 above. After dissection, samples were transferred to the BioMasher column

and stored on ice until all dissections were complete. All dissections were performed using equipment that had been washed with RNaseZap (Sigma-Aldrich, R2020).

4.2.6 – RNA Quantification

RNA was quantified using spectrophotometry. To do this, two dilutions were prepared: i) a 1:200 dilution containing 1 µl of extracted RNA and 199 µl of Tris-Cl buffer, pH 7.2, and ii) a 1:50 dilution containing 2 µl of extracted RNA and 98 µl of Tris-Cl buffer, pH 7.2. The spectophotometer was then blanked using Tris-Cl buffer prior to analysis. In order to perform spectrophotometry, 100 µl of each dilution was loaded into a cuvette and the absorbance was recorded at OD_{230}, OD_{260}, and OD_{280}. The concentration of RNA was determined in each sample using the following equation:

44 x [absorption at OD_{260}] x dilution factor = sample concentration

The purity of each sample was then calculated using the OD_{260}/OD_{280} ratio; a result of approximately 1.8 indicating purity. Finally, the OD_{260}/OD_{230} ratio was used as a measure of contamination; a result of approximately 1.5 indicating very little contamination.

4.2.7 – cDNA Synthesis

Extracted RNA was converted into a cDNA library using the SuperScript III First Strand Synthesis System (Invitrogen; 18080-051). The full protocol is given in Appendix 1. This system is designed to convert 1 pg – 5 µl of total RNA into first-strand cDNA. Following conversion of RNA to cDNA, samples were stored at -20°C until use.

4.2.8 – Polymerase Chain Reaction

In order to amplify the genes of interest, polymerase chain reaction (PCR) was performed using the primer pairs for each of the candidate genes and the chick cDNA created at HH 30 and 34 above. The protocol and binding temperatures for each gene are

described in Appendix 1. All PCR reactions were done in triplicate (at a minimum). In addition, during set-up a master mix was always used to ensure that all samples received the same distribution of ingredients.

4.2.9 – Gel Electrophoresis and Imaging

Gel electrophoresis was used in order to determine whether the primer pairs specific to each candidate gene were binding to the gene of interest. To do this, a 1% agarose gel was prepared by dissolving 0.6 g of agarose (Fisher Scientific, 9012-36-6) in 60 ml of 1X Tris-Borate-EDTA Buffer (Appendix 1). Once cooled, 3 µl of GelRed Nucleic Acid Gel Stain (Biotium, 41003) was added to the agarose in order to facilitate the visualization of the DNA product after electrophoresis. Once set, 2-5 µl of PCR product or ladder was added to each well. As the Crimson Taq Polymerase Buffer doubles as a loading dye, no dye was added to the PCR samples. Based on the size of the target DNA, a 100 bp ladder (Promega, G210A) was used. All gels were visualized using the AlphaImager HP System (Protein Simple) at a 350 nm wavelength. An image of each gel was captured using the AlphaImager Software.

4.2.10 – Primer Validation

Once PCR had been performed in triplicate and analyzed using gel electrophoresis, it was possible to determine whether the primers were binding to the band of interest by determining the approximate size of each DNA band. For all of the candidate genes (*Prox1, Eya1, Inhba, Ednrb, Gsc,* and *Dlx5*), the primers yielded a band of the appropriate size for the target gene sequence (Figure 4.4).

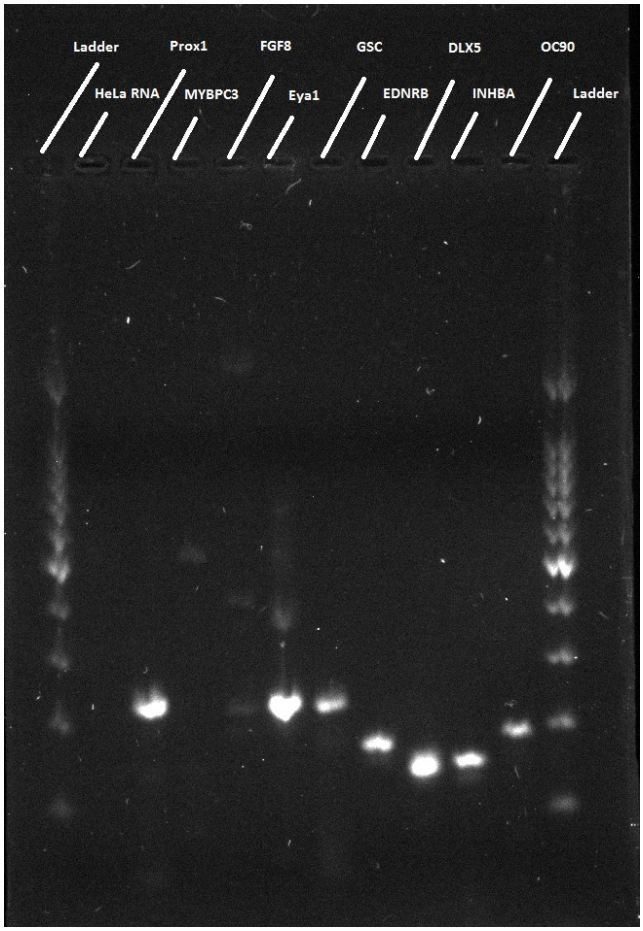

Figure 4.4: Summarizing the results of PCR for the candidate genes. A 100 bp ladder was run on either side of the gel in order to determine the size of each band. A band of approximately 230 bp was present for *Prox1*. A band of approximately 230 bp was present for *Eya1*. The band for *Gsc* also appeared to be approximately 230 bp. The bands for *Ednrb, Dlx5,* and *Inhba* were shorter, sitting at around 180 bp, 150 bp, and 150 bp respectively. All of the bands corresponded to the size of the target gene sequences.

4.2.11 – Gene Sequencing

After the primers had been validated, they were sequenced to confirm that the primers bound only to the mRNA sequence of interest. Sequencing was performed in Dr. Timothy Frasier's laboratory at Saint Mary's University (Halifax, N.S., Canada). The full protocol for this protocol is given in Appendix 1. Once samples had been prepared following Dr. Frasier's protocol, samples were analyzed by a 3500xl Genetic Analyzer (Applied Biosystems). Results of the sequencing indicated that the primers were targeted

to the gene of interest. Once the target gene sequence for each primer pair had been confirmed, another RNA extraction was performed as described below.

4.2.12 – RNA Extraction with Tissue Separation

In order to obtain individual RNA samples of the epithelium and the mesenchyme from the tissue of interest at HH 30 and 34, additional RNA extractions were performed. The protocol used was the same as that described in section 4.2.5 above with a single exception. After the tissue had been dissected from the eye, it was placed in a small volume of pre-warmed Dispase II in Hank's Balanced Salt Solution (Stemcell Technologies, 07913). The tissue was then incubated at 37°C in Dispase II until the epithelium began to separate from the underlying mesenchyme. After the tissue had begun to separate, fine tungsten needles were used to fully separate the epithelium from the underlying mesenchyme. The samples of epithelium and mesenchyme tissue were subsequently washed in autoclaved 1X PBS prior to being transferred to the BioMasher column.

4.2.13 – Presence versus Absence Analysis

Once the RNA had been extracted from the individual samples of epithelium and mesenchyme separately at HH 30 and 34 and transformed into cDNA, PCR was used to determine whether each candidate gene was present or absent in the tissue of interest. This PCR reaction and its subsequent analysis by gel electrophoresis were performed as described above.

4.2.14 – Primer Design with Conjugated T3 and T7 Binding Sites

Once presence and/or absence had been determined for each candidate gene, a new set of primers were designed for each gene that had a T7 polymerase (forward) promoter conjugated to the 5'-end of the original forward primer and a T3 polymerase (reverse)

promoter conjugated to the 5'-end of the original reverse primer. The design of these polymerase conjugated primers was based on a protocol published by David & Wedlich (2001). These primers were designed in order to facilitate the use of PCR for the creation of DIG-RNA labeled riboprobes for *in situ* hybridization.

Once the primers had been designed, they were validated using NCBI's BLAST to ensure that the addition of polymerase binding sites did not alter their specificity to the target sequence. These new primers were only selected if they were 100% complementary to the target sequence. Primers were again ordered through IDT. These new primer sequences are given below. The added T3 and T7 polymerase binding sites are underlined for clarity.

PROX1

Forward: TAATACGACTCACTATAGGGAAGCAGGCAAACCAAGAGAA

Reverse: AATTAACCCTCACTAAAGGGAAAGGCATCATGGCATCTTC

EDNRB

Forward: TAATACGACTCACTATAGGGTGACTTGCTGCACATCATCA

Reverse: AATTAACCCTCACTAAAGGGAGCAACTGCTCGGTACCTGT

INHBA

Forward: TAATACGACTCACTATAGGGGCCACCAAGAAACTCCATGT

Reverse: AATTAACCCTCACTAAAGGGGCAACGTTTTCTTGGGTGTT

DLX5

Forward: TAATACGACTCACTATAGGGACAAACAAACGACGACGACA

Reverse: AATTAACCCTCACTAAAGGGCCATTGACAGTGTCCACAGC

GSC

Forward: TAATACGACTCACTATAGGGCCACGTCTGGGTATTTCGTT

Reverse: AATTAACCCTCACTAAAGGGTCGTCTCGTCTGTCTGTTCG

EYA1

Forward: TAATACGACTCACTATAGGGAAATTGGCATTCCGCTACAG

Reverse: AATTAACCCTCACTAAAGGGCCAGAGCCGGAATTAGTTGA

4.2.15 – Validation of New Primers

In order to confirm that these new primers were binding to the same gene targets, PCR was performed and the results were analyzed using gel electrophoresis. The annealing temperatures for the new primer pairs are given in Appendix 1. The new primers were considered to be specific if they yielded a band that was 40 bp larger than the original sequence, due to the addition of a 20 bp sequence to each primer. Unfortunately, due to the similarity between the T7 and T3 polymerase binding sequences, these new primers also gave rise to primer dimers. In some samples, only a 40 bp primer dimer was present in the sample while in others, such as *Prox1* two primer dimers were present in the sample of 40 bp and 20 bp. Additionally, in order to further determine the specificity of the new primer pairs, I repeated the presence versus absence analysis. The results were the same for each gene using the new primers. A representative image of a presence versus absence analysis is shown below for *Prox1* (Figure 4.5).

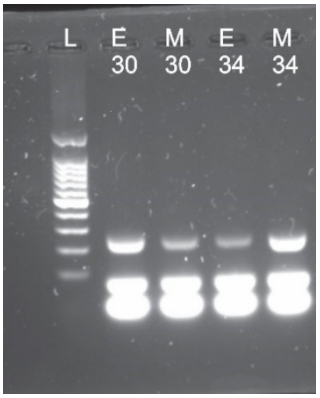

Figure 4.5: Results of *Prox1* PCR using the new primers to which T3 and T7 binding sites have been conjugated. The top band is the band of interest (approximately 230 bp), while the bottom two bands (40 bp and 20 bp, respectively) are the primer dimers created by the new primers.

4.2.16 – Ethanol Precipitation of DNA

In order to purify the PCR products for the creation of DIG-RNA labeled riboprobes, the primer dimers created by the T3 and T7 polymerases had to be removed from the sample. This was achieved by first concentrating the PCR sample using EtOH precipitation of the DNA (Appendix 1) based on the protocol from the Lamitina lab (2007) with slight modification. This modification, which was an increase in the volume of 3M sodium acetate (pH 5.2) added to the PCR sample, was due to the viscosity of the Crimson Taq Polymerase Buffer used for PCR.

4.2.17 – Purification of DNA from an Agarose Gel

Once concentrated, the DNA sample was run on an agarose gel in order to separate the band of interest from the contaminating primer dimer. The desired band of target DNA was then isolated from the agarose gel using the High Pure PCR Purification kit (Roche, 11 732 668 001) (Appendix 1). These purified DNA samples were then used to generate DIG-RNA labeled riboprobes for *Inhba, Ednrb,* and *Prox1*. This procedure is described in 4.2.23 below. In order to expedite the trouble-shooting of the PCR-generated riboprobes,

plasmids were obtained for the rest of the candidate genes, namely *Gsc, Eya1,* and *Dlx5* (described below).

4.2.18 – Plasmids

The plasmid for *goosecoid* (*Gsc*) was generously provided by Dr. Susan Chapman (Clemson University, S.C., U.S.A.) while the plasmids for *Eya1* and *Dlx5* were generously provided by Dr. Andrea Streit (University of King's College, London, U.K.). An additional plasmid was obtained for *β-catenin* in order to investigate epithelial competency in the conjunctival papilla system, as discussed in Chapter 3, which was generously provided by Dr. Randall Widelitz (University of Southern California, California, U.S.A.). Sequences for each of these plasmids is given below.

GSC (Chapman *et al*., 2002)

ATGCCTGCGAGCATGTTCAGCATCGACAACATCCTGGCGGCCAGACCT
CGCTGCAAGGACTCGGTGCTGCTGCCCCCGAGCGCGCCCGTCGTCTTC
CCCAGCCTGCACGGGGACTCCCTCTACGGCGCTGCCTCCGACTACGGA
GGATTTTACTCCCGGGCTGTGGCTCCCGGCTCGGCGCTGCCGGCGGTC
GGCCGGTCCCGCCTGGGCTACAACAACTACTACTACGGGCAGCTGCAT
GTCGCCACGTCTCCCGTGGGCCCGTCGTGTTGCGGGGCCGTGCCGCCG
CTGGGGGCCCAGCAGTGCTCCTGCGTGCCCCCCGCAGGTTACGAGGGC
GCTGGGTCGGTGCTGATGTCCCCTGTTCCCCATCAGATGTTGCCTTACA
TGAACGTAGGCACTTTGTCCCGAACGGAGCTGCAGTTACTCAACCAGC
TGCACTGCAGGAGGAAAAGACGGCACCGGACTATCTTCACTGACGAG
CAGCTCGAAGCGCTGGAAAACCTCTTCCAGGAAACGAAATACCCAGA
CGTGGGCACCAGGGAACAGCTGGCGAGGAAGGTGCACTTAAGAGAGG
AGAAAGTGGAGGTTTGGTTCAAAAACCGCCGGGCGAAATGGAGGAGG
CAAAAGCGGTCGTCTTCCGAGGAGTCGGAAAATGCACAGAAATGGAA
TAAAGCGTCTAAAACGTCTCCGGAGAAGAGGCAAGAAGACGGGAAAA
GCGATTTGGACTCCGACAGCTGATGCCGCGCAGGGGGATGCTCCCCGT
GGACTGTAGGATACGCTCCGGAGGATGCTACTATCTTGCACAAGCTCT
GCCTTGTCGGAGGGGGGAAACTATCTGTATATAATGTACAATACCCCG
AGTCGATTTCGTGTAAATAAAATGTGTTGCGGAGGTGTTGCACAGGCA

EYA (Christophorou *et al*., 2010)

CTTATCTCCAAATAGCACCTATAACTTGGAACGGATGGCTTTCCCGCA
GCTGCCACCAGCGCTAATTGTGCCTCGCGACAGGGGTGCGTGGAGGA
GTGGATTGGATGAGAAAATGGCATTCCGCTACAGACGAGTAAAAGAA
ATATATAATACCTACAAAAACAATGTTGGAGGTCTTCTTGGTCCAGCA
AAAAGAGAGGCTTGGCTACAACTAAGAGCAGAAATTGAAGCTTTGAC
GGATTCCTGGTTAACACTTGCACTGAAAGCACTCACCCTTATTCATTCA
AGGACAAATTGTGTGAACATCCTTGTAACAACTACTCAACTAATTCCG
GCTCTGGCAAAAGTCTTGTTGTATGGATTAGGGGTTGTATTTCCCATAG
AGAATATTTACAGTGCAACTAAAATAGGAAAGGAAAGTCGTTTGAGC
GAATAATTCAAAGATTTGGAAGAAAAGTAGTGTATGTGGTTATAGGA
GATGGTGTAGAAGAAGAACAAGGCGCTAAAAAGCATGCTATGCCATT
TGGAGGATCTCAAGCCACTCTGACCTTATGGCCCTTCACCATGCCTTG
GAAACTGGAGTACTTGTAGCAGCTCAGCAGCACTTTGAAACCCCAGAG
CCTCCTTCTGCCCATGGACGGTACGCCTGTGTCTTGTGTCAGCATTGGA
CTACAGAACTTTGTGATTTCAACATGTTGACGTACAGCTGCAATGGTC
TTAACCCTTGTCCCTTTCAGTAACGGAG

DLX5 (Bhattacharyya *et al*., 2004)

GGGCGCCGAGCCGCCTCCCCCGGCCATGTCCGCCTGAGCCCGGCGATC
CGCGCTATGACAGCAGTGTTTGACAGAAGGGTCCCCGGCATCAGGTCC
TCCGACTTCCAGCCGCCTTTCCAGAGCGCCGCAGCCATGCACCACCCG
TCCCAGGAATCTCCCACTTTACCCGAGTCCTCGGCTACGGATTCCGAC
TACTACAGCCCGACGGGGGCGGCCCCGCACGGCTACTGCTCGCCTACC
TCGGCTTCCTACGGCAAAGCGCTCAACCCCTACCAGTACCAGTACGGC
ATGAACGGCTCCGCCGGCACCTACCCCGCCAAAGCCTACGCGGACTAC
GGCTACGGCAGCCCCTACCACCAGTACGGAGGAGCCTACGGCCGCGG
GCAAAGCTCCGCGGGGCAGCCAGAGAAGGAGGTGGCGGAGCCCGAG
GTGAGGATGGTGAACGGCAAGCCAAAGAAAGTGCGCAAACCGCGGAC
TATTTATTCCAGCTTTCAGCTGGCGGCGTTGCAGAGGAGGTTCCAGAA
GACCCAATACCTCGCCCTGCCCGAGCGGGCCGAGCTGGCCGCCTCGCT
GGGACTCACGCAGACGCAGGTGAAAATCTGGTTCCAGAACAAAAGGT
CCAAGATCAAGAAGATCATGAAGAACGGGGAGATGCCCCCGGAGCAC
AGCCCCAGCTCCAGCGACCCCATGGCCTGCAACTCCCCGCAGTCGCCG
GCGGTGTGGGAACCTCAGGGCTCGTCGCGCTCCCTCGGCCACCACGGG
CACGGGCACCCGCCCGCCGCCAACCCGTCCCCCGGCAGCTACCTGGAG
AGCCCCTCGGCCTGGTACCCCGCCGCCAGCCCCCTCGGCTCCCACCTG
CAGCCCCACGGCTCCCTACAGCATCCCTTGGCGCTGCCCTCCGGGACG
ATCTACTGAGGGCCGAACCCTCGTGCTTCTTTTGTATTCCGCTCCCTGG
ACTCCTGTGTTTTACTGTTAAGGAAGAATAACGAAAGGAATGCGGATG
GGGGATTTTTAAAGGGAAACGAAACAAACAAACGACGACGACAACGA
CAAACAAACAAACAAACAAAAAAGGTTAAAATGTGTAAAGCTTGTGC
ATGTAACTTATTGCATTTCAAAGGAACCCTTTTTTATACCGTGCGGACG
TTTTTCGGCTCAGCTGTGGACACTGTCAATGGTGCCTTCAAATCTATGA

CCTCAACTTTTCCAGAGACTTTTTTTCAATGTTATTTTAACCCTTGTAA
ATAATTGTAGATAGAGGAATTAAACTGTATATTCTGAATAAAATAAAA
TTATTTCGACC

β-CATENIN (Suksaweang *et al*., 2004)

GGCACGAGAGCAGCAGCAGCCGGAGCCCGGGGGGACGCTGCGCTCTC
GCCTCCGTGCCACAGTCTCTGAAAGGTAGCAGGAAAGAGTTCTGGGA
GCACAGCAAGGAACATGGCAACCCAAGCTGACTTGATGGAGTTGGAT
ATGGCCATGGAGCCAGACAGAAAAGCTGCAGTCAGTCATTGGCAGCA
GCAGTCATATCTGGACTCTGGTATCCATTCCGGTGCCACGACAACTGC
TCCCTCTTTGAGTGGCAAAGGAAATCCTGAAGAGGAAGATGTGGACA
CAACGCAAGTCCTGTATGAGTGGGAGCAAGGGTTCTCTCAGTCCTTTA
CCCAGGAGCAAGTTGCTGATATTGATGGCCAATATGCAATGACTAGAG
CTCAGAGAGTGCTTTCTGCTATGTTCCCCGAAACACTGGATGAAGGAA
TGCAAATCCCATCCACACAATTTGATGCTGCCCATCCAACTAATGTGC
AGCGCCTGGCTGAGCCATCCCAGATGCTAAAACATGCTGTTGTTAATT
TGATAAACTATCAGGATGATGCTGAACTTGCAACTCGTGCAATCCCAG
AACTGACCAAACTGTTGAATGATGAGGACCAGGTGGTGGTAAACAAG
GCTGCGGTTATGGTTCATCAGCTATCCAAAAAGGAAGCATCTCGCCAT
GCTATTATGAGGTCTCCTCAAATGGTATCTGCAATTGTGCGTACCATGC
AAAATACAAACGATGTGGAAACAGCCCGCTGTACTGCAGGCACACTA
CACAATCTCTCACATCACCGTGAAGGCTTGTTGGCAATCTTCAAATCA
GGAGGCATCCCTGCGTTGGTTAAAATGCTTGGGTCTCCGGTGGATTCT
GTGTTGTTCTATGCCATTACTACTCTTCACAATCTCCTGTTACATCAGG
AGGGAGCCAAAATGGCTGTCCGTCTGGCTGGAGGGCTGCAAAAAATG
GTTGCCCTGCTCAACAAGACAAATGTGAAATTCTTGGCCATCACGACA
GACTGTCTTCAGATTTTAGCCTATGGCAATCAAGAAAGTAAGCTGATT
ATTCTGGCAAGCGGTGGACCCCAAGCTCTAGTAAACATAATGAGGACC
TACACTTATGAGAAACTATTGTGGACCACAAGTAGGGTGCTGAAGGTG
TTGTCAGTCTGCTCCAGCAACAAACCTGCTATTGTTGAGGCTGGTGGG
ATGCAAGCTTTAGGACTCCACCTTACAGATCCAAGCCAGCGTCTTGTC
CAGAACTGTCTCTGGACCCTGAGAAATTTGTCAGATGCAGCAACCAAG
CAGGAGGGAATGGAAGGCCTTCTAGGAACTCTTGTTCAGCTTTTAGGA
TCAGATGACATTAATGTTGTGACTTGCGCTGCCGGAATCCTTTCTAACC
TTACTTGCAACAATTACAAGAACAAGATGATGGTCTGCCAGGTTGGTG
GCATCGAGGCTCTTGTGCGCACAGTTCTTCGGGCTGGAGACAGGGAAG
ACATCACAGAACCTGCTATTTGTGCGCTCCGTCACCTCACCAGCAGAC
ATCAGGAAGCTGAAATGGCTCAAAATGCAGTACGTCTCCATTACGGAC
TCCCAGTGGTGGTTAAACTGTTGCACCCACCTTCACACTGGCCTTTGAT
CAAGGCTACTGTTGGGTTGATTCGCAATCTCGCGCTCTGCCCTGCAAA
CCATGCCCCACTGCGTGAACAAGGTGCTATCCCACGGCTAGTTCAGCT
GCTGGTTAGAGCACATCAAGATACCCAGCGACGTACTTCCATGGGTGG
AACGCAACAGCAGTTTGTGGAGGGTGTGCGCATGGAGGAAATCGTTG
AGGGCTGTACTGGAGCCCTGCATATTCTTGCACGTGATGTTCACAATC
GAATTGTAATCAGGGGTCTAAATACCATTCCACTATTTGTGCAGTTGTT

GTACTCCCCCATTGAGAATATCCAGAGAGTAGCTGCGGGTGTACTTTG
TGAACTTGCTCAAGACAAGGAAGCAGCTGAAGCAATTGAAGCTGAAG
GCGGAACTGCCCCTTTAACAGAACTGCTTCATTCCAGGAATGAGGGTG
TTGCAACATATGCAGCTGCAGTGCTGTTCAGAATGTCGGAGGACAAAC
CACAAGACTACAAGAAGCGACTTTCAGTTGAACTGACAAGCTCTCTGT
TCCGGACTGAGCCAATGGCTTGGAACGAGACAGCGGATCTTGGACTTG
ACATTGGTGCCCAGGGAGAACCTCTTGGATACCGCCCAGATGATCCTA
GCTACCGTTCTTTCCACTCTGGCGGATACGGTCAGGATGCCTTGGGTAT
GGACCCTATGATGGAACATGAAATGGGTGGCCACCACCCTGGTGCTGA
CTACCCAGTTGATGGTCTGCCAGATCTTGGCCATGCCCAGGACCTTAT
GGATGGGCTGCCTCCAGGTGACAGTAATCAGTTGGCCTGGTTCGATAC
TGACCTGTAAATCATCCTTTAGCTGTATCATCTGAATGAACTTGCATTG
ATTGGCCTGTAGAGTTGCTGAGAGGGCTCGAGGGGTGGGCTAGTATCT
CAGAAAGTGCCTGACACACTAACCAAGCTGAGTTTCCTATGGGAACAA
TTGAAGTAAACTTTTTGTTCTGGTCCTTTTTGGTCGAGGAGTAATAATA
CAAATGGATTTTGGGAGTGATTCAAGAAACGAGGAATGCACAAGAAT
GAATTGCAAGATGGAATTTATCAAACCCTAGCCTTGCTTGTTAAAAAT
TTATTATTTTTTTTAAATCTCTGTAATGGTACTGACCTTTGCTTGCTTTG
AAAGTAGCCTTTCTTTTCGCAGTAATTGTTGTTAGGGTTTTTTTTTTAA
GTCTCTCGTAGTATTAAGTTATAGTGAATATGCTACAGCCGTTTCTAAT
TTTTAAGGATTGAGTAAAGGTGTAGAACACTAATTCATAATCGCTCTA
ACTGTATTCTGAATAAAGTGTAACATTGTGTAGCCTTTTTGTATAAAAA
AAACTAGACAAATAGAAATGGTCCAATTAGTTTCCTTTTTAATATGCTT
AAAATAAGCAGGTGGATCTATTTCATGTTTTTGATCAAAAACTTTATCT
GGATATGTCTGGGTAGGGGCCAGTAAGAACTGTTTATTTGGAACCTTG
TATTGGACAGTTTACCAGTTGCCTTTTATCCCAAAGTTATTGTAGCCTG
CTGTGATACAGATGCTTCATGAGAAAAATGCAGTTATAAAATGGTTCA
AAATTAAAGTAAACTTTTAATTCAAAAAAAAAAAAAAAAAA

4.2.19 – Removing the Plasmids from Filter Paper

The filter paper containing the plasmid was dissected and placed in a 1.5 ml Eppendorf tube to which 100 µl of TE Buffer was added. The tube was incubated at room temperature for 5 minutes. After incubation, the tube was thoroughly mixed and collected by centrifugation at 3,000 rpm for 1 minute. The sample was then incubated for a further 30 minutes at room temperature. Following this incubation, the filter paper was removed from the Eppendorf tube and transferred to a new, 1.5 ml Eppendorf tube. Both the filter paper and the plasmid were stored at -20°C.

4.2.20 – Cloning

Cloning was performed following standard protocols, using proper aseptic techniques (Appendix 1).

4.2.21 – Mini-Prep

Mini-Prep was also performed following standard protocol. The complete protocol is given in Appendix 1.

4.2.22 – DNA Digest

The specific DNA digest protocols used for each gene are presented in Appendix 1. The protocol for DLX5 is given as a representative protocol.

DNA digests were prepared in a large volume; where 10 µg of DNA was digested in a 100 µl volume. For DLX5 (antisense), the following reagents were combined in a 0.2 ml PCR tube: 70 µl of DepC treated H_2O, 10 µl of Buffer SH, 10 µl of BSA, 5 µl of *Dlx5* mini-prep, and 5 µl of restriction enzyme NcoI. The solution was gently mixed and then briefly centrifuged before being incubated overnight at 37°C. The following day, the reaction was heat inactivated at 65°C for 15 minutes.

4.2.23 – Gene Sequencing

In order to confirm that the plasmids obtained for the candidate gene analysis were the genes of interest, *Eya1*, *Gsc*, and *Dlx5* were sent for sequencing to the Center for Applied Genomics at the Sick Kid's Hospital in Toronto (Canada). Plasmids were prepared for sequencing by diluting the mini-prep purified plasmid DNA to a concentration of 200-300 ng of DNA in 7 µl of water.

4.2.24 – DIG-RNA Labeling (Riboprobe Generation)

All riboprobes for the candidate gene analysis were made using the DIG-RNA Labeling Kit (SP6/T7) from Roche (11 175 025 910). The specific protocol for each riboprobe is given in Appendix 1.

4.2.25 – DIG-High Prime DNA Labeling and Detection (Dot-Blot)

Once created, the riboprobe was verified using the DIG-High Prime DNA Labeling and Detection Dot-Blot Protocol by Roche (11 745 832 910), for which the entire protocol is given in Appendix 1.

4.2.26 – *In Situ* Hybridization

All *in situ* hybridization reactions were performed as described in Chapter 3. The riboprobe concentration, however, varied depending on the specific riboprobe used. Riboprobe concentrations are listed in Appendix 2.

In addition, a number of controls were used to verify the *in situ* hybridization reactions. The first, a stage-matched embryo with no riboprobe was used as a negative control. Furthermore, *in situ* hybridization using the sense riboprobe was performed for each gene as a measure of non-specific binding.

4.2.27 – Cryosectioning

After *in situ* hybridization, select stages of each gene were cryosectioned in order to determine the spatial expression pattern of the candidate genes. The stage selected for cryosectioning varied based on the type and timing of gene expression. For most genes, this corresponded to the stage with the strongest expression (i.e. HH 33 for *Ednrb* and *Inhba* and HH 34 for *Eya1,* and *Prox1*). Cryosectioning was performed at HH 35.5 for both *Dlx5* and *Gsc* in order to investigate the possible expression in the underlying scleral

condensations. The corresponding stage for the sense riboprobe was also cryosectioned if expression was present in the whole mount samples. Cryosectioning was performed as described in Chapter 3; save for *Gsc*, for which all sections were cut at 25 μm intervals.

4.3 – Results

4.3.1 - Part A: Epithelial Competency Factors

In order to investigate the potential requirement for epithelial competency prior to the induction of the first conjunctival papillae, *in situ* hybridization was performed at HH 28, HH 29, and HH 30 using the antisense riboprobe for *β-catenin.* No *β-catenin* expression was detected in either the epithelium or mesenchyme at either HH 28 or HH 29 (n=4 at each stage) (not shown). At HH 30, on the other hand, prior to the induction of the first conjunctival papilla in the ring, there was expression of *β-catenin* in the temporal region directly above the ciliary artery (N=8, Figure 4.6A). There also appeared to be faint expression of *β-catenin* dorsal to the ciliary artery at the location of the adjacent conjunctival papilla (Figure 4.6A). These results suggest that *β-catenin* expression may be required for the acquisition of epithelial competency prior to the induction of the conjunctival papillae.

Next, I wanted to determine whether this expression pattern was the same during the induction of the rest of the conjunctival papillae. To investigate this, *in situ* hybridization was performed for *β-catenin* between HH 31 and HH 33 (N=8), at HH 34 (N=6), and at HH 35 (N=3). In all cases, between HH 31 and HH 34, there was widespread mesenchymal expression of *β-catenin* and localized, strong expression of *β-catenin* in the papillae themselves (Figure 4.6B, C, I). Furthermore, within the mesenchyme, there was very strong expression of *β-catenin* in the papilla-contiguous region directly beneath the

epithelium but almost no expression of *β-catenin* in the mesenchyme underlying the papilla, the site of the future scleral condensation (Figure 4.6I). This mesenchymal expression of *β-catenin* was surprising as in hair, feather, and tooth the expression of *β-catenin* is required in the epithelium for the induction and specification of the placode (Wolpert, 1998; Eames & Schneider, 2005; Widelitz, 2008; Duverger & Morasso, 2009; Dhouailly, 2009; Sayama *et al*., 2010; Enshell-Seijffers *et al*., 2010; Jiang *et al*., 2011; Painter *et al*., 2012; Sennett & Rendl, 2012; Huang *et al*., 2012; Woo *et al*., 2012; Suksaweang *et al*., 2012; Wells *et al*., 2012 Chuong *et al*., 2013; Myung *et al*., 2013; O'Connor *et al*., 2013). However, by HH 34, all of the conjunctival papillae have been induced and this may indicate that *β-catenin*, in the sclerotic ring system, is serving an additional function. By HH 35, all papillae appear to have down regulated their expression of *β-catenin* and the mesenchymal expression appears to have become restricted to the region where the scleral condensations will form (Figure 4.6D).

The sense riboprobe for *β-catenin* was used as a control during *in situ* hybridization. In all cases, no signal was detected using the sense riboprobe for *β-catenin* at any of the stages examined (Figure 4.6E to H).

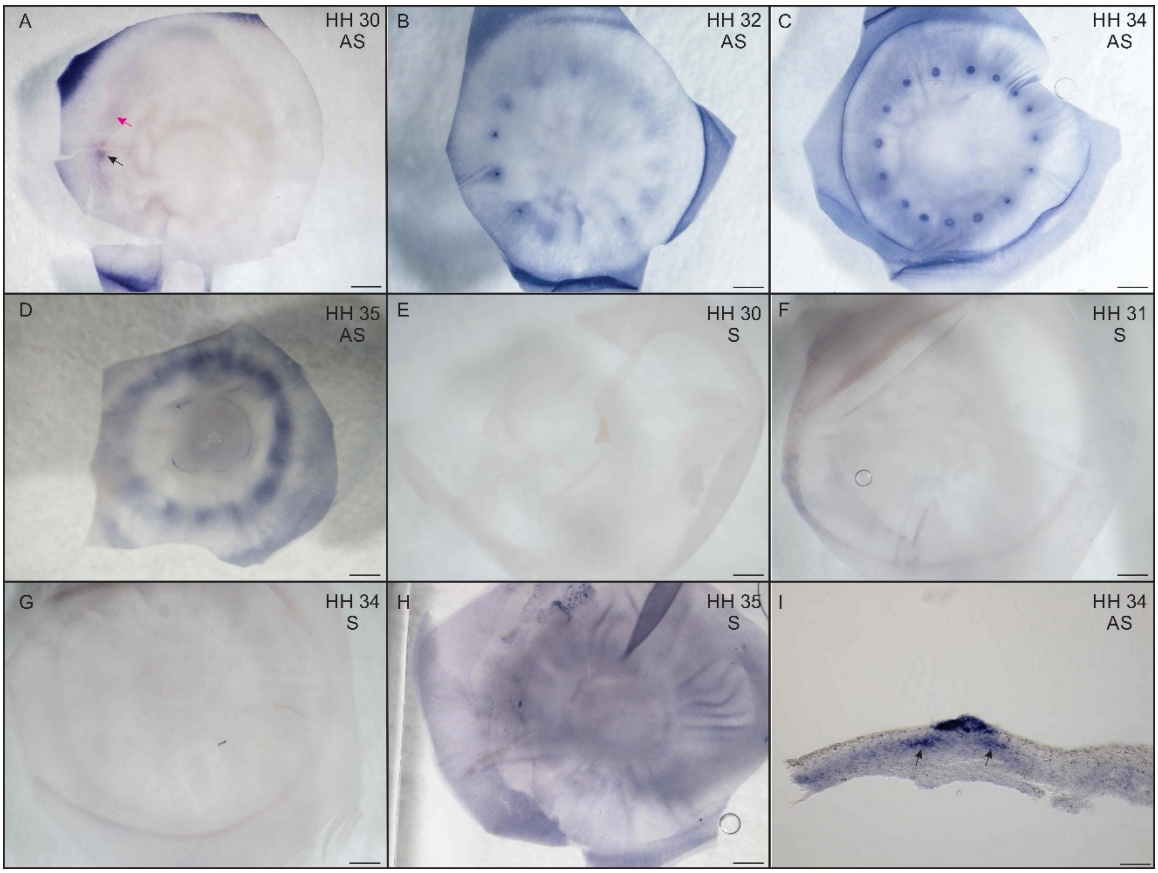

Figure 4.6: Summarizing the results of *in situ* hybridization of *β-catenin* at HH 30, HH 32, HH 34 and HH 35. **A**) There is widespread expression of *β-catenin* in the temporal region, with localized expression of *β-catenin* at the site of the presumptive papilla directly above the ciliary artery (black arrow) and faint *β-catenin* expression that appears to be localized at the site of the papilla dorsal to the ciliary artery (pink arrow). **B**) There is widespread expression of *β-catenin* throughout the eye with strong, localized expression of *β-catenin* in the temporal conjunctival papillae. There is also faint, localized expression of *β-catenin* at the presumptive nasal and dorsal conjunctival papillae. The most ventral nasal papilla has begun to express *β-catenin.* There is no localized expression in the ventral region. **C**) There is strong, localized expression in all of the conjunctival papillae in the eye by HH 34. The widespread expression of *β-catenin* is maintained. **D**) The papillae have downregulated their expression of *β-catenin* and the mesenchymal expression has become restricted to the corneal-scleral limbus. **E-H)** No signal was detected using the sense riboprobe for *β-catenin* at any of the stages examined as shown by **E**) HH 30, **F**) HH 32, **G**) HH 34, and **H**) HH 35. **I**) Cryosection showing the widespread mesenchymal expression of *β-catenin*. This expression seems to be concentrated in the superficial mesenchyme. Mesenchymal expression is strongest in the mesenchyme underlying the papilla-contiguous region (arrows). Additionally, there is very strong expression of *β-catenin* in the conjunctival papilla. AS: antisense riboprobe; S: sense riboprobe. Scale bars for **A-H** are 500 µm while that of **I** is 20 µm.

4.3.2 - Part B: Candidate Gene Analysis

4.3.2.1 – Description of Selected Candidate Genes

This section will address the rationale for selecting the six candidate genes (*i.e. Prox1, Ednrb, Inhba, Dlx5, Gsc,* and *Eya1*) based on validation via GO enrichment and literature assessment.

Prospero-Related Homeobox 1

Prox1, a transcription factor, was upregulated by a fold change of 1.80 at HH 34 as compared to HH 30. In the literature, *Prox1* has been shown to play a role in cell-cycle exit in the lens (Cvelk & Mitton, 2010; Cavalheiro *et al*., 2014), lateral line development (Pistocchi *et al*., 2009; Chen *et al*., 2011; Loh *et al*., 2014), hair cell development in the inner ear (Bermingham-McDonogh *et al*., 2006; Nichols *et al*., 2008; Fritzsch *et al*., 2010), hippocampal neurogenesis (Karalay *et al*., 2011), neurogenesis (Kaltezioti *et al*., 2010; Stergiopoulos *et al*., 2015), vascular endothelial cell development (Yoo *et al*., 2010), the induction and patterning of the paratympanic organ placode (O'Neill *et al*., 2012), renal development (Kim *et al*., 2015), and lens development (Lengler *et al*., 2001; Carmona *et al*., 2008; Chen *et al*., 2008a; Chen *et al*., 2008b). Interestingly, *Prox1* has also been shown to play a role in the ectopic activation of downstream effectors of the Hh signaling pathway during lens development (Kerr *et al*., 2012). As two members of the Hh family (*Ihh* and *Shh*) have been shown to be expressed in the conjunctival papillae during the induction of the scleral condensations (Duench & Franz-Odendaal, 2012), it will be interesting to determine whether and when *Prox1* is expressed in this system and to also whether it may be involved in the regulation of *Hh* during the development of the scleral ossicles.

Endothelin Receptor B

Ednrb, a G-protein coupled receptor, was upregulated by a fold change of 2.26 at HH 34 as compared to HH 30. Additionally, based on the literature, *Ednrb* has been shown to be involved in feather development and pigmentation (Kinoshita *et al*., 2014; Li *et al*., 2015), melanoma (Saldana-Caboverde & Kos, 2010; Cruz-Munoz *et al*., 2012); hair development and pigmentation (Lee & Tumbar, 2012), pigmentation (Dorshorst *et al*., 2011; Shinomiya *et al*., 2012), NC and melanocytes (Lecoin *et al*., 1998; Hakami *et al*., 2006; Kelsh *et al*., 2009; Clouthier *et al*, 2010), vasculature of the eye (McGlinn *et al*., 2007), and has been associated with Waardenburg syndrome (Welch *et al*., 2011). Additionally, *Ednrb* has also been shown to play a substantial role in vascular development and function (Thorin & Clozel, 2010; Mazzuca & Khalil, 2012; Paradis & Zhang, 2013).

Inhibin Beta A

Inhba, a growth and differentiation factor that was previously known as *Activin-βA*, was upregulated by a fold change of 1.60 at HH 34 as compared to HH 30. *Inhba* was also a very strong candidate based on the literature, where it has been shown to be involved with palatogenesis and cleft palate (Zhu *et al*., 2012; Ozturk *et al*., 2013; Iwata *et al*., 2014), renal branching morphogenesis (Costantini, 2012), regenerative proliferation in the cochlea (White *et al*., 2012), tooth development (Dangaria *et al*., 2011; Vieira *et al*., 2013; Jheon *et al*., 2013; Lan *et al*., 2014; Kaukua *et al*., 2015), eyelid development (Meng *et al*., 2014), hair development (Sennet & Rendl, 2012; Geng *et al*., 2013; Huh *et al*., 2013; Tsai *et al*., 2014), and has been found in osteoblasts (Hopwood *et al*., 2007). Inhba has also been shown, in pancreas development in the rat, to be required for the induction of *Shh* (van Eyll *et al.*, 2004).

Distal-Less Homeobox 5

Dlx5, a transcription factor, was upregaulted by a fold change of 2.73 at HH 34 as compared to HH 30. *Dlx5* was also a very strong candidate based on its involvement in tooth (Cho *et al*., 2010), inner ear (Chatterjee *et al*., 2010; Sajan *et al*., 2011), cranial placode (Steventon & Mayor, 2012; Leung *et al*., 2013; Moody & LaMantia, 2015), tongue (Barron *et al*., 2011), and limb development (Vieux-Rochas *et al*., 2013; Restelli *et al*., 2014). Dlx5 has also been shown to be involved in chondrocyte hypertrophy and endochondral ossification (Zhu & Bendall, 2009), osteoblast differentiation (Itoh *et al*., 2009), molecular regulation of matrix extracellular phosphoglycoproteins (Cho *et al*., 2009), post-natal bone growth (Zhang *et al*., 2008), craniofacial and mandibular development (Brown *et al*., 2010; Gitton *et al*., 2014), development of the frontal bone (Chung *et al*., 2010), osteoblastogenesis (Samee *et al*., 2008; Baek & Baek, 2013; Hagh *et al*., 2015), as well as craniofacial, axial, and appendicular skeletal development (Robledo *et al*., 2002). Furthermore, expression of *Dlx5* has been linked to tumor proliferation (Xu & Testa, 2009) and ovarian cancer cell proliferation (Tan *et al*., 2010); Interestingly, Dlx5 has also been shown to play a role in the indirect modulation of Shh signaling during the oral-nasal patterning of the palate and can rescue cleft palate in *Msx1*-null mice (Han *et al*., 2009). Depending on the timing of *Dlx5* expression in the eye of the chicken, it may be important to investigate this relationship between *Dlx5* and *Shh* in the scleral ossicle system.

Goosecoid Homeobox

Gsc, a transcription factor, was downregulated by a fold change of 1.98 at HH 34 as compared to HH 30. *Gsc* has been shown to be involved in craniofacial development

(Zou *et al*., 2011); mouth formation in echinoderms (Saudemont *et al*., 2010); SAMS or short-stature, auditory-canal atresia, skeletal abnormalities (Parry *et al*., 2013); mandible and tooth development (Denaxa *et al*., 2009), limb development (Belo *et al*., 1998), and middle ear and cochlear development (Rivolta *et al*., 2002; Chapman, 2011). Additionally, Gsc has been shown to interact with HNF-3beta during notochord and ventral neural tube development in mice to regulate the expression of *Shh* and thus, dorsal ventral patterning of the neural tube (Filosa *et al*., 1997). Therefore, although it does not have a strong association with the induction and patterning of the placodes, the involvement of Gsc in tooth, middle ear, and skeletogenesis along with its role in the regulation of *Shh* in the notochord make Gsc a candidate for the regulation of the induction and patterning of the conjunctival papillae.

Eyes Absent Homolog 1 (Drosophila)

Eya1, a transcriptional coactivator and phosphatase, was downregulated by a fold change of 1.26 at HH 34 as compared to HH 30. While this fold change was not large enough to have justified the selection of this gene, *Eya1* is a critical regulator of the induction and patterning of the cranial placodes in the literature (Zou *et al*., 2004; Schlosser *et al*., 2008; Saint-Jeannet & Moody, 2014). Eya1 has also been shown to be involved in inner ear and hair cell development (Zou *et al*., 2006; Zou *et al*., 2008; Freyer & Morrow, 2010; Ahmed *et al*., 2012), Branchio-oto-renal (BOR) syndrome (Landgraf *et al*., 2010; Li *et al*., 2010; Musharraf *et al*., 2014; Sun & Li, 2014), vascular morphogenesis in the mammalian lung (El-Hashash *et al*., 2011), and craniofacial morphogenesis (Guo *et al*., 2011). Therefore, although the fold change for *Eya1* is not very large, its prominent role in the induction and patterning of other placodes make it a prime candidate.

4.3.2.2 – Candidate Gene Expression in the Epithelium and/or Mesenchyme: Presence versus Absence

After the primer had been selected, I wanted to determine whether each candidate gene was present or absent in the epithelium and/or mesenchyme of the eye at HH 30 and 34 respectively. This presence versus absence analysis allowed for a qualitative validation of the microarray data for each gene of interest in the target tissue and served as a validation for the use of these primers for the subsequent generation of riboprobes for *in situ* hybridization. All genes were expressed in both the epithelium and mesenchyme at both HH 30 and HH 34 (Figure 4.7).

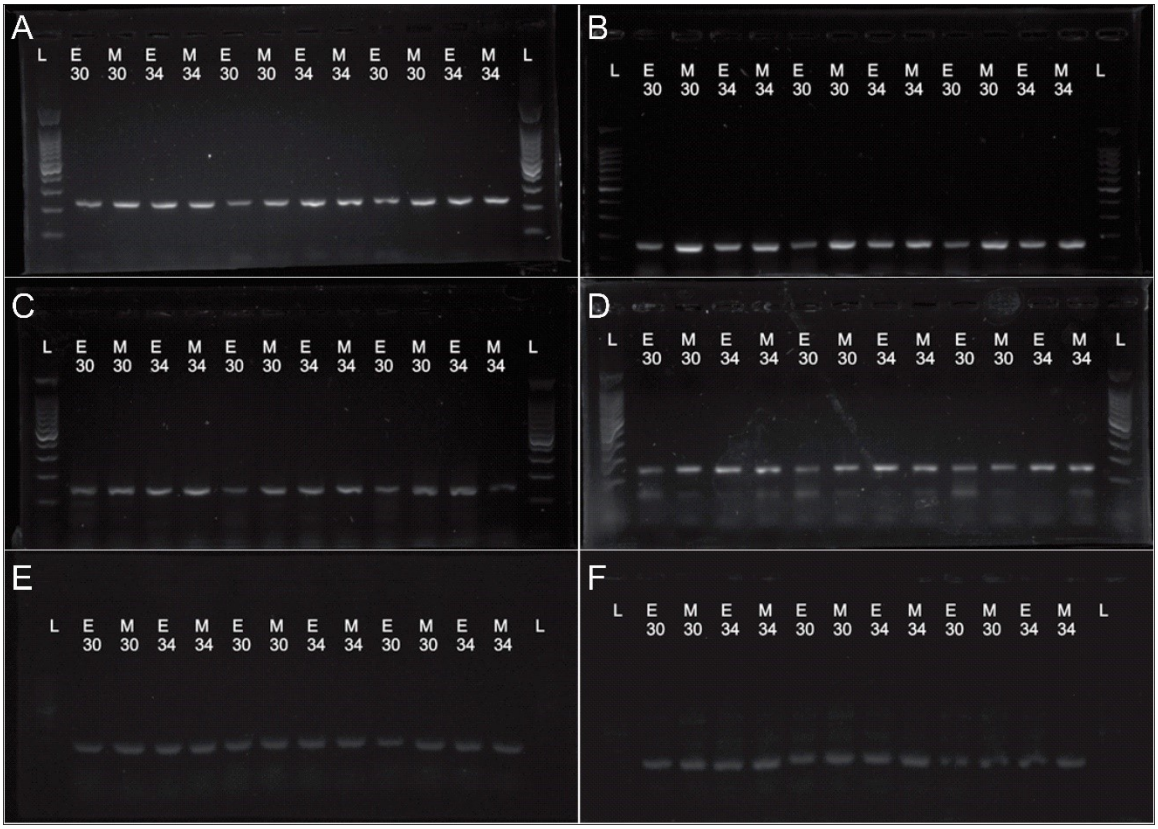

Figure 4.7: The results of gel electrophoresis for the six candidate genes. **A**) The results for *Prox1*. *Prox1* was expressed in both the epithelium and mesenchyme at HH 30 and 34. **B**) The results for *Ednrb*. *Ednrb* was expressed in both the epithelium and mesenchyme at HH 30 and HH 34. **C**) The results for *Inhba*. *Inhba* was expressed in both the epithelium and mesenchyme at HH 30 and HH 34. **D**) The results for *Dlx5*. *Dlx5* was expressed in both the epithelium and mesenchyme at HH 30 and HH 34. **E**) The results for *Gsc*. *Gsc*

was expressed in both the epithelium and mesenchyme at HH 30 and HH 34. **F**) The results for *Eya1*. *Eya1* was expressed in both the epithelium and mesenchyme at HH30 and HH 34. L: ladder, E: epithelium, M: mesenchyme.

4.3.2.3 – Results of In Situ Hybridization

As the presence versus absence analysis above could not provide any information about the spatiotemporal expression of these six candidate genes, I subsequently performed *in situ* hybridization at HH 30, between HH 31 and 33, at HH 34, and at HH 35. The results of *in situ* hybridization for each candidate genes are presented below.

PROX1

Based on the results of *in situ* hybridization, *Prox1* is not expressed in the eye of the chicken at a detectible level at either HH 30 (N=8) or HH 31 (N=4; Figure 4.8A-B). There is faint expression in the conjunctival papillae at HH 33 (N=4; Figure 4.8C). By HH 34, there is a moderate level of expression in all of the conjunctival papillae in the eye (N=7; Figure 4.8D and K) which is downregulated by HH 35.5, when the conjunctival papillae only faintly express *Prox1* (N=6; Figure 4.8E). There is no expression of *Prox1* in the mesenchyme at any of the stages examined (Figure 4.8A-E). Furthermore, there was no signal detected using the sense riboprobe for *Prox1* at any of the stages examined (N=10 for all stages examined; Figure 4.8F-J). In summary, *Prox1* is upregulated in the epithelium of the conjunctival papilla just prior to the induction of the underlying scleral condensations.

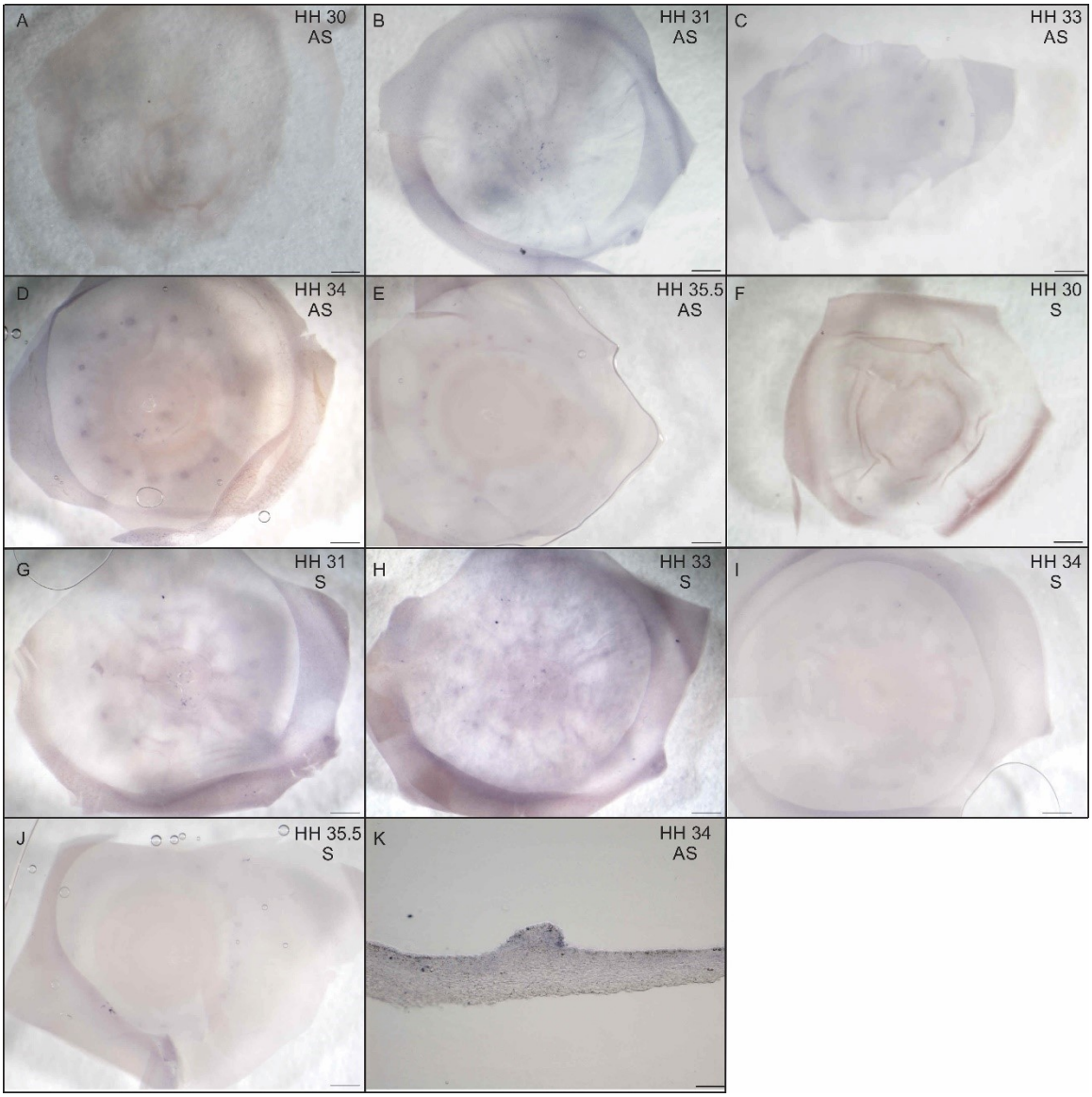

Figure 4.8 Results of *in situ* hybridization for *Prox1*. **A-E** show the results of *in situ* hybridization using the antisense riboprobe for *Prox1* while **F-J** show the results of *in situ* hybridization using the sense riboprobe. There is no expression of *Prox1* in the eye at **A**) HH 30 and **B**) HH 31. **C**) There is faint expression in the conjunctival papillae. **D**) The conjunctival papillae all express *Prox1*. No signal was detected using the sense riboprobe at any of the stages examined (**F-J**). **K**) A cryosection through a conjunctival papilla at HH 34 confirms that expression of *Prox1* is restricted to the conjunctival papillae. Additionally, this expression is quite faint. AS: antisense riboprobe; S: sense riboprobe. **A-J** scale bars are 500 μm. **K** scale bar is 20 μm.

EDNRB

Based on the results of *in situ* hybridization, *Ednrb* is not expressed at HH 30 (N=10; Figure 4.9A). By HH 31 (N=4), *Ednrb* is faintly expressed in the conjunctival papillae of the temporal and nasal groups (Figure 4.9B). At this stage, *Ednrb* is also strongly expressed in the vasculature of the eye, particularly in the small capillaries in the temporal region and surrounding the lens (Figure 4.9B). This vasculature expression continues into HH 33 (N=4), at which point the conjunctival papillae of the temporal region have begun to downregulate their expression of *Ednrb*; while the nasal papillae continue to express *Ednrb* (Figure 4.9C). When a section was cut through a conjunctival papilla of the nasal region at HH 33, *Ednrb* expression was restricted to the conjunctival papilla (Figure 4.9K). Furthermore, this expression seemed to be concentrated at the bottom of the papilla, within the mesenchymal tongue (Figure 4.9K). A section through the eye closer to the lens shows the expression of *Ednrb* within the vasculature (Figure 4.9L). By HH 34 (N=7), the network of vasculature surrounding the lens has increased in size and is still strongly expressing *Ednrb* (Figure 4.9D). At this stage, the nasal papillae have begun to downregulate their expression of *Ednrb* while it has been upregulated in the dorsal and ventral papillae (Figure 4.9D). All expression of *Ednrb* has begun to be downregulated by HH 35.5, at which stage the vasculature only weakly expresses *Ednrb* and the expression in the conjunctival papillae is very faint (Figure 4.9E). These results suggest that *Ednrb* may be involved in the induction and patterning of the conjunctival papillae but may not be required for the induction of the scleral condensations. No signal was detected using the sense riboprobe for *Ednrb* at any of the stages examined (N=11 across all stages; Figure 4.9F-J).

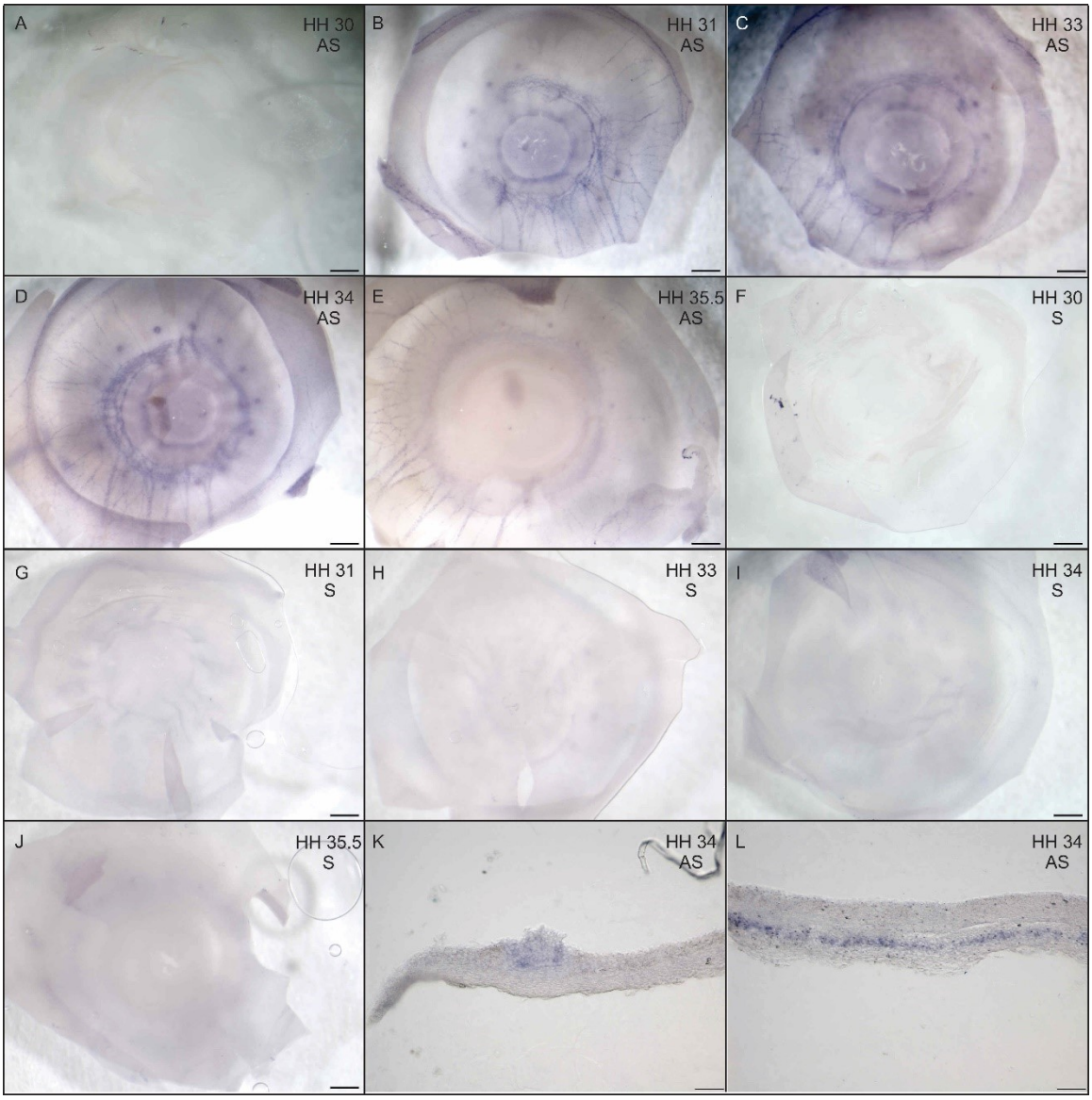

Figure 4.9: Results of *in situ* hybridization for *Ednrb*. **A-E** show the results of *in situ* hybridization using the antisense riboprobe for *Ednrb* while **F-J** show the results of *in situ* hybridization using sense riboprobe for *Ednrb*. **A**) There is no *Ednrb* expression in the eye. **B**) *Ednrb* is expressed in both the temporal (strong) and nasal (faint) conjunctival papillae. Additionally, the vasculature in the eye is strongly expressing *Ednrb*. **C**) The temporal and nasal conjunctival papillae still express *Ednrb*, although the temporal papillae have begun to downregulate their expression of *Ednrb*. *Ednrb* is still strongly expressed in the vasculature. **D**) The conjunctival papillae of the nasal, dorsal, and ventral regions all express *Ednrb*. There is still faint expression in the temporal conjunctival papillae. The vasculature continues to express *Ednrb* and appears to be restricted to the temporal half of the eye. **E**) The conjunctival papillae no longer express *Ednrb* and it is downregulated in the vasculature. No signal was detected using the sense riboprobe at any of the stages examined: **F**) HH 30, **G**) HH 31, **H**) HH 33, **I**) HH 34, and **J**) HH 35.5. **K**) Cryosectioning reveals strong expression of *Ednrb* in only the conjunctival papillae. **L**) A cryosection

through the epithelium and mesenchyme closer to the lens highlights the expression of *Ednrb* in the vasculature. AS: antisense riboprobe, S: sense riboprobe. **A-J** scale bars are 500 μm. **K-L** scale bars are 20 μm.

INHBA

Based on the results of *in situ* hybridization, *Inhba* is not expressed in the eye at HH 30 (N=10) (Figure 4.10A). By HH 31 (N=4), *Inhba* is strongly expressed in the temporal group of conjunctival papillae. Interestingly, there appears to be a "halo" of *Inhba* expression around all of the conjunctival papillae (Figure 4.10B). By HH 33 (N=4), *Inhba* is expressed in both the temporal and nasal papillae as well as the center papilla of the dorsal group (Figure 4.10C). These papillae all still appeared to have a halo of expression in the papilla-contiguous region (Figure 4.10C). When this expression pattern was investigated by sectioning, it was determined that *Inhba* is only expressed in the basal lamina beneath the conjunctival papillae (Figure 4.10K). This expression of *Inhba* in the basal lamina extends slightly into the papilla-contiguous region, which explains why the conjunctival papillae appear to be surrounded by a halo of expression (Figure 4.10L). By HH 34 (N=7), the temporal and nasal papillae have both downregulated their expression of *Inhba* whereas *Inhba* has been upregulated in the dorsal and ventral groups of conjunctival papillae (Figure 4.10D). By HH 35 (N=5), all of the conjunctival papillae have begun to downregulate their expression of *Inhba*, which is now only faintly visible in the dorsal and ventral papillae (Figure 4.10E). These results suggest that *Inhba* may be required for the induction and patterning of the conjunctival papillae but does not seem to be required for the induction of the scleral condensations. No signal was detected using the sense riboprobe for *Inhba* at any of the stages examined (N=11, Figure 4.10F-J).

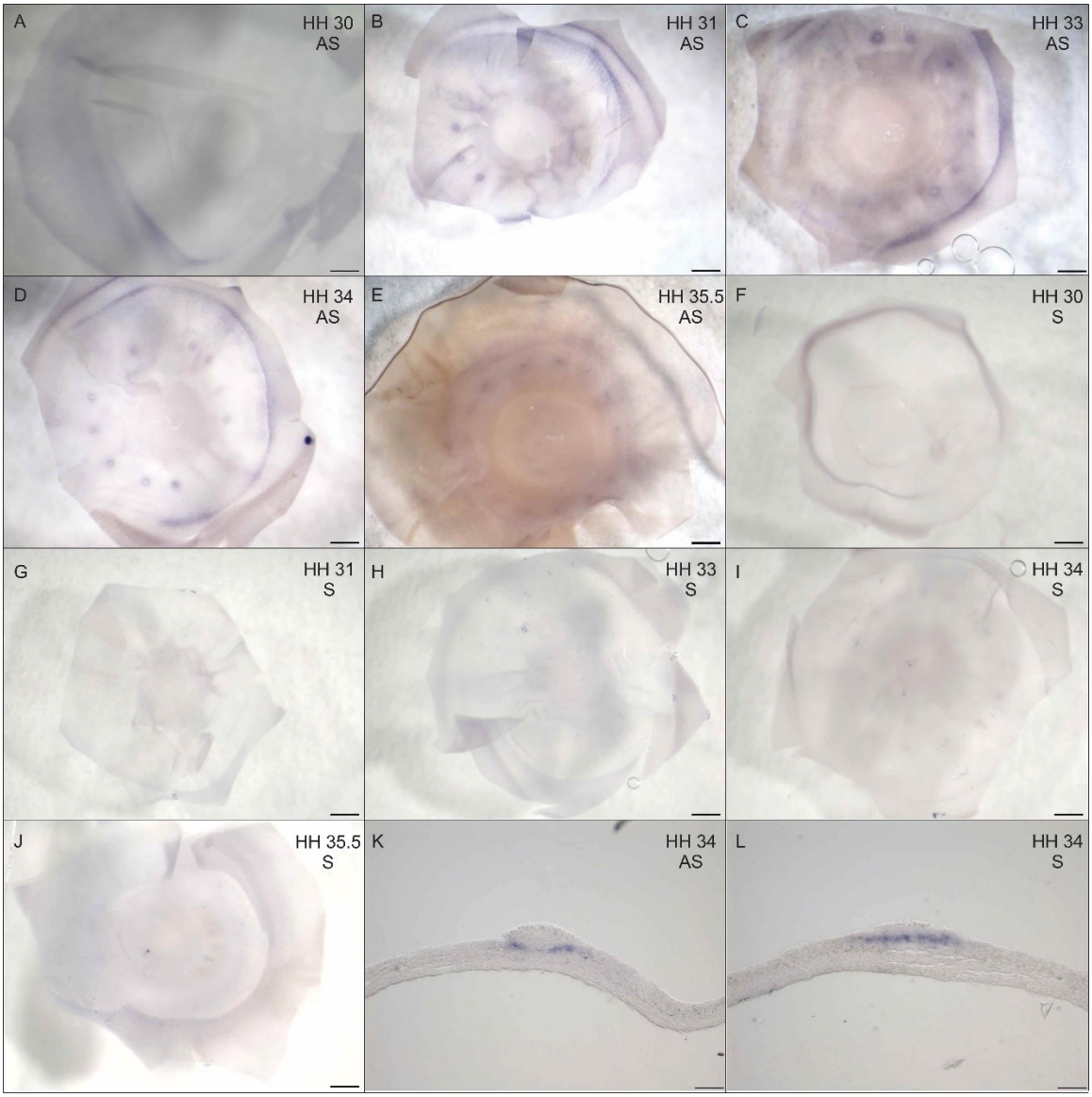

Figure 4.10: Results of *in situ* hybridization for *Inhba*. **A-E** show the results of *in situ* hybridization using the antisense riboprobe for *Inhba* while **F-J** show the results of *in situ* hybridization using the sense riboprobe. **A**) There is no expression in the eye. **B**) There is expression of *Inhba* in the temporal conjunctival papillae. **C**) The temporal, nasal and dorsal papillae all express *Inhba*. **D**) The temporal and nasal papillae have begun to downregulate *Inhba.* There is strong expression in the dorsal and ventral papillae. **E**) The dorsal and ventral papillae have begun to downregulate their expression of *Inhba*. No signal was detected using the sense riboprobe for *Inhba* at any of the stages examined: **F**) HH 30, **G**) HH 31, **H**) HH 33, **I**) HH 34, and **J**) HH 35. **K**) Cryosectioning reveals that the papilla expression is restricted to the basal lamina. **L**) A later section through the border of the conjunctival papilla shown in K shows the expression of *Inhba* in the basal lamina extending into the papilla-contiguous region. AS: antisense riboprobe, S: sense riboprobe. **A-J** scale bars are 500 µm. **K-L** scale bars are 20 µm.

DLX5

Based on the results of *in situ* hybridization, *Dlx5* is not expressed in the eye at HH 30 (N=10) (Figure 4.11A). By HH 31 (N=4), *Dlx5* is strongly expressed in the conjunctival papillae of the temporal and nasal groups (Figure 4.11B). At the next stage examined, HH 33 (N=4), *Dlx5* is strongly expressed in the temporal, nasal, and dorsal groups (Figure 4.11C). By HH 34 (N=7), all of the conjunctival papillae in the eye express *Dlx5* (Figure 4.11D). Between HH 35-36.5 (N=12), the temporal conjunctival papillae begin to downregulate their expression of *Dlx5* and induce the expression of *Dlx5* in the underlying condensation (Figure 4.11E). This condensation is at first small and ovoid in shape but by HH 36 is large and trapezoidal, reflective of the final shape of the condensation (Figure 4.11E). This expression of *Dlx5* in the condensations of the temporal region was confirmed by cryosectioning (Figure 4.11M). In the nasal, dorsal, and ventral regions at HH 35-35.5, the conjunctival papillae still express *Dlx5* (Figure 4.11E). These papillae also appeared to have begun to induce expression of *Dlx5* in the underlying condensations. Interestingly, when this region was sectioned, it was determined that this expression of *Dlx5* extended from the papilla into the papilla-contiguous region and a short distance into the interpapillary region in both the epithelium and the mesenchyme (Figure 4.11K and L). Furthermore, this expression seemed to be descending from the papilla, papilla-contiguous region, and part of the interpapillary region down through the mesenchyme to the underlying scleral condensation (Figure 4.11K and L). It should be noted that there is a distinct region of the interpapillary zone that is devoid of *Dlx5* expression (Figure 4.11K, dotted outline). These results strongly suggest that *Dlx5* is required for both the induction and patterning of the conjunctival papillae and the underlying scleral condensations.

Unlike with *Prox1, Ednrb,* and *Inhba* above, the *in situ* hybridization with the sense riboprobe for *Dlx5* detected signal. The expression pattern detected using this sense riboprobe was quite interesting as it was very different from that observed using the antisense riboprobe. Faint signal using the sense riboprobe for *Dlx5* was first detected in the conjunctival papillae of the temporal and nasal groups beginning at HH 31 (N=2) (Figure 4.11G). By HH 33 (N=2), this signal was detected in all of the currently present conjunctival papillae (Figure 4.11H) and by HH 34 (N=2), the signal from the sense riboprobe for *Dlx5* was strongly expressed in all of the conjunctival papillae while faint expression was detected in the mesenchyme beneath each papilla (Figure 4.11I). However, between HH 35 and 36, signal for the sense riboprobe of *Dlx5* was not expressed in the mesenchyme and/or the scleral condensations at has the antisense riboprobe; instead, instead, the signal for the sense riboprobe was still strongly detected within conjunctival papillae (Figure 4.11J). In order to determine the nature of this sense riboprobe signaling for *Dlx5*, the gene sequence was re-examined. This verification showed that *Dlx6* is located very nearby, on the same chromosome. It is, however, oriented in the reverse direction. In order to determine whether the sense probe was binding to *Dlx6,* this plasmid was sent for sequencing. Unfortunately, the sequencing for the sense riboprobe was inconclusive, as the sequence provided to me by the Center for Applied Genomics (Toronto, Ontario) was only 199 bp long as compared to the 1303 bp of the original riboprobe. When this sequence was analyzed using NCBI BLAST, it did not bind to any target sequence. I was therefore unable to determine whether the signal generated by the sense riboprobe for *Dlx5* may also be generating antisense expression for a different gene. The results of the sequencing analysis, however, confirmed that the antisense riboprobe

was that of *Dlx5*. Interestingly, when the gene sequence for *Dlx5* (NCBI gene ID 373969) was BLASTed against the chicken genome, it generated a 125 bp overlap, in the antisense direction, of 81.6% homology with *Dlx3*. Therefore, as this probe was generated from a published plasmid (which did not show evidence of sense expression at HH 7 [the stage examined]) and the sense expression was different than the antisense expression, I hypothesize that this sense expression is the expression of either *Dlx3* or *Dlx6*. This will require further analysis.

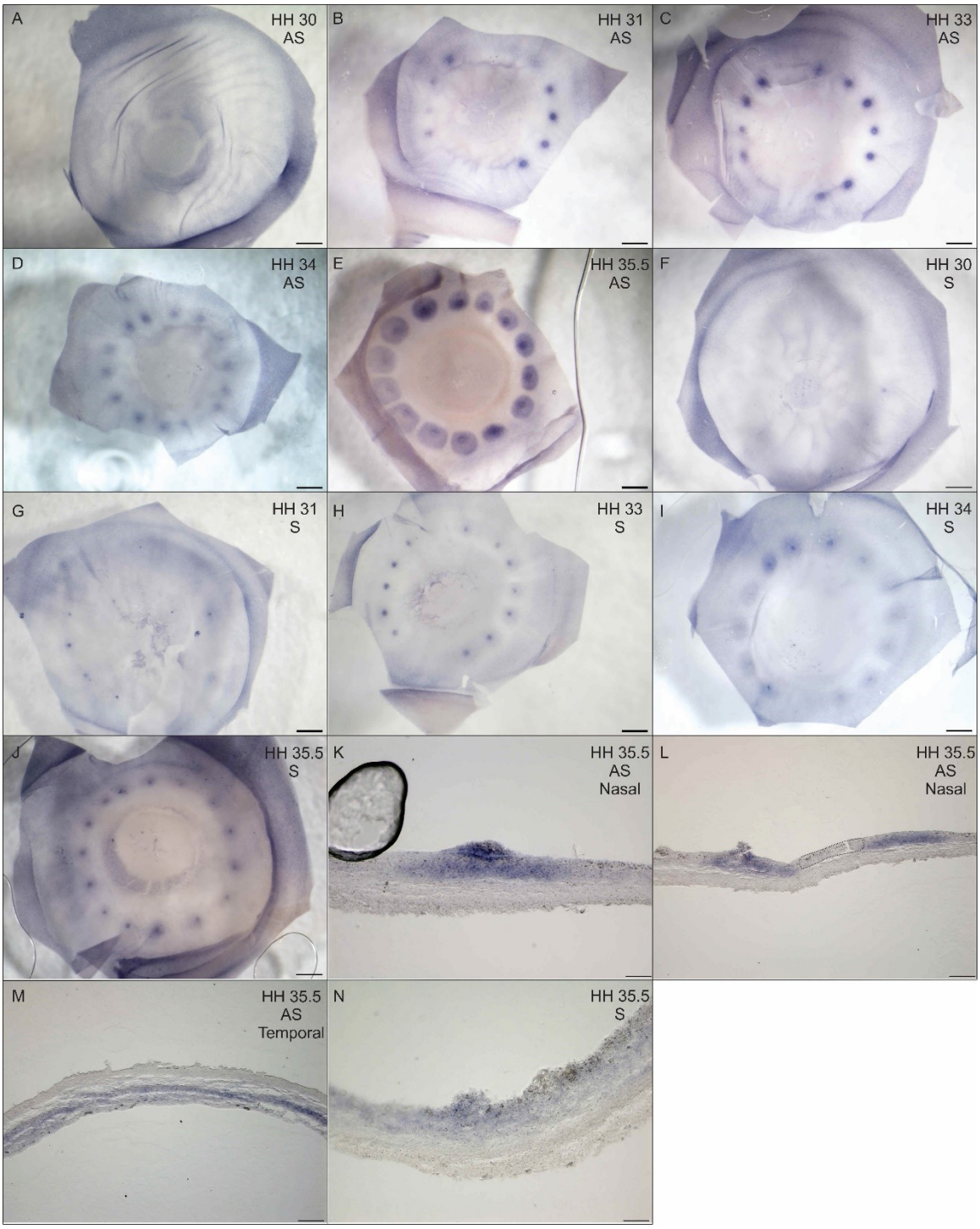

Figure 4.11: Results of *in situ* hybridization for *Dlx5*. **A-E, K-M** show the results of *in situ* hybridization using the antisense riboprobe for *Dlx5* while **F-J, N** show the results of *in situ* hybridization using the sense riboprobe. **A**) There is no expression in the eye. **B**) The temporal and nasal conjunctival papillae strongly express *Dlx5*. **C**) The temporal, nasal, and dorsal papillae all express *Dlx*. **D**) All of the conjunctival papillae in the ring express *Dlx5*. **E**) The papillae in the nasal, dorsal, and ventral region still express *Dlx5*

while the temporal papillae have downregulated *Dlx5*. There appears to be strong mesenchymal expression in the shape of a condensation under each of the papillae. **F**) There is no expression in the eye. **G**) There is faint expression in the temporal and nasal conjunctival papillae. **H**) There is faint expression in the temporal, nasal, and dorsal conjunctival papillae. **I**) There is faint expression in all of the conjunctival papillae and there appears to be faint mesenchymal expression underneath each of the papillae. **J**) There is expression in all of the conjunctival papillae but no mesenchymal expression. **K**) A cryosection through a nasal papilla reveals expression of *Dlx5* in the epithelium and first few layers of the mesenchyme of the papilla and papilla-contiguous region. There is no expression of *Dlx5* in the inter-papillary region. **L**) A section through the same region as K at a lower magnification shows that both the papilla and papilla-contiguous region express *Dlx5* while the inter-papillary region is devoid of *Dlx5* expression (dotted outline). **M**) Cryosectioning through the temporal region at the same stage reveals that this expression becomes localized to the underlying condensation and that these condensations have begun to overlap. **N**) Cryosectioning reveals that the signal detected by the sense riboprobe is expressed throughout the epithelium and first few layers of mesenchyme with faint expression in the papilla. No signal was detected in the underlying scleral condensations. AS: antisense riboprobe, S: sense riboprobe. **A-J** scale bars are 500 μm. **K, M,** and **N** scale bars are 20 μm. **L** scale bar 10 μm.

GSC

Based on the results of *in situ* hybridization, *Gsc* is not expressed in the eye at HH 30 (N=10), 31 (N=4), 33 (N=4), 34 (N=7), or 35 (N=3) (Figure 4.12A-D). By HH 35.5 (N=4), however, *Gsc* is faintly expressed in all of the conjunctival papillae (Figure 4.12E). Surprisingly, however, there also appeared to be widespread, albeit faint, expression of *Gsc* throughout the mesenchyme except in a large circular area directly beneath each of the conjunctival papillae which was devoid of *Gsc* expression; this area corresponds to the area in which the scleral condensations will form (Figure 4.29E). Furthermore, these large circular areas devoid of *Gsc* expression were separated from one another by a narrow rim of *Gsc* expression (Figure 4.12E). Cryosectioning at HH 35.5 confirmed that this expression between the presumptive scleral condensations was mesenchymal and restricted to only a few cells (Figure 4.12K circle). Furthermore, sectioning also revealed that the papilla expression seemed to be restricted only to the surface of the M-stage 5 papilla

(Figure 4.12L). These results therefore suggest that *Gsc* is not required for the induction and patterning of the conjunctival papillae, but may play a role in the induction and patterning of the scleral condensations. Moreover, this is the first gene to ever be recorded in the inter-condensation zone, which may indicate that *Gsc* plays a role in establishing the boundaries between condensations.

Unlike with *Prox1, Ednrb,* and *Inhba* above, the *in situ* hybridization with the sense riboprobe for *Gsc* detected signal. The expression pattern detected using this sense riboprobe was quite interesting as it was very different from that observed using the antisense riboprobe. Similarly, to the antisense riboprobe above, there was no signal detected using the sense riboprobe at HH 30 (N=3). Surprisingly, however, signal was detected using the sense riboprobe in the temporal conjunctival papillae beginning at HH 31 (N=2; Figure 4.12G). By HH 33, there was strong signal detected using the sense riboprobe in both the temporal and nasal conjunctival papillae (N=2; Figure 4.12H). This signal was maintained through to HH 34 (N=2), where it was detected in all of the conjunctival papillae in the ring. By HH 35.5 (N=2), on the other hand, only faint signal was detected in the conjunctival papillae and there was no obvious signal in the underlying mesenchyme (Figure 4.12J). Cryosectioning confirmed that there was no mesenchymal signal detected in the mesenchyme (not shown). That signal was detected using the sense riboprobe was somewhat surprising as there are no nearby genes that coded in the reverse direction. In order to validate the observed signal that was detected with the sense riboprobe, the plasmid for *Gsc* was sent for sequencing. Results of sequencing showed that the antisense riboprobe was targeting only the sense strand of *Gsc.* The sense riboprobe, on the other hand, which primarily targeted the antisense strand of *Gsc,* also

targeted a small region (34 bp in length) of the sense strand of an un-identified gene product on chromosome 20. It is therefore possible that the signal detected with the sense riboprobe represents either binding of the sense riboprobe to the antisense strand of *Gsc* or expression of the unidentified gene product on chromosome 20. Therefore, the signal detected using the sense riboprobe will require further study in order to identify which gene it may be attributed to and, therefore, will not be discussed further.

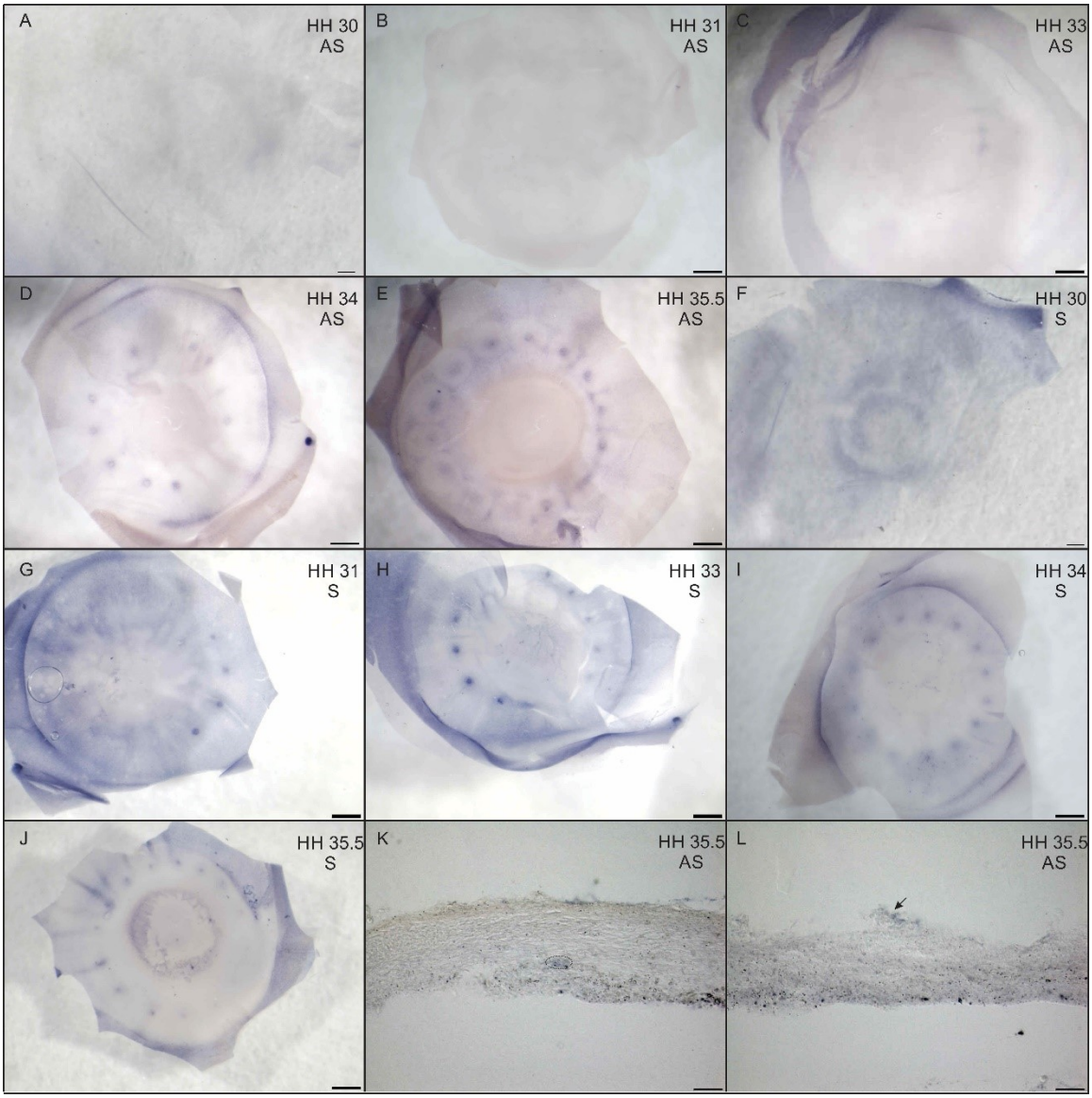

Figure 4.12: Results of *in situ* hybridization for *Gsc*. **A-E, K, L** show the results of *in situ* hybridization using the antisense riboprobe for *Gsc* while **F-J** show the results of *in situ*

hybridization using the sense riboprobe. There is no expression of *Gsc* in the eye at **A**) HH 30, **B**) HH 31, **C**) HH 33, or **D**) HH 34. **E**) There is expression of *Gsc* in all of the conjunctival papillae in the eye and expression throughout the mesenchyme save for a large area directly beneath each of the papillae where the condensations will form. These areas devoid of *Gsc* expression are separated from one another by a thin band of *Gsc* expression. **F**) There is no expression in the eye. **G**) There is expression in the temporal conjunctival papillae. **H**) There is expression in the temporal and nasal conjunctival papillae. **I**) There is faint expression in all of the conjunctival papillae. **J**) The conjunctival papillae appear to begun downregulating *Gsc* and there is no mesenchymal expression. Sectioning confirmed that there is no mesenchymal expression at this stage (not shown). **K**) Cryosectioning reveals a small, few cell layer thick band of expression in the mesenchyme on the same plane as the conjunctival papillae (circle). This expression in located in the inter-condensation zone. **L**) Cryosectioning through a papilla reveals that expression is located only on the surface epithelium and not throughout the papilla (arrow). AS: antisense riboprobe, S: sense riboprobe. **A-J** scale bars are 500 μm. **K** and **L** scale bars are 20 μm.

EYA1

Based on the results of *in situ* hybridization, *Eya1* is not expressed in the eye at HH 30 (N=8; Figure 4.13A). The first expression of *Eya1* is visible in the conjunctival papillae of the temporal and dorsal groups at HH 31 (N=2), although there also appears to be faint expression throughout the eye (Figure 4.13B). By HH 33 (N=2), *Eya1* is also expressed in the dorsal conjunctival papillae and is faintly expressed throughout the epithelium (Figure 4.13C). By HH 34 (N=9), all of the conjunctival papillae in the eye express *Eya1* and *Eya1* is also faintly expressed throughout the epithelium (Figure 4.13D). Cryosectioning of a sample at HH 34 revealed faint, widespread expression throughout the epithelium and mesenchyme, with stronger expression in the papilla itself (Figure 4.13K). By HH 35.5 (N=3), *Eya1* is downregulated in the conjunctival papillae and is now only expressed in the underlying mesenchyme, but does not appear to be restricted to the future sites of condensation formation as evidenced in other genes (compare Figure 4.13E and Figure 4.11E). These results suggest that *Eya1* may be required for the induction and patterning

of the conjunctival papillae, but does not appear to be involved in the induction of the underlying condensations. The role of *Eya1* at HH 35.5 is currently unclear.

Unlike with *Prox1, Ednrb,* and *Inhba* above, the *in situ* hybridization performed with the sense riboprobe for *Eya1* detected signal. No signal was detected at HH 30 (N=2; Figure 4.13F). However, signal for the sense riboprobe was detected in all of the visible conjunctival papillae at each HH 31 (N=2), HH 33 (N=2), HH 34 (N=2) (Figure 4.13H-I). At HH 35.5 (N=2), there was strong, widespread signal detected throughout the eye and strong signal detected in all of the conjunctival papillae (Figure 4.13J). This expression pattern was very different than that observed using the antisense riboprobe at HH 35.5 (above). Cryosectioning at HH 34 revealed that this signal detected using the sense riboprobe was located throughout the epithelium and mesenchyme, with stronger expression in the conjunctival papillae (Figure 4.13L). An analysis of the chromosome upon which *Eya1* is found did not find any genes coding in the reverse direction nearby. Therefore, the plasmid for *Eya1* was sequenced. The results of sequencing did not elucidate the matter, as both the antisense and sense strands of the plasmid were specific to *Eya1*. To further test this plasmid and the validity of this sense expression, I examined the publication in which this gene was described and replicated the *in situ* hybridization at HH 13-14. The results of *in situ* hybridization using both the antisense and sense riboprobes was similar to what is described in the literature, with expression of *Eya1* in the somites and otic region (Figure 4.14A and B). This may suggest that the signal detected with the sense riboprobe represents binding of the sense riboprobe to the antisense strand of *Eya1* and not non-specific binding. There are, however, seven isoforms of *Eya1* that have been identified in the chicken and sequence of both the sense and antisense riboprobes

were able to bind to at least four of the isoforms. This may thus suggest that the antisense expression described above may be for a different isoform of *Eya1*. This will require further research.

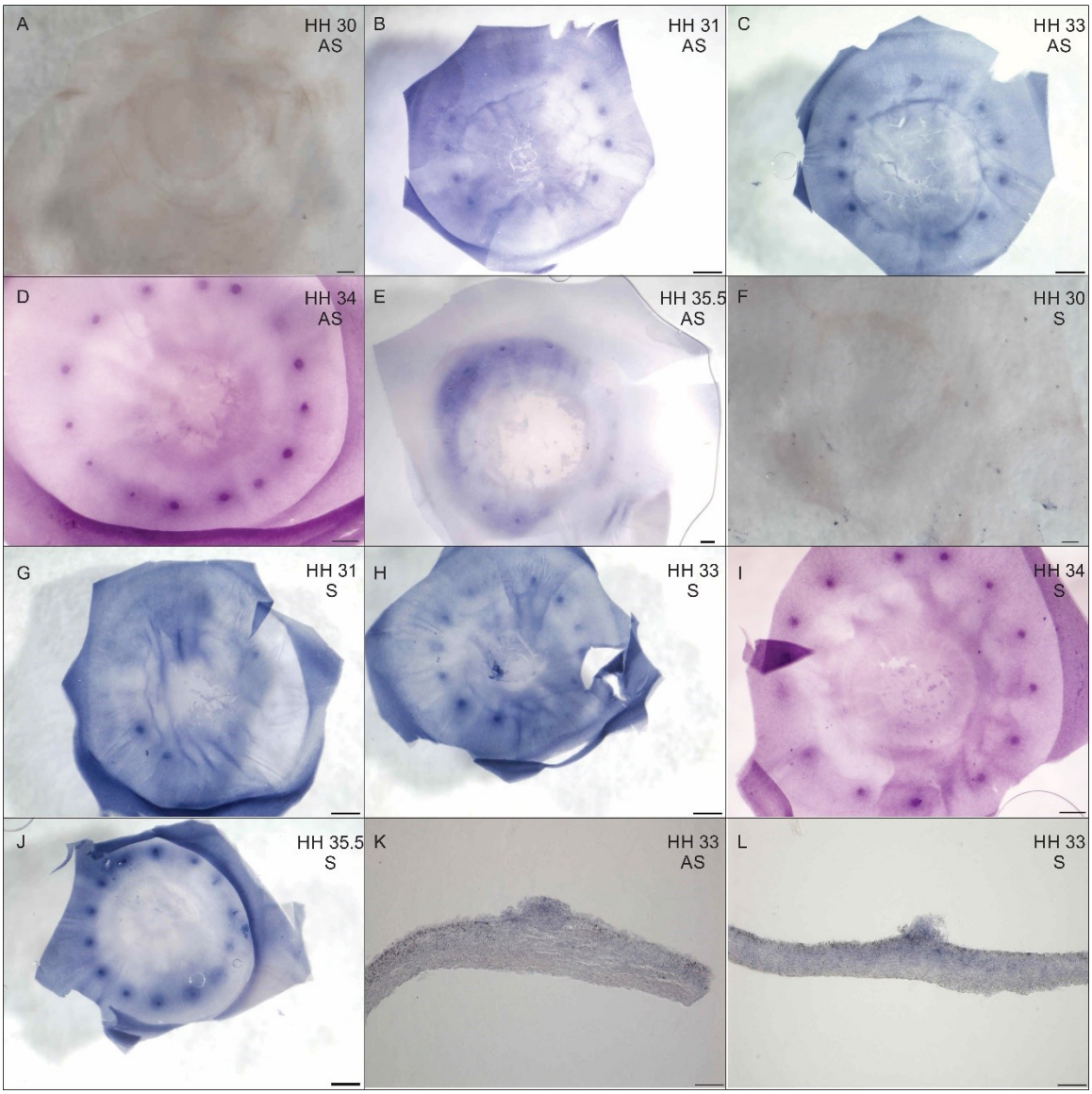

Figure 4.13: Results of *in situ* hybridization for *Eya1*. **A-E, K** show the results of *in situ* hybridization using the antisense riboprobe for *Eya1* while **F-J, L** show the results of *in situ* hybridization using the sense riboprobe for *Eya1*. **A**) There is no expression in the eye. **B**) There is expression in the temporal and nasal conjunctival papillae as well as faint expression throughout the eye. **C**) There is expression in the temporal, nasal, and dorsal conjunctival papillae and widespread expression throughout the eye. **D**) All of the conjunctival papillae strongly express *Eya1* and there is widespread expression throughout the eye. **E**) The conjunctival papillae have downregulated their expression. There is now

expression in the underlying mesenchyme that does not appear to be restricted to the future sites of condensation formation. **F**) There is no expression in the eye. **G**) There is expression in the temporal conjunctival papillae and widespread expression throughout the eye. **H**) There is expression in the temporal, nasal, and dorsal papillae and widespread expression throughout the eye. **I**) All of the conjunctival papillae in the ring express *Eya1* and there is widespread expression throughout the eye. **J**) There is strong expression in all of the conjunctival papillae in the eye as well as widespread expression throughout the eye. **K**) Cryosectioning reveals that there is expression in the conjunctival papillae as well as the rest of the epithelium and the surface mesenchyme. **L**) Cryosectioning reveals strong expression in the papillae as well as widespread expression throughout the epithelium and surface mesenchyme. AS: antisense riboprobe, S: sense riboprobe. **A-J** scale bars are 500 µm. **K** and **L** scale bars are 20 µm.

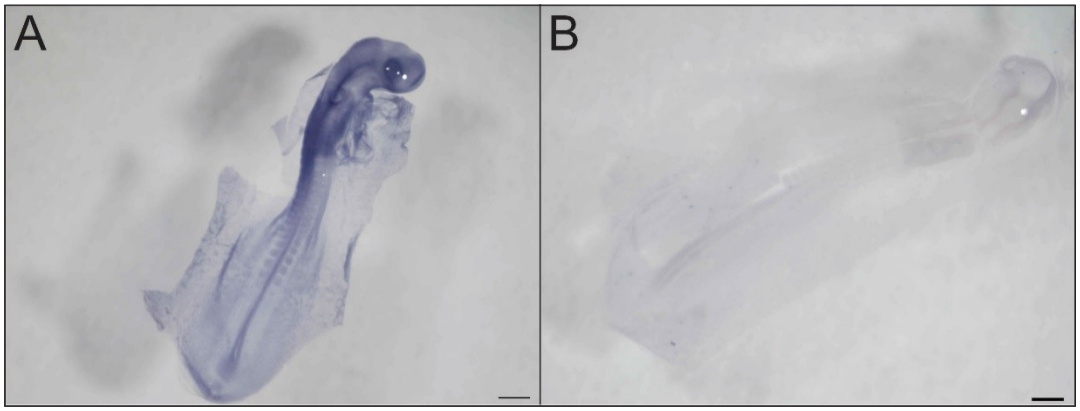

Figure 4.14: Results of *in situ* hybridization for *Eya1*. **A**) Antisense riboprobe expression of *Eya1* at HH 14 is found in the eye, the otic region, neural tube and in the somites. **B**) No signal was detected using the sense riboprobe at HH 13.

4.3.2.4 – Summary of Candidate Gene Analysis

Interestingly, all six of the candidate genes were expressed during the induction and patterning of the scleral ossicle system (summarised in Figure 4.15). While none of these candidates were expressed at HH 30 (i.e. patterning the epithelium prior to the induction of the conjunctival papillae); four genes (*Eya1, Dlx5, Inhba,* and *Ednrb*) were expressed in the conjunctival papillae as they developed (HH 31 through to HH 34). Two of these genes, *Inhba* and *Ednrb* were expressed transiently while *Prox1* was only strongly expressed in the conjunctival papillae at HH 34, when all the conjunctival papillae had been induced and patterned. Furthermore, during this study, two genes were identified

which likely play a role in the induction and patterning of the underlying scleral condensations. The first, *Dlx5* is expressed in both the conjunctival papillae and the underlying scleral condensations at HH 35.5. This suggests that *Dlx5* may be aiding in fate determination of the scleral condensations, a similar role to that described for *Bmp2* in Chapter 3. *Gsc*, on the other hand, is only expressed in the area around the scleral condensations and is therefore likely acting to delimitate the boundaries of the scleral condensations. While the functions of these candidate genes cannot be conclusively stated without further experimentation, the timing of their expression and their spatial patterning can allow an approximation of the roles they may be playing during the induction and patterning of the sclerotic ring. Additionally, this candidate gene analysis has identified some of the genes involved in the induction and patterning of the conjunctival papillae and at least one gene which may be involved in delimitating the size of the scleral condensations. This research paves the way for future analyses of new genes involved in the scleral ossicle system.

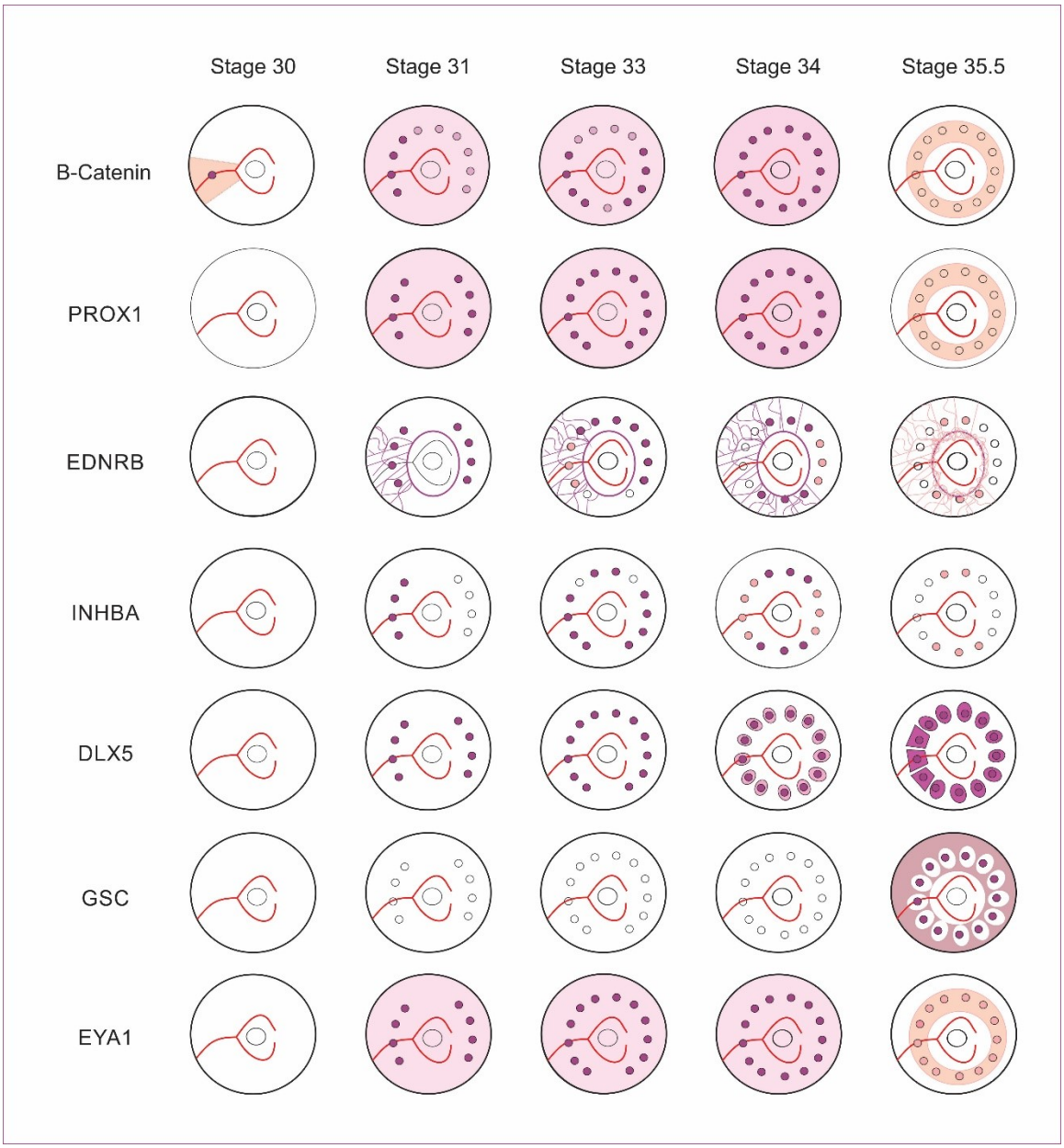

Figure 4.15: A schematic summarizing the expression of all my candidate genes during the induction and patterning of the conjunctival papillae and scleral ossicles between HH 30 and 35.5. Strong expression (dark purple), medium expression (light purple), faint expression (pink), ciliary artery: red.

4.4 – Discussion

As described in the introduction to this chapter, during the course of this thesis project it has become difficult to ignore the similarities between the conjunctival papillae and the other placodes. All currently identified placodes are epithelial thickenings that give rise to a diverse array of derivative structures including sensory organs and cutaneous appendages such as hair, feather, scales and teeth. In all cases, the placodes are transient in nature, are similarly induced, and are responsible for the temporospatial patterning of their respective derivative structures. While not all of the genetic factors required for their induction are the same, the induction of a placode typically includes: i) an initial inductive phase or pre-patterning of the epithelium, ii) the induction of the epithelial thickening in the epithelium via signaling from the underlying mesenchyme, and iii) the induction of a subsequent structure by the placode. The aim of this discussion is therefore to demonstrate the similarities between the conjunctival papillae and other placodes based on the results of my candidate gene analysis (summarized in Figures 4.15 and 4.16). To do this, I will begin by discussing my results pertaining to the pre-patterning of the epithelium, namely that of *in situ* hybridization for *β-catenin*. I will then present my hypothesis for the induction of the epithelial thickening, in light of the results of *in situ* hybridization for my six candidate genes. Following this, I will briefly discuss the induction and patterning of the subsequent structure by the conjunctival papillae, as I hypothesize that I have identified two genes that appear to be involved in the induction and patterning of the scleral condensations. It is important to note that much of this discussion will be speculative, presenting possible ways in which these genes could interact to govern the induction and patterning of both the conjunctival papillae and the scleral condensations. The exact role

of these genes will not be able to be conclusively determined until functional analyses have been conducted, which is outside of the scope of the present study.

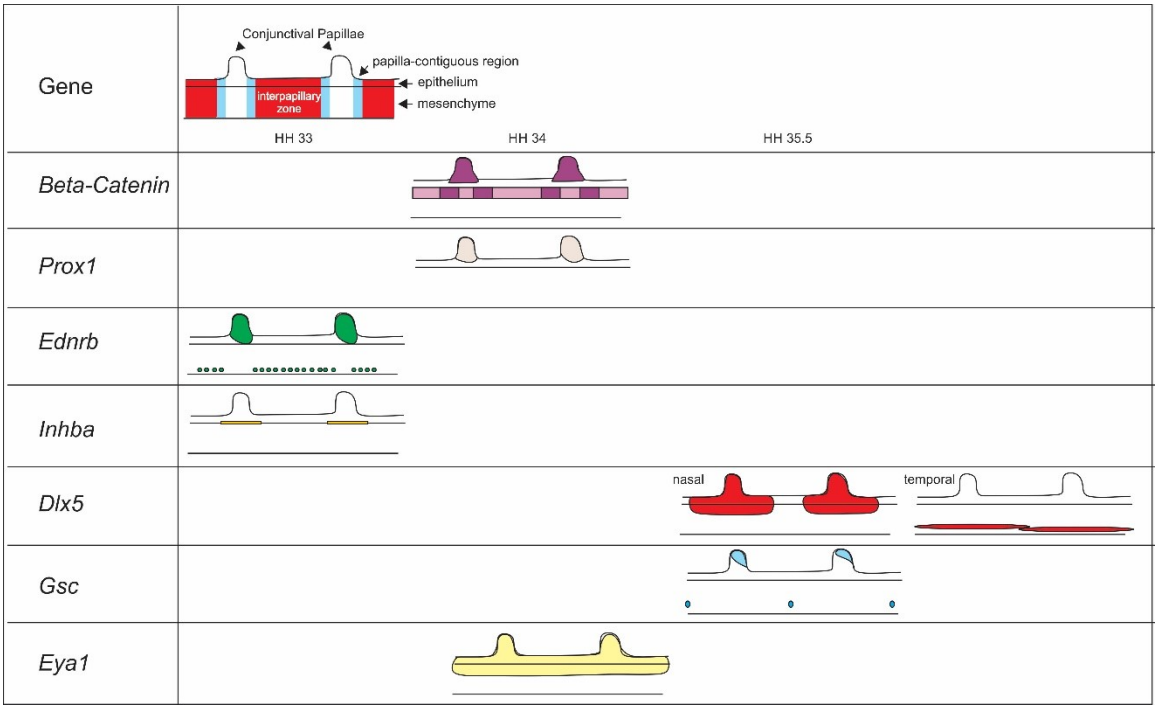

Figure 4.16: A schematic summarizing the results of cryosectioning at the stage of strongest expression for each of the candidate genes. The dots of expression in Ednrb represent the vasculature expression and the dots in Gsc represent the tiny zones of expression between the developing scleral condensations. Each gene is presented in a different color in order to differentiate them in Figure 4.17 below. Strong expression is shown by darker colors and faint expression by pastels.

4.4.1 – Pre-Patterning of the Epithelium

In order to begin addressing the similarity of the conjunctival papillae to other placodes, it is necessary to demonstrate that there is an initial induction phase or some sort of pre-patterning of the epithelium. I first addressed the idea of epithelial competency in Chapter 3, where the results of surgical ablation of a single papilla suggest that there is some sort of epithelial competency factor restricting the regeneration of the ablated conjunctival papilla to only the area in which the conjunctival papilla was removed. Furthermore, the ability of the conjunctival papilla to regenerate suggest both that the

epithelium remains competent to respond to the mesenchymally-derived inductive cue and that the inductive signal is still expressed.

When the literature was queried for epithelial competency factors in other placodal systems, *β-catenin* was identified as an epithelial competency factor during placode formation in tooth, feather, and hair (Wolpert, 1998; Eames & Schneider, 2005; Widelitz, 2008; Duverger & Morasso, 2009; Dhouailly, 2009; Sayama *et al*., 2010; Enshell-Seijffers *et al*., 2010; Jiang *et al*., 2011; Painter *et al*., 2012; Sennett & Rendl, 2012; Huang *et al*., 2012; Woo *et al*., 2012; Suksaweang *et al*., 2012; Wells *et al*., 2012 Chuong *et al*., 2013; Myung *et al*., 2013; O'Connor *et al*., 2013). In these systems, there is initial widespread expression of *β-catenin* in the epithelium, followed by localized expression in the placode (Wolpert, 1998; Eames & Schneider, 2005; Widelitz, 2008; Duverger & Morasso, 2009; Dhouailly, 2009; Sayama *et al*., 2010; Enshell-Seijffers *et al*., 2010; Jiang *et al*., 2011; Painter *et al*., 2012; Sennett & Rendl, 2012; Huang *et al*., 2012; Woo *et al*., 2012; Suksaweang *et al*., 2012; Wells *et al*., 2012 Chuong *et al*., 2013; Myung *et al*., 2013; O'Connor *et al*., 2013). Therefore, I used *in situ* hybridization to determine the expression pattern of *β-catenin* prior to the induction and patterning of the conjunctival papillae. As described in the results above, *β-catenin* was not expressed at either HH 28 or 29. It was, however, expressed in the temporal region of the eye beginning at HH 30, prior to the induction of the first conjunctival papilla. Expression was centered directly above the ciliary artery and seemed to be strongest in the presumptive papilla region. This expression of *β-catenin* in the temporal epithelium, prior to condensation induction and the expression of any other papilla genes, strongly suggests that *β-catenin* is required to establish epithelial competency and is required for conjunctival papilla induction as it is in tooth,

hair, and feather. However, as the conjunctival papillae form over a period of days, I extended the *in situ* hybridization analysis to include HH 31, 33, 34, and 35.5. Throughout these stages, there was widespread expression of *β-catenin* in the eye which resolved to strong expression in each of the presumptive papillae (Figure 4.6B and C). This is similar to what was described in the induction of the hair, feather, and tooth placodes above. It is, however, interesting to note that this widespread expression of *β-catenin* does not disappear after the induction of the conjunctival papillae, but is instead maintained through to HH 34. Furthermore, sectioning determined that this widespread expression of *β-catenin* at HH 34 was primarily in the mesenchyme, where there was strong expression in the mesenchyme of the papilla-contiguous region, subjacent to the epithelium (Figure 4.16). The localization of *β-catenin* expression to the mesenchyme of the papilla-contiguous region at HH 34 is quite interesting as it precedes the expression of *Dlx5* in this region at HH 35 (Figure 4.11K), which may suggest that *β-catenin* has an additional role in the induction and/or patterning of the scleral condensations. Of particular interest is that canonical Wnt signaling, which is mediated through the expression of *β-catenin*, has been shown to be involved in the fate determination of osteoblasts, a process in which *Dlx5* is considered to be one of the master regulators (Kang *et al*., 2007). Equally interesting is that, at HH 35.5, *Dlx5* has been induced in this papilla-contiguous region, while the expression of *β-catenin* has been downregulated in the papillae and seems to be confined to the area in which the scleral condensations will be induced. This may therefore suggest that this maintained, widespread expression of *β-catenin* in the mesenchyme, after the conjunctival papillae have been induced, may have to do with the skeletogenic nature of the tissue. As neither hair, tooth, nor feather will give rise to an osteogenic derivative, they

may not require the sustained expression of *β-catenin*. It is also possible that this prolonged mesenchymal expression of *β-catenin* (until HH 35.5) may be required to maintain epithelial competency in the conjunctival epithelium, which permits the regeneration of a conjunctival papilla after surgical ablation. This hypothesis has some experimental support as in the ablations performed by Coulombre & Coulombre (1962), the surface mesenchyme was also ablated and the papillae did not regenerate. This will provide an interesting avenue for future research. Furthermore, after determining that *β-catenin* is expressed within the conjunctival papillae and may be required for the induction of the underlying scleral condensations, I wanted to determine whether *β-catenin* could be the factor identified by Pinto and Hall (1991) of 3.5 to 6 kDa required for the induction of the underlying scleral condensations. Unfortunately, this does not seem to be the key inductive factor as β-catenin is quite large, with a weight of 85 kDa.

It will be interesting, in future, to further examine the way in which epithelial competency is established during the induction of the conjunctival papillae. If *β-catenin* is required for papilla induction, inhibition of *β-catenin* would abrogate papilla development. On the other hand, over-expression of *β-catenin* would possibly increase the papilla field, either extending it beyond the corneal-scleral limbus or increasing the number of papillae in the ring. Additionally, if *β-catenin* is also required for the induction and patterning of the scleral condensations, it will be important to determine the nature of this interaction. It will therefore be important, in future, to investigate the function of other epithelial competency genes such as *Eda* and Wnts in order to determine the similarity between this and other placodal systems.

4.4.2 – Investigating the Induction and Patterning of the Conjunctival Papillae and the Induction of the Underlying Scleral Condensations

After the initial patterning or pre-patterning of the epithelium, the second step in placode induction is the induction of the placode itself via a mesenchymal signal. As in all other placodal systems, it is quite difficult to identify the components of a mesenchymal-epithelial inductive cascade as the events are all taking place simultaneously. The following section will address the results of *in situ* hybridization for each of the six candidate genes (*Prox1, Ednrb, Inhba, Dlx5, Gsx,* and *Eya1*) and will speculate as to the roles that they may be playing during the induction and patterning of the conjunctival papillae.

4.4.2.1– PROX1

As described in the results section above, *Prox1* is only faintly expressed in the conjunctival papillae beginning at HH 33. This expression becomes stronger at HH 34. As almost all of the conjunctival papillae in the ring have been induced prior to the expression of *Prox1*, it is not likely that *Prox1* expression is required for the induction and patterning of the conjunctival papillae. *Prox1* may rather be involved in the morphological development of the papillae and the onset of condensation induction. The timing of onset of *Prox1* expression is interesting as *Prox1* has been shown to play a role in the ectopic activation of some downstream effectors of the Hh signaling pathway during lens development (Kerr *et al*., 2012). As *Ihh*, *Ptc*, and *Shh* are all expressed in the conjunctival papillae beginning at HH 35 during the induction and patterning of the underlying scleral condensations (Franz-Odendaal, 2008a; Duench & Franz-Odendaal, 2012), it is possible that *Prox1* is upregulated at HH 34 in order to play a role in regulating the onset of expression of the Hh family beginning at HH 35, at which point *Prox1* has begun to be

downregulated. A link between these two genes has not yet been identified in this system and will require further research. One such study could, through bead implantation, knock-down the expression of *Prox1* at HH 34 and perform *in situ* hybridization for *Shh* and/or *Ihh* in order to determine whether *Prox1* is upstream of *Hh* expression in the conjunctival papillae.

Other studies have identified *Prox1* as a target of *β-catenin-TCF/LEF* signaling (Karalay *et al*., 2011, Loh *et al*., 2014). As *β-catenin* expression was shown during this study to be expressed in the conjunctival papillae until at least HH 34, it is possible that the onset of *Prox1* expression may, in turn, be regulated by canonical Wnt signaling. As no members of the Wnt family have yet been investigated in the sclerotic ring system, this will require further study. It will be particularly interesting to conclusively determine the role played by *Prox1* in the induction and patterning of the scleral condensations due to its recorded role in the literature as both a transcriptional activator and repressor (Chen *et al*., 2008). Furthermore, *Prox1* has a weight of 83 kDa, much larger than the size identified by Pinto and Hall (1991), making it unlikely to be the key factor required for the induction and patterning of the scleral condensations.

4.4.2.2 - EDNRB

As described in the results section above, *Ednrb* was transiently expressed in the conjunctival papillae beginning at HH 31, when it was faintly expressed in the conjunctival papillae of the temporal and nasal groups. This temporal and nasal expression was downregulated by HH 33 prior to the onset of *Ednrb* expression in the dorsal and ventral conjunctival papillae at HH 34, which, in turn, was downregulated by HH 35.5. This transient expression of *Ednrb* may suggest a role in the induction and patterning of the

conjunctival papillae themselves. *Ednrb* is unlikely, however, to be involved in papilla maintenance as its expression is not sustained. *Ednrb* is also unlikely to be involved in either the induction or patterning of the scleral condensations as it is not expressed during their induction. Additionally, *Ednrb* has a weight of 49 kDa, indicating that it is unlikely to be the key inductive factor of 3.5 to 6 kDa identified by Pinto and Hall (1991).

This expression of *Ednrb* during the induction and patterning of the conjunctival papillae was somewhat surprising because, although *Ednrb* is expressed in NC-derived cells, its expression is primarily linked to the NCCs of the melanoblastic lineage (Lecoin *et al*., 1998; Hakami *et al*., 2006; Kelsh *et al*., 2009; Clouthier *et al*, 2010). As the exact nature of the NCCs which make up the periocular mesenchyme is not currently known, it is possible that there is a component of the periocular mesenchyme which is derived from the melanoblastic NCC lineage. Interestingly, endothelin-3 (*Edn3*), which is the ligand that binds to *Ednrb*, has been shown to be directly regulated by canonical Wnt expression (i.e. highly induced upon the activation of *β-catenin*) in the NC-derived melanocyte stem cells (Lee & Tumbar, 2012). It will be interesting to determine whether a similar interaction is required for the expression of *Edn3* in the conjunctival papilla and what effect this may have on the expression of *Ednrb*. Furthermore, it will be interesting to determine the way in which the expression of *Ednrb* is mediated in the sclerotic ring system and to identify whether the expression of *Ednrb* in the conjunctival papillae is induced by the underlying NC.

Interestingly, *Ednrb* has also been associated with vascular development and function (Thorin & Clozel, 2010; Mazzuca & Khalil, 2012; Paradis & Zhang, 2013) as well as the development of the vasculature in the eye (McGlinn *et al*., 2007). Indeed, I detected

strong expression of *Ednrb* in the developing vasculature in the temporal scleral mesenchyme. This vascular expression of *Ednrb* was particularly interesting as previous studies in the Franz-Odendaal lab have demonstrated that there is significant remodeling of the vasculature taking place in the eye during conjunctival papilla development which, in turn, leads to the establishment of an avascular zone directly beneath each of the conjunctival papillae (Jourdeuil & Franz-Odendaal, 2012; Jabalee & Franz-Odendaal, 2015). These avascular zones are required for scleral condensation formation and therefore, it is possible that *Ednrb* may be involved in this vascular remodeling. The regulatory network controlling the expression of *Ednrb* as well as the role played by *Ednrb* in the induction and patterning of the conjunctival papillae will require further study.

4.4.2.3 - INHBA

Similarly, to *Ednrb* above, *Inhba* was transiently expressed in the conjunctival papillae beginning in the temporal group at HH 31. Surprisingly, at this stage, there appeared to be a halo of *Inhba* expression in the papilla-contiguous region, just beyond the papilla itself. This temporal expression of *Inhba* was downregulated by HH 33, by which time *Inhba* was weakly expressed in the nasal papillae and strongly expressed in the dorsal papillae. Again, the conjunctival papillae in each group appeared to be surrounded by a halo of *Inhba* expression. By HH 35.5, there was no obvious expression of *Inhba* in the eye. Cryosectioning revealed that this halo of *Inhba* expression was likely due to the specific expression of *Inhba* in only the basal lamina underlying the conjunctival papillae, which toward the edge of the papilla extended slightly into the papilla-contiguous region. This expression pattern seems to suggest that *Inhba* is involved in the induction and patterning of the conjunctival papillae. Like *Ednrb*, as this *Inhba* expression is not

maintained, it is unlikely to be involved in the maintenance of the conjunctival papillae and, as all expression has been downregulated by HH 35.5, is unlikely to be involved in the induction of the scleral condensations. Similar to Prox1 and Ednrb, Inhba appears to be too large to be the key factor required for condensation induction, as it has a molecular weight of 47 kDa which is much larger than the 3.5 to 6 kDa factor identified by Pinto and Hall (1991). I have so far been unable to find any references to expression of *Inhba* (which was previously known as *Activin-βA*) in the basal lamina, and therefore, this specific localization of *Inhba* will require further investigation.

That *Inhba* may play a role in the induction and patterning of the conjunctival papillae is not altogether surprising, as Lan and colleagues (2014) identified a requirement for *Inhba* expression in tooth placode development. This study indicated that mice lacking *Inhba* function exhibit early developmental arrest of incisors and mandibular molar tooth germs (Lan *et al*., 2014). This *Inhba* expression in tooth placode is mediated by the expression of *Fgf8*, and therefore, it will be important to determine whether *Fgf8* is expressed during the induction and patterning of the conjunctival papillae and its spatiotemporal pattern. A study in hair development has placed *Inhba* expression downstream of *β-catenin* in the dermal papilla (Tsai *et al*., 2014). As *β-catenin* is expressed in the conjunctival papillae during their development, it is possible that the onset of *Inhba* expression is regulated by *β-catenin*. This is particularly interesting because the expression of *Inhba* is located directly above the strong expression of *β-catenin* in the papilla-contiguous region. This will require further research. It will also be interesting to extend the analysis of *Inhba* function beyond HH 35.5 as *Inhba* expression has been linked to the differentiation and function of osteoblasts (Hopwood *et al*., 2007). As the induction

of the scleral condensations has begun at HH 35.5, it is possible that *Inhba* expression is required for osteoblastogenesis during later condensation development.

4.4.2.4 - DLX5

As described in the results section above, *Dlx5* is first expressed in the conjunctival papillae of the temporal and nasal groups beginning at HH 31. By HH 33, the dorsal conjunctival papillae have also begun to express *Dlx5*. At HH 34, when all of the conjunctival papillae in the ring have been induced, they all strongly express *Dlx5* and there appeared to be faint mesenchymal expression of *Dlx5* directly beneath each of the conjunctival papillae. Cryosectioning determined that this condensation shaped expression begins first in the epithelium and first few layers of the mesenchyme of the papilla and papilla-contiguous region before being upregulated in the scleral condensations. This expression pattern for *Dlx5* suggests that *Dlx5* could play a role in the induction and patterning of the conjunctival papillae. In addition, this continued expression of *Dlx5* in the conjunctival papillae may indicate that it is required for papilla maintenance. Furthermore, *in situ* hybridization for *Dlx5* strongly suggests that it is involved in condensation induction.

The expression of *Dlx5* in the conjunctival papillae is somewhat surprising as, during cranial placode induction, *Dlx5* is required in the NPB prior to cranial placode formation in order to establish the competence of the PPR but is not expressed in the placodes themselves (Leung *et al.*, 2013; Moody & LaMantia, 2015). The cranial placodes, however, do not give rise to any skeletogenic derivatives (Zou *et al*., 2004; Meulemans & Bronner-Fraser, 2007; Harlow & Barlow, 2007; Kourakis & Smith, 2007; Schlosser *et al*., 2008; Canning *et al*., 2008; Knabe *et al*., 2009; O'Neill *et al*., 2012; Saint-Jeannet &

Moody, 2014; Steventon *et al*., 2014); therefore, the expression of *Dlx5* in the conjunctival papillae may be a tissue specific requirement. Furthermore, it is possible that this early expression of *Dlx5* confers upon the papillae the ability to induce skeletogenic derivatives. This will require further study.

It is interesting to note, however, that this critical function of *Dlx5* during the induction and patterning of the PPR is thought to be driven by the *Dlx*-mediated regulation of a BMP antagonist in the NPB and subsequent binding to a PPR-specific enhancer in the *Six1* gene (Moody & LaMantia, 2015). As *Six1* is known to interact with another of my candidate genes, *Eya1*, it will be interesting to determine whether there is a regulatory *Dlx5-Six1-Eya1* interaction taking place in the sclerotic ring system. Furthermore, *Msx1*, which has been shown to interact with *Dlx5* and is required for the activation of two other NPB specifying genes *Pax3* and *Zic1* (another candidate gene for this study), has also been shown to be capable of binding to this PPE-specific *Six1* enhancer (Moody & LaMantia, 2015). It will therefore be important, in future, to evaluate the role of *Msx1* during the induction and patterning of the conjunctival papillae.

Additionally, the mesenchymal expression of *Dlx5* during the induction and patterning of the scleral condensations is quite interesting. *Dlx5* has been shown in the literature to play a role in osteoblast differentiation and therefore this mesenchymal expression was not altogether unexpected (Lee *et al*., 2003a; Zhang *et al*., 2008; Samee *et al*., 2008; Cho *et al*., 2009; Itoh *et al*., 2009; Baek & Baek, 2012; Hagh *et al*., 2015). However, the size and shape of the mesenchymal expression of *Dlx5* at HH 35.5 was fairly surprising. To date, the only other gene which has been shown to be expressed in the scleral condensations during their induction is *Bmp2*, as was described in Chapter 3. This

Bmp2 expression at HH 35 and 35.5 is still ovoid in shape and does not yet reveal the final shape of the developing condensation. This therefore seems to suggest that expression of *Dlx5* is required prior to that of Bmp2 and may play a role in the fate determination of osteoblasts in the skeletogenic condensation. While this needs to be verified by further experimentation, there is support for this hypothesis in the literature. Many studies into the hierarchical regulatory relationships among the master regulators of osteogenesis; namely *Bmp2*, *Runx2*, *Osx*, and *Dlx5*; have suggested that *Dlx5* acts upstream of *Bmp2* during osteoblastogenesis (Lee *et al.*, 2003a; Itoh *et al*., 2009; Baek & Baek, 2012). Furthermore, *Dlx5* has been shown to mediate the expression of *Bmp2* in both early inner ear development and the induction of matrix extracellular phosphoglycoproteins in mineralized tissues (Cho *et al*., 2009; Sajan *et al*., 2010). Additionally, *Dlx5* expression in palatogenesis results in downregulation of *Fgf7* and expanded *Shh* expression, which suggests that it may also be playing a role in the regulation of *Shh* in this system (Han *et al*., 2009). Finally, during frontal bone development, *Dlx5* and *Msx1* has been shown to function synergistically to regulate osteogenesis (Chung *et al*., 2010). However, *Dlx5* does not seem to be the key factor required for the induction and patterning of the scleral condensations identified by Pinto and Hall (1991) as it has a molecular weight of 31 kDa.

Therefore, while further research needs to be conducted in order to unravel the role of *Dlx5* during the induction and patterning of the conjunctival papillae and the scleral condensations, current evidence suggests that it confers upon the papillae the ability to induce a skeletogenic placode and may be responsible for the subsequent regulation of osteoblastogenesis in the scleral condensations. In addition, this research suggests that

Msx1 would be a good candidate for future study due to its interactions with *Dlx5* during both osteogenesis and establishment of the PPR.

4.4.2.5 - GSC

As described in the results section above, *Gsc* was not expressed during the induction and patterning of the conjunctival papillae; and therefore is unlikely to be required for either the induction and patterning of the conjunctival papillae or papilla maintenance. Surprisingly, however, *Gsc* was expressed in the papillae at HH 35.5. Furthermore, at this stage there was widespread expression of *Gsc* in the mesenchyme except for large circular areas directly beneath each of the conjunctival papillae, the site of the future condensations. This expression pattern is particularly exciting previous work has suggested that the borders of the scleral condensations are being delimitated by some inhibitory factor, which to date has remained elusive (Franz-Odendaal, 2008a; Duench & Franz-Odendaal, 2012). In addition, *Gsc* does not appear to be the key factor required for the induction of the scleral condensations identified by Pinto and Hall (1991) as it has a molecular weight of 28 kDa. This, however, is not surprising if, indeed, *Gsc* is required for the establishment and/or maintenance of distinct boundaries between the scleral condensations. A study by Filosa *et al*. (1997) demonstrated that Gsc and HNF-3β interact to regulate *Shh* expression, and thus dorsal-ventral patterning in the neural tube; it is therefore possible that *Gsc* is playing a similar role during condensation induction. Interestingly, Bmp2/4 signaling has also been shown to repress *Gsc* promoter activity in *Xenopus* development (Candia *et al*., 1997). However, I was unable to find any regulatory interactions between *Gsc* and *Dlx5*. These gene interactions hint of a possible signaling cascade required for the induction and patterning of the scleral condensations:

1. *β-catenin* upregulates the expression of *Dlx5* in the papilla and/or papilla-contiguous region
2. This *Dlx5* expression upregulates the expression of *Bmp2* in the papilla and/or condensation
3. The expression of *β-catenin* and/or *Dlx5* may also be responsible for the expression of the *Hh* family of genes
4. Once *Dlx5* and/or *Bmp2* have been induced (HH 35), the condensations begin to increase in size, and *Gsc* is upregulated (perhaps through *Activin* signaling (Candia *et al*., 1997).
5. Mutual repression between Gsc and Bmp2/Shh then restricts the expression of Gsc to a small group of cells in the inter-condensation region, establishing a sharp boundary between condensations.
6. Upon downregulation of *Gsc,* the condensations would expand and overlap to form the completed sclerotic ring.

While this hypothesis provides a possible mechanism by which *Gsc* could act to delineate the boundaries of the scleral condensations, further research is required to unravel the mechanisms governing the patterning of the scleral condensations.

4.4.2.6 - EYA1

As described in the results section above, *Eya1* is first expressed in the conjunctival papillae at HH 31. *Eya1* is then expressed in each group of conjunctival papillae as they are induced until all conjunctival papillae express *Eya1* at HH 34. By HH 35.5, this expression of *Eya1* has become downregulated. Therefore, while *Eya1* seems likely to be involved in the induction and patterning of the conjunctival papillae it is unlikely to be

involved with either papilla maintenance or the induction of the scleral condensations. In addition, *Eya1* does not seem to be the key factor required for the induction of the scleral condensations that was identified by Pinto and Hall (1991) as it has a molecular weight of 64 kDa.

That *Eya1* was expressed in the conjunctival papillae was not particularly surprising as *Eya1* is critical for the induction and patterning of the cranial placodes (Zou *et al*., 2004; Schlosser *et al*., 2008; Saint-Jeannet & Moody, 2014). In the literature, *Eya1* (along with the *Six* family members) has been shown to be involved in both the pre-patterning of the PPR (Saint-Jeannet & Moody, 2014) and the development of all cranial placodes other than the lens placode in the *Xenopus* (David *et al*., 2001). Furthermore, the expression of both *Eya1* and *Dlx5* in the conjunctival papillae may suggest that *Six1* would be a promising new candidate gene, especially as it may provide the context for the role played by *Eya1* in the eye. As *Eya1* is a co-factor for *Six1* expression and *Dlx5* is capable of binding to a PPR-specific enhancer of *Six1* it is possible that some similar regulatory network is involved during the induction and patterning of the conjunctival papillae (Baker, 2005; Schlosser, 2005; Schlosser, 2006; Bhat *et al*., 2013; Groves & LaBonne, 2014; Schlosser *et al*., 2014; Saint-Jeannet & Moody, 2014). Therefore, the expression of *Eya1*, a critical factor for cranial placode induction, during papilla induction seems to suggest that the conjunctival papillae are induced and patterned in a very similar way to the other placodes.

4.4.2.7 – Summary of the Candidate Gene Analysis

The results of the candidate gene analysis have, for the first time, identified four genes which are likely involved in the induction and patterning of the conjunctival papillae. I hypothesize, based on the literature and the spatiotemporal expression patterns that I

obtained that these four genes (*Eya1, Dlx5, Inhba,* and *Ednrb*) are important for the induction and patterning of the conjunctival papillae. This will require further testing, such as knock-down and over-expression studies, in order to determine the functional role played by each of these genes during in the induction and patterning of the conjunctival papillae.

This candidate gene analysis further identified three new genes (*Prox1*, *Dlx5*, and *Gsc*) which are likely to be involved in the induction and patterning of the scleral condensations; however, none of these are the key factor identified by Pinto and Hall (1991) that are critical for the induction of the underlying scleral condensations. The first of these genes, *Prox1* is only induced beginning at HH 33, near the end of papilla induction. As *Prox1* has been shown in the literature to be upregulated by the expression of *β-catenin* and suggested to play a role in the regulation of *Shh* (Kerr *et al*., 2012), the timing of *Prox1* onset in the conjunctival papillae may suggest a role in initiating the inductive cascade for the underlying scleral condensations. Expression of *Dlx5* in the scleral condensations at HH 35.5 may suggest that *Dlx5* is required upstream of *Bmp2* in order to restrict the scleral condensation to a skeletogenic fate. While more research will be required to establish the gene regulatory network responsible for the induction of the scleral condensations, this is surprising as the literature suggests that *Dlx5* is downstream of *Bmp2* during osteoblastogenesis in a number of different systems (Lee *et al*., 2003b; Ulsamer *et al*., 2008; Chen *et al*., 2012). Finally, the expression of *Gsc* at HH 35.5 seems to have identified, for the first time, a gene that is responsible for the patterning of the scleral condensations. Based on the regulatory networks governing *Gsc* expression in other systems, *Gsc* can be repressed by *Bmp2* (Marom *et al*., 2005) which is expressed in the

condensation prior to *Gsc* expression in the surrounding mesenchyme. *Gsc*, in turn, has been shown to repress *Shh* in combination with *HNK-3β* during dorsoventral patterning of the neural tube (Filosa *et al*., 1997). A summary of the possible gene interactions taking place during the induction and patterning of both the conjunctival papillae and scleral condensations based on the results of *in situ* hybridization is presented in Figure 4.17.

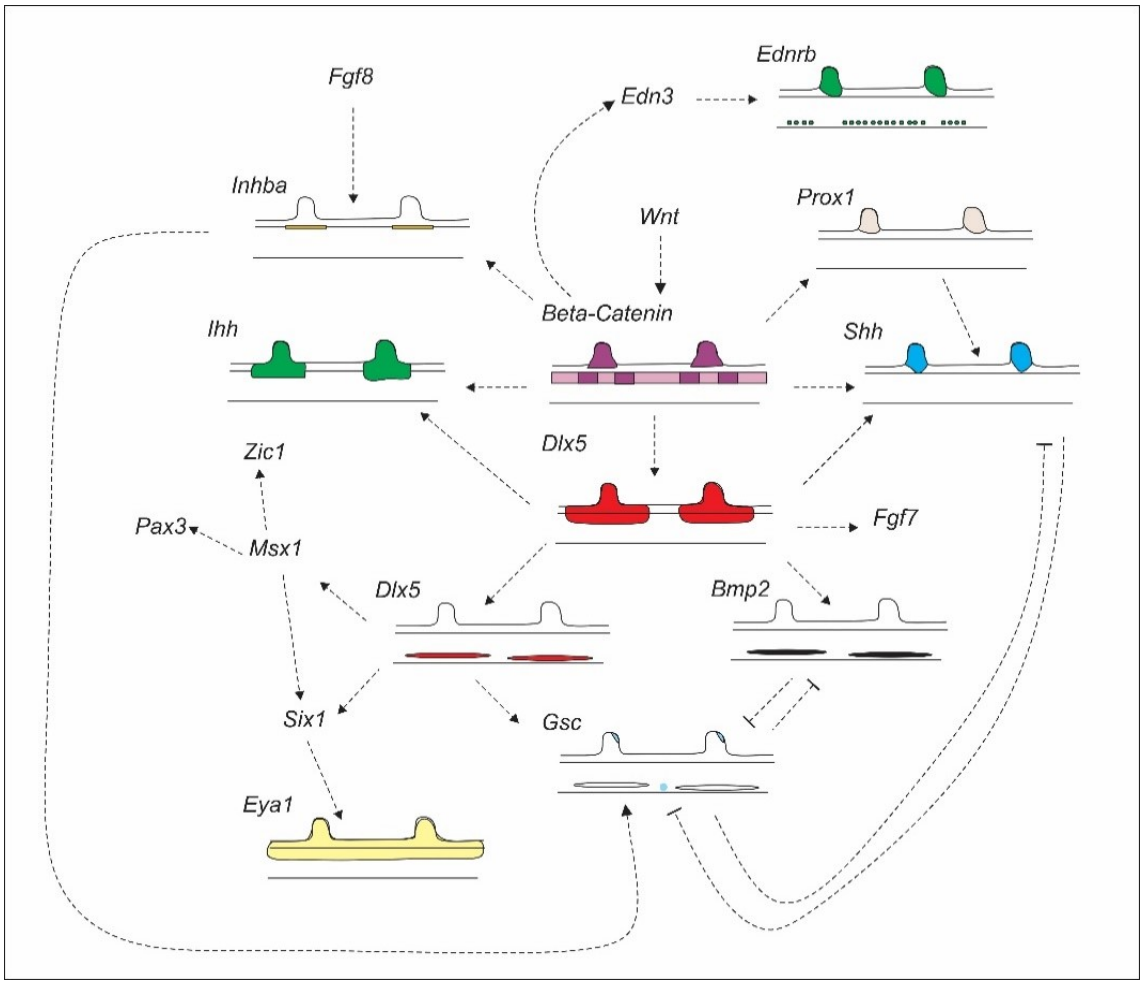

Figure 4.17: Schematic illustrating the possible gene interactions taking place during the induction of the conjunctival papillae and scleral condensations. As these represent hypothesized interactions, dotted lines are used to represent gene interactions.

Therefore, the results of this candidate gene analysis has enabled a first glimpse into some of the regulatory relationships that may be governing the induction and patterning of the conjunctival papillae. While many of the conclusions above are

conjecture at this point, these hypotheses set the stage for future experimental testing of the proposed relationships between these genes and suggests a course for further focused study.

4.4.3 – Conclusion

The candidate gene analysis presented in this Chapter has identified novel genes that are likely required i) to establish epithelial competency prior to the induction of the conjunctival papillae (*β-catenin*), ii) for the induction and patterning of the conjunctival papillae (*Eya1, Dlx5, Inhba*, and *Ednrb*), and iii) for the induction and patterning of the scleral condensations (*Gsc, Prox1,* and *Dlx5*). As these are the three steps required for the induction of a placode, these results strongly suggest that the conjunctival papillae are similar to the cranial and cutaneous placodes at both a morphological and genetic level. Based on these similarities, this study has identified a new stage of conjunctival papilla development: the conjunctival placode. This conjunctival placode represents the first stages of papilla development (approximately M-stages 1 and 2) prior to the extension of the conjunctival papilla into the underlying mesenchyme and above the surface epithelium. After this stage, the conjunctival placode becomes a conjunctival papilla, similar to what has been described in feather and hair. Furthermore, this study has identified a number of possible gene interactions that are taking place during the induction and patterning of both the conjunctival papillae and the scleral condensations. While the functional analyses for these genes must now be undertaken, this study provides a good baseline for future studies. Finally, this study has also identified, for the first time, a gene that may be required to establish the sharp boundaries between condensations, validating a long-held hypothesis

for the patterning of the scleral ossicles. The broader implications of these results are discussed in Chapter 5.

Chapter 5: Discussion and Conclusion

5.1 – Discussion

The broad objective of this thesis was to investigate the mechanisms governing the induction and patterning of the conjunctival papillae. As very little was previously known about the development of the conjunctival papillae, it was necessary to approach this study using a variety of techniques in order to begin to tease apart the various facets of induction and patterning that may be at play in this system. The results of this investigation have generated a number of new, and in some cases, unexpected insights into the development of the conjunctival papillae and will serve as a good basis for future studies in this field.

5.1.1 - Patterning of the Conjunctival Papillae

In Chapter 2, I hypothesized that the that surgical ablation of NC signaling centers or the epithelium along NCC migratory routes prior to papillae formation will alter the induction and patterning of derivative structures such as the scleral ossicles. The results of these experiments were inconclusive and it will be important to unravel the migration of the NCCs into the periocular mesenchyme in the future, in order to better target the NCC of the periocular mesenchyme for surgical manipulation. The next question I wanted to address was the way in which the pattern was generated in the conjunctival papillae (Chapter 3). From these experiments, I concluded that the ablation of a single papilla cannot alter the patterning of nearby papillae, that the first papillae does not seem to provide signaling information for the placement of adjacent papillae, and that there may be two independent levels of patterning for the conjunctival papillae (temporal and spatial). In Chapter 4, the expression patterns of seven candidate genes enabled me to hypothesize about their involvement in the induction and patterning of the scleral ossicle system.

Collectively, the results from Chapters 2, 3, and 4 have allowed me to develop these new hypotheses for the induction and patterning of the conjunctival papillae:

1. The conjunctival epithelium only acquires competency to respond to an inductive cue at a specific time in a specific place in the eye.

    In this hypothesis, the inductive cue for the development of the conjunctival papillae is expressed throughout the corneal-scleral limbus but competence is acquired in a temporal pattern (temporal, nasal, dorsal, and ventral), thereby restricting the induction of the conjunctival placodes to only the competent epithelium. This hypothesis, however, currently has little support as preliminary investigations into epithelial competency factors (described in Chapter 4) do not show this temporal pattern of competency; rather, by HH 31, there is widespread expression of *β-catenin* throughout the eye which becomes localized to the conjunctival papillae as they are induced. It is, however, possible that other epithelial competency factors are required for the patterning of the conjunctival placodes which may show this temporal pattern of expression. Further research into the question of epithelial competency will be required.

2. Temporal patterning governs the specification of the four different regions that can give rise the conjunctival placodes.

    This hypothesis is particularly interesting as the temporal patterning of the conjunctival placodes is dissimilar to the patterning models described in the other placodal systems. In these other systems (i.e. tooth, feather, hair) a temporal pattern establishes the location of the initial group of placodes;

however, all subsequent placodes are patterned in a linear fashion (Wolpert, 1998; Eames & Schneider, 2005; Drew *et al*., 2007; Duverger & Morasso, 2009; Koussoulakou *et al*., 2009; Bei, 2009; Catón & Tucker, 2009; Cobourne & Sharpe, 2010; Lin *et al*., 2011; Jiang *et al*., 2011; Porntaveetus *et al*., 2011; Matalova *et al.*, 2012; Sennett & Rendl, 2012; Painter *et al*., 2012; Yue *et al*., 2012; Chuong *et al*., 2013). In the conjunctival papilla system, on the other hand, these groups of placodes form independently from one another and only combine to create a complete circle after all of the groups have been initiated (Coulombre & Coulombre, 1962; Franz-Odendaal, 2008a; Duench & Franz-Odendaal, 2012; Jourdeuil & Franz-Odendaal, 2012). It is possible that this initial temporal patterning is established through epithelial competency, as hypothesized above. It is also possible that this temporal patterning is established through the migration of the NCCs into the periocular mesenchyme in the temporal, nasal, dorsal, and ventral regions at different times or through some currently unknown mechanism. This will require further study. To facilitate this study, it will be important to try to replicate this system using mathematical or computer models in order to generate new hypotheses that can be tested experimentally.

3. Spatial patterning coordinates the distance between the placodes both within each group and between groups; furthermore, this spatial patterning is likely regulated by a LALI model.

I hypothesize that the spatial patterning of the conjunctival placodes is regulated separately from the temporal patterning of the conjunctival papillae because this spatial patterning is established as soon as a group is induced but is also maintained between groups. Furthermore, when a conjunctival papilla is ablated, the regenerated papilla always forms at the site of ablation as described in Chapter 3. This spatial patterning seems to best fit a LALI model because of the way in which spatial patterning is achieved between different groups of papillae that are induced at different times. As described in Chapter 3, in a LALI model: an activator and inhibitor (which can be made up of a cascade of factors) are paired such that the activator (which is autocatalytic) becomes restricted to localized areas due to the long-range diffusion of an inhibitor (Roth, 2011; Szalai *et al*., 2012; Diambra *et al*., 2014; Ball, 2015). In the conjunctival papilla system, this would mean that the first papillae to form (in the temporal and nasal groups) would establish the spatial pattern between the papillae in these groups. However, the activity of the long-range inhibitors expressed by the conjunctival papillae in the temporal and nasal groups would also pattern the dorsal and ventral groups that will form between them. Furthermore, in other systems (i.e. hair, tooth, and feather) which are also believed to be patterned through a LALI model, β-catenin forms part of the hypothesized activator cascade (Wolpert, 1998; Eames & Schneider, 2005; Widelitz, 2008; Duverger & Morasso, 2009; Dhouailly, 2009; Sayama *et al*., 2010; Enshell-Seijffers *et al*., 2010; Jiang *et al*., 2011; Painter *et al*., 2012; Sennett

& Rendl, 2012; Huang *et al*., 2012; Woo *et al*., 2012; Suksaweang *et al*., 2012; Wells *et al*., 2012 Chuong *et al*., 2013; Myung *et al*., 2013; O'Connor *et al*., 2013). Additionally, if the papillae are restricted to the corneal-scleral limbus by mutual repression of the cornea and the sclera (similar to what occurs between the odontogenic and non-odontogenic regions in tooth development [Zhou *et al*., 2011]), the induction of the first group of conjunctival papillae would be able to pattern the entire papilla field if pattern is governed by a LALI model. This will require further study.

5.1.2 – Papillae Induction and Regeneration

One of the most surprising, and perhaps most exciting, results of this project was discovering that the conjunctival papillae are capable of regeneration, as described in Chapter 3. These data strongly suggest that the factor responsible for the induction (and regeneration) of a conjunctival papilla is mesenchymal in nature (as was previously suggested by Hall [1981a]) because a papilla will not regenerate in the absence of the mesenchyme and/or basal lamina. Through these experiments, I was able to determine that the regenerated papilla matures faster in order to induce the underlying scleral condensation with only a slight delay as compared to the adjacent scleral condensations within the timeline of normal condensation induction (HH 35-36). This condensation quickly compensates for its delay in induction, expressing *Bmp2* similarly to the adjacent condensations before it begins to downregulate its expression of *Bmp2* concomitant with the other condensations in the eye at HH 36.5.

Furthermore, through the study of the limits of regeneration, I was able to determine that the inductive factor(s) responsible for papilla induction remain in the eye until at least

HH 35.5, a full day and a half longer than had been previously identified in this system. Additionally, these results suggest that the epithelium remains competent to respond to this inductive cue until at least HH 35.5. These results are significant because they demonstrate that there is a mechanism in place, in the epithelium, to ensure the development of a complete ring of scleral condensations. Previous research in this field identified a similar mechanism in the mesenchyme that compensates for a missing ossicle through in-growth of the adjacent ossicles to form a complete ring (Coulombre & Coulombre, 1962; Franz-Odendaal, 2008a; Duench & Franz-Odendaal, 2012). These compensatory mechanisms appear to create redundancies, in both the epithelium and the mesenchyme, to ensure that a complete sclerotic ring is induced and normally patterned prior to adulthood. These redundancies likely developed in the sclerotic ring system due to its importance in visual accommodation (Slonaker, 1918; Slonaker, 1921; Curtis & Miller, 1938). Further research will be required to determine the nature of these redundancies and the severity of the perturbations that they can overcome. For instance, can two papillae regenerate? Can the sclerotic ring recover from the ablation of an entire group of conjunctival papillae?

5.1.3 – A New Stage of Conjunctival Papilla Development: The Conjunctival Placode

The most important and significant new facet of conjunctival papilla development that I discovered during this study is that the development of the conjunctival papillae includes a placodal stage. As described in Chapter 4, the development of a placode typically includes three phases: i) an initial inductive phase or pre-patterning of the epithelium, ii) the induction of the epithelial thickening in the epithelium via signaling from the underlying mesenchyme, and iii) the induction of a subsequent structure by the placode (Ferguson *et al*., 1998; Wolpert, 1998; Baker & Bronner-Fraser, 2001; Baker, 2005;

Schlosser, 2005; Eames & Schneider, 2005; Schlosser, 2006; Zhang *et al*., 2009; Dhouailly, 2009; Duverger & Morasso, 2009; Catón & Tucker, 2009; Chen *et al*., 2009; Koussoulakou *et al*., 2009; Bei, 2009; Takahashi *et al*., 2010; Cui et al., 2010; Sayama *et al*., 2010; Jiang *et al*., 2011; Painter *et al*., 2012; Sennett & Rendl, 2012; Chuong *et al*., 2013; O'Connor *et al*., 2013; Groves & LaBonne, 2014; Saint-Jeannet & Moody, 2014; Schlosser *et al*., 2014). During this study, all three of these phases have been identified in the conjunctival papillae via molecular signals.

The first, an initial induction phase in which the epithelium gains competency to respond to a subsequent inductive cascade, was demonstrated for the first time during the induction and patterning of the conjunctival papilla by the expression of *β-catenin* in the epithelium at HH 30, prior to the induction of any other papilla-specific genes. Additionally, this pre-patterning of the epithelium has been confirmed to be required for the induction and patterning of all conjunctival papillae. Furthermore, this expression of *β-catenin* is required for epithelial competency in a number of other placodal systems, including tooth, hair, and feather (Wolpert, 1998; Eames & Schneider, 2005; Widelitz, 2008; Duverger & Morasso, 2009; Dhouailly, 2009; Sayama *et al*., 2010; Enshell-Seijffers *et al*., 2010; Jiang *et al*., 2011; Painter *et al*., 2012; Sennett & Rendl, 2012; Huang *et al*., 2012; Woo *et al*., 2012; Suksaweang *et al*., 2012; Wells *et al*., 2012 Chuong *et al*., 2013; Myung *et al*., 2013; O'Connor *et al*., 2013). While *β-catenin* is only a single gene that has been associated with epithelial competency during cutaneous placode induction, this suggests that other epithelial competency genes would make good candidates for future studies, including such genes as *Eda* and Wnt (Zhang *et al*., 2009; Cui et al., 2010; Sayama *et al*., 2010; Duverger & Morasso, 2009; Sennett & Rendl, 2012).

The similarity between the conjunctival papillae and other placodes continues into the second phase of placode development, which is defined as the induction of the epithelial thickening in the epithelium via signaling, usually, from the underlying mesenchyme. While this study did not identify a gene that was first expressed in the mesenchyme and subsequently in the developing conjunctival papillae; this expression pattern has not yet been identified for any of the other placodes (Ferguson *et al*., 1998; Wolpert, 1998; Eames & Schneider, 2005; Schlosser, 2006; Zhang *et al*., 2009; Dhouailly, 2009; Duverger & Morasso, 2009; Catón & Tucker, 2009; Chen *et al*., 2009; Koussoulakou *et al*., 2009; Bei, 2009; Takahashi *et al*., 2010; Cui et al., 2010; Sayama *et al*., 2010; Jiang *et al*., 2011; Painter *et al*., 2012; Sennett & Rendl, 2012; Chuong *et al*., 2013; O'Connor *et al*., 2013; Groves & LaBonne, 2014; Saint-Jeannet & Moody, 2014; Schlosser *et al*., 2014). As the inductive cascade is complex and many genes are all signaling at the same time, it is difficult to isolate the way in which these placode-specific genes are induced in the placodes themselves. The results of the candidate gene analysis have identified, for the first time, four genes that are expressed during early conjunctival papilla development; visible in the epithelial thickenings as early as HH 31. It should be noted here that these genes are likely slightly expressed earlier, however, as samples for HH 30 were fixed prior to the induction of the first conjunctival papilla to match the samples used for both the microarray analysis and the qualitative PCR analysis, this was not shown during this study. Furthermore, the majority of these genes (*Eya1*, *Dlx5*, and *Inhba*) are critical regulators of placode induction in other systems. This similar gene expression pattern further suggests that the initial stages of conjunctival papillae development should rather be known as the conjunctival placodes. One of these genes (*Ednrb*) has not previously been recorded during

the induction and patterning of other placodes, however, each placode has some variation in gene expression that gives rise to its particular derivatives. For instance, after the pre-placodal region has been established during cranial placode induction, this placodal region is subdivided into two distinct regions (anterior and posterior) that have distinct expression patterns (Schlosser, 2005; Schlosser, 2006; Schlosser *et al*., 2014). After this subdivision, the pre-placodal field is further refined until each placode has its own distinct molecular code (Saint-Jeannet & Moody, 2014). Therefore, that a novel gene was identified during this candidate gene analysis likely identifies some of the particularities of the conjunctival placode inductive code and also reflect its later skeletogenic requirements.

The final step during the development of a placode is the induction of the subsequent structure by the placode. As the derivatives of all placodes are so diverse, this induction is generally highly variable, including different inductive methodologies (i.e. invagination into the underlying mesenchyme during tooth placode morphogenesis or neuronal determination and delamination during neurogenic cranial placode morphogenesis) and different genetic cascades (Wolpert, 1998; Zou *et al*., 2004; Eames & Schneider, 2005; Drew *et al*., 2007; Meulemans & Bronner-Fraser, 2007; Whitlock, 2008; McCabe & Bronner-Fraser, 2009; Duverger & Morasso, 2009; Liu *et al*., 2008; Bei, 2009; Catón & Tucker, 2009; Koussoulakou *et al*., 2009; Chen *et al*., 2009; Enchell-Seijffers *et al*., 2010; Sayama *et al*., 2010; Jackman *et al*., 2010; Garcia *et al*., 2011; Jiang *et al*., 2011; Landin *et al*., 2012; Painter *et al*., 2012; Yue *et al*., 2012; Clavel *et al*., 2012; Sennett & Rendl, 2012; Chuong *et al*., 2013; Bhat *et al*., 2013; Lassiter *et al.*, 2014; Saint-Jeannet & Moody, 2014; Maier *et al*., 2014). In the conjunctival papilla system, the conjunctival placode undergoes a complex morphological development to form the conjunctival papilla

(Murray, 1943). This conjunctival papilla, throughout its morphological development, becomes inductively active in order to induce the underlying scleral condensation. Interestingly, previous studies have placed this inductive event between HH 35-36 (Coulombre & Coulombre, 1962; Hall, 1981a; Franz-Odendaal, 2008a), however, the results of this study suggest that it may in fact be occurring slightly earlier, between HH 34 and 35. The induction of the underlying scleral condensations has been shown to be mediated in part by the expression of *Bmp2*, *Shh*, *Ihh*, and *Ptc* in the conjunctival papillae between HH 34.5 and 36 (Duench & Franz-Odendaal, 2012). During this thesis, the molecular cascade required for the induction of the scleral condensations was further elucidated as it was discovered that *Bmp2* is subsequently induced in the underlying scleral condensation at HH 35 (Chapter 3). Initially ovoid in shape, both the condensation and the area of *Bmp2* expression increase over subsequent stages until expression is down-regulated beginning at HH 36.5. This expression of *Bmp2* was the first to be identified in the scleral condensations themselves. Furthermore, this candidate gene analysis, as described above, identified three other genes that are likely involved in the induction and patterning of the scleral condensations. The first, *Prox1* seems most likely to be involved in establishing the inductive cascade in the conjunctival papillae. The second, *Dlx5* is first expressed in the conjunctival papillae and then subsequently becomes induced in the underlying scleral condensation. As the expression of *Dlx5* in the underlying condensation is larger in size than that of *Bmp2* at HH 35.5 and is already trapezoidal in shape, it is possible that *Dlx5* expression is required upstream of *Bmp2* during osteogenesis. Finally, *Gsc* is expressed in the conjunctival papillae beginning at HH 35.5 and in the mesenchyme delimitating the area in which the scleral condensations will form.

Therefore, during the course of this study we have determined that the conjunctival papillae exhibit all three phases that are typical of placode induction. Furthermore, many of the genes that are involved in both establishing epithelial competency and the induction of the conjunctival papillae themselves are critical for the induction and patterning of other placodes. Finally, similar to other placodes, the conjunctival papillae are responsible for the induction of a subsequent structure; although the way in which this structure is induced is somewhat different from that of the other currently described placodes. Therefore, these data suggest that the initial stages of papilla development consist of a conjunctival placode. Furthermore, by delineating this new stage of development (the conjunctival placode) it will facilitate our rapid understanding of the way in which these conjunctival placodes are induced, as it creates a list of candidate genes that should be investigated; specifically, those that are involved in the induction and patterning of a large number of other placodes.

Moreover, as these conjunctival placodes and papillae give rise to the sclerotic ring, a calvarial bone, unravelling their induction and patterning will provide further insights into the way in which other calvarial and intramembranous bones are induced and patterned; an issue that has significant impacts on human health and development. This could be particularly important in the fields of craniosynostosis and cleft lip and palate; developmental disorders that affect large numbers of children (Shillito & Matson, 1968; Vanderas, 1987; Wilkie, 1997; Kabbani & Raghuveer, 2004; Arosarena, 2007)

5.1.4 – A Third Category of Placodes – The Skeletogenic Placodes

The conjunctival placodes are also similar to another group of epithelial thickenings, which, to date, have all been considered individually. These epithelial thickenings, which include the apical ectodermal ridge and the epithelium above the

mandible and maxilla, are responsible for the induction of a broad range of skeletogenic derivatives that, with the exception of the apical ectodermal ridge, are poorly understood. In the following section, I will discuss each of the epithelial thickenings, which I believe should be considered together as skeletogenic placodes. By redefining the way in which these epithelial thickenings are considered, it may be possible to change the way in which these skeletogenic thickenings are studied and further shed new light on the way in which epithelial thickenings are responsible for the induction and patterning of various bones.

5.1.4.1 – Limb development: The Apical Ectodermal Ridge

In vertebrates, the fore- and hind-limb buds will emerge at defined somite positions perpendicular to the primary body axis where an ectodermal outpocketing, initially filled with naïve and undetermined mesenchymal cells derived from the embryonic flank mesoderm, will form (Bénazet & Zeller, 2009; Romereim & Dudley, 2011). This outgrowth and subsequent development of distinct limb zones (stylopod, zeugopod, and autopod) is mediated by a distinct ectodermal thickening that is known as the apical ectodermal ridge (Lu *et al.,* 2008; Bénazet & Zeller, 2009, Boehm *et al.*, 2010; Zhu *et al*., 2010; Talamillo *et al*., 2010; Taher *et al.,* 2011; Gross *et al.,* 2011; Vieux-Rochas *et al*., 2013). If this apical ectodermal ridge is removed during limb development, it results in developmental arrest and truncation of the limb skeleton, similar to the way in which development is arrested when other placodes are removed (Lu *et al.,* 2008; Bénazet & Zeller, 2009; Zeller *et al.,* 2009; Zhu *et al*., 2010; Danopoulos *et al*., 2013).

Apical ectodermal ridge development begins are around E8.5 in the mouse, the pre-specification of the limb tissue (Capellini *et al*., 2011; Danopoulos *et al*., 2013). This "pre-patterning" is thought to be mediated by expression of Fgfs, as a loss of Fgfr2b at this stage,

prior to the induction of a visible limb bud, results in the attenuation of limb development (Lu *et al.,* 2008; Bénazet & Zeller, 2009; Capellini *et al.,* 2011; Danopoulos *et al*., 2013). It has been determined that early expression of Fgf10, which binds to Fgfr2b, allows for the stabilization of *β-catenin* in the epithelium (Capellini *et al*., 2011; Danopoulos *et al*., 2013), a gene that is similarly required for the pre-patterning of the epithelium in most other placodes as described above. This stabilized expression of β-catenin then upregulates the expression of *Fgf8*, *Dkk1,* and *Wnt3* in the epithelium; genes critical for the development and maintenance of the apical ectodermal ridge (Talamillo *et al*., 2010; Danopoulos *et al*., 2013). It is also responsible for regulating changes in the adhesion properties of the epithelium via expression of E-cadherin, p63, and β1-integrin; a process similar to that described in hair and feather placode development (Danopoulos *et al*., 2013). Placodal expression of Fgf8 subsequently signals to the underlying mesenchyme, inducing the expression of Fgfr1 and Tw1 which initiate the localized expression of Shh in the zone of polarized activity (Bénazet & Zeller, 2009; Krawchuk *et al.,* 2010; Romereim & Dudley, 2011; Capellini *et al*., 2011; Vieux-Rochas *et al*., 2013). This Shh expression is required to drive localized cell proliferation and to regulate gene expression in the ventral portion of the limb bud (Romereim & Dudley, 2011). The early expression of Fgf8 also induces mesenchymal expression of *Dlx5/6*, *Msx1/2*, and *Bmp2/4*, genes that are responsible for the restriction of Wnt expression to the surrounding dorsal and ventral epithelium and thus maintaining expression of Fgf in the apical ectodermal ridge, which coordinates the growth of the limb (Vieux-Rochas *et al*., 2013). As the mechanisms that drive further limb outgrowth are well characterized in the literature and not the focus of the present discussion, they will not be further discussed (Berge *et al*., 2008; Bénazet & Zeller, 2009;

Krawchuk *et al*., 2010; Romereim & Dudley, 2011; Capellini *et al*., 2011; Feenstra *et al*., 2013).

Thus, it is apparent that the apical ectodermal ridge shares many characteristics with the other placodes. There is an initial pre-patterning of the epithelium required to establish epithelium competency to respond to a mesenchymal inductive cue. This pre-patterning is mediated by the expression of *β-catenin* and Wnts, similarly to both the cutaneous placodes and the conjunctival placodes (Wolpert, 1998; Eames & Schneider, 2005; Widelitz, 2008; Duverger & Morasso, 2009; Dhouailly, 2009; Sayama *et al*., 2010; Enshell-Seijffers *et al*., 2010; Jiang *et al*., 2011; Painter *et al*., 2012; Sennett & Rendl, 2012; Huang *et al*., 2012; Woo *et al*., 2012; Suksaweang *et al*., 2012; Wells *et al*., 2012 Chuong *et al*., 2013; Myung *et al*., 2013; O'Connor *et al*., 2013). Furthermore, the apical ectodermal ridge itself is induced by a complex, reciprocal mesenchymal-epithelial signaling cascade. Finally, the apical ectodermal ridge drives the induction and patterning of the underlying skeletogenic condensations before degenerating. That the apical ectodermal ridge is larger than other placodes does not discount the function it plays in the induction and patterning of the underlying limb nor does it preclude it from being considered a placode. Additionally, many of the factors responsible for the induction and maintenance of the apical ectodermal ridge are similar to those responsible for the induction and maintenance of other placodes (e.g. β-catenin, Fgfs, Bmps, Wnts, *etc.*). Finally, as the gene regulatory network responsible for the induction and patterning of the apical ectodermal ridge is better understood, it may provide critical information required to unravel the mesenchymal-epithelial signaling cascade responsible for the induction and patterning of other placodes.

5.1.4.2 – Evidence of Other Skeletogenic Placodes

There are a number of instances in the literature where epithelial thickenings have been described which play a critical role in the induction and patterning of skeletogenic structures, however these have not been well researched. These include the epithelial thickenings required for the induction and patterning of the maxilla and mandible (Tyler & Hall, 1977; Bee & Thorogood, 1980; Tyler & McCobb, 1980; Tyler & McCobb, 1981; Hall, 1981b). That these epithelial thickenings are involved in the induction and patterning of the mandible and maxilla was demonstrated by Hall (1981b) in an elegant series of experiments. In these experiments, the epithelium was removed from the underlying mesenchyme by an enzymatic digestion prior to the induction of the mandibular condensation. In all cases, the mesenchyme alone was incapable of forming bone (Hall, 1981b). However, when recombined with other inductive epithelia (mandible or conjunctival), a skeletogenic condensation formed (Hall, 1981b). While the epithelium directly above the mandible does not form a small, distinct placode, it is thickened and serves an inductive role during osteogenesis in the mandible (Hall, 1981b). This would also suggest that, as three separate and independent craniofacial bones require an inductive cue from an initial epithelial thickening, other craniofacial bones may also require this epithelial-mesenchymal induction. Therefore, by considering these epithelial thickenings as placodes and using the current literature in the field as a way in which to create an initial list of candidate genes responsible for this inductive interaction, it may be possible to more rapidly unravel the mechanisms governing the induction and patterning of craniofacial bones.

5.2 – Conclusion

This chapter has highlighted the similarities between the cranial and cutaneous placodes to the conjunctival papillae and has identified a new stage of papilla development, the conjunctival placode. Furthermore, this research suggests that a third category of placodes should be established, that of the skeletogenic placodes. This third category of placodes, which would include the conjunctival placodes, the apical ectodermal ridge, and the epithelial thickenings required for the induction and patterning of the maxilla and mandible, could be expanded in the future to include other epithelial thickenings responsible for induction of the skeleton as they are uncovered. As very little is currently known about the role played by the epithelium in the induction and patterning of skeletogenic condensations, with the obvious exception of the apical ectodermal ridge, changing the way in which these epithelial thickenings are considered opens up a number of new avenues in which to study the induction and patterning of bone. Furthermore, creating a new category of placodes will provide a rich history of scientific literature from which to draw; especially as the induction and patterning of the apical ectodermal ridge, the cutaneous placodes, and the cranial placodes have become better understood. Additionally, the study of these different families of placodes may provide critical information to the way in which placodes have evolved and the roles they have played in vertebrate adaptation and evolution. Thus, by changing our approach to the study of placodes and extending this field to include a new, third category of placodes, that of the skeletogenic placode, we stand to make interesting discoveries in both evolutionary developmental biology as well as issues that are paramount to human health, including craniosynostosis, cleft palate, and tooth abnormalities to name but a few.

References

Abu-Daya, A., Khokha, M.K., Zimmerman, M.L.B. (2012). The Hitchhiker's Guide to *Xenopus* genetics. *Genesis.* 50(3): 164-175.

Ahmed, M., Wong, E.Y.-M., Sun, J., Xu, J., Wang, F., Xu, P-X. (2012). Eya1-Six1 interaction is sufficient to induce hair cell fate in the cochlea by activating Atoh1 expression in cooperation with Sox2. *Dev. Cell*. 22(2): 377-390.

Arosarena, O.A. (2007). Cleft lip and palate. *Otolaryngol. Clin. N. Am.* 40(1): 27-60.

Atchley, W.R. and Hall, B.K. (1991). A model for development and evolution of complex morphological structures. *Biol. Rev.* 66(2): 101-157.

Baek, K. and Baek, J.-H. (2013). The transcription factors myeloid elf-1-like factor (MEF) and distal-less homeobox 5 (Dlx5) inversely regulate the differentiation of osteoblasts and adipocytes in bone marrow. *Adipocyte.* 2(1): 50-54.

Bailey, A.P., Bhattacharyya, S., Bronner-Fraser, M., Streit, A. (2006). Lens specification is the ground state of all sensory placodes, from which FGF promotes olfactory identity. *Dev. Cell*. 11(4): 505-517.

Baker, C.V.H. and Bronner-Fraser, M. (2001). Vertebrate cranial placodes I. Embryonic induction. *Dev. Biol.* 232(1): 1-61.

Baker, C. (2005). Neural crest and cranial ectodermal placodes. *Developmental Neurobiology*. 4th edn. Kluwer Academic / Plenum Publishers. New York.

Ball, P. (2015). Forging patterns and making waves from biology to geology: A commentary on Turing (1952) "The chemical basis of morphogenesis". *Phil. Trans. R. Soc. B.* 370: 20140218.

Banerjee, S., Isaacman-Beck, J., Schneider, V.A., Granato, M. (2013). A novel role for Lh3 dependent ECM modification during neural crest cell migration in zebrafish. *PLoS One.* 8(1): e54609.

Barron, F., Woods, C., Kuhn, K., Bishop, J., Howard, M.J., Clouthier, D.E. (2011). Downregulation of Dlx5 and Dlx6 expression by Hand2 is essential for initiation of tongue morphogenesis. *Development.* 138(11): 2249-2259.

Basch, M.L., Bronner-Fraser, M., and García-Castro, M.I. (2006). Specification of the neural crest occurs during gastrulation and requires pax7. *Nature*. 441: 218-222.

Bee, J. and Thorogood, P.V. (1980). The role of tissue interactions in the skeletogenic differentiation of avian neural crest cells. *Dev. Biol*. 78(1): 47-62.

Bei, M. (2009). Molecular genetics of tooth development. *Curr. Opin. Genet. Dev.* 19(5): 504-510.

Belo, J.A., Leyns, L., Yamada, G., De Robertis, E.M. (1998). The prechordal midline of the chondrocranium is defective in *Goosecoid*-1 mouse mutants. *Mech. Dev.* 72: 15-25.

Bénazet, J.-D. and Zeller, R. (2009). Vertebrate limb development: moving from classical morphogen gradients to an integrated 4-dimensional patterning system. *Cold Spring Harb. Perspect. Biol*. 1: a001339.

Berge, D.t., Brugmann, S.A., Helms, J.A., Nusse, R. (2008). Wnt and FGF signals interact to coordinate growth with cell fate specification during limb development. *Development*. 135(19): 3247-3257.

Bermingham-McDonogh, O., Oesterle, E.C., Stone, J.S., Hume, C.R., Huynh, H.M., Hayashi, T. (2006). The expression of Prox1 during mouse cochlear development. *J. Comp. Neurol.* 496(2): 172-186.

Betters, E., Liu, Y., Kjaeldgaard, A., Sundström, E., García-Castro, M.I. (2010). Analysis of early human neural crest development. *Dev Biol*. 344(2): 578-592.

Bhat, N. and Riley, B.B. (2011). Integrin-α5 coordinates assembly of posterior cranial placodes in zebrafish and enhances Fgf-dependent regulation of otic/epibranchial cells. *PLoS ONE*. 6(12): e277778.

Bhat, N., Kwon, H.-J., Riley, B.B. (2013). A gene network that coordinates pre placodal competence and neural crest specification in zebrafish. *Dev. Biol.* 373(1): 107-117.

Bhattacharyya, S., Bailey, A.P., Bronner-Fraser, M., Streit, A. (2004). Segregation of lens and olfactory precursors from a common territory: cell sorting and reciprocity of Dlx5 and Pax6 expression. *Dev. Biol.* 271(2): 403-414.

Boehm, B., Westerberg, H., Lesnicar-Pucko, G., Raja, S., Rautschka, M., Cotterell, J., Swoger, J., Sharpe, J. (2010). The role of spatially controlled cell proliferation in limb bud morphogenesis. *PLoS Biol.* 8(7): e1000420.

Bronner-Fraser, M. (1994). Neural crest cell formation and migration in the developing embryo. *FASEB J.* 8: 699-706.

Bronner, M.E. (2012). Formation and migration of neural crest cells in the vertebrate embryo. *Histochem. Cell Biol.* 138(2): 179-186.

Bronner, M.E. and Le Douarin, N.M. (2012). Evolution and development of the neural crest: an overview. *Dev Biol.* 366(1): 2-9.

Brown, K.K., Reiss, J.A., Crow, K., Ferguson, H.L., Kelly, C., Fritzsch, B., Morton, C.C. (2010). Deletion of an enhancer near DLX5 and DLX6 in a family with hearing loss, craniofacial defects, and an inv(7)(q21.3q35). *Hum. Genet.* 127(1): 19-31.

Candia, A.F., Watabe, T., Hawley, S.H., Onichtchouk, D., Zhang, Y., Derynck, R., Niehrs, C., Cho, K.W. (1997). Cellular interpretation of multiple TGF-beta signals: intracellular antagonism between activing/BVg1 and BMP-2/4 signaling mediated by Smads. *Development*. 124(22): 4467-80.

Canning, C.A., Lee, L., Luo, S.X., Graham, A., Jones, C.M. (2008). Neural tube derived Wnt signals cooperate with FGF signaling in the formation and differentiation of the trigeminal placodes. *Neural Dev.* 3: 35.

Capellini, T.D., Zappavigna, V., Selleri, L. (2011). Pbx homeodomain proteins: TALEnted regulators of limb patterning and outgrowth. *Dev. Dyn.* 240(5): 1063-1086.

Carmona, F.D., Jiménez, R., Collinson, J.M. (2008). The molecular basis of defective lens development in the Iberian mole. *BMC Biol.* 6: 44.

Catón, J. and Tucker, A.S. (2009). Current knowledge of tooth development: patterning and mineralization of the murine dentition. *J. Anat*. 214: pp 502-515.

Cavalheiro, G.R., Matos-Rodrigues, G.E., Gomes, A.L., Rodrigues, P.M.G., Martins, R.A.P. (2014). c-myc regulates cell proliferation during lens development. *PLoS ONE*. 9(2): e87182.

Chapman, S.C., Schubert, F.R., Schoenwolf, G.C., Lumsden, A. (2002). Analysis of spatial and temporal gene expression patterns in blastula and gastrula stage chick embryos. *Dev. Biol.* 245(1): 187-199.

Chapman, S.C. (2011). Can you hear me now? Understanding vertebrate middle ear development. *Front. Biosci.* 16: 1675-1692.

Chatterjee, S., Kraus, P., Lufkin, T. (2010). A symphony of inner ear developmental control genes. *BMC Genet.* 11: 68.

Chen, Y., Zhang, Y., Jiang, T.-X., Barlow, A.J., St. Amand, T.R., Hu, Y., Heaney, S., Francis-West, P., Chuong, C.-M., Maas, R. (2000). Conservation of early odontogenic signaling pathways in *Aves*. *PNAS.* 97(18): 10044-10049.

Chen, X., Taube, J.R., Simirskii, V.I., Patel, T.P., Duncan, M.K. (2008a). Dual Roles for Prox1 in the regulation of the chicken βB1-crystallin promoter. *Invest. Ophthalmol. Vis. Sci.* 49(4): 1542-1552.

Chen, X., Patel, T.P., Simirskii, V.I., Duncan, M.K. (2008b). PCNA interacts with Prox1 and represses its transcriptional activity. *Mol. Vis.* 14: 2076-2086.

Chen, J., Lan, Y., Baek, J.-A., Gao, Y., Jiang, R. (2009). Wnt/beta-catenin signaling plays an essential role in activation of odontogenic mesenchyme during early tooth development. *Dev. Biol*. 334(1): 174-185.

Chen, X., Lou, Q., He, J., Yin, Z. (2011). Role of zebrafish Lbx2 in embryonic lateral line development. *PLoS ONE*. 6(12): e29515.

Chen, J. and Chuong, C.-M. (2012). Patterning skin by planar cell polarity: the multi-talented hair designer. *Exp. Dermatol.* 21(2): 81-85.

Chen, G., Deng, C., Li, Y.-P. (2012). TGF-β and BMP signaling in osteoblast differentiation and bone formation. *Int. J. Biol. Sci.* 8(2): 272-288.

Cho, Y.-D., Yoon, W.-J., Woo, K.-M., Baek, J.-H., Lee, G. Cho, J.-Y., Ryoo, H.-M. (2009). Molecular regulation of matrix extracellular phosphoglycoprotein expression by bone morphogenetic protein-2. *J. Biol. Chem*. 284(37): 25230-25240.

Cho, Y.-D., Yoon, W.J., Woo, K.-M., Baek, J.-H., Park, J.-C., Ryoo, H.-M. (2010). The canonical BMP signaling pathway plays a crucial part in stimulation of dentin sialophosphoprotein expression by BMP2. *J. Biol. Chem.* 285(47): 36369-36376.

Christophorou, N.A., Mende, M., Lleras-Forero, L., Grocott, T., Streit, A. (2010). Pax2 coordinates epithelial morphogenesis and cell fate in the inner ear. *Dev. Biol.* 345(2): 180-190.

Chung, I.-H., Han, J., Iwata, J., Chai, Y. (2010). Msx1 and Dlx5 function synergistically to regulate frontal bone development. *Genesis.* 48(11): 645-655.

Chuong, C.-M., Yeh, C.-Y., Jiang, T.-X., Widelitz, R. (2013). Module based complexity formation: Periodic patterning in feathers and hairs. *Wiley Interdiscip. Rev. Dev. Biol.* 2(1): 97-112.

Clavel, C., Grisanti, L., Zemla, R., Rezza, A., Barros, R., Sennett, R., Mazloom, A., Chung, C.-Y., Cai, X., Cai, C.-L., Pevny, L., Nicolis, S., Ma'ayan, A., Rendl, M. (2012). Sox2 in the dermal papilla niche controls hair growth by fine-tuning Bmp signaling in differentiating hair shaft progenitors. *Dev. Cell.* 23(5): 981-994.

Clouthier, D.E., Garcia, E., Schilling, T.F. (2010). Regulation of facial morphogenesis by Endothelin signaling: insights from mice and fish. *Am. J. Med. Genet. A.* 152A(12): 2962-2973.

Cobourne, M.T. and Sharpe, P.T. (2010). Making up the numbers: The molecular control of mammalian dental formula. *Semin. Cell Dev. Biol.* 21: 314-324.

Costantini, F. (2012). Genetic controls and cellular behaviors in branching morphogenesis of the renal collecting system. *Wiley Interdiscip. Rev. Dev. Biol.* 1(5): 693-713.

Coulombre, A.J. and Coulombre, J.L. (1962). The skeleton of the eye I. conjunctival papillae and scleral ossicles. *Dev. Biol.* 5: 382-401.

Creuzet, S., Couly, G., Le Douarin, N.M. (2005). Patterning the neural crest derivatives during development of the vertebrate head: insights from avian studies. *J. Anat.* 207: pp 447-459.

Cruz-Munoz, W., Jaramillo, M.L., Man, S., Xu, P., Banville, M., Collins, C., Nantel, A., Francia, G., Morgan, S.S., Cranmer, L.D., O'Connor-McCourt, M.D., Kerbel, R.S. (2012). Roles for Endothelin receptor B and BCL2A1 in spontaneous CNS metastasis of melanoma. *Cancer Res.* 72(19): 4909-4919.

Cui, C.-Y., Kunisada, M., Piao, Y., Childress, V., Ko, M.S.H., Schlessinger, D. (2010). Dkk4 and Eda regulate distinctive developmental mechanisms for subtypes of mouse hair. *PLoS ONE*. 5(4): e10009.

Curtis, E.L. & Miller, R.C. (1938). The sclerotic ring in North American birds. *Auk*. 55: 225-243.

Cvekl, A. and Mitton, K.P. (2010). Epigenetic regulatory mechanisms in vertebrate eye development and disease. *Heredity (Edinb.)*. 105(1): 135-151.

Dangaria, S.G., Ito, Y., Luan, X., Diekwisch, T.G.H. (2011). Differentiation of neural crest-derived intermediate pluripotent progenitors into committed periodontal populations involves unique molecular signature changes, cohort shifts, and epigenetic modifications. *Stem Cell Devel.* 20(1).

Danopoulos, S., Parsa, S., Al Alam, D., Tabatabai, R., Baptista, S., Tiozzo, C., Carraro, G., Wheeler, M., Barreto, G., Braun, T., Li, X., Hajihosseini, M.K., Bellusci, S. (2013). Transient inhibition of FGFR2b-ligands signaling leads to irreversible loss of cellular β-catenin organization and signaling in AER during mouse limb development. *PLoS ONE.* 8(10): e76248.

David, R. and Wedlich, D. (2001). PCR-based RNA probes, a quick and sensitive method to improve whole mount embryo *in situ* hybridizations. *Biotechniques*. 30: 769-772.

Deans, M.R, Peterson, J.M., Wong, G.W. (2010). Mammalian otolin: A multimeric glycoprotein specific to the inner ear that interacts with otoconial matrix protein Otoconin-90 and Cerebellin-1. *PLoS ONE.* 5(9): e12765.

Denaxa, M., Sharpe, P.T., Pachnis, V. (2009). The LIM homeodomain transcription factors Lhx6 and Lhx7 are key regulators of mammalian dentition. *Dev. Biol.* 333(2): 324-336.

Dhouailly, D. (2009). A new scenario for the evolutionary origin of hair, feather, and avian scales. *J. Anat*. 214: pp 587-606.

Diambra, L., Senthivel, V.R., Menendez, D.B., Isalan, M. (2014). Cooperativity to increase Turing pattern space for synthetic biology. *ACS. Synth. Biol.* 4: 177-186.

Donoghue, P.C.J., Graham, A., and Kelsh, R.N. (2008). The origin and evolution of the neural crest. *Bioessays.* 30(6): 530-541.

Dorshorst, B., Molin, A.-M., Rubin, C.-J., Johansson, A.M., Strömstedt, L., Pham, M.-H., Chen, C.-F., Hallböök, F., Ashwell, C., Andersson, L. (2011). A complex genomic rearrangement involving the Endothelin 3 locus causes dermal hyperpigmentation in the chicken. *PLoS Genet*. 7(12): e1002412.

Drew, C.F., Lin, C.M., Jiang, T.X., Blunt, G., Mou, C., Chuong, C.M., Headon, D.J. (2007). The Edar subfamily in feather placode formation. *Dev. Biol*. 305(1): 232-245.

Duench, K. and Franz-Odendaal, T.A. (2012). BMP and Hedgehog signaling during the development of scleral ossicles. *Dev. Biol*. 365: 251-258.

Duverger, O. and Morasso, M.I. (2009). Epidermal patterning and induction of different hair types during mouse embryonic development. *Birth Defects Res. C. Embryo Today*. 87(3): 263-272.

Eames, B.F. and Schneider, R.A. (2005). Quail-duck chimeras reveal spatiotemporal plasticity in molecular and histogenic programs of cranial feather development. *Development.* 132(7): 1499-1509.

Economou, A.D. and Green, J.B.A. (2014). Modelling from the experimental developmental biologist's viewpoint. *Semin. Cell Dev. Biol.* 0: 58-65.

El-Hashash, A.H.K., Alam, D.A., Turcatel, G., Bellusci, S., Warburton, D. (2011). Eyes absent 1 (Eya1) is a critical coordinator of epithelial, mesenchymal and vascular morphogenesis in the mammalian lung. *Dev. Biol.* 350(1): 112-126.

Enshell-Seijffers, D., Lindon, C., Kashiwagi, M., Morgan, B.A. (2010). β-catenin activity in the dermal papilla regulates morphogenesis and regeneration of hair. *Dev. Cell.* 18(4): 633-642.

Ezin, A.M., Sechrist, J.W., Zah, A., Bronner, M., Fraser, S.E. (2011). Early regulative ability of the neuroepithelium to form cardiac neural crest. *Dev. Biol*. 349(2): 238-249.

Feenstra, J.M., Kanaya, K., Pira, C.U., Hoffman, S.E., Eppey, R.J., Oberg, K.C. (2012). Detection of genes regulated by Lmx1b during limb dorsalization. *Dev. Growth Differ.* 54(4): 451-462.

Ferguson, C.A., Tucker, A.S., Christensen, L., Lau, A.L., Matzuk, M.M., Sharpe, P.T. (1998). Activin is an essential early mesenchymal signal in tooth development that is required for patterning of the murine dentition. *Genes Dev.* 12: 2636-2649.

Filosa, S., Rivera-Pérez, J.A., Gómez, A.P., Gansmuller, A., Sasaki, H., Behringer, R.R., Ang, S.-L. (1997). Goosecoid and HNF-3β genetically interact to regulate neural tube patterning during mouse embryogenesis. *Development.* 124: 2843-2854.

FitzPatrick, D.R. and van Heyningen, V. (2005). Developmental eye disorders. *Curr. Opin. Genetics Dev.* 15(3): 348-353.

Fortunato, S.A.V., Leininger, S., Adamska, M. (2014). Evolution of the Pax-Six-Eya-Dach network: the calcisponge case study. *EvoDevo*. 5: 23.

Franz-Odendaal, T.A. (2006). Intramembranous ossification of scleral ossicles in *Chelydra serpentina*. *Zoology*. 109: 75-81.

Franz-Odendaal, T.A. and Hall, B.K. (2006). Skeletal elements within teleost eyes and a discussion of their homology. *J. Morph.* 267: 1326-1337.

Franz-Odendaal, T.A. and Vickaryous, M.K. (2006). Skeletal elements in the vertebrate eye and adnexa: morphological and developmental perspectives. *Dev. Dyn.* 235: 1244-1255.

Franz-Odendaal, T.A., Ryan, K., Hall, B.K. (2007). Developmental and morphological variation in the teleost craniofacial skeleton reveals an unusual mode of ossification. *J. Exp. Zool. (Mol. Dev. Evol.)*. 308B: 709-721.

Franz-Odendaal, T.A. (2008a). Towards understanding the development of scleral ossicles in the chicken, *Gallus gallus*. *Dev. Dyn.* 237: 3240-3251.

Franz-Odendaal, T.A. (2008b). Scleral ossicles of teleostei: evolutionary and developmental trends. *Anat. Rec.* 291: 161-168.

Franz-Odendaal, T.A. (2011). The ocular skeleton through the eye of evo-devo. *J. Exp. Zool. (Mol. Dev. Evol.)*. 316: 393-401.

Freyer, L. and Morrow, B.E. (2010). Canonical Wnt signaling modulates Tbx1, Eya1, and Six1 expression, restricting neurogenesis in the otic vesicle. *Dev. Dyn.* 239(6): 1708-1722.

Fritzsch, B. and Beisel, K.W. (2003). Molecular conservation and novelties in vertebrate ear development. *Curr. Top. Dev. Biol*. 57: 1-44.

Fritzsch, B., Dillard, M., Lavado, A., Harvey, N.L., Jahan, I. (2010). Cranal cristae growth and fiber extension to the outer hair cells of the mouse ear require Prox1 activity. *PLoS ONE.* 5(2): e9377.

Fuchs, E. (2007). Scratching the surface of skin development. *Nature.* 445(7130): 834-842.

Fukushige, T., Brodigan, T.M., Schriefer, L.A., Waterston, R.H., Krause, M. (2006). Defining the transcriptional redundancy of early bodywall muscle development in *C. elegans*: evidence for a unified theory of animal muscle development. *Genes & Development.* 20: 3395-3406.

Fuhrmann, S. (2010). Eye morphogenesis and patterning of the optic vesicle. *Curr. Top. Dev. Biol.* 93: 61-84.

Fyfe, D.M. and Hall, B.K. (1981). A scanning electron microscopic study of the developing epithelial scleral papillae in the eye of the embryonic chick. *J. Morph.* 167: 201-209.

Fyfe, D.M. and Hall, B.K. (1983). The origin of the ectomesenchymal condensations which precede the development of the bony scleral ossicles in the eyes of embryonic chicks. *J. Embryol. exp. Morph.* 73: 69-86.

Fyfe, D.M., Ferguson, M.W.J., and Chiquet-Ehrismann, R. (1988). Immunocytochemical localization of tenascin during the development of scleral papillae and scleral ossicles in the embryonic chick. *J. Anat.* 159: pp. 117-127.

Gage, P.J., Rhoades, W., Prucka, S.K., Hjalt, T. (2005). Fate maps of neural crest and mesoderm in the mammalian eye. *IOVS.* 46(11): 4200-4208.

Gammill, L.S. and Roffers-Agarwal, J. (2010). Division of labor during trunk neural crest development. *Dev. Biol*. 344(2): 555-565.

Gans, C. and Northcutt, G. (1983). Neural crest and the origin of vertebrates: A new head. *Science.* 220(4594): 268-273.

Garcia, C.M., Huang, J., Madakashira, B.P., Liu, Y., Rajagopal, R., Dattilo, L., Robinson, M.L., Beebe, D.C. (2011). The function of FGF signaling in the lens placode. *Dev. Biol*. 351(1): 176-185.

Geng, R., Yuan, C., Chen, Y. (2013). Exploring differentially expressed genes by RNA-Seq in Cashmere goat (*Capra hircus*) skin during hair follicle development and cycling. *PLoS ONE.* 8(4): e62704.

Gitton, Y., Narboux-Nême, N., Levi, G. (2014). Transitory expression of Dlx5 and Dlx6 in maxillary arch epithelial precursors is essential for upper jaw morphogenesis. *F1000Res*. 2: 261.

Golding, J.P., Dixon, M., Gassmann, M. (2002). Cues from neuroepithelium and surface ectoderm maintain neural crest-free regions within cranial mesenchyme of the developing chick. *Development.* 129: 1095-1105.

Golding, J.P., Sobieszczuk, D., Dixon, M., Coles, E., Christiansen, J., Wilkinson, D., Gassman, M. (2004). Roles of erbB4, rhombomere-specific, and rhombomere-independent cues in maintaining neural crest-free zones in the embryonic head. *Dev. Biol.* 266: 361-372.

Graw, J. (2010). Eye development. *Curr. Top. Dev. Biol*. 90: 343-386.

Graham, A., Blentic, A., Duque, S., Begbie, J. (2007). Delamination of cells from neurogenic placodes does not involve an epithelial-to-mesenchymal transition. *Development*. 134: 4141-4145.

Grocott, T., Johnson, S., Bailey, A.P., Streit, A. (2011). Neural crest cells organize the eye via TGF-β and canonical Wnt signaling. *Nature Commun.* 2: 265.

Grocott, T., Tambalo, M., Streit, A. (2012). The peripheral sensory nervous system in the vertebrate head: a gene regulatory perspective. *Dev. Biol*. 370: 3-23.

Gross, J.B. and Hanken, J. (2008). Review of fate-mapping studies of osteogenic cranial neural crest in vertebrates. *Dev Biol*. 317(2): 389-400.

Gross, J.B., Kerney, R., Hanken, J., Tabin, C.J. (2011). Molecular anatomy of the developing limb in the coqui frog, *Eleutherodactylus coqui* limb bud development in the coqui frog. *Evol. Dev.* 13(5): 415-426.

Groves, A.K. and LaBonne, C. (2014). Setting appropriate boundaries: Fate, patterning and competence at the neural plate border. *Dev. Biol.* 389: 2-12.

Gunhaga. L. (2011). The lens: a classical model of embryonic induction providing new insights into cell determination in early development. *Phil. Trans. R. Soc. B.* 266: 1193-1203.

Guo, C., Sun, Y., Zhou, B., Adam, R.M., Li, X., Pu, W.T., Morrow, B.E., Moon, A., Li, X. (2011). A Tbx1-Six1/Eya1-Fgf8 genetic pathway controls mammalian cardiovascular and craniofacial morphogenesis. *J. Clin. Invest.* 121(4): 1585-1595.

Hagh, M.F., Noruzinia, M., Mortazavi, Y., Soleimani, M., Kaviani, S., Abroun, S., Fard, A.D., Maymand, M.M. (2015). Different methylation patterns of RUNX2, OSX, DLX5 and BSP in osteoblastic differentiation of mesenchymal stem cells. *Cell J.* 17(1): 71-82.

Hakami, R.M., Hou, L., Baxter, L., Loftus, S., Southard-Smith, E.M., Incao, A., Cheng, J., Pavan, W.J. (2006). Genetic evidence does not support direct regulation of EDNRB by Sox10 in migratory neural crest and the melanocyte lineage. *Mech. Dev.* 123(2): 124-134.

Hall, B.K. (1981a). Specificity in the differentiation and morphogenesis of neural crest-derived scleral ossicles and of epithelial scleral papillae in the eye of the embryonic chick. *J. Embryol. exp. Morph.* 66: 175-190.

Hall, B.K. (1981b). The induction of neural crest-derived cartilage and bone by embryonic epithelia: an analysis of the mode of action of an epithelial-mesenchymal interaction. *J. Embryol. exp. Morph.* 66: 305-320.

Hall, B.K. and Miyake, T. (1995). Divide, accumulate, differentiate: cell condensation in skeletal development revisited. *Int. J. Dev. Biol*. 39: 881-893.

Hall, B.K. (2000). The neural crest as a fouth germ layer and vertebrates as quadroblastic not triploblastic. *Evol Dev*. 2: 3-5.

Hamburger, V. and Hamilton, H.L. (1951). A series of normal stages in the development of the chick embryo. *J. Morph.* 68(3).

Han, J., Mayo, J., Xu, X., Li, J., Bringas, P., Maas, R.L., Rubenstein, J.L.R., Chai, Y. (2009). Indirect modulation of Shh signaling by Dlx5 affects the oral-nasal patterning of palate and rescues cleft palate in Msx1-null mice. *Development.* 136(24): 4225-4233.

Harlow, D.E. and Barlow, L.A. (2007). Embryonic origin of gustatory cranial sensory neurons. *Dev. Biol*. 310(2): 317-328.

Hartman, B.H., Durruthy-Durruthy, R., Laske, R.D., Losorelli, S., Heller, S. (2015). Identification and characterization of mouse otic sensory lineage genes. *Front. Cell. Neurosci.* 9: 79.

Hopwood, B., Tsykin, A., Findlay, D.M., Fazzalari, N.L. (2007). Microarray gene expression profiling of osteoarthritic bone suggests altered bone remodelling, WNT and transforming growth factor-β/bone morphogenic protein signaling. *Arthritis Res. Ther.* 9(5): R100.

Hu, D. and Marcucio, R.S. (2012). Neural crest cells pattern the surface cephalic ectoderm during FEZ formation. *Dev. Dyn.* 241(4): 732-740.

Huang, S., Zhu, X., Liu, Y., Tao, Y., Feng, G., He, L., Guo, X., Ma, G. (2012). WIs is expressed in the epidermis and regulates embryonic hair follicle induction in mice. *PLoS ONE*. 7(9): e45904.

Huh, S.-H., Närhi, K., Lindfors, P.H., Häärä, O., Yang, L., Ornitz, D.M., Mikkola, M.L. (2013). Fgf20 governs formation of primary and secondary dermal condensations in developing hair follicles. *Genes & Development*. 27: 450-458.

Hynes, R.O. (2009). The extracellular matrix: not just pretty fibrils. *Science.* 326: 1216-1219.

Ishii, M., Arias, A.C., Liu, L., Chen, Y.-B., Bronner, M.E., Maxson, R.E. (2012). A stable cranial neural crest cell line from mouse. *Stem Cells Dev*. 21(17): 3069-3080.

Itoh, T., Nozawa, Y., Akao, Y. (2009). MicroRNA-141 and -200a are involved in bone morphogenetic protein-2-induced mouse pre-osteoblast differentiation by targeting distal-less homeobox 5. *J.Biol. Chem.* 284(29): 19272-19279.

Ivashkin, E. and Adameyko, I. (2013). Progenitors of the protochordate ocellus as an evolutionary origin of the neural crest. *EvoDevo*. 4: 12.

Iwata, J., Suzuki, A., Pelikan, R.C., Ho, T.-V., Sanchez-Lara, P.A., Chai, Y. (2014). Modulation of lipid metabolic defects rescues cleft palate in Tgfbr2 mutant mice. *Human Mol. Gen.* 23(1): 182-193.

Jabalee, J. and Franz-Odendaal., T.A. (2015). Vascular endothelial growth factor signaling affects both angiogenesis and osteogenesis during the development of scleral ossicles. *Dev. Biol.* 406(1): 52-62.

Jackman, W.R., Yoo, J.J., Stock, D.W. (2010). Hedgehog signaling is required at multiple stages of zebrafish tooth development. *BMC Dev. Biol*. 10: 119.

Jacques-Fricke, B.T., Roffers-Agarwal, J., Gammill, L.S. (2012). DNA methyltransferase 3b is dispensible for mouse neural crest development. *PLoS One*. 7(10): e47794.

Jeong, J., Mao, J., Tenzen, T., Kottmann, A.H., McMahon, A.P. (2004). Hedgehog signaling in the neural crest cells regulates the patterning and growth of facial primordia. *Genes Dev*. 18: 937-951.

Jeong, A.H. and Schneider, R.A. (2009). The cells that fill the bill: Neural crest and the evolution of craniofacial development. *J. Dent. Res.* 88(1): 12-21.

Jheon, A.H., Seidel, K., Biehs, B., Klein, O.D. (2013). From molecules to mastication: the development and evolution of teeth. *Wiley Interdiscip. Rev. Dev. Biol.* 2(2): 165-183.

Jhingory, S., Wu, C.-Y., Taneyhill, L.A. (2010). Novel insight into the function and regulation of αN-catenin by snail2 during chick neural crest cell migration. *Dev Biol.* 344(2): 896-910.

Jiang, X., Rowitch, D.H., Soriano, P., McMahon, A.P., Sucov, H.M. (2000). Fate of the mammalian cardiac neural crest. *Development.* 127: 1607-1616.

Jiang, T.-X., Tuan, T.L., Wu, P., Widelitz, R.B., Chuong, C.-M. (2011). From buds to follicles: Matrix metalloproteinases in developmental tissue remodeling during feather morphogenesis. *Differentiation.* 81(5): 307-314.

Jidigam, V.K. and Gunhaga, L. (2013). Development of cranial placodes: insights from studies in chick. *Dev. Growth Differ.* 55(1): 79-95.

Jourdeuil, K. and Franz-Odendaal, T.A. (2012). Vasculogenesis and the induction of skeletogenic condensations in the avian eye. *Anat. Rec*. 295: 691-698.

Juuri, E., Jussila, M., Seidel, K., Holmes, S., Wu, P., Richman, J., Heikinheimo, K., Chuong, C.-M., Arnold, K., Hochedlinger, K., Klein, O., Michon, F., Thesleff, I. (2013). Sox2 marks epithelial competence to generate teeth in mammals and reptiles. *Development.* 140: 1424-1432.

Kabbani, H. and Raghuveer, T.S. (2004). Craniosynostosis. *Am. Fam. Physician*. 69(12): 2863-2870.

Kaltezioti, V., Kouroupi, G., Oikonomaki, M., Mantouvalou, E., Stergiopoulos, A., Charonis, A., Rohrer, H., Matsas, R., Politis, P.K. (2010). Prox1 regulates the Notch1-mediated inhibition of neurogenesis. *PLoS Biol.* 8(12): e1000565.

Kanakubo, S., Nomura, T., Yamamura, K., Miyazaki, J., Tamai, M., Osumi, N. (2006). Abnormal migration and distribution of neural crest cells in Pax6 heterozygous mutant eye, a model for human eye diseases. *Genes Cells*. 11(8): 919-33.

Kang, H.-W., Zheng, L., Othmer, H.G. (2012). The effect of the signalling scheme on the robustness of pattern formation in development. *Interface Focus*. 2: 465-486.

Karalay, Ö., Doberauer, K., Vadodaria, K.C., Knobloch, M., Berti, L., Miquelajauregui, A., Schwark, M., Jagasia, R., Taketo, M.M., Tarabykin, V., Lie, D.C. (2011). Prospero-related homeobox 1 gene (Prox1) is regulated by canonical Wnt signaling and has a stage-specific role in adult hippocampal neurogenesis. *PNAS.* 108(14): 5807-5812.

Kaukua, N., Chen, M., Guarnieri, P., Dahl, M., Lim, M.L., Yucel-Lindberg, T., Sundström, E., Adameyko, I., Mao, J.J., Fried, K. (2015). Molecular differences between stromal cell populations from deciduous and permanent human teeth. *Stem Cell Research & Therapy*. 6: 59.

Kawakami, K., Sato, S., Ozaki, H., Ikeda, K. (2000). Six family genes – structure and function as transcription factors and their roles in development. *Bioessays*. 22: 616-626.

Kelsh, R.N., Harris, M.L., Colanesi, S., Erickson, C.A. (2009). Stripes and belly-spots - a review of pigment cell morphogenesis in vertebrates. *Semin. Cell Dev. Biol.* 20(1): 90-104.

Kerosuo, L. and Bronner-Fraser, M. (2012). What's bad in cancer is good in the embryo: Importance of EMT in neural crest development. *Semin. Cell Dev. Biol*. 23(3): 320-332.

Kerr, C.L., Huang, J., Williams, T., West-Mays, J.A. (2012). Activation of the Hedgehog signaling pathway in the developing lens stimulates ectopic *FoxE3* expression and disruption in fiber cell differentiation. *Invest. Ophthalmol. Vis. Sci.* 53(7): 3316-3330.

Kim, Y.-M., Kim, W.-Y., Nam, S.A., Choi, A.-R., Kim, H., Kim, Y.-K., Kim, H.-S., Kim, J. (2015). Role of Prox1 in the transforming ascending thin limb of Henle's Loop during mouse kidney development. *PLoS ONE*. 10(5): e0127429.

Kinoshita, K., Akiyama, T., Mizutani, M., Shinomiya, A., Ishikawa, A., Younis, H.H., Tsudzuki, M., Namikawa, T., Matsuda, Y., (2014). Endothelin receptor B2 (EDNRB2) is responsible for the Tyrosinase-Independent recessive white (mo^w) and Mottled (mo) plumage phenotypes in the chicken. *PLoS ONE.* 9(1): e86361.

Knabe, W., Obermayer, B., Kuhn, H.-J., Brunnett, G., Washausen, S. (2009). Apoptosis and proliferation in the trigeminal placode. *Brain Struct. Funct.* 214: 49-65.

Kourakis, M.J. and Smith, W.C. (2007). A conserved role for FGF signaling in chordate otic/atrial placode formation. *Dev. Biol.* 312(1): 245-257.

Koussoulakou, D.S., Margaritis, L.H., Koussoulakos, S.L. (2009). A curriculum vitae of teeth: Evolution, generation, regeneration. *Int. J. Biol. Sci.* 5(3): 226-243.

Krawchuk, D., Weiner, S.J., Chen, Y.-T., Lu, B., Costantini, F., Behringer, R.R., Laufer, E. (2010). Twist1 activity thresholds define multiple functions in limb development. *Dev. Biol*. 347(1): 133-146.

Krimm, R.F. (2007). Factors that regulate embryonic gustatory development. *BMC Neurosci*. 8(Suppl 3): S4.

Kulesa, P.M. and Fraser, S.E. (2000). In ovo time-lapse analysis of chick hindbrain neural crest cell migration shows cell interactions during migration to the branchial arches. *Development.* 127: 1161-1172.

Kulesa, P.M., Ellies, D.L., Trainor, P.A. (2004). Comparative analysis of neural crest cell death, migration, and function during vertebrate embryogenesis. *Dev. Dyn*. 229: 14-29.

Kulesa, P.M., Bailey, C.M., Kasemeier-Kulesa, J.C., McLennan, R. (2010). Cranial neural crest migration: New rules for an old road. *Dev. Biol.* 344: 543-554.

LaBonne, C. and Bronner-Fraser, M. (1998). Neural crest induction in Xenopus: evidence for a two-signal model. *Development.* 125(1): 2403-2414.

Lamb, T.D., Collin, S.P., Pugh, E.N. (2007). Evolution of the vertebrate eye: opsins, photoreceptors, retina and eye cup. *Nat. Rev. Neurosci.* 8(12): 960-976.

Lan, Y., Jia, S., Jiang, R. (2014). Molecular patterning of the mammalian dentition. *Semin. Cell Dev. Biol.* 0: 61-70.

Landin, M.A.S.S., Shabestari, M., Babaie, E., Reseland, J.E., Osmundsen, H. (2012). Gene expression profiling during murine tooth development. *Front. Genet.* 3: article 139

Landgraf, K., Bollig, F., Trowe, M-O., Besenbeck, B., Ebert, C., Kruspe, D., Kispert, A., Hänel, F., Englert, C. (2010). Sipl1 and Rbck1 are novel Eya-1 binding proteins with a role in craniofacial development. *Mol. Cell Biol.* 30(24): 5764-5775.

Langenberg, T., Kahana, A., Wszalek, J.A., Halloran, M.C. (2008). The eye organizes neural crest cell migration. *Dev. Dyn.* 237: 1645-1652.

Lassiter, R.N.T., Stark, M.R., Zhao, T., Zhou, C.J. (2014). Signaling mechanisms controlling cranial placode neurogenesis and delamination. *Dev. Biol.* 389: 39-49.

Lecoin, L., Sakurai, T., Ngo, M.-T., Abe, Y., Yanagisawa, M., Le Douarin, N.M. (1998). Cloning and characterization of a novel endothelin receptor subtype in the avian class. *Proc. Natl. Acad. Sci. USA*. 95: 3024-3029.

Le Douarin, N.M. (2004). The avian embryo as a model to study the development of the neural crest: a long and still ongoing study. *Mech. Dev*. 121: 1089-1102.

Lee, M.-H., Kwon, T.-G., Park, H.-S., Wozney, J.M., Ryoo, H.-M. (2003a). BMP-2-induced Osterix expression is mediated by Dlx5 but is independent of Runx2. *Biochem. Biophys. Res. Commun.* 309: 689-694.

Lee, M.-H., Kim, Y.-J., Kim, H.-J., Park, H.-D., Kang, A.-R., Kyung, H.-M., Sung, J.-H., Wozney, J.M., Kim, H.-J., Ryoo, H.-M. (2003b). BMP-2-induced Runx2 expression is mediated by Dlx5, and TGF-β1 opposes the BMP-2-induced osteoblast differentiation by suppression of Dlx5 expression. *J. Biol. Chem*. 278: 34387-34394.

Lee, J. and Tumbar, T. (2012). Hairy tale of signaling in hair follicle development and cycling. *Semin. Cell Dev. Biol.* 23(8): 906-916.

Lengler, J., Krausz, E., Tomarev, S., Prescott, A., Qinlan, R.A., Graw, J. (2001). Antagonistic action of Six3 and Prox1 at the γ-crystallin promoter. *Nucleic Acid Res.* 29(2): 515-526.

Leung, A.W., Morest, D.K., Li, J.Y.H. (2013). Differential BMP signaling controls formation and differentiation of multipotent preplacodal ectoderm progenitor from human embryonic stem cells. *Dev. Biol.* 379(2): 208-220.

Li, Y., Manaligod, J.M., Weeks, D.L. (2010). EYA1 mutations associated with the branchio-oto-renal syndrome result in defective otic development in *Xenopus laevis*. *Biol. Cell*. 102: 277-292.

Li, A., Chen, M., Jiang, T.-X., Wu, P., Nie, Q., Widelitz, R., Chuong, C.-M. (2012). Shaping organs by a wingless-int/Notch/nonmuscle myosin module which orients feather bud elongation. *PNAS*. E1452-E1461.

Li, L., Li, D., Li, S., Feng, Y., Peng, X., Gong, Y. (2015). Endothelin receptor B2 (EDNRB2) gene is associated with spot plumage pattern in domestic ducks (*Anas platyrhynchos*). *PLoS ONE*. 10(5): e0125883.

Lin, M., Li, L., Liu, C., Liu, H., He, F., Yan, F., Zhang, Y., Chen, Y. (2011). Wnt5a regulates growth, patterning, and odontoblast differentiation of developing mouse tooth. *Dev. Dyn.* 240(2): 432-440.

Lines, M.A., Kozlowski, K., Kulak, S.C., Allingham, R.R., Héon, E., Ritch, R., Levin, A.V., Shields, M.B., Damji, K.F., Newlin, A., Walter, M.A. (2004). Characterization and prevalence of PITX2 microdeletions and mutations in Axenfeld-Rieger malformations. *Invest. Ophthalmol. Vis. Sci.* 45(3): 828-833.

Liu, F., Chu, E.Y., Watt, B., Zhang, Y., Gallant, N.M., Andl, T., Yang, S.H., Lu, M.-M., Piccolo, S., Schmidt-Ullrich, R., Taketo, M.M., Morrisey, E.E., Atit, R., Dlugosz, A.A., Millar, S.E. (2008). Wnt/beta-catenin signaling directs multiple stages of tooth morphogenesis. *Dev. Biol.* 313(1): 210-224.

Loh, S.-L., The, C., Muller, J., Guccione, E., Hong, W., Korzh, V. (2014). Zebrafish yap1 plays a role in differentiation of hair cells in posterior lateral line. *Sci. Rep.* 4: 4289.

Lu, P., Yu, Y., Perdue, Y., Werb, Z. (2008). The apical ectodermal ridge is a timer for generating distal limb progenitors. *Development.* 135(8): 1395-1405.

Maier, E.C., Saxena, A., Alsina, B., Bronner, M.E., Whitfield, T.T. (2014). Sensational placodes: Neurogenesis in the otic and olfactory systems. *Dev. Biol.* 389: 50-67.

Mammoto, T., Mammoto, A., Torisawa, Y., Tat, T., Gibbs, A., Derda, R., Mannix, R., de Bruijn, M., Yung, C.W., Huh, D., Inbger, D.E. (2011). Mechanochemical control of mesenchymal condensation and embryonic tooth organ formation. *Dev. Cell.* 21(4): 758-769.

Marom, K., Levy, V., Pillemer, G., Fainsod, A. (2005). Temporal analysis of the early BMP functions identifies distinct anti-organizer and mesoderm patterning phases. *Dev. Biol.* 282(2): 442-454.

Martinez-Morales, J.R. and Wittbrodt, J. (2009). Shaping the vertebrate eye. *Curr. Opin. Genet. Dev.* 19*:* 511-517.

Matalova, E., Svandova, E., Tucker, A.S. (2012). Apoptotic signaling in mouse odontogenesis. 16: 60-70.

Matsuzaki, T. and Yoshizato, K. (1998). Role of hair papilla cells on induction and regeneration processes of hair follicles. *Wound Rep. Reg.* 6: 524-530.

Mazzuca, M.Q. and Khalil, R.A. (2012). Vascular endothelin receptor type B: structure, function, and dysregulation in vascular disease. *Biochem. Pharmacol.* 84(2): 147-162.

McCabe, K.L. and Bronner-Fraser, M. (2009). Molecular and tissue interactions governing induction of cranial ectodermal placodes. *Dev. Biol*. 332(2): 189-195.

McGlinn, A.M., Baldwin, D.A., Tobias, J.W., Budak, M.T., Khurana, T.S., Stone, R.A. (2007). Form-deprivation myopia in chick induces limited changes in retinal gene expression. *Invest. Ophthalmol. Vis. Sci*. 48(8): 3430-3436.

McLennan, R., Teddy, J.M., Kasemeier-Kulesa, J.C., Romine, M.H., Kulesa, P.M. (2010). Vascular endothelial growth factor (VEGF) regulates cranial neural crest migration in vivo. *Dev. Biol*. 339: 114-125.

Meinhardt, H. (2012). Turing's theory of morphogenesis of 1952 and the subsequent discovery of the crucial role of local self-enhancement and long-range inhibition. *Interface Focus.* 2: 407-416.

Meng, Q., Jin, C., Chen, Y., Chen, J., Medvedovic, M., Xia, Y. (2014). Expression of signaling components in embryonic eyelid epithelium. *PLoS ONE.* 9(2): e87038.

Meulemans, D. and Bronner-Fraser, M. (2007). The amphioxus SoxB family : Implications for the evolution of vertebrate placodes. *Int. J. Biol. Sci.* 3(6): 356-364.

Minoux, M. and Rijli, F.M. (2010). Molecular mechanisms of cranial neural crest cell migration and patterning in craniofacial development. *Development*. 137: 2605-2621.

Miura, T. (2007). Modulation of activator diffusion by extracellular matrix in Turing system. *RIMS Kôkyûroku Bessatsu*. B3: 165-176.

Moody, S.A. and LaMantia, A.-S. (2015). Transcriptional regulation of cranial sensory placode development. *Curr. Top. Dev. Biol.* 111: 301-350.

Moreland, K.T., Hong, M., Lu, W., Rowley, C.W., Ornitz, D.M., De Yoreo, J.J., Thalmann, R. (2014). In vitro calcite crystal morphology is modulated by otoconial proteins Otolin-1 and Otoconin-90. *PLoS ONE*. 9(4): e95333.

Mou, C., Pitel, F., Gourichon, D., Vignoles, F., Tzika, A., Tato, P., Yu, L., Burt, D.W., Bed'hom, B., Tixier-Boichard, M., Painter, K.L., Headon, D.J. (2011). Cryptic patterning of avian skin confers a developmental facility for loss of neck feathering. *PLoS Biol*. 9(3): e1001028.

Murray, P.D.F. (1943). The development of the conjunctival papillae and of the scleral bones in the embryo chick. *J. Anat.* 77(Pt 3): 225-240.2.

Musharraf, A., Kruspe, D., Tomasch, J., Besenbeck, B., Englert, C., Landgraf, K. (2014). BOR-syndrome-associated Eya1 mutations lead to enhanced proteasomal degradation of Eya1 protein. *PLoS ONE*. 9(1): e87407.

Myung, P., Takeo, M., Ito, M., Atit, R. (2013). Epithelial Wnt ligand secretion is required for adult hair follicle growth and regeneration. *J. Invest. Dermatol*. 133(1): 31-41.

Neilson, K.M., Pignoni, F., Yan, B., Moody, S.A. (2010). Developmental expression patterns of candidate co-factors for vertebrate Six family transcription factors. *Dev. Dyn.* 239(12): 3446-3466.

Ng, C.S., Wu, P., Foley, J., Foley, A., McDonald, M.-L., Juan, W.-T., Huang, C.-J., Lai, Y.-T., Lo, W.-S., Chen, C.-F., Leal, S.M., Zhang, H., Widelitz, R.B., Patel, P.I., Li, W.-H., Chuong, C.-M. (2012). The chicken frizzle feather is due to an α-Keratin (KRT75) mutation that causes a defective rachis. *PLoS Genet.* 8(7): e1002748.

Nichols, D.H., Pauley, S., Jahan, I., Beisel, K.W., Millen, K.J., Fritzsch, B. (2008). Lmx1a is required for segregation of sensory epithelia and normal ear histogenesis and morphogenesis. *Cell Tissue Res.* 334(3): 339-358.

Nodder, S. and Martin, P. (1997). Wound healing in embryos: a review. *Anat. Embryo. (Berl).* 195(3): 215-228.

Northcutt, R.G. and Gans, C. (1983). The genesis of neural crest and epidermal placodes: A reinterpretation of vertebrate origins. *Q. Rev. Biol*. 58(1): 1-28.

O'Connor, J.K., Chiappe, L.M., Chuong, C.-M., Bottjer, D.J., You, H. (2013). Homology and potential cellular and molecular mechanisms for development of unique feather morphologies in early birds. *Geosciences (Basel).* 2(3): 157-177.

Olesnicky Killian, E.C., Birkholz, D.A., Artinger, K.B. (2009). A role for chemokine signaling in neural crest cell migration and craniofacial development. *Dev. Biol*. 333: 161-172.

O'Neill, P., Mak, S.-S., Fritzsch, B., Ladher, R.K., Baker, C.V.H. (2012). The amniote paratympanic organ develops from a previously undiscovered sensory placode. *Nat. Commun.* 3: 1041.

Ojeda, A.F., Munjaal, R.P., Lwigale, P.Y. (2013). Expression of CXCL12 and CXCL14 during eye development in chick and mouse. *Gene Exp. Patterns.* 13: 303-310.

Ozturk, F., Li, Y., Zhu, X., Guda, C., Nawshad, A. (2013). Systematic analysis of palatal transcriptome to identify cleft palate genes within TGFβ3-knockout mice alleles: RNA-Seq analysis of TGFβ3 mice. *BMC Genomics*. 14: 113.

Painter, K.J., Hunt, G.S., Wells, K.L., Johansson, J.A., Headon, D.J. (2012). Towards an integrated experimental-theoretical approach for assessing the mechanistic basis of hair and feather morphogenesis. *Interface Focus*. 2: 433-450.

Padanad, M.S. and Riley, B.B. (2011). Pax2/8 proteins coordinate sequential induction of otic and epibranchial placodes through differential regulation of foxi1, sox3, and fgf24. *Dev. Biol*. 351(1): 90-98.

Paradis, A. and Zhang, L. (2013). Role of endothelin in uteroplacental circulation and fetal vascular function. *Curr. Vasc. Pharmacol.* 11(5): 594-605.

Parry, D.A., Logan, C.V., Stegmann, A.P.A., Abdelhamed, Z.A., Calder, A., Khan, S., Bonthron, D.T., Clowes, V., Sheridan, E., Ghali, N., Chudley, A.E., Dobbie, A., Stumpel, C.T.R.M., Johnson, C.A. (2013). SAMS, a syndrome of short stature, auditory-canal atresia, mandibular hypoplasia, and skeletal abnormalities is a unique neurocristopathy caused by mutations in Goosecoid. *Am. J. Hum. Genet*. 93: 1135-1142.

Peterkin, T., Gibson, A., Patient, R. (2007). Redundancy and evolution of GATA factor requirements in development of the myocardium. *Dev. Biol.* 311(2): 623-635.

Petko, J.A., Millimaki, B.B., Canfield, V.A., Riley, B.B., Levenson, R. (2008). Otoc1: A novel Otoconin-90 ortholog required for Otolith mineralization in zebrafish. *Dev. Neurobiol.* 68(2): 209-222.

Pinto, C.B. and Hall, B.K. (1991). Toward an understanding of the epithelial requirement for osteogenesis in scleral mesenchyme of the embryonic chick. *J. Exp. Zool.* 258(1): 92-108.

Pinyopich, A., Ditta, G.S., Savidge, B., Liljegren, S.J., Baumann, E., Wisman, E., Yanofsky, M.F. (2003). Assessing the redundancy of MADS-box genes during carpel and ovule development. *Nature.* 424: 85-88.

Piotrowski, T. and Baker, C.V.H. (2014). The development of lateral line placodes: Taking a broader view. *Dev. Biol.* 389: 68-81.

Pistocchi, A., Feijóo, C.G., Cabrera, P., Villablanca, E.J., Allende, M.L., Cotelli, F. (2009). The zebrafish prospero homolog prox1 is required for mechanosensory hair cell differentiation and functionality in the lateral line. *BMC Devel. Biol.* 9: 58.

Prasad, M.S., Sauka-Spengler, T., LaBonne, C. (2012). Induction of the neural crest state: Control of stem cell attributes by gene regulatory, post-transcriptional and epigenetic interactions. *Dev. Biol*. 366(1): 10-21.

Prum, R.O. (1999). Development and evolutionary origin of feather. *J. Exp. Zool*. 285(4): 291-306.

Porntaveetus, T., Otsuka-Tanaka, Y., Basson, M.A., Moon, A.M., Sharpe, P.T., Ohazama, A. (2011). Expression of fibroblast growth factors (Fgfs) in murine tooth development. *J. Anat.* 218: pp 534-543.

Rendl, M., Lewis, L., Fuchs, E. (2005). Molecular dissection of mesenchymal-epithelial interactions in the hair follicle. *PLoS Biol.* 3(11): e331.

Restelli, M., Lopardo, T., Iacono, N.L., Garaffo, G., Conte, D., Rustighi, A., Napoli, M., Del Sal, G., Perez-Morga, D., Costanzo, A., Merlo, G.R., Guerrini, L. (2014). DLX5, FGF8, and the Pin1 isomerase control ΔNp63α protein stability during limb development: a regulatory loop at the basis of the SHFM and EEC congenital malformations. *Human Mol. Gen.* 23(14): 3830-3842.

Rivolta, M.N., Halsall, A., Johnson, C.M., Tones, M.A., Holley, M.C. (2002). Transcript profiling of functionally related groups of genes during conditional differentiation of a mammalian cochlear hair cell line. *Genome Res.* 12: 1091-1099.

Robinson, V., Smith, A., Flenniken, A.M., Wilkinson, D.G. (1997). Roles of Eph receptors and ephrins in neural crest pathfinding. *Cell Tissue Res.* 290: 265-274.

Robledo, R.F., Rajan, L., Li, X., Lufkin, T. (2002). The Dlx5 and Dlx6 homeobox genes are essential for craniofacial, axial, and appendicular skeletal development. *Genes & Development.* 16: 1089-1101.

Roffers-Agarwal, J., Hutt, K.J., and Gammill, L.S. (2012). Paladin is an antiphosphatase that regulates neural crest cell formation and migration. *Dev Biol*. 371(2): 180-190.

Romereim, S.M. and Dudley, A.T. (2011). Cell polarity: The missing link in skeletal morphogenesis. *Organogenesis*. 7(3): 217-228.

Ronaghi, M., Nasr, M., Ealy, M., Durruthy-Durruthy, R., Waldhaus, J., Diaz, G.H., Joubert, L.-M., Oshima, K., Heller, S. (2014). Inner ear hair cell-like cells from human embryonic stem cells. *Stem Cells Dev.* 23(11): 1275-1284.

Roth, S. (2011). Mathematics and biology: a Kantian view on the history of pattern formation theory. *Dev. Genes Evol.* 221: 255-279.

Saint-Jeannet, J.-P. and Moody, S.A. (2014). Establishing the pre-placodal region and breaking it into placodes with distinct identities. *Dev. Biol.* 389: 13-27.

Sajan, S.A., Rubenstein, J.L.R., Warchol, M.E., Lovett, M. (2011). Identification of direct downstream targets of Dlx5 during early inner ear development. *Human Mol. Gen.* 20(7): 1262-1273.

Saldana-Caboverde, A. and Kos, L. (2010). Roles of Endothelin signaling in melanocyte development and melanoma. *Pigment Cell Melanoma Res.* 23(2): 160-170.

Samee, N., Geoffroy, V., Marty, C., Schiltz, C., Vieux-Rochas, M., Levi, G., de Vernejoul, M.-C. (2008). Dlx5, a positive regulator of osteoblastogenesis, is essential for osteoblast-osteoclast coupling. *Am. J. Pathol.* 173(3): 773-780.

Sato, S., Ikeda, K., Shioi, G., Ochi, H., Ogino, H., Yajima, H., Kawakami, K. (2010). Conserved expression of mouse Six1 in the pre-placodal region (PPR) and identification of an enhancer for the rostral PPR. *Dev. Biol.* 344: 158-171.

Sato, S., Ikeda, K., Shioi, G., Nakao, K., Yajima, H., Kawakami, K. (2012). Regulation of Six1 expression by evolutionarily conserved enhancers in tetrapods. *Dev. Biol*. 368: 95-108.

Saudemont, A., Haillot, E., Mekpoh, F., Bessodes, N., Quirin, M., Lapraz, F., Duboc, V., Röttinger, E., Range, R., Oisel, A., Besnardeau, L., Wincker, P., Lepage, T. (2010). Ancestral regulatory circuits governing ectoderm patterning downstream of Nodal and BMP2/4 revealed by gene regulatory network analysis in an echinoderm. *PLoS Genet*. 6(12): e1001259.

Sauka-Spengler, T. and Bronner-Fraser, M. (2008). A gene regulatory network orchestrates neural crest formation. *Nat. Rev. Mol. Cell Biol*. 9: 557-568.

Sayama, K., Kajiya, K., Sugawara, K., Sato, S., Hirakawa, S., Shirakata, Y., Hanakawa, Y., Dai, X., Ishimatsu-Tsuji, Y., Metzger, D., Chambon, P., Akira, S., Paus, R., Kishimoto, J., Hashimoto, K. (2010). Inflammatory mediator TAK1 regulates hair follicle morphogenesis and anagen induction shown by using keratinocyte-specific TAK1-deficient mice. *PLoS ONE.* 5(6): e11275.

Scarpa, E., Szabó, A., Bibonne, A., Theveneau, E., Parsons, M., Mayor, R. (2015). Cadherin switch during EMT in neural crest cells leads to contact inhibition of locomotion via repolarization of forces. *Dev. Cell.* 34: 421-434.

Schlosser, G. and Northcutt, R.G. (2000). Development of neurogenic placodes in *Xenopus laevis*. *J. Comp. Neurol*. 418: 121-146.

Schlosser, G. (2005). Evolutionary origins of vertebrate placodes: Insights from developmental studies and from comparisons with other deuterostomes. *J. Exp. Zool. (Mol. Dev. Evol.)*. 304B: 347-399.

Schlosser, G. (2006). Induction and specification of cranial placodes. *Dev. Biol.* 294: 303-351.

Schlosser, G., Awtry, T., Brugmann, S.A., Jensen, E.D., Neilson, K., Ruan, G., Stammler, A., Voelker, D., Yan, B., Zhang, C., Klymkowsky, M.W., Moody, S.A. (2008). Eya1 and Six1 promote neurogenesis in the cranial placodes in a SoxB1-dependent fashion. *Dev. Biol*. 320(1): 199-214.

Schlosser, G. (2014). Development and evolution of vertebrate cranial placodes. *Devel. Biol*. 389: 1.

Schlosser, G., Patthey, C., Shimeld, S.M. (2014). The evolutionary history of vertebrate cranial placodes II. Evolution of ectodermal patterning. *Dev. Biol.* 389: 98-119.

Sechrist, J., Serbedziji, G.N., Scherson, T., Fraser, S.E., Bronner-Fraser, M. (1993). Segmental migration of the hindbrain neural crest does not arise from its segmental generation. *Development.* 118: 691-703.

Sengel, P. (1990). Pattern formation in skin development. *Int. J. Dev. Biol*. 64: 33-50.

Sennett, R. and Rendl, M. (2012). Mesenchymal-epithelial interactions during hair follicle morphogenesis and cycling. *Semin Cell Dev. Biol*. 23(8): 917-927.

Shillito, J. and Matson, D.D. (1968). Craniosynostosis: A review of 519 surgical patients. *Pediatrics*. 41(4): 829-853.

Shinomiya, A., Kayashima, Y., Kinoshita, K., Mizutani, M., Namikawa, T., Matsuda, Y., Akiyama, T. (2012). Gene duplication of endothelin 3 is closely correlated with the hyperpigmentation of the internal organs (*Fibromelanosis*) in Silky chickens. *Genetics.* 190: 627-638.

Sick, S., Reinker, S., Timmer, J., Schlake, T. (2006). WNT and DKK determine hair follicle spacing through a reaction-diffusion mechanism. *Science*. 314: 1447-1450.

Silver, P.H.S. (1960). Special problems of experimenting in ovo on the early chick embryo and a solution. *J. Embryol. exp. Morph.* 8(4): 369-375.

Simard, A., Di Pietro, E., Ryan, A.K. (2005). Gene expression pattern of Claudin-1 during chick embryogenesis. *Gene Exp. Patterns.* 5: 553-560.

Simões-Costa, M.S., McKeown, S.J., Tan-Cabugao, J., Sauka-Spengler, T., and Bronner, M.E. (2012). Dynamic and differential regulation of stem cell factor FoxD3 in the neural crest is encrypted in the genome. *PLoS Genet*. 8(12): e1003142.

Simões-Costa, M. and Bronner, M.E. (2013). Insights into neural crest development and evolution from genomic analysis. *Genome Research*. 23: 1069-1080.

Sinn, R. and Wittbrodt, J. (2013). An eye on eye development. *Mech. Dev.* 130: 347-358.

Slonaker, J.R. (1918). A physiological study of the anatomy of the eye and its accessory parts in the English sparrow (*Passer domesticus*). *J. Morph*. 31: 351-459.

Slonaker, J.R. (1921). The development of the eye and its accessory parts in the English Sparrow (*Passer domesticus*). *J. Morph.* 35: 263-359.

Stergiopoulos, A., Elkouris, M., Politis, P.K. (2015). Prospero-related homeobox 1 (Prox1) at the crossroads of diverse pathways during adult neural fate specification. *Front. Cell Neurosci.* 8: 454.

Steventon, B. and Mayor, R. (2012). Early neural crest induction requires an initial inhibition of Wnt signals. *Dev. Biol.* 265(1): 196-207.

Steventon, B., Mayor, R., Streit, A. (2014). Neural crest and placode interaction during the development of the cranial sensory system. *Dev. Biol.* 389: 28-38.

Stuart, E.S., Garber, B., Moscona, A.A. (1972). An analysis of feather germ formation in the embryo and in vitro, in normal development and in skin treated with hydrocortisone. *J. Exp. Zool*. 179: 97-118.

Stuhlmiller, T.J. and García-Castro, M.I. (2012). Current perspectives of the signaling pathways directing neural crest induction. *Cell. Mol. Life Sci*. 69: 3715-3737.

Suskaweang, S., Lin, C.M., Jaing, T.X., Hughes, M.W., Widelitz, R.B., Chuong, C.M. (2004). Morphogenesis of chicken liver: identification of localized growth zones and the role of beta-catenin/Wnt in size regulation. *Dev. Biol.* 266(1): 109-122.

Suksaweang, S., Jiang, T.-X., Roybal, P., Chuong, C.-M., Widelitz, R. (2012). Roles of EphB3/Ephrin-B1 interactions in feather morphogenesis. *Int. J. Dev. Biol*. 56(9): 719-728.

Sun, Y. and Li, X. (2014). The canonical wnt signal restricts the glycogen synthase kinase 3/fbw7-dependent ubiquitination and degradation of eya1 phosphatase. *Mol. Cell Biol.* 34(13): 2409-2417.

Suzuki, A., Tsuda, M., Saga, Y. (2007). Functional redundancy among Nanos proteins and a distinct role of Nanos2 during male germ cell development. *Development.* 134: 77-83.

Szalai, I., Cuinas, D., Takács, N., Horváth, J., De Kepper, P., (2012). Chemical morphogenesis: recent experimental advances in reaction-diffusion systems design and control. *Interface Focus*. 2: 417-432.

Taher, L., Collette, N.M., Murugesh, D., Maxwell, E., Ovcharenko, I., Loots, G.G. (2011). Global gene expression analysis of murine limb development. *PLoS One*. 6(12): e28358.

Takahashi, K.F., Kiyoshima, T., Kobayashi, I., Xie, M., Yamaza, H., Fujiwara, H., Ookuma, Y., Nagata, K., Wada, H., Sakai, T., Terada, Y., Sakai, H. (2010). Protogenin, a new member of the immunoglobulin superfamily, is implicated in the development of the mouse lower first molar, *BMC Dev. Biol*. 10: 115

Takuma, N., Sheng, H.Z., Furuta, Y., Ward, J.M., Sharma, K., Hogan, B.L., Pfaff, S.L., Westphal, H., Kimura, S., Mahon, K.A. (1998). Formation of Rathke's pouch requires dual induction from the diencephalon. *Development*. 125: 4835-4840.

Talamillo, A., Delgado, I., Nakamura, T., de-Vega, S., Yoshitomi, Y., Unda, F., Birchmeier, W., Yamada, Y., Ros, M.A. (2010). Role of epiprofin, a zinc-finger transcription factor, in limb development. *Dev. Biol*. 337(2): 363-374.

Tan, Y., Cheung, M., Pei, J., Menges, C.W., Godwin, A.K., Testa, J.R. (2010). Up regulation of Dlx5 promotes ovarian cancer cell proliferation by enhancing IRS-2-AKT signaling. *Cancer Res.* 70(22): 9197-9206.

Teddy, J.M. and Kulesa, P.M. (2004). In vivo evidence for short- and long-range cell communication in cranial neural crest cells. *Development.* 131: 6141-6151.

Theveneau, E. and Mayor, R. (2012). Neural crest delamination and migration: From epithelium-to-mesenchyme transition to collective cell migration. *Dev. Biol.* 366: 34-54.

Theveneau, E., Steventon, B., Scarpa, E., Garcia, S., Trepat, X., Streit, A., Mayor, R. (2013). Chase-and-run between adjacent cell populations promotes directional collective migration. *Nat. Cell Biol*. 15: 763-772.

Thorin, E. and Clozel, M. (2010). The cardiovascular physiology and pharmacology of endothelin-1. *Adv. Pharmacol.* 60: 1-26.

Törnqvist, G., Sandberg, A., Hägglund, A.-C., Carlsson, L. (2010). Cyclic expression of Lhx2 regulates hair formation. *PLoS ONE*. 6(4): e1000904.

Trainor, P.A., Sobieszczuk, D., Wilkinson, D., Krumlauf, R. (2002). Signaling between the hindbrain and paraxial tissues dictates neural crest migration pathways. *Development.* 129: 433-442.

Tsai, S.-Y., Sennett, R., Rezza, A., Clavel, C., Grisanti, L., Zemla, R., Najam, S., Rendl, M. (2014). Wnt/β-catenin signaling in dermal condensates is required for hair follicle formation. *Dev. Biol.* 385(2): 179-188.

Tucker, A.S. and Sharpe, P. (2004). The cutting-edge of mammalian development; How the embryo makes teeth. *Nat. Rev. Genet.* 5(7): 499-508.

Tucker, A.S. and Fraser, G.J. (2014). Evolution and developmental diversity of tooth regeneration. *Semin. Cell Dev. Biol.* 25-26: 71-80.

Tyler, M.S. and Hall, B.K. (1977). Epithelial influences on skeletogenesis in the mandible of the embryonic chick. *Anat. Rec*. 188: 229-240.

Tyler, M.S. and McCobb, D.P. (1980). The genesis of membrane bone in the embryonic chick mandible: epithelial-mesenchymal tissue recombination studies. *J. Embryol. exp. Morph.* 56: 269-281.

Tyler, M.S. and McCobb, D.P. (1981). Tissue interactions promoting osteogenesis in the embryonic chick palate. *Archs. Oral Biol.* 26(7): 585-590.

Ulsamer, A., Ortuno, M.J., Ruiz, S., Susperregui, A.R.G., Osses, N., Rosa, J.L., Ventura, F. (2008). BMP-2 induces osterix expression through up-regulation of Dlx5 and its phosphorylation by p38. *J. Biol. Chem.* 283(7): 3816-3826.

Van de Kamp, M. and Hilfer, S.R. (1985). Cell proliferation in condensing scleral ectomesenchyme associated with the conjunctival papillae in the chick embryo. *J. Embryol. Exp. Morph.* 88: 25-37.

Vanderas, A.P. (1987). Incidence of cleft lip, cleft palate, and cleft lip and palate among races: a review. *Cleft Palate J.* 24(3): 216-225.

van Eyll, J.M., Pierreux, C.E., Lemaigre, F.P., Rousseau, G.G. (2004). Shh-dependent differentiation of intestinal tissue from embryonic pancreas by activin A. *J. Cell. Sci.* 117(Pt 10): 2077-2086.

Vergara, M.N. and Canto-Soler, M.V. (2012). Rediscovering the chick embryo as a model to study retinal development. *Neural Devel.* 7: 22.

Verma, A.S. and FitzPatrick, D.R. (2007). Anopthalmia and micropthalmia. *Orphanet. J. Rare Dis.* 2: 47.

Vernon, A.E. and LaBonne, C. (2006). Slug stability is dynamically regulated during neural crest development by the f-box protein ppa. *Dev.* 133: 3359-3370.

Viera, A.R., D'Souza, R.N., Mues, G., Deeley, K., Hsin, H.-S., Küchler, E.C., Meira, R., Patir, A., Tannure, P.N., Lips, A., Costa, M.C., Granjeiro, J.M., Seymen, F., Modesto, A. (2013). Candidate gene studies in hypodontia suggest role for FGF3. *Eur. Arch. Paediatr. Dent.* 14(6): doi:10.1007/s40368-013-0010-2.

Vieux-Rochas, M., Bouhali, K., Mantero, S., Garaffo, G., Provero, P., Astigiano, S., Barbieri, O., Caratozzolo, M.F., Tullo, A., Guerrini, L., Lallemand, Y., Robert, B., Levi, G., Merlo, G.R. (2013). BMP-mediated functional cooperation between *Dlx5;Dlx6* and *Msx1;Msx2* during mammalian limb development. *PLoS ONE*. 8(1): e51700.

Walls, G.L. (1942). The vertebrate eye and its adaptive radiation (Bulletin No. 19). Michigan: Cranbook Institute of Science. 785 p.

Wang, Y., Kowalski, P.E., Thalmann, I., Ornitz, D.M., Mager, D.L., Thalmann, R. (1998). Otoconin-90, the mammalian otoconial matrix protein, contains two domains of homology to secretory phospholipase A_2. *Proc. Natl. Acad. Sci. USA*. 95: 15345-15350.

Wang, W.-D., Melville, D.B., Montero-Balaguer, M., Hatzopoulos, A.K., Knapik, E.W. (2011). Tfap2a and foxd3 regulate early steps in the development of the neural crest progenitor population. *Dev Biol*. 360(1): 173-185.

Welch, A.K., Jacobs, M.E., Wingo, C.S., Cain, B.D. (2011). Early progress in epigenetic regulation of endothelin pathway genes. *Br. J. Pharmacol.* 168: 327-334.

Wells, K.L., Hadad, Y., Ben-Avraham, D., Hillel, J., Cahaner, A., Headon, D.J. (2012). Genome-wide SNP scan of pooled DNA reveals nonsense mutation in FGF20 in the scaleless line of featherless chickens. *BMC Genomics*. 13: 257.

White, P.M., Stone, J.S., Groves, A.K., Segil, N. (2012). EGFR signaling is required for regenerative proliferation in the cochlea: Conservation in birds and mammals. *Dev. Biol.* 363(1): 191-200.

Whitlock, K.E. (2008). Developing a sense of scents: Plasticity in olfactory placode formation. *Brain Res. Bull.* 75(2-4): 340-347.

Widelitz, R.B. (2008). Wnt signaling in skin organogenesis. *Organogenesis*. 4(2): 123-133.

Wilkie, A.O.M. (1997). Craniosynostosis: Genes and Mechanisms. *Hum. Mol. Gen.* 6(10): 1647-1656.

Wolpert, L. (1998). Pattern formation in epithelial development: the vertebrate limb and feather bud spacing. *Phil. Trans. R. Soc. Lond. B*. 353: 871-875.

Woo, W.-M., Zhen, H.H., Oro, A.E. (2012). Shh maintains dermal papilla identity and hair morphogenesis via a Noggin-Shh regulatory loop. *Genes Dev.* 26: 1235-1246.

Wu, M.Y., Ramel, M.-C., Howell, M., and Hill, C.S. (2011). SNW1 is a critical regulator of spatial BMP activity, neural plate border formation, and neural crest specification in vertebrate embryos. *PLoS Biol*. 9(2): e1000593.

Xu, Q., Mellitzer, G., Wilkinson, D.G. (2000). Roles of Eph receptors and ephrins in segmental patterning. *Phil. Trans. R. Soc. Lond.* 355: 993-1002.

Xu, J. and Testa, J.R. (2009). DLX5 (distal-less homeobox 5) promotes tumor cell proliferation by transcriptionally regulating MYC-. *J. Biol. Chem.* 284(31): 20593-20601.

Xu, Y., Zhang, H., Yang, H., Zhao, X., Lovas, S., Lundberg, Y.W. (2010). Expression, functional and structural analysis of proteins critical for otoconia development. *Dev. Dyn.* 239(10): 2659-2673.

Yang, H., Zhao, X., Xu, Y., Wang, L., He, Q., Lundberg, Y.W. (2011). Matrix recruitment and calcium sequestration for spatial specific otoconia development. *PLoS ONE.* 6(5): e20498.

Yoo, J., Kang, J., Lee, H.N., Aguilar, B., Kafka, D., Lee, S., Choi, I., Lee, J., Ramu, S., Haas, J., Koh, C.J., Hong, Y.-K. (2010). Kaposin-B enhances the PROX1 mRNA stability during lymphatic reprogramming of vascular endothelial cells by Kaposi's sarcoma herpes virus. *PLoS Pathog.* 6(8): e1001046.

Yue, Z., Jiang, T.X., Wu, P., Widelitz, R.B., Chuong, C.-M. (2012). Sprouty/FGF signaling regulates the proximal-distal feather morphology and the size of dermal papillae. *Dev. Biol*. 372(1): 45-54.

Zeller, R., López-Ríos, J., Zuniga, A. (2009). Vertebrate limb bud development: moving towards integrative analysis of organogenesis. *Nat. Rev. Genet.* 10: 845-858.

Zhang, J., Zhu, J., Valverde, P., Li, L. Pageau, S., Tu, Q., Nishimura, R., Yoneda, T., Yang, P., Zheng, W., Ma, W., Chen, J. (2008). Phenotypic analysis of Dlx5 overexpression in post-natal bone. *J. Dent. Res.* 87(1): 45-50.

Zhang, Y., Tomann, P., Andl, T., Gallant, N.M., Huelsken, J., Jerchow, B., Birchmeier, W., Paus, R., Piccolo, S., Mikkola, M.L., Morrisey, E.E., Overbeek, P.A., Schneidereit, C., Millar, S.E., Schmidt-Ullrich, R. (2009). Reciprocal requirements for Eda/Edar/NF-κB and Wnt/β-catenin signaling pathways in hair follicle induction. *Dev. Cell.* 17(1): 49-61.

Zhao, X., Yang, H., Yamoah, E.N., Lundberg, Y.W. (2007). Gene targeting reveals the role of Oc90 as the essential organizer of the otoconial organic matrix. *Dev. Biol.* 304(2): 508-524.

Zhao, X., Jones, S.M., Thoreson, W.B., Lundberg, Y.W. (2008a). Osteopontin is not critical for otoconia formation or balance function. *JARO.* 9: 191-201.

Zhao, X., Jones, S.M., Yamoah, E.N., Lundberg, Y.W. (2008b). Otoconin-90 deletion leads to imbalance but normal hearing: A comparison with other Otoconia mutans. *Neurosci*. 153(1): 289-299.

Zhou, J., Gao, Y., Zhang, Z., Zhang, Y., Maltby, K.M., Liu, Z., Lan, Y., Jiang, R. (2011). Osr2 acts downstream of Pax9 and interacts with both Msx1 and PAx9 to pattern the tooth developmental field. *Dev. Biol*. 353(2): 344-353.

Zhu, H. and Bendall, A.J. (2009). Dlx5 is a cell autonomous regulator of chondrocyte hypertrophy in mice and functionally substitutes for Dlx6 during endochondral ossification. *PLoS ONE.* 4(11): e8097.

Zhu, J., Zhang, Y.-T., Alber, M.S., Newman, S.A. (2010). Bare bones pattern formation: A core regulatory network in varying geometries reproduces major features of vertebrate limb development and evolution. *PLoS ONE*. 5(5): e10892.

Zhu, W., Pao, G.M., Satoh, A., Cummings, G., Monaghan, J.R., Harkins, T.T., Bryant, S.V., Voss, S.R., Gardiner, D.M., Hunter, T. (2012). Activation of germline-specific genes is required for limb regeneration in the Mexican axolotl. *Dev. Biol.* 370(1): 42-51.

Zhu, X., Ozturk, F., Pandey, S., Guda, C., Nawshad, A. (2012). Implications of TGFβ on transcriptome and cellular biofunctions of palatal mesenchyme. *Front. Physiol.* 3: 85.

Zou, D., Silvius, D., Fritzsch, B., Xu, P.-X. (2004). Eya1 and Six1 are essential for early steps of sensory neurogenesis in mammalian cranial placodes. *Development*. 131(22).

Zou, D., Silvius, D., Rodrigo-Blomqvist, S., Enerbäck, S., Xu, P.-X. (2006). Eya1 regulates the growth of otic epithelium and interacts with Pax2 during the development of all sensory areas in the inner ear. *Dev. Biol.* 298(2): doi:10.1016/j.ydbio.2006.06.049.

Zou, D., Erickson, C., Kim, E.-H., Jin, D., Fritzsch, B., Xu, P.-X. (2008). Eya1 gene dosage critically affects the development of sensory epithelia in the mammalian inner ear. *Hum. Mol. Genet.* 17(21): 3340-3356.

Zou, W., Chen, X., Shim, J., Huang, Z., Brady, N., Hu, D., Drapp, R., Sigrist, K., Glimcher, L.H., Jones, D. (2011). The E3 ubiquitin ligase Wwp2 regulates craniofacial development through monoubiquitination of Goosecoid. *Nat. Cell Biol.* 13(1): 59-65.

Appendix 1: Protocols

3% Neutral Red (stock)

- Add 0.3 g neutral red (Sigma-Aldrich, N7005) to 10 ml dH_2O
- Separate into 1 ml aliquots
- Store at 4°C

0.3% Neutral Red (working solution)

- Add 1 ml neutral red stock to 10 ml of dH_2O

10% Nile Blue Phosphate

- Add 0.1 g of nile blue phosphate (Sigma-Aldrich, N5632) to 10 ml of dH_2O
- Add 0.25 g of agarose (Fisher Scientific, 9012-36-6) to the nile blue phosphate solution
- Heat with stirring until dissolved (do not boil)
- Pour into a small petri dish and allow to cool but not completely set
- Dip blunted needles (below) into this solution and allow to set
- Store solution, wrapped with parafilm at 4°C
- To re-use, remove from petri dish and melt in a beaker before repeating above steps

1N NaOH (1 L)

- Add 40 g of sodium hydroxide (NaOH; Sigma-Aldrich, S5881) to 1 L of dH_2O
- Stir until dissolved at low heat

0.85% Chick Saline (1 L)

- Add 8.5 g sodium chloride (NaCl, EMD; SX0420-3) to 1 L of dH_2O
- Stir until dissolved

70% EtOH (500 ml)

- 375 ml 100% ethanol (EtOH; Central Stores, Dalhousie, N.S., Canada)
- 125 ml dH_2O

50% EtOH (500 ml)

- 250 ml 100% EtOH
- 250 ml dH_2O

25% EtOH (500 ml)

- 125 ml 100% EtOH
- 375 ml dH_2O

1X Phosphate Buffered Saline (PBS) pH 7.4 (1 L)

- To a 1000 ml beaker, add:
    - 8 g NaCl
    - 0.2 g potassium chloride (KCl; MP Biomedicals LLC, 191427)
    - 1.15 g sodium phosphate, dibasic (Na_2HPO_4; EMD, SX0720-1)

    - 0.2 g monopotassium phosphate (KH_2PO_4; Simga-Aldrich, P0662)
- Add 800 ml of dH_2O to the beaker
- Stir until dissolved
- pH to 7.4
- Top up to 1 L with dH_2O

4% Paraformaldehyde (PFA) pH 7.4 (500 ml)
- Add 20 g paraformaldehyde (Simga-Aldrich, P6148) to 400 ml of 1X PBS
- Stir with heat (covered with foil) until the PFA is completely mixed into the solution
- When completely stirred in, add NaOH pellets one at a time until the solution goes clear
- Allow to cool
- pH to 7.4
- Top up to 500 ml with 1X PBS
- Divide into 30 ml aliquots and store at -20°C

1M Tris-HCl (100 ml)
- Add 12.1 g trisma (Fluka, 93362) to 70 ml dH_2O
- pH to 8.0 with hydrochloric acid (HCl; Sigma-Aldrich, 258148)
- Top up to 100 ml

0.5M EDTA (100 ml)
- Add 18.6g ethylenediaminetetraacetic acid (EDTA; Simga-Aldrich, E5134) to 70 ml dH_2O
- pH to 8.0 with NaOH

TE Buffer (100 ml)
- To a 200 ml beaker, add:
    - 1 ml of 1M Tris-HCl
    - 0.2 ml of 0.5M EDTA
    - 80 ml of dH_2O
- pH to 8.0
- Top up to 100 ml with dH_2O

5X Tris-Borate-EDTA (TBE) Buffer (500 ml)
- To a 600 ml beaker, add:
    - 27 g trisma
    - 13.75 g boric acid (Sigma-Aldrich, B7901)
    - 0.37 g EDTA
- Add 400 ml of dH_2O
- Heat until dissolved
- Top up to 500 ml with dH_2O

1X TBE (500 ml)

- 50 ml of 1X TBE
- 450 ml dH_2O

1% Agarose Gel (60 ml)

- Add 0.6 g agarose to an Erlenmeyer flask
- Add 60 ml 1X TBE
- Microwave for 3 x 20 seconds at highest temperature, swirling in between
- Microwave for 1 x 10 seconds
- Once cooled enough to touch, add 3 µl of gel red (Biotium, 41003)
- Pour into casting tray with combs

Making Blunted Needles

- Set up a Bunsen burner and set flame so that it is mostly blue
- Place the center of the Pasteur pipet tip (VWR, 14673-010) into the flame
- When the center is heated and has become malleable, remove from heat and pull
- Cut the pulled pipet close to the base of the pipet using a diamond scorer
- Place the cut tip back into the flame and allow to melt
- Remove from heat and tap against hard surface to form a rounded tip
- Allow to cool

Making Fine Tungsten Needles

- Begin as described for the blunted needles above
- After the pipets have been pulled, cut with the diamond scorer further away from the base of the pipet
- Insert a piece of tungsten wire into the cut opening of the pipet
- Return pipet to the flame and heat until the glass melts around the wire
- Remove from flame and allow to cool

Sharpening Tungsten Needles

- Pour 500 ml of 1N NaOH into a plastic beaker
- Place an opened paper clip over the lip of the beaker and attach the red electrode
- Once set up, turn on the transformer
    - If sharpening fine needles, use a low current
    - If sharpening coarse needles, use a high current
- Place tip of needle into the 1N NaOH and touch the needle with the black electrode
- As long as it is touching the wire, it will be oxidizing (and removing) metal beneath the surface of the solution
- Check the sharpness of the wire under the scope

Alkaline Phosphatase Protocol (in glass vials)

- Rehydrate embryos from 70% EtOH
    - 1 hour in 50% EtOH

    - 1 hour in 25% EtOH
- 3 x 15 minute washes in dH_2O
- 1 hour in tris-maleate buffer (pH 8.3) at room temperature
    - Make AP-substrate solution here
- 1 hour in AP substrate solution at room temperature
- 3 x 15 minutes in saturated sodium borate water
    - Make bleach solution here
- Bleach overnight using 3% bleach solution
- In the morning, process embryos to 80% glycerol (BDH, BDH1172-4LP)
    - 1 hour in 25% glycerol
    - 1 hour in 50% glycerol
    - 1 hour in 80% glycerol

Alkaline Phosphatase Solutions

Tris-Maleate Buffer (25 ml)

- 0.605 g Tris base
- 0.55 g maleic acid (Fisher-Scientific, 03417)
- pH to 8.3 using NaOH
- Top up to 25 ml with dH_2O

1% KOH (100 ml)

- 1 g KOH (Sigma-Aldrich, 221473)
- 100 ml dH_2O

Saturated Sodium Borate Water (100 ml)

- 5 g sodium tetraborate decahydrate (Sigma-Aldrich, B9876)
- 100 ml dH_2O

25% Glycerol (25 ml)

- 6.25 ml glycerol
- 18.75 ml 100% EtOH

50% Glycerol (25 ml)

- 12.5 ml glycerol
- 12.5 ml 100% EtOH

80% Glycerol (25 ml)

- 20 ml glycerol
- 5 ml 100% EtOH

AP Substrate Solution

- 0.01 g napthol AS-TR phosphate disodium salt (Sigma-Aldrich, N6125)
- 1 ml DMF (Sigma-Aldrich, 319937)
- 10 ml tris-maleate buffer

- 0.008 g fast blue B salt (Sigma-Aldrich, D9805)

3% Bleach Solution (20 ml)

- 2 ml 3% H_2O_2 (from local store)
- 18 ml 1% KOH

Cryosectioning Protocol

Embedding for Cryosectioning

- Make 1% agar solution as follows:
  - 0.1g agar (Sigma-Aldrich, A7002)
  - 10 ml dH_2O
  - Stir with heat until clear
- Pour agar into a small petri dish and allow to cool for 1-2 minutes
- Carefully dry specimen with a KimWipe and place in agar
- Fix orientation under microscope
- Place in fridge for 30 minutes to cool (4°C)
- Make 30% sucrose solution as follows:
  - 6g sucrose (Sigma-Aldrich, 179949)
  - 20 ml dH_2O
- Cut a large block from the agar containing the sample
- Place in 30% sucrose solution and leave at 4°C until blocks have sunk

Cryosectioning

- Once blocks have sunk, pour block and sucrose solution into a petri dish
- Determine orientation under the microscope
- Dry the block with a KimWipe
- Mount the block on the chuck using a small amount of Tissue Freezing Medium (Jung, 020108926)
- Put block (mounted on the chuck) into the cryostat and freeze
- Cut sections at -25°C at either 16 μm or 25 μm thickness
- Once cut, put sections onto APTES coated slides

APTES Coated Slides

- Rack slides
- Wash in 100% EtOH
- Wash in dH_2O
- Dry overnight at 38°C
- The next day, remove from oven and allow to cool
- Dip in 2% 3-aminopropylthioethoxy saline in acetone:
  - 6 ml 3-aminopropylthioethoxy saline (APTES; Sigma-Aldrich, A3648)
  - 294 ml acetone (Fisher Scientific, A18-4)
- Dip in acetone
- Dip in acetone
- Dip in dH_2O

- Dry overnight at 38°C
- Store in slide box until use

Primer Design

- Obtain the mRNA sequence from the NCBI website using the RefSeq Transcript ID provided with the microarray data
- Load the mRNA sequence in Serial Cloner 2.1 (http://serialbasics.free.fr/Serial_Cloner.html)
- Determine correct reading frame and coding region
- Upload target coding region in Primer3 (bioinfo.ut.ee/primer3-0.4.0)
- Use General Primer Picking Conditions with slight modification:
  - Size: 18 to 22 bp
  - Optimal melting temperature (TM): 60°C
  - GC content: 45-60%
- Compare generated primer pairs to genome using a Basic Local Alignment Search Tool (BLAST) (blast.ncbi.nln.gov/Blast.cgi) to confirm that primer specified target gene sequence is 100% specific to gene of interest
- Target gene sequence should fall between approximately 200 to 500 bp
- Order primer sequences from Integrated DNA Technologies (IDT)

RNA Extraction Protocol

Several reagents are from the RNeasy Microarray Tissue Mini Kit (Qiagen, 73304)
Before starting:

- Create RNA free benchtop by washing with 70% EtOH and then spraying RNaseZap on counters
- Turn on centrifuge to 4°C
- Take out Chloroform and set up station in fume hood
- Take tubes out of the -80°C and put on ice
- Make 70% EtOH with DepC water
- Prewarm Dispase II in Hank's balanced salt solution to 37°C

Protocol:

- Excise the tissue sample from the animal
- Place in an Eppendorf tube in autoclaved chick saline on ice
- Rinse the tissue in autoclaved chick saline on ice
- Place the tissue in the biomasher and disrupt tissue using the biomasher (VWR, 82031-456)
- Add 150 µl lysate buffer, homogenize, and then add another 3 x 150 µl then spin at 10, 000 xg for 30 seconds
- Place tube containing the homogenate on the benchtop at room temperature for 5 minutes
- Add 200 µl chloroform. Securely cap the tube containing the homogenate and shake vigorously for 15 seconds
- Place the tube on the benchtop at room temperature for 2-3 minutes
- Centrifuge at 12, 000 xg for 15 minutes at 4°C

- Transfer 80% of upper aqueous phase to a new tube (from unlabeled bag). Add 1 volume of 70% EtOH (RNase-free). Mix thoroughly by pipetting up and down. Do not centrifuge. Proceed immediately to the next step.
- Transfer up to 700 µl of the sample to an RNeasy mini-spin column in a 2 ml collection tube. Close lid gently. Centrifuge for 5 seconds at 11, 000 xg at room temperature. Discard flow-through.
- Repeat above step using the remainder of the sample
- Using same collection tube, add 700 µl Buffer RW1. Close lid and centrifuge for 15 seconds at 11, 000 xg. Discard flow-though.
- Add 500 µl Buffer RPE. Centrifuge for 15 seconds at 11, 000 xg. Discard flow-through.
- Reconnect tube to the same spin column and add 500 µl Buffer RPE. Centrifuge for 2 minutes at 11, 000 xg.
- Place collection column into a new collection tube.
- Centrifuge at 13, 000 xg for 1 minute
- Place in a 1.5 ml collection tube and add 30 µl RNase-free water directly to the membrane
- Centrifuge 1 minute at 13, 000 xg
- Repeat step 20

SuperScript III First-Strand cDNA Synthesis Protocol (Invitrogen, 18080-051)

- Mix and briefly centrifuge each component before use
- Combine the following in each 0.2 ml tube:
  - 5 µl 0.65 µg RNA
  - 1 µl 50 µM Oligo$(DT)_{20}$
  - 1 µl 10 mM dNTP mix
  - 3 µl DepC H_2O
- Incubate at 65°C for 5 minutes
- Place on ice for at least 1 minute
- Prepare the following cDNA synthesis mix, adding each component as indicated:
  - 2 µl 10X RT Buffer
  - 4 µl 25 mM $MgCl_2$
  - 2 µl 0.1 M DTT
  - 1 µl RNase OUT
  - 1 µl SuperScript III
- Add 10 µl cDNA mix to each RNA mixture, mix gently, and collect by brief centrifugation
- Incubate for 50 minutes at 50°C
- Terminate the reaction at 85°C for 5 minutes
- Chill on ice
- Collect reactions by brief centrifugation
- Add 1 µl RNase H to each tube
- Incubate for 20 minutes at 37°C
- Once incubated, proceed directly to PCR purification

High Pure PCR Purification Kit Protocol (Roche, 11 732 668 001)

- After PCR is complete, adjust total column for each PCR tube (reaction components and DNA products) to 100 µl
- Add 500 µl Binding Buffer to each 100 µl PCR tube and mix well
- Insert one High Pure Filter Tube into one Collection Tube
- Transfer the sample from above steps using a pipette to the upper reservoir of the filter tube
- Centrifuge 30-60 seconds at 13,000 xg in a standard table top centrifuge at +15°C to +25°C
- Disconnect the filter tube and discard the flow-through solution
- Reconnect the filter tube to the same collection tube
- Add 500 µl Wash Buffer to the upper reservoir
- Centrifuge 1 minute at 13,000 xg (as above)
- Discard the flow-through solution
- Recombine the filter tube with the same collection tube
- Add 200 µl Wash Buffer
- Centrifuge 1 minute at 13,000 xg (as above)
- Discard the flow-through solution and collection tube
- Reconnect the filter tube to a clean 1.5 ml micro-centrifuge tube
- Add 50-100 µl Elution Buffer to the upper reservoir of the filter tube
- Centrifuge 1 minute at 13,000 xg
- Repeat above two steps
- Store at -20°C

Polymerase Chain Reaction Protocol

- Create a master mix containing: (per sample)
    - 34.75 µl DepC H_2O
    - 10 µl crimson taq buffer
    - 1 µl dNTP
    - 0.25 µl crimson taq polymerase
- Separate into separate tubes for each gene. Add: (per sample)
    - 1 µl forward primer
    - 1 µl reverse primer
- Separate each gene's tube by desired stage. Add: (per sample)
    - 2 µl DNA
- Mix and briefly centrifuge
- Incubate according to the cycling conditions below:
    - 95°C 30 seconds
    - 95°C 20 second
    - *** 30 seconds (gene specific, listed below)
    - 68°C 1 minute
    - Repeat above three temperature cycles 40 times
    - 68°C 5 minutes
    - 4°C hold

Annealing Temperatures for Original Primers

Prox1: 54.1°C
Oc90: 55.7°C
Ednrb: 56.3°C
Inhba: 55.0°C
Dlx5: 55.7°C
Gsc: 55.7°C
Eya1: 54.1°C

Annealing Temperatures for T3 and T7 Primers

Prox1: 64.2°C
Oc90: 64.8°C
Ednrb: 65.2°C
Inhba: 65.2°C
Dlx5: 64.5°C
Gsc: 65.4°C
Eya1: 64.5°C

Gene Sequencing (with permission, January 22, 2015)
This protocol is from Dr. Timothy Frasier's Lab at Saint Mary's University, Halifax, Canada.

Frasier Lab Protocols
Sequencing
Last Updated: January 9, 2015

- For sequencing, you want to aim for ~5 ng of DNA per 100 bp of sequence. Therefore, if you are sequence a 500 bp fragment, you will need ~25 ng of DNA.
- The total volume of a sequencing reaction can be up to 9.5 µl

Cleaning the PCR Product: ExoSAP

- Clean only the volume of PCR intended for sequencing
- Ensure that the volume of all samples is standardize using water so that they all contain the same amount of DNA in the same volume
- The sample calculations below are for a sample volume of 5 µl

Reagent	Volume to Add Per µl	For 5 µl of sample
Antarctic Phosphatase Buffer	0.129 µl	0.65 µl
Antarctic Phosphatase	0.02 µl	0.1 µl
Exonuclease I	0.00614 µl	0.03 µl

- Samples should be prepared as for a normal PCR cocktail (i.e. using a master mix, where the total volumes required of all reagents for the total number of samples are mixed together and then an appropriate volume is aliquoted for each sample)
- Below is a sample calculation for 10 samples, each of 5 µl
    - 10 samples + 1 negative control + 1 positive control + 3 extra = 15 reactions

Reagent	Volume to Add Per µl	Total Volume
Antarctic Phosphatase Buffer	0.65 µl	9.75 µl
Antarctic Phosphatase	0.1 µl	1.5 µl
Exonuclease I	0.03 µl	0.45 µl
		11.7 µl

- Create master mix for target number of samples, including positive and negative controls as well as extra reactions in case of error
- Mix thoroughly
- Add appropriate amount of cocktail to each sample
- Run PCR using program EXOSAP
    - 15 minutes at 37ºC
    - 15 minutes at 80ºC
    - Hold at 10ºC for at least 2 minutes

Sequencing Reaction

- The required volume for sequencing is 15 µl
- For sequencing, you should prepare an aliquot of the primer you want to sequence (concentration: 5 µM) and then use 1 µl of that primer for each sample
- Sample calculations given below:

Reagent	Stock concentration	Desired concentration	Volume to Add
Reaction Mix	2.5X	0.25X	22.5 µl
Sequencing Buffer	5X	1X	45 µl
Primer	5 µM	1 µl/rxn	15 µl
DNA		5.78 µl/rxn	86.7 µl
Water		To 225 µl	55.8 µl
			225 µl

- Mix cocktail thoroughly
- Add the appropriate amount of cocktail to each sample.
- Run PCR using the program Sequencing
    - 2 minutes at 96ºC
    - 20 seconds at 96ºC
    - 20 seconds at 50ºC
    - 4 minutes at 60ºC
    - Hold at 4ºC
    - Conduct steps 2-4 for 30 cycles before moving to step 5

Ethanol Precipitation

(Based on a 15 µl sequencing reaction)

- All 10% of the PCR volume (1.5 µl) of 7.5 M ammonium acetate to each sample, for a final concentration of 0.68 M
- Add 46.2 µl of 95% ethanol to each sample for a final concentration of 70%
- Pipette up and down twice to mix
- Seal the plate

- Spin plate for 35 minutes at 2,550 x g
- Decant the ethanol by dumping the ethanol into the sink gently
- Tap plate gently on two KimWipes placed on the lab bench
- Tape two KimWipes to the top of the plate and spin, inverted, up to 300 rpm
- Remove the KimWipes and add 100 µl of 70% ethanol to each sample and pipette up and down twice to mix
- Seal the plate and spin at maximum speed (4,500 x g) for 2 minutes
- Decant the ethanol by dumping the ethanol into the sink gently, then tap the plate gently on two KimWipes placed on the lab bench
- Tape two KimWipes to the top of the plate and spin, inverted, up to 300 rpm.
- Resuspend DNA in 10 µl HiDi formamide.
- Also add 10 µl of formamide to any wells in your injection that will be empty (injections are 24 samples each, 3 columns)
- Label the plate with the next run number (found in the ABI book) and place in the amplified section of the freezer
- Enter a plate map into the ABI computer and save (this can be done by opening the "**3500 Data Collection Software – Enter plate information** [then enter preliminary information] – **Assign plate contents** [enter plate contents] – **Save plate**).
- Write a plate run number in ABI logbook to indicate plate is ready to be run

Ethanol Precipitation of DNA Protocol

- Measure the volume of the DNA sample
- Add 1/5 volume of sodium acetate, pH 5.2
- Mix well
- Place on ice or at -20°C for over 20 minutes
- Spin at maximum speed for 10-15 minutes
- Carefully decant supernatant
- Add 1 ml of 70% EtOH (DepC).
- Mix and spin briefly.
- Carefully decant supernatant
- Air dry or briefly vacuum dry pellet
- Resuspend pellet in appropriate volume of TE or DepC H_2O

3M Sodium Acetate (50 ml)

- 12.3045 g sodium acetate (Sigma-Aldrich, S2889)
- pH to 5.2
- Top up to 50 ml with DepC H_2O

Purification of DNA Fragments from an Agarose Gel Protocol (Roche, 11 732 668 001)

- Isolate DNA band of interest electrophoretically as follows:
  - Load PCR reaction mixture on a 0.8-2% agarose gel
  - Use 1X TBE as running buffer
  - Electrophorese until DNA band of interest is isolated from adjacent contaminating fragments

- Identify bands by staining gel with gel red
- Cut desired DNA band from gel using an ethanol-cleaned scalpel or razor blade
- Place excised agarose gel-slice in a sterile 1.5 ml micro-centrifuge tube
    - Determine gel mass by first pre-weighting the tube and then re-weight the tube with excised gel slice
- Add 300 µl Binding Buffer for every 100 mg agarose gel slice
- Dissolve the agarose gel slice in order to release the DNA
    - Vortex the micro-centrifuge tube for 15-30 seconds to resuspend the gel slice in the Binding Buffer
    - Incubate the suspension for 10 minutes at 56°C
    - Vortex the tube briefly every 2-3 minutes during the incubation
- After the agarose gel slice is completely dissolved:
    - Add 150 µl isopropanol for every 100 mg agarose gel slice to the tube
    - Vortex thoroughly
- Insert one High Pure Filter Tube into one collection tube
    - Pipette the entire contents of the micro-centrifuge tube into the upper reservoir of the filter tube
        - Do not exceed 700 µl total volume – if mixture is greater than 700 µl, split the volume into two separate tubes
- Centrifuge 30-60 seconds at 13,000 xg in a standard tabletop centrifuge at room temperature
- Discard the flow-through solution and then reconnect the filter tube with the same collection tube
- Add 500 µl Washing Buffer to the upper reservoir
    - Centrifuge 1 minute at 13,000 xg
- Discard the flow-through solution. Reconnect the filter tube with the same collection tube
    - Add 200 µl Washing Buffer
    - Centrifuge 1 minute at 13,000 xg
        - This second 200 µl wash step ensures optimal purity and complete removal of wash buffer from the glass fibers
- Discard the flow-through solution and collection tube
    - Recombine filter tube with a clean 1.5 ml collection tube
- Add 50-100 µl Elution Buffer to the upper reservoir of the filter tube
    - Centrifuge 1 minute at maximum speed
    - Added 100 µl Elution Buffer
- Micro-centrifuge tube now contains the purified DNA

Removing a Plasmid from Filter Paper Protocol

- Cut out the part of the filter with the plasmid
- Place in a 1.5 ml Eppendorf tube
- Add 100 µl of TE buffer
- Allow tube to sit for 5 minutes at room temperature
- Vortex the tube and centrifuge at 3,000 rpm for 1 minute
- Allow tube to sit for 30 minutes at room temperature

- Remove filter and place it in a separate tube
- Store both tubes at -20°C

Cloning Protocol

Day 1

Preparing agar plates and LB broth

- Make 3 plates/gene – 2 experimental and 1 control
- Agar plates and LB broth must be prepared prior to starting the cloning process. Once plates/broth have been made, store at 4°C

LB Broth (100 ml)

- 2.5 g Difco LB broth, Miller (BD, 244620)
- 100 ml dH_2O
- Autoclave (covered with foil)

Agar Plates (6 plates)

- 6.25 g Difco LB broth
- 250 ml dH_2O
- 3.75 g Difco agar (BD, 214530)
- Heat and stir until dissolved, covered with foil
- Autoclave
- Allow to come to room temperature
- Add 0.025 g ampicillin trihydrate (Sigma-Aldrich, A6140)
- Pour solution into plates and allow to cool
- Parafilm and store upside down at 4°C

At this time, autoclave glass Nalgene tubes at this time (needed 4, autoclaved 6) – cover with tin foil and lay in autoclave tray.

Day 2

- Before beginning:
  - Put plates in 37°C incubator
  - Chill tips (200 µl and 1 ml) and Nalgene tubes by placing them in a ziplock bag on ice
  - Set water bath to 42°C
- Remove HB101 competent *E.Coli* cells (Promega, L2011) from the -80°C freezer and place on ice until just thawed (~5 minutes)
- Gently mix the thawed cells then pipette (using chilled tips) 100 µl of bacteria into each chilled Nalgene tube
- Add either 1 µl concentrated stock DNA or 10 µl filter stock DNA to each tube
- For the control samples, add 10 µl TE buffer instead of DNA
- Heat shock tubes for 45-50 seconds in 42°C in water bath
- Put tubes on ice for 2 minutes

- Add 900 µl LB broth (cold, chilled tips) to each tube. Incubate for 60 minutes at 37°C with shaking (145-185 rpm).
    - At this time, make sure the plates are in the incubator (upside down) to warm up
- For each gene, set up two experimental plates and 1 control as follows:
    - Experimental Plate 1: dispense 100 µl of DNA transfected cells onto the plate and spread using a bent pipet.
    - Experimental Plate 2: dispense 10 µl of DNA transfected cells onto the plate and spread using a bent pipet.
    - Control Plate: dispense 100 µl of TE transfected cells onto the plate and spread using a bent pipet.
- Incubate overnight at 37°C overnight.

Day 3

- Place LB broth into the incubator at 37°C to warm up
- Pour 20 ml of LB broth into an autoclave Nalgene tube after flaming the lip of the Nalgene tube and the lip of the broth container
- Remove one colony from each plate using an autoclaved tip and dropped it into the broth
- Incubate overnight at 37°C with shaking at 145 rpm

Day 4

- Proceed to mini-prep protocol

Mini-Prep Protocol

- Take 2 ml from each overnight culture and place it in a 2 ml Eppendorf tube
- Spin at 13,000 rpm for 1 minute
    - Repeat above steps twice to increase the pellet size
    - Store overnight cultures in the fridge for the short term or in glycerol for the long term
- Pour off supernatant and keep the pellet
- Combine:
    - 0.82 µl RNase A (ribonuclease A – Sigma Aldrich, R4642)
    - 250 µl cold buffer
- Add the cold buffer and RNase A to the pellet and re-suspend by dragging the tube over a rack 5-10 times
- Add 250 µl cold fresh lysis solution and mix by inverting 3 times and let sit on ice for 5 minutes
- Add 250 µl cold potassium acetate solution and mix by inverting 3 times (solution will go cloudy)
- Place on ice for 5 minutes
- Centrifuge at 13, 000 rpm for 5 minutes.
- Pour supernatant into a new tube and keep it – discard the previous tube

- In the fume hood, add 200 µl phenol-chloroform (take bottom layer) and shake for 30 seconds (phenol; Sigma-Aldrich, P4682; chloroform, Sigma-Aldrich, 288306)
- Centrifuge at 13,000 rpm for 5 minutes
- Remove top layer with a pipette and dispense into a new tube to keep and dispose of bottom layer
- Add an equal volume of room temperature isopropanol and then mix by inversion for 30 seconds
- Let stand for 2 minutes at room temperature and then spin for 5 minutes at 13,000 rpm
- Carefully decant the supernatant
- Add 200 µl of cold 95% EtOH, invert, and then centrifuge at 13,000 rpm for 5 minutes
- Discard supernatant and allow pellet to dry on bench
- Resuspend the pellet in 50 µl of DepC H_2O
- Store at -20°C

Mini-Prep Solutions

Catalogue numbers were provided in Appendices 1 and 2

2M NaOH (50 ml)

- 4 g NaOH
- 50 ml dH_2O

10% SDS (50 ml)

- 5 g SDS
- 50 ml dH_2O

3M Potassium Acetate (50 ml)

- 30 ml 5M potassium acetate (KOAc; Sigma-Aldrich, P1190)
- 5.75 ml glacial acetic acid (Fisher Scientific; A38 212)
- 14.25 ml dH_2O

5M KoAc Stock (10 ml)

- 4.9075 g KOAc
- 10 ml dH_2O

Cold Buffer (50 ml)

- 2.5 ml 1M tris
- 1 ml 0.5M EDTA
- pH to 8.0
- Top up to 50 ml dH_2O

Cold Lysis (1 ml)

- 100 µl 2M NaOH
- 100 µl 10% SDS

- 800 µl dH_2O

Potassium Acetate (6.2 ml)

- 3.75 ml 5M KOAc
- 0.7 ml glacial acetic acid
- 1.75 ml dH_2O

Long Term Storage of Transfected E. Coli Cells Protocol

- Make 50% glycerol
- Add 1 ml glycerol to 5 ml screw cap-tube
- Add 1 ml overnight culture of *E. coli* cells containing your plasmid
- Gently mix by inverting
- Store at -50°C

50% Glycerol (50 ml)

- 25 ml glycerol
- 25 ml dH_2O

DNA Digest Protocol

- Prepare digests in a large volume
- Digestion of 10 µg DNA should be done in a 100 µl volume (or 50 µl for a longer time)
    - Enzyme concentration should not exceed 10% of total volume
        - For 10 µg DNA – 50U enzyme
- In a small 0.2 ml PCR tube, combine:
    - 70 µl DepC H_2O
    - 10 µl Buffer (see below)
    - 10 µl BSA
    - 5 µl DNA
    - 5 µl Digestion enzyme (see below)
- Mix with pipette and centrifuge briefly
- Incubate overnight at 37°C
- In the morning, heat inactivate enzyme at 65°C for 15 minutes

Buffer and Digestion Enzymes Used for Each Gene

Bmp2 antisense: Buffer E (Promega, R005A); Enzyme: BamHI (Promega, R602A)

β-catenin antisense: Buffer D (Promega. R004A); Enzyme: XhoI (Promega, R616A)

β-catenin sense: Buffer E; Enzyme: BamHI

Dlx5 antisense: Buffer SH (Sigma-Aldrich, B3657); Enzyme: NCOI (Sigma-Aldrich, R8761)

Dlx5 sense: Buffer E; Enzyme: BamHI

Gsc antisense: Buffer D; Enzyme: XhoI

Gsc sense: Buffer 3 (NEB, B70035); Enzyme: NotI (NEB; R0189S)

Eya1 antisense: Buffer H (Promega, R008A); Enzyme: EcoRI (Promega, R601A)
Eya1 sense: Buffer 3; Enzyme: NotI

DIG-RNA Labeling Protocol

- Add 1 µg of purified template DNA or 4 µl control DNA to a sterile, RNase-free reaction vial. Then, add enough water (DepC) to the vial to make the total volume of the sample 13 µl
- Place reaction vial on ice, then add the following:
  - 2 µl 10X DIG RNA labeling mix (Roche, 11 277 073 910)
  - 2 µl 10X transcription buffer
  - 1 µl protector RNase inhibitor (Roche, 03 335 399 001)
  - 2 µl RNA polymerase T7 (Roche, 10 881 767 001), or RNA polymerase T3 (Roche, 11 031 163 001)
- Mix gently and centrifuge briefly then incubate for 2 hours at 37°C
- Add 2 µl DNase-I RNase-free to remove template DNA then incubate for 15 minutes at 37°C
- Stop the reaction by adding 2 µl of 0.2M EDTA (pH 8.0)

DIG-RNA Labeling Volumes for Each Gene

Bmp2 antisense: 10 µl DNA + 3 µl dH_2O
β-catenin antisense: 3 µl DNA + 10 µl dH_2O
β-catenin sense: 3 µl DNA + 10 µl dH_2O
Prox1 antisense: 9 µl DNA + 4 µl dH_2O
Prox1 sense: 9 µl DNA + 4 µl dH_2O
Oc90 antisense: 10 µl DNA + 3 µl dH_2O
Oc90 sense: 10 µl DNA + 3 µl dH_2O
Ednrb antisense: 10 µl DNA + 3 µl dH_2O
Ednrb sense: 10 µl DNA + 3 µl dH_2O
Inhba antisense: 13 µl DNA
Inhba sense: 13 µl DNA
Dlx5 antisense: 3 µl DNA + 10 µl dH_2O
Dlx5 sense: 3 µl DNA + 10 µl dH_2O
Gsc antisense: 3 µl DNA + 10 µl dH_2O
Gsc sense: 3 µl DNA + 10 µl dH_2O
Eya1 antisense: 3 µl DNA + 10 µl dH_2O
Eya1 sense: 3 µl DNA + 10 µl dH_2O

DIG-High Prime DNA Labeling and Detection Protocol (Dot-Blot) (Roche, 11 745 832 910)

- Make sure oven is on and pre-heated to 120°C
- Cut out membrane big enough to fit the petri dish (nylon membranes, positively charged; Roche, 11 209 299 001)
- Cut a wedge out of one corner in order to indicate the top left corner
- Set up a Dilution Series as follows

5:3:2 Dilution Buffer (1 ml)
- 500 µl DepC H_2O
- 300 µl 20X SSC
- 200 µl formaldehyde (Sigma-Aldrich, F8775)

Dilution Series /probe

Tube Number	Probe/Tube	Buffer
Tube 1	1 µl probe	40.6 µl
Tube 2	2 µl from Tube 1	18 µl
Tube 3	2 µl from Tube 2	198 µl
Tube 4	15 µl from Tube 3	35 µl
Tube 5	5 µl from Tube 3	45 µl

- Apply a 1 µl spot of your labeled probe and labeled control probe to the nylon membrane
- Fix the nucleic acid by baking for 30 minutes at 120°C (in wax oven) in a sterile glass petri dish
- Transfer membrane into sterile plastic petri dish with enough maleic acid buffer to cover the membrane
- Incubate for 2 minutes with gentle shaking at room temperature
- Incubate for 20 minutes in blocking solution with gentle shaking
    - Prepare antibody solution during this step. Store in fridge until required
- Wash for 5 minutes with 1X TBST at room temperature with shaking
- Incubate in 10 ml of antibody solution for 30 minutes at room temperature with shaking
- Wash in washing buffer at room temperature with gentle shaking for 2 x 15 minutes
    - Prepare the color substrate solution during the second wash above; wrap in tinfoil to above any light
- Equilibrate for 5 minutes in detection buffer at room temperature with shaking
- Incubate at room temperature in dark drawer in 10 ml of freshly prepare color substrate solution.
    - Check every 30 seconds until first dot appears and then check every 5 minutes until color stops developing
- When ready, stop the reaction by removing the color substrate solution and add TE buffer (pH 8.0). Incubate at room temperature at room temperature with shaking.
- Removed the membrane from the dish and store in a ziplock bag at room temperature

DIG-High Prime DNA Labeling and Detection Recipes

Catalogue numbers provided above

Washing Buffer (100 ml)
- 1.1607 g 1M maleic acid
- 0.8766 g 0.15M NaCl

- pH to 7.5
- 0.3 ml Tween20
- Top up to 100 ml with DepC H_2O

Maleic Acid Buffer (100 ml)
- 1.1607 g 1M maleic acid
- 0.8766 g 0.15M NaCl
- pH to 7.5 with solid NaOH (Sigma-Aldrich, S5881)
- Top up to 100 ml with DepC H_2O

Detection Buffer (100 ml)
- 10 ml 1M Tris-HCl
- 0.5844 g 0.1M NaCl
- Top up to 100 ml with DepC H_2O

TE Buffer (100 ml)
- 1 ml 1M Tris-HCl
- 0.2 ml 0.5M EDTA
- pH to 8.0
- Top up to 100 ml with DepC H_2O

10X TBST (500 ml)
- 140 ml 5M NaCl
- 3.37 ml 4M KCl
- 125 ml 1M Tris-Cl pH 7.5
- 0.5 ml Tween20
- Top up to 500 ml with DepC H_2O

Make the following solutions fresh – store in fridge until used
Blocking Solution (10 ml)
- 200 µl sheep serum (Sigma-Aldrich, S2263)
- 0.3 g milk powder (from grocery store)
- 10 ml DepC H_2O

Antibody Solution (10 ml)
- 2 µl Anti-Digoxigenin-AP Fab fragments
- 10 ml 1X TBST

Color Substrate Solution (10 ml)
- 1 tablet Sigma*Fast* NBT/BCIP tablets
- 10 ml dH_2O

Appendix 2: *In Situ* Hybridization

In Situ Hybridization – Protocol

WMISH – Pre Day 1 – Part 1

- 2 x 10 minutes in 1X PBST on ice in sterile 50 ml tube
- 15 minutes in 12.5% MeOH on ice in 50 ml tube
- 15 minutes in 25% MeOH on ice in 50 ml tube
- 15 minutes in 50% MeOH on ice in 50 ml tube
- 15 minutes in 75% MeOH on ice in 50 ml tube
- 15 minutes in 85% MeOH on ice in 50 ml tube
- Store in 100% MeOH for at least one overnight at -20C in 50 ml tubes

WMISH – Day 1

Rehydrate embryos:

- 15 mins in 85% MeOH on ice with shaking or until embryos sink in 50 ml tube
- 15 mins in 75% MeOH on ice with shaking or until embryos sink in 50 ml tube
- 15 mins in 50% MeOH on ice with shaking or until embryos sink in 50 ml tube
- 15 mins in 25% MeOH on ice with shaking or until embryos sink in 50 ml tube
- 15 mins in 12.5% MeOH on ice with shaking or until embryos sink in 50 ml tube
- 2 x 10 mins in 1X PBST at room temperature with shaking in 50 ml tubes
    - Make 10% H_2O_2 solution here
- Leave in 10% bleach solution overnight at room temperature with shaking in 50 ml tube (made with fresh hydrogen peroxide from fridge)

WMISH – Day 2

- 2 x 10 minutes in 1X PBST at room temperature with shaking
    - At start of second wash take ProK out of the freezer
    - Also, take out 4% PFA/1X PBS and glutaraldehyde and allow to thaw
- 30 minutes in 50 mg/ml ProK/1X PBST at room temperature with shaking

  50 mg/ml ProK/1X PBST (40 ml)
    - 200 µl 50 mg/ml stock ProK
    - 40 ml 1X PBST (DepC)
- 20 minutes in 4% PFA/1X PBS + 0.25% glutaraldehyde/1X PBS (50:50) at room temperature with shaking

  4% PFA/PBS + 0.25% glutaraldehyde/PBS (40 ml)
    - 200 µl glutaraldehyde
    - 20 ml 1X PBS
    - 20 ml 4% PFA/1X PBS
- 2 x 10 minutes in 1X PBST at room temperature with shaking
    - Make fresh Prehyb here
- Place in preheated Prehyb at 60°C for 2 hours with shaking
- Hybridization
    - Add probe to fresh Prehyb made above
    - 1 µl probe in 10 ml Prehyb

- Incubate overnight at 60°C with shaking

WMISH – Day 3

- Pre-warm both wash solutions to 60°C (just what is needed in a 15 ml tube)
- 3 x 20 minutes in Wash I at 60°C with shaking
- 3 x 20 minutes in Wash II at 60°C with shaking
    - During last wash (~1/2 way), put the sheep serum into the 60°C incubator for 30 minutes in order to inactivate
- 3 x 10 minutes in 1X TBST at room temperature with shaking
- Antibody Block
    - 2 hour in 20% inactivated sheep serum/TBST at room temperature with shaking
- Pre-Absorb Antibody
    - Combine approximately 1 ml of 20% inactivated sheep serum/TBST made during block step with the required amount of antibody and a tiny amount of chick powder in an Eppendorf tube
    - Shake tube
    - Let the powder settle for 30 minutes on ice
    - Remove the antibody and add it to the rest of the 20% inactivated serum/TBST to make the correct dilution
- Add antibody solution to embryos and incubate overnight at 4°C with shaking

WMISH – Day 4

- 3 x 10 minutes in 1X TBST at room temperature with shaking
- Wash in 1X TBST + 2 mM levamisole overnight at 4°C with shaking
    - Change 1X TBST + 2 mM levamisole 1-3 time a day for 1-3 days

WMISH – Day 5

- Wash in 1X TBST + 2 mM levamisole overnight at 4°C with shaking
    - Change 1X TBST + 2 mM levamisole once a day for 3 days

WMISH – Day 6

- Wash in 1X TBST + 2 mM levamisole overnight at 4°C with shaking
    - Change 1X TBST + 2 mM levamisole once a day for 2 days

WMISH – Day 7

- Wash in 1X TBST + 2 mM levamisole overnight at 4°C with shaking
    - Change 1X TBST + 2 mM levamisole once a day

WMISH – Day 8

- Make 1X NTMT and 1X NTMT + 2mM levamisole
- Boil PVA

Develop Color Reaction (30 ml)

1X NTMT for color detection (30 ml)

- 600 µl 5M NaCl

- 3 ml 1M Tris-Cl pH 9.5
- 150 µl Tween20
- Top up to 25 ml with DepC H_2O

- Add 3 g of PVA (10% w/v) to the 25 ml 1X NTMT made above
  - This solution needs to be boiled in order to dissolve the PVA. To do this, dissolve it in a 50 ml falcon tube floating in a water bath
- When PVA is cooled to room temperature, add:
  - 750 µl 1M $MgCl_2$-$6H_2O$
  - 99 µl Nitrotetrazolium blue chloride (NBT; Sigma-Aldrich, N6876) in 70% N,N-dimethyl formamide (DMF; Sigma-Aldrich, 319937) (68.2 mg/ml stock)
  - 69 µl 5-Bromo-4-chloro-3-indolyl phosphate p-toluidine sald (BCIP; Sima-Aldrich, B6777) in 100% DMF(50 mg/ml stock)
  - Top up solution to 30 ml
- 3 x 10 minutes in 1X NTMT + 2 mM levamisole at 4°C with shaking
- Incubate embryos in the dark at room temperature in the color substrate solution. This should be done in glass vials. Change color solution if it goes pink.

<u>WMISH – Day 7 (or after color)</u>
- 2 x 10 minutes in 1X PBST + 5 mM EDTA at room temperature without shaking
- Post fix in 4% PFA for 20 minutes at room temperature without shaking
- 2 x 10 minutes in 1X PBST at room temperature without shaking
- Leech background from embryos in 90% MeOH overnight at 4°C without shaking

<u>WMISH – 8</u>
- Quick rinse in dH_2O
- Store in 50:50 Glycerol/water at 4°C

In Situ Hybridization – Solutions

<u>0.1% Diethyl Pyrocarbonate (DepC) Treated Water</u> (1 L)
- Add 1 ml DepC to 1 L of dH_2O
- Shake vigorously for 30 minutes
- Let stand, with lid cracked, in the fume hood for at least 1 hour
- Autoclave
- Allow to cool

<u>5M NaCl</u> (500 ml)
- 146.1 g NaCl
- Top up to 500 ml with DepC H_2O

<u>4M KCl</u> (50 ml)
- 14.912 g KCl
- Top up to 50 ml with DepC H_2O

1M Na_2HPO_4 (50 ml)

- 7.098 g Na_2HPO_4
- Top up to 50 ml with DepC H_2O

1M KH_2PO_4 (50 ml)

- 6.805 g KH_2PO_4
- Top up to 50 ml with DepC H_2O

1M Tris-Cl pH 7.5 (250 ml)

- 30.275 g Tris base
- pH to 7.5 HCl
- Top up to 250 ml with DepC H_2O

1M Tris-Cl pH 9.5 (50 ml)

- 6.055 g Tris base
- pH to 9.5 HCl
- Top up to 50 ml with DepC H_2O

1M $MgCl_2$-$6H_2O$ (50 ml)

- 10.165 g $MgCl_2$-$6H_2O$
- Top up to 44.6 ml with DepC H_2O

10X PBS (500 ml)

- 137 ml 5M NaCl
- 3.37 ml 4M KCl
- 21.5 ml 1M Na_2HPO_4
- 7 ml 1M KH_2PO_4
- pH to 7.4
- Top up to 500 ml with DepC

1X PBS (500 ml)

- 50 ml 10X PBS
- 450 ml DepC H_2O

1X PBST (1L)

- 100 ml 10X PBST
- 900 ml DepC H_2O
- 1 ml Tween20

4% PFA (100 ml)

- 80 ml PBST in graduated cylinder
- Pour into beaker
- 4 g PFA
- Add to 80 ml PBST

- Mix (heat and cover with foil)
- When completely stirred in, add 1 pellet of NaOH
- pH to 7.4 when cooled
- Top up to 100 ml with 1X PBST
- Divide into 3 aliquots of 35 ml

12.5% MeOH (100 ml)
- 12.5 ml 100% MeOH
- 87.5 ml 1X PBST (DepC)

25% MeOH (100 ml)
- 25 ml 100% MeOH
- 75 ml 1X PBST (DepC)

50% MeOH (100 ml)
- 50 ml 100% MeOH
- 50 ml 1X PBS (DepC)

75% MeOH (100 ml)
- 75 ml 100% MeOH
- 25 ml DepC H_2O

85% MeOH (100 ml)
- 85 ml 100% MeOH
- 15 ml DepC H_2O

90% MeOH (100 ml)
- 90 ml 100% MeOH
- 10 ml dH_2O

10% Hydrogen Peroxide in PBST
- 25 ml 30% H_2O_2
- 50 ml 1X PBST (DepC)

Prehyb (30 ml)
- 15 ml deionized formamide
- 7.5 ml 20X SSC
- 3 ml 10% SDS
  (0.3g SDS in 3 ml DepC H_2O)
- 4.5 ml DepC H_2O
- 0.0015 g 50 g/ml yeast tRNA
- 0.0015 g 50 g/ml heparin

10X TBST (500 ml)
- 140 ml 5M NaCl

- 3.37 ml 4M KCl
- 125 ml 1M Tris-Cl pH 7.5
- Top up to 500 ml with DepC H_2O

1X TBST (1L)
- 100 ml 10X TBST
- 900 ml DepC H_2O
- 1 ml Tween20

Wash I (50 ml)
- 25 ml deionized formamide
- 10 ml 20X SSC
- 2.5 ml 20% SDS
  (0.5g SDS in 2.5 ml DepC H_2O)
- 12.5 ml DepC H_2O

Wash II (50 ml)
- 25 ml deionized formamide
- 5 ml 20X SSC
- 20 ml DepC H_2O

1X NTMT (100 ml)
- 2 ml 5M NaCl
- 10 ml 1M Tris-Cl pH 9.5 with HCl
- 2.5 ml 1M $MgCl_2$-$6H_2O$
- 0.5 ml Tween 20
- Top up to 100 ml with DepC H_2O

Chick Powder
- Cool acetone
- Collect 4 four-five day embryos in a small amount of PBS
- Add 4 volumes of cold acetone
- Homogenize embryos in acetone
- Incubate on ice for 30 minutes
- Spin at 10,000 xg for 10 minutes
- Pour off acetone
- Pour embryos onto clean filter paper and crush or cut into a powder
- Store at -20°C

20% Sheep Serum in TBST (20 ml)
- 4 ml sheep serum
- 16 ml 1X TBST

Antibody Solution (10 ml)
- 1 µl Anti-DIG-AP Fab Fragments

- 10 ml 20% inactivated sheep serum

1X TBST + 2 mM Levamisole (20 ml)
- 0.00963 g levamisole
- 20 ml 1X TBST

1X NTMT + 2 mM Levamisole (20 ml)
- 0.00963 g levamisole
- 20 ml 1X TBST

1X PBST + 5 mM EDTA (50 ml)
- 0.093 g EDTA
- 50 ml 1X PBST

In Situ Hybridization – Probe Concentrations Used

- *Bmp2* antisense: 2 µl/5 ml
- *β-catenin* antisense: 1 µl/5 ml
- *β-catenin* sense: 1 µl/5 ml
- *Prox1* antisense: 2 µl/5 ml
- *Prox1* sense: 2 µl/5 ml
- *Ednrb* antisense: 2 µl/5 ml
- *Ednrb* sense: 2 µl/5 ml
- *Inhba* antisense: 2 µl/5 ml
- *Inhba* sense: 2 µl/5 ml
- *Dlx5* antisense: 2 µl/5 ml
- *Dlx5* sense: 1 µl/5 ml
- *Gsc* antisense: 2 µl/5 ml
- *Gsc* sense: 1 µl/5 ml
- *Eya1* antisense: 2 µl/5 ml
- *Eya1* sense: 1 µl/5 ml
- *Oc90* antisense: 2 µl/5 ml
- *Oc90* sense: 3 µl/5 ml

Appendix 3: *Oc90*

As described in the methodology for Chapter 4, the gene sequence from which the primers for *Oc90* were designed has since been removed from NCBI because it was found to be erroneous. As I cannot, therefore, be sure of the results obtained for *Oc90*, they are presented here.

Gene Sequence:

GCTATGAGGAAGCGATGGAGATGGAGTGCACATGGGACCCATCAAAA
>>>>>>>>>>>>>>>>>>>>>>>>>
ATTTCCACAGATGTCACGTGCTCTGCAGAAAACCTGAGCTGTGAAAAT

GGGGATCCCTGTGAACAGTTCCTCTGCACCTGTGACAAAGATGCCATT

GAGTGTTTTGGGAACGCTCATATTAACTCTTCCCTGAATGGCCT
<<<<<<<<<<<<<<<<<<<<<<<<<

Product size: 187 bp

Start	Len	TM	GC%	Seq
419	20	49.94	55.00	GCTATGAGGAAGCGATGGAG
605	20	60.07	50.00	AGGCCATTCAGGGAAGAGTT

T3 and T7 Conjungated Primers:

Forward: TAATACGACTCACTATAGGGGCTATGAGGAAGCGATGGAG

Reverse: AATTAACCCTCACTAAAGGGAGGCCATTCAGGGAAGAGTT

Description of Candidate Gene:

Oc90, a calcium ion binding protein, was upregulated by a fold change of 1.30 at HH 34 as compared to HH 30. However, what was most interesting about *Oc90* was its upregulation by a fold change of 29.67 at HH 36 when compared to HH 30. This huge upregulation of *Oc90* between HH 30 and 36 may therefore indicate a strong involvement of *Oc90* in the induction and patterning of the conjunctival papillae and scleral condensations, as those are the major developmental processes underway in the eye during that period. This large upregulation could indicate a false positive, especially considering that *Oc90* has never been associated in the literature with the development of any structure other than the otoconia and hair cells in the inner ear (Wang *et al*., 1998; Zhao *et al*., 2007; Zhao *et al*., 2008a; Zhao *et al*., 2008b; Petko *et al*., 2008; Deans *et al*., 2010; Xu *et al*., 2010; Yang *et al*., 2011; Abu-Daya *et al*., 2012; Moreland *et al*., 2014; Ronaghi *et al*., 2014; Hartman *et al*., 2015).

Presence versus Absence Analysis:

Oc90 was expressed in both the epithelium and mesenchyme at both HH 30 and HH 34 (Figure 1). In the mesenchyme, however, there also appeared to be a band at both 1,500 bp and 190 bp. As this 1,500 bp band was not present in the PCR triplicates of *Oc90* performed on the unseparated tissues and the sequencing of these primers was 100% specific to the gene of interest, I am not sure what this 1,500 bp band may represent.

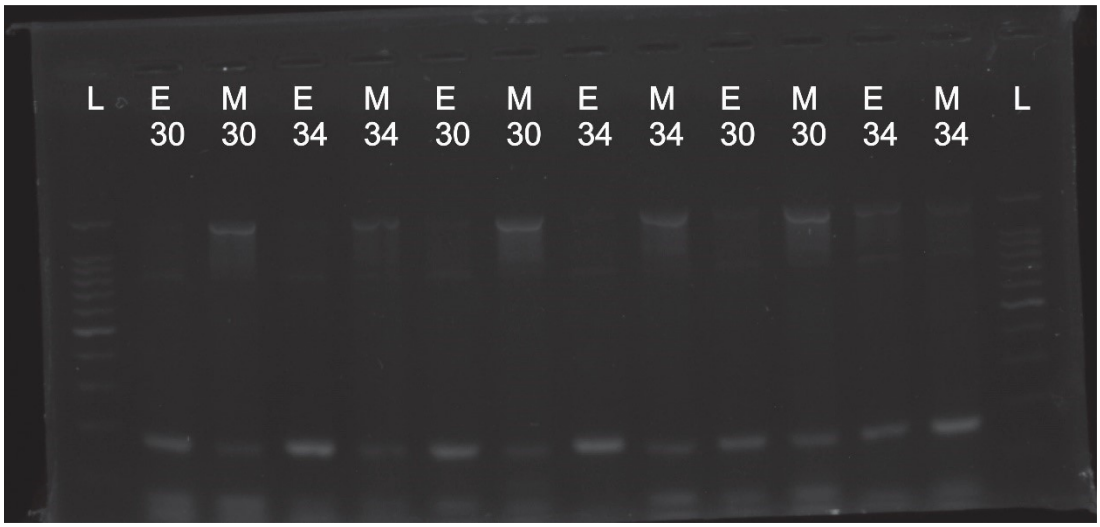

Figure 1: The results of PCR for *Oc90*. *Oc90* was expressed in both the epithelium and mesenchyme at HH 30 and HH34. L: ladder, E: epithelium, M: mesenchyme.

Spatiotemporal Gene Expression Pattern:

Based on the results of *in situ* hybridization, *Oc90* was not expressed at HH 30 (N=8; Figure 2A). By HH 31 (N=2), *Oc90* is faintly expressed in the temporal and nasal papillae, the only groups present at this stage (Figure 2B). This faint expression of *Oc90* continues through to HH 33 (N=2), when *Oc90* is faintly expressed in all visible conjunctival papillae (Figure 2C). By HH 34 (N=6), *Oc90* is strongly expressed in all of the conjunctival papillae in the ring with faint expression of *Oc90* throughout the eye (Figure 2D). There also appears to be some faint mesenchymal expression at the future site of the scleral condensations (Figure 2D). The results of cryosectioning confirm that this expression of *Oc90* is widespread in both the epithelium and the mesenchyme, with stronger expression in the conjunctival papillae and the epithelium of the papilla-contiguous region (Figure 2K). By HH 35.5 (N=3), *Oc90* is downregulated throughout both the epithelium and mesenchyme and has been downregulated in the conjunctival papillae, which now only faintly express *Oc90* (Figure 2E). These results suggest that *Oc90* may be important for the induction and patterning of the conjunctival papillae but is likely not required for the induction and patterning of the scleral condensations.

In situ hybridization using the sense riboprobe for *Oc90* detected signal (N=8; Figure 2F-J). The expression pattern detected using the sense riboprobe was very similar to that described using the antisense riboprobe with the exception of HH 35.5, at which

stage these was strong sense riboprobe signal detected in the conjunctival papillae (Figure 2J). When this signal was further examined by cryosectioning at HH 34, it was determined that the signal detected by the sense riboprobe was located both throughout the epithelium and mesenchyme (Figure 2K). Additionally, the conjunctival papilla was almost indistinguishable from the surrounding epithelium and mesenchyme due to the intensity of the staining. In order to determine the nature of this sense riboprobe signaling for *Oc90*, the gene sequence was re-examined. There were no nearby genes. As the primers were 100% specific to the gene of interest, it is possible that the small size of the probe for *Oc90* (187 bp) resulted in the trapping of the sense and antisense riboprobes in the tissue and therefore, all of the expression I detected may represent non-specific binding. Furthermore, as the gene sequence from which they were designed has since been removed from NCBI because it was found to be erroneous, it is difficult to identify the nature of the signal detected by the sense riboprobe.

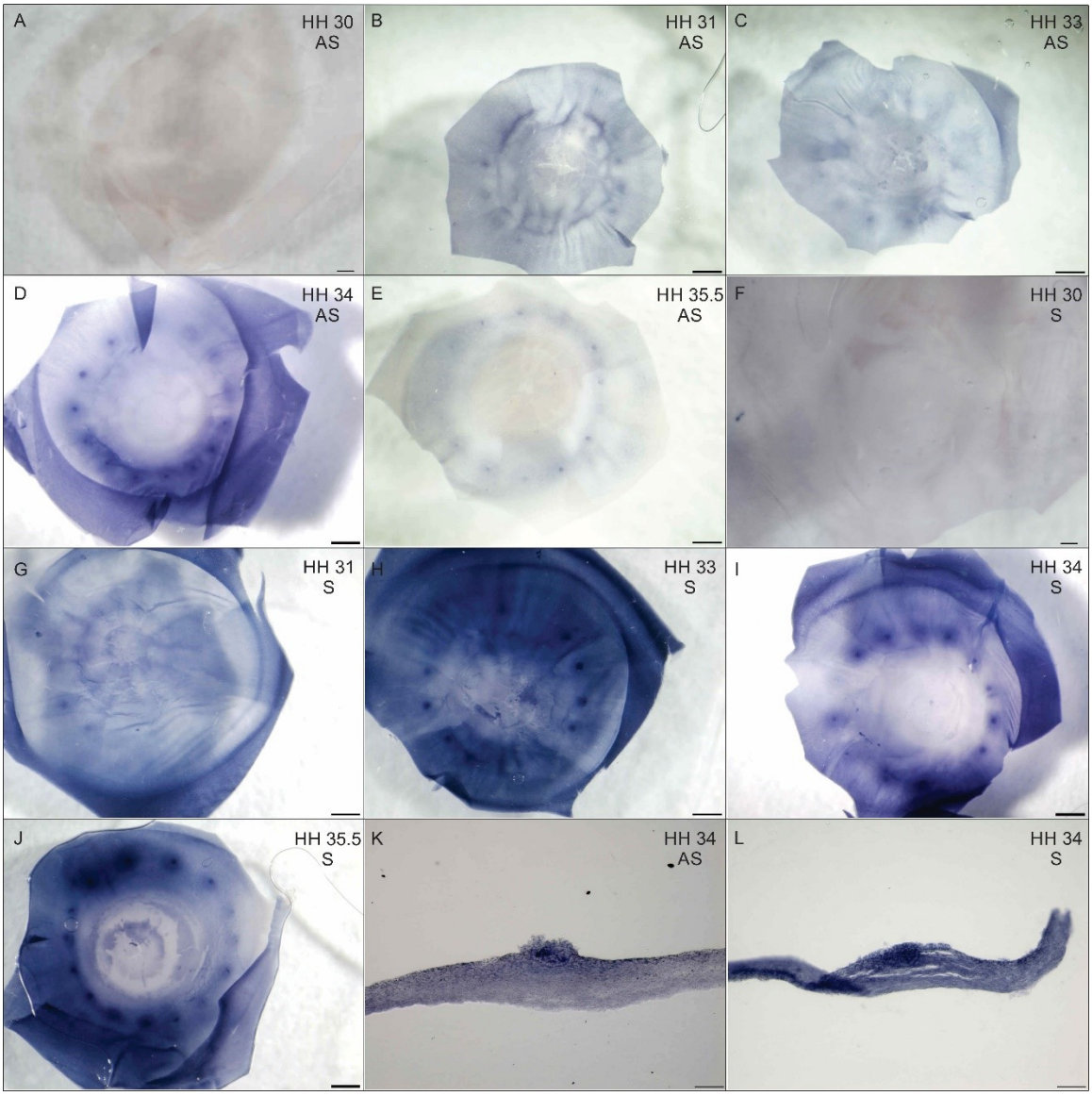

Figure 2: Results of *in situ* hybridization for *Oc90*. **A-E, K** show the results of *in situ* hybridization using the antisense riboprobe while **F-J, L** show the results of *in situ* hybridization using the sense riboprobe. **A**) There is no expression in the eye. **B**) There is faint expression in the temporal and nasal conjunctival papillae. **C**) The temporal, nasal, and dorsal conjunctival papillae faintly express *Oc90*. **D**) All of the conjunctival papillae express *Oc90*. There also appears to be faint, widespread expression in the epithelium and mesenchyme. **E**) There is now only faint expression in the conjunctival papillae. **F**) There is no expression. **G**) There is expression in the temporal and nasal conjunctival papillae. **H**) There is expression in the temporal, nasal, and dorsal conjunctival papillae. **I**) There is expression in all of the conjunctival papillae in the eye and there appears to be some faint mesenchymal expression. **J**) Expression is detected in the conjunctival papillae at HH 35.5. **K**) Cryosectioning shows widespread, faint expression in the epithelium and underlying mesenchyme and stronger expression in the conjunctival papilla and papilla-contiguous region. **L**) Cryosectioning reveals ubiquitously strong expression throughout both the epithelium and mesenchyme. The papilla is almost indistinguishable from the surrounding tissue. AS: antisense riboprobe, S: sense riboprobe. **A-J** scale bars are 500 μm. **K-L** scale bars are 20 μm.

Discussion of *Oc90* Expression:

As described above, previous to this study, *Oc90* was believed to be expressed during only the development of the otoconia and hair cells in the inner ear where it is required for the formation of the organic matrix of the otoconia (Wang *et al*., 1998; Zhao *et al*., 2007; Zhao *et al*., 2008a; Zhao *et al*., 2008b; Petko *et al*., 2008; Deans *et al*., 2010; Xu *et al*., 2010; Yang *et al*., 2011; Abu-Daya *et al*., 2012; Moreland *et al*., 2014; Ronaghi *et al*., 2014; Hartman *et al*., 2015). Very little is known, however, about the gene interactions or regulatory elements that govern the expression of *Oc90.* Surprisingly, *Oc90* was expressed in each group of conjunctival papillae as they were induced and by HH 34, *Oc90* was strongly expressed in all of the conjunctival papillae in the ring. Additionally, cryosectioning of a sample at HH 34 revealed widespread expression of *Oc90* throughout the epithelium and mesenchyme. However, as I also detected signal using the sense riboprobe for *Oc90,* therefore, it is possible that this expression represented non-specific binding of the probe. Thus, it will be important to do functional analyses for this gene in order to determine whether it is required for the induction and patterning of either the conjunctival papillae or scleral ossicles. If, however, this expression of *Oc90* does represent specific expression, the results of *in situ* hybridization described above would suggest that *Oc90* may play a role in the induction and patterning of the conjunctival papillae, as it is expressed coincident with the appearance of the first conjunctival papillae. Additionally, the continued expression of *Oc90* across all examined stages of papilla development may suggest that *Oc90* is involved in the maintenance of the conjunctival papillae. It is, however, unlikely that *Oc90* is required for the induction of the condensations themselves as it is substantially down-regulated by HH 35.5, during the inductive period of the condensations (Coulombre & Coulombre, 1962). This will require further research.